NASA TECHNICAL MEMORANDUM

NASA TM X-73998

NASA TM X-73998

AUGMENTATION OF MANEUVER PERFORMANCE BY SPANWISE BLOWING

BY

Gary E. Erickson, Joint Institute for the Advancement of Flight Sciences, George Washington University

James F. Campbell, NASA Langley Research Center

January 1977

National Aeronautics and Space Administration

Langley Research Center
Hampton, Virginia 23665

1. Report No.	2. Government Accession No.	3. Recipient's Catalog No.
NASA TM X-73998		

4. Title and Subtitle	5. Report Date
AUGMENTATION OF MANEUVER PERFORMANCE BY SPANWISE BLOWING	January 1977
	6. Performing Organization Code

7. Author(s)	8. Performing Organization Report No.
Gary E. Erickson, George Washington University, JIAFS and James F. Campbell, NASA Langley Research Center	
	10. Work Unit No.

9. Performing Organization Name and Address	11. Contract or Grant No.
NASA Langley Research Center Hampton, VA 23665	
	13. Type of Report and Period Covered
12. Sponsoring Agency Name and Address	Technical Memorandum
National Aeronautics and Space Administration Washington, DC 20546	14. Sponsoring Agency Code

15. Supplementary Notes

16. Abstract

A generalized wind tunnel model was tested to investigate new component concepts utilizing spanwise blowing to provide improved maneuver characteristics for advanced fighter aircraft with primary emphasis on high angle-of-attack performance, stability, and control at subsonic speeds. Test data were obtained in the Langley 7- by 10-foot high speed facility at free-stream Mach numbers up to 0.50 for a range of model angle-of-attack, jet momentum coefficient, and leading- and trailing-edge flap deflection angles.

Spanwise blowing on a 44^{o} swept trapezoidal wing resulted in leading-edge vortex enhancement with subsequent large vortex-induced lift increments and drag polar improvements at the higher angles-of-attack. Small deflections of a leading-edge flap delayed these lift and drag benefits to higher angles-of-attack. In addition, blowing was more effective at higher Mach numbers. Spanwise blowing in conjunction with a deflected trailing-edge flap resulted in lift and drag benefits that exceeded the summation of the effects of each high-lift device acting alone. Asymmetric blowing was an effective lateral control device at the higher angles-of-attack. Spanwise blowing on the wing reduced horizontal tail loading and improved the lateral-directional stability characteristics of a wing-horizontal tail-vertical tail configuration. The effects of spanwise blowing in the channel formed by extension of upper surface leading- and trailing-edge flaps were limited due to wing flap design and jet location.

17. Key Words (Suggested by Author(s))

Spanwise blowing
Vortex lift
Maneuver performance
Locked vortex

18. Distribution Statement

Unclassified-Unlimited

Star Category-02

19. Security Classif. (of this report)	20. Security Classif. (of this page)	21. No. of Pages	22. Price*
Unclassified	Unclassified	239	$8.00

*For sale by the National Technical Information Service, Springfield, Virginia 22161

ABSTRACT

A generalized wind tunnel model was tested to investigate new component concepts utilizing spanwise blowing that will provide improved maneuver characteristics for advanced fighter aircraft with primary emphasis on high angle-of-attack performance, stability, and control at subsonic speeds. The investigation was focused on various methods of controlling and delaying the leading-edge vortex breakdown and of optimizing component interactions. In particular, spanwise blowing was utilized on a 44° swept trapezoidal wing to determine the effect of leading-edge vortex enhancement on leading- and trailing-edge flap effectiveness, horizontal and vertical tail loads, and to assess the concept as a roll control device. In addition, the effect of spanwise blowing on the canard or wing on close-coupled canard-wing effectiveness was investigated. Additional studies were conducted with a trapezoidal wing featuring a unique leading- and trailing-edge flap arrangement which, when combined with spanwise blowing created a "locked vortex" system for high lift at take-off, approach, and during maneuvering flight.

Test data were obtained in the Langley high speed wind tunnel at free-stream Mach numbers up to 0.50 for a range of model angle-of-attack, jet momentum coefficient, and leading- and trailing-edge flap deflection angle. Spanwise blowing resulted in significant vortex-induced lift increments at the higher angles-of-attack with consequent improvement in the drag polar, and the data suggested that blowing was more effective at the higher Mach number. Small deflections of a leading-edge flap delayed the beneficial effects on lift due to blowing to higher angles-of-attack, but the data suggested a forward rotation of the vortex-lift vector resulted in leading-edge

thrust recovery and, hence, polar improvement. Spanwise blowing in conjunction with a deflected trailing-edge flap resulted in lift and drag benefits that exceeded the effect of each high-lift device acting alone. Spanwise blowing on the canard in the presence of the wing was more effective than blowing on the wing in the presence of the canard. The data suggested that blowing on the canard enhanced the canard leading-edge vortex and improved the favorable canard-wing interference at higher angles-of-attack. Horizontal tail loading at higher angles-of-attack was reduced by spanwise blowing on the wing. In addition, blowing resulted in stabilizing increments in the effective dihedral and directional stability parameters of the wing-vertical tail and wing-horizontal tail-vertical tail configurations and delayed the unfavorable break in the directional stability parameter to much higher angles-of-attack. Spanwise blowing was an effective lateral control device at the higher angles-of-attack and compared favorably to a theoretical estimate of the effect of trailing-edge flap ailerons. Spanwise blowing in the channel formed by extension of upper surface leading- and trailing-edge flaps of the "locked vortex" wing resulted in large vortex-induced lift increments but the data suggested that further refinements in the wing flap design and nozzle location are necessary in order to achieve more favorable lift benefits.

The leading-edge suction analogy was used for selected configurations and provided reasonable estimates for the longitudinal aerodynamic characteristics resulting from spanwise blowing.

TABLE OF CONTENTS

LIST OF TABLES

LIST OF FIGURES

Figure

Figure

Figure

Figure

Figure

Figure

Figure

SYMBOLS

The International System of Units (SI), with the U.S. Customary Units presented in parentheses, is used for the physical quantities in this paper. Measurements and calculations were made in the U.S. Customary Units. All data presented in this report are referred to the stability-axis system as indicated in figure 1.

AF_J	axial force due to nozzle thrust components, N(lbf)
AR	aspect ratio, b^2/S
A_e	nozzle exit area, cm^2 (in^2)
b	wing span, 54.36 cm (21.40 in.)
C_D	aerodynamic drag coefficient, $\frac{Drag}{q_\infty S}$
$C_{D,J}$	drag coefficient due to nozzle thrust components
$C_{D,L}$	aerodynamic drag-due-to-lift coefficient ($C_D - C_{D,o}$)
$C_{D,T}$	total drag force coefficient, including nozzle thrust components
$C_{D,o}$	minimum aerodynamic drag coefficient
C_L	aerodynamic lift coefficient, $\frac{Lift}{q_\infty S}$
$C_{L,J}$	lift coefficient due to nozzle thrust components
$C_{L,ind}$	lift coefficient at zero angle-of-attack due to jet-induced camber effect
$C_{L,max}$	maximum lift coefficient
$C_{L,o}$	aerodynamic lift coefficient without blowing ($C_{L,jet\ off}$)
$C_{L,p}$	potential lift coefficient
$C_{L,T}$	total lift force coefficient, including nozzle thrust components
$C_{L,vle}$	leading-edge vortex lift coefficient
$C_{L,vse}$	side-edge vortex lift coefficient

$C_{L,tot}$	$C_{L,p} + C_{L,vle} + C_{L,vse}$
C_{L_α}	lift curve slope
C_m	aerodynamic pitching moment coefficient, $\frac{\text{pitching moment}}{q_\infty S \bar{c}}$
$C_{m,J}$	pitching moment coefficient due to nozzle thrust components
$C_{m,T}$	total pitching moment coefficient, including nozzle thrust components
C_ℓ	aerodynamic rolling moment coefficient, $\frac{\text{Rolling moment}}{q_\infty Sb}$
$C_{\ell,J}$	rolling moment coefficient due to nozzle thrust components
$C_{\ell,T}$	total rolling moment coefficient, including nozzle thrust components
C_{ℓ_β}	rolling moment due to sideslip, $\frac{\partial C_\ell}{\partial \beta}$, per deg
C_n	aerodynamic yawing moment coefficient, $\frac{\text{Yawing moment}}{q_\infty Sb}$
$C_{n,J}$	yawing moment coefficient due to nozzle thrust components
$C_{n,T}$	total yawing moment coefficient, including nozzle thrust components
C_{n_β}	yawing moment due to sideslip, $\frac{\partial C_n}{\partial \beta}$, per deg
C_Y	aerodynamic side force coefficient, $\frac{\text{Side force}}{q_\infty S}$
$C_{Y,J}$	side force coefficient due to nozzle thrust components
$C_{Y,T}$	total side force coefficient, including nozzle thrust components
C_{Y_β}	side force due to sideslip, $\frac{\partial C_Y}{\partial \beta}$, per deg
C_μ	jet momentum coefficient, $\dot{w}V_j/gq_\infty S$
$C_{\mu,avg}$	average jet momentum coefficient
c	local wing chord, cm (in.)
c_f	local flap chord, cm (in.)

c_{th}	theoretical wing root chord with leading and trailing edges extended to plane of symmetry, cm (in.)
$\bar{c}$	wing mean geometric chord, cm (in.)
d	nozzle diameter, cm (in.)
g	gravitational acceleration, 9.8m/sec^2 (32.2ft/sec^2)
h	height of nozzle center-line above lifting surface, cm (in.)
i_C	canard incidence angle, deg
LE	leading edge
M_∞	free-stream Mach number
NF_J	normal force due to nozzle thrust components, N (lbf)
p_∞	free-stream static pressure, Pa (psi)
$p_{t,plen}$	stagnation pressure in settling chamber, Pa (psi)
$p_{t,n}$	stagnation pressure at nozzle exit, Pa (psi)
PM_J	pitching moment due to nozzle thrust components, N-m (in-lbf)
q_∞	free-stream dynamic pressure, Pa (lbf/ft^2)
R_n	Reynolds number (based on wing mean geometric chord, $\bar{c}$)
RM_J	rolling moment due to nozzle thrust components, N-m (in-lbf)
S	wing reference area with leading and trailing edges extended to plane of symmetry, cm^2 (in.^{2})
S_C	exposed canard area, cm^2 (in^2)
S_T	exposed tail area, cm^2 (in^2)
SF_J	side force due to nozzle thrust components, N (lbf)
$T_{t,plen}$	average stagnation temperature in settling chamber, ^oR
TE	trailing edge
t	local wing thickness, cm (in.)

V_j	jet velocity reached by isentropic expansion from the stagnation pressure at the nozzle exit to free-stream pressure, m/sec (ft/sec)
$\dot{w}$	nozzle-air weight flow rate, N/sec (lbf/sec)
x_n	chordwise distance of nozzle from leading edge of wing root chord, cm (in.)
YM_J	yawing moment due to nozzle thrust components, N-m (in-lbf)
α	angle-of-attack, deg
β	angle-of-sideslip, deg
δ_{left}	left aileron deflection angle, deg
δ_{right}	right aileron deflection angle, deg
δ_{LE}	leading-edge flap deflection angle, deg
δ_{TE}	trailing-edge flap deflection angle, deg
Λ_{LE}	sweep angle of lifting surface leading edge, deg
Λ_n	sweep angle of nozzle, deg
γ	ratio of specific heats, 1.4 (air)
ΔC_D	aerodynamic drag increment due to blowing, $C_{D,\text{jet on}} - C_{D,\text{jet off}}$
$\Delta C_{D,L}$	aerodynamic drag-due-to-lift increment due to blowing, $(C_{D,L})_{\text{jet on}} - (C_{D,L})_{\text{jet off}}$
ΔC_L	aerodynamic lift increment due to blowing, $C_{L,\text{jet on}} - C_{L,\text{jet off}}$
η_i	trailing-edge flap aileron inboard span station
η_o	trailing-edge flap aileron outboard span station

CHAPTER I

INTRODUCTION

The flow on thin, highly-swept-back wings at moderate-to-high angles-of-attack is characterized by a leading-edge separation which forms a stable vortex over the wing and provides significant vortex-induced lift increments. This characteristic of slender wings, of the supersonic cruise type, has been understood for many years (refs. 1-5). For moderately-swept higher aspect ratio wings suitable for fighter aircraft, however, these vortex-induced lift increments are not achieved due to vortex bursting, or breakdown, at low angles-of-attack. If vortex breakdown could be delayed to higher angles-of-attack, the resulting vortex lift would significantly improve fighter maneuver performance.

A promising technique for enhancing the leading-edge vortex on moderately-swept wings and effectively delaying vortex breakdown to higher angles-of-attack consists of blowing a concentrated jet over the wing's upper surface in a direction essentially parallel to the wing leading-edge. The results reported in refs. 6-20 have demonstrated the control of separated flow regions by transverse blowing, applied the spanwise blowing concept to different types of lifting surfaces, and determined the amount of vortex lift achievable on wings typical of current fighter aircraft. It is desirable to extend these studies to evaluate the effect of spanwise blowing on fighter performance, stability, and control for a variety of aircraft-component arrangements.

Accordingly, the present investigation was conducted utilizing a 44° swept trapezoidal wing configuration to determine (1) the effects of spanwise

blowing on leading- and trailing-edge flap effectiveness, (2) on horizontal and vertical tail effectiveness, (3) on close-coupled canard-wing interactions, (4) to assess spanwise blowing on a roll control device, and (5) to evaluate a unique leading- and trailing-edge flap arrangement which creates a "locked vortex" system.

The wind tunnel tests were performed in the Langley high speed 7- by 10-foot facility at Mach numbers up to 0.50. Six-component force and moment data were acquired for a range of angle-of-attack and jet momentum coefficient.

CHAPTER II

BACKGROUND

The contradictory requirements for thin, low aspect ratio wings for efficient supersonic performance and for thicker, higher aspect ratio wings for subsonic maneuver and take-off and landing performance have led to considerable investigation of design concepts that take advantage of vortex-induced lift. Stable, leading-edge vortices are characteristic of the flow over thin, highly swept-back wings at moderate-to-high angles-of-attack. This flow situation occurs because the favorable spanwise pressure gradient causes the separated leading-edge flow to form a stable spiral vortex, as illustrated in figure 2. The take-off and landing performance of the Anglo-French supersonic transport "Concorde" relies on favorable leading-edge vortex-induced effects. In addition, a strong vortex flow generated by a maneuver strake is very important to the high angle-of-attack maneuverability of the F-16 fighter, which is shown in the photograph in figure 3. Many researchers, for example ref. 1, have investigated sharp-edge delta and delta-related planforms and have shown that a fully-developed leading-edge vortex induces substantial increases in lift beyond that obtainable with attached flow. These trends are illustrated in figure 4, which shows the effect of leading-edge sweep angle on the lift of flat-plate delta wings at $\alpha = 20^{\circ}$. For moderately-swept, higher aspect ratio wings typical of fighter aircraft, these vortex-induced effects are not achieved due to vortex breakdown at low angles-of-attack. It is of interest, therefore, to incorporate into aircraft design either an active of passive means, or perhaps a synthesis of both, of augmenting the leading-edge vortex flow for such

wings in order to improve the maneuver performance at moderate-to-high angles-of-attack.

Spanwise blowing is one active method of enhancing the leading-edge vortex on moderately-swept wings and delaying vortex bursting to greater span distances at a given angle-of-attack. This is accomplished by directing a concentrated jet spanwise over the wing's upper surface in a direction essentially parallel to the wing leading edge. A sketch of the concept is shown in figure 5 and illustrates how the air is drawn over the leading-edge vortex and reattaches to the wing surface behind the jet, much like the reattachment behind a two-dimensional separation bubble. Spanwise blowing induces a flow along the vortex axis which delays vortex breakdown to greater span distances and higher wing angles-of-attack with consequent increases in lift, and hence enables a stable vortex flow to be maintained over a wider range of flight attitudes and Mach numbers. Some original work related to this concept was performed in refs. 6-9 which demonstrated the control of separated flow regions by transverse blowing. Additional work performed in refs. 10-14 applied the concept to different types of lifting surfaces, such as wings, leading- and trailing-edge flaps, horizontal tails, and vertical tail rudders. More recently, wind tunnel tests and theoretical studies have been conducted in refs. 15-19 to determine the effects of spanwise blowing on wings of moderate sweep angles typical of current fighter aircraft. Reference 20 has also investigated the application of spanwise blowing on the canard of a large-scale, semi-span canard-wing transport configuration and has indicated that canard blowing may possibly enable a reduction in canard size required for low-speed flight and permit a more optimum canard to be used in cruise.

Another concept utilizing spanwise blowing to augment a vortex flow has been investigated in ref. 21 which consists of "locking" a vortex flow over a semi-span, rectangular wing by spanwise blowing in the channel formed by extension of upper surface leading-and trailing-edge flaps. This concept is illustrated in the sectional view in figure 6 which shows how the flow separates from the upper end of the leading-edge flap and rolls up into two discrete vortices within the channel. Two co-rotating vortices were found in flow visualization studies conducted in reference 22 using neutrally-buoyant helium-filled bubbles to visualize the flow. Ref. 21 did not discern the vortex ahead of the jet, which is probably due to an inherent disadvantage in generating smoke in front of the model as a flow visualization technique. At sufficient blowing rates, the separated flow reattaches to the trailing-edge flap after passing over the vortex channel. It is this flow reattachment that results in large increases in lift. The vortex flow appears to energize the flow such that attached flow is provided over an "effective" airfoil shape possessing a large amount of camber and thickness. Ref. 23 initially proposed application of spanwise blowing in conjunction with the unique flap arrangement to improve the low speed flight performance of fighter aircraft. By extending the flaps and blowing spanwise in the channel during take-off and landing, it may be possible to generate high lift at relatively low angles-of-attack, thereby improving pilot visibility and possibly decreasing the required runway length. Such a configuration may also augment maneuvering lift at higher subsonic speeds by appropriate extension of the flaps and sufficient blowing rates. Ref. 23 has also suggested that the "locked vortex" flap system for a swept-back wing be retracted to form a thin wing for efficient cruising flight.

Flow visualization tests were conducted in refs. 22 and 24 to determine qualitative effects of spanwise blowing on flat-plate, semi-span models which included a wing planform typical of fighter aircraft with leading- and trailing-edge flaps, and also unswept and swept-back wings featuring the "locked vortex" wing channel. Typical results are shown in figures 7(a)and 7(b) which suggest high-lift conditions when spanwise blowing is present.

Based on the results of the flow visualization tests in references 22 and 24, and in order to supplement the previous research just discussed, the present wind tunnel force test program was designed to provide experimental data to quantify the effects of leading-edge vortex enhancement by spanwise blowing on a 44° swept trapezoidal wing configuration featuring conventional leading- and trailing-edge flaps. Blowing was initiated on the "clean" wing and also in conjunction with a deflected leading-edge flap and/or a deflected trailing-edge flap in an attempt to conform wing geometry to best utilize the effectiveness of blowing. Specifically, the tests were designed to determine if spanwise blowing in conjunction with a deflected leading-edge flap would result in drag polar improvement as a result of an increase in suction forces on the cambered wing surface and, in addition, to evaluate spanwise blowing in combination with a deflected trailing-edge flap as a means of improving trailing-edge flap effectiveness. Two leading-edge flap deflection angles and two trailing-edge flap deflection angles were investigated, along with one configuration having simultaneously-deflected leading- and trailing-edge flaps. In addition, one case was investigated for a differentially-deflected leading-edge flap, in an attempt to modify the wing leading-edge across the span to best utilize the highly-effective jet at inboard wing stations and to

maintain attached flow near the leading-edge farther outboard where jet spreading and vortex bursting occur. A further application of spanwise blowing may be as a roll control device where differential wing blowing alone or in combination with small deflections of conventional lateral control devices may prove an effective means of improving lateral control characteristics. In this regard, spanwise blowing was initiated on the right wing only. The effects of spanwise blowing on the lateral-directional stability characteristics of a wing- horizontal tail-vertical tail configuration were evaluated at two side-slip angles, along with the effect of blowing on the wing on horizontal tail and vertical tail effectiveness. The favorable interaction effects between canard and wing are limited due to leading-edge vortex breakdown at moderate-to-high angles-of-attack, on either or both of the lifting surfaces. Spanwise blowing was therefore investigated in conjunction with a close-coupled canard-wing configuration by blowing on the wing in the presence of the canard and blowing on the canard in the presence of the wing for two canard incidence angles. The present study is also designed to provide an initial evaluation of the "locked vortex" concept for a moderately-swept-back wing featuring a unique upper surface leading- and trailing-edge flap arrangement.

The wind tunnel tests were performed in the Langley high speed 7- by 10-foot facility, and data were acquired at a free-stream Mach number of 0.30 for the 44° swept trapezoidal wing configuration (data were acquired at $M_{\infty} = 0.50$ for selected configurations) and at free-stream Mach numbers of 0.15 and 0.20 for the "locked vortex" wing configuration. Six-component force and moment data were obtained for a range of angle-of-attack, leading- and trailing-edge flap deflection angle, and jet momentum coefficient.

CHAPTER III

EXPERIMENTAL INVESTIGATION

Model and Apparatus

A three-view drawing of the general research model showing the canard, wing, horizontal tail, and vertical tail is presented in figure 8(a), and a three-view drawing of the "locked vortex" wing presented in figure 8(b). Photographs of the various model configurations installed in the wind tunnel are shown in figures 9(a) - 9(e). It should be noted that the horizontal and vertical tails shown in figure 9(e) were not investigated with the "locked vortex" wings. Table I contains the pertinent geometric parameters associated with the model.

The canard had a leading-edge sweep angle of 51.7° and an exposed area (S_C) of approximately 20 per cent of the wing reference area (S), and was tested in a position in the wing chordal plane and also at an incidence angle, i_C, of $+10^{\circ}$. The canard was untwisted and had uncambered circular arc airfoil sections. The thickness varied linearly from 6 per cent at the root to 4 per cent at the tip.

The horizontal and vertical tails had a leading-edge sweep angle of 51.7° and an exposed area (S_T) of approximately 25 percent of the wing reference area. Both tails were untwisted and had uncambered circular arc airfoil sections. The thickness varied linearly from 6 percent at the root to 4 per cent at the tip. The horizontal tail was tested in a position in the wing chordal plane and the vertical tail was located along the centerline of the model.

The untwisted wing planform shown on the model in figure 8(a) is shown in more detail in figure 10(a) and had a leading-edge sweep angle, Λ_{LE}, of 44° and a 64A006 airfoil section at the wing root (the root of the wing is taken at the intersection of the fuselage and wing) which varied linearly to a 64A004 airfoil section at the tip. The full-span leading-edge flap, which twisted and cambered the wing when deflected, had a constant chord of 15 percent of the wing root chord, and consisted of five spanwise segments which are shown in detail in figure 10(a). The trailing-edge flap was 20 percent of the local wing chord and extended from the wing-fuselage intersection to 70 percent of the wing span. The moment reference center is taken to be at 25 per cent of the theoretical wing root chord at the fuselage center line, which is illustrated in figures 8(a) and 8(b).

The untwisted "locked vortex" wing planform shown in figure 8(b) is shown in more detail in figure 10(b). The wing had a leading-edge sweep angle, Λ_{LE}, of 44° and flat-plate airfoil section at all span stations (when the flaps are retracted) with a rounded leading-edge and sharp trailing edge. The thickness ratio, t/c, was 6 per cent for the wing, hence the thickness varied linearly from the root to the tip. The leading-edge flap chord was 30 per cent of the wing chord at the root and 36 per cent at the tip. The leading-edge flap hinge-line was located at 25 per cent of the flap chord at the root and 50 percent of the flap chord at the tip. The trailing-edge flap chord was 35 per cent of the wing chord at the root and 58 per cent at the tip. The trailing-edge flap hinge-line was located at 65 per cent of the flap chord at the root and 26 per cent at the tip.

The continuous-flow air system that was used to provide the desired dry high-pressure air to each set of convergent nozzles is shown in figure 11. High pressure air was delivered through 0.953 cm-diameter brass tubing which was fed through the high speed sting (#5) and coupled to the aft end of a six-component strain gage balance in the model by means of a flare fitting. Air flow was routed around the balance and piped into a single cylindrical plenum chamber located in the forward section of the model.

Details of the convergent nozzle geometry and location are shown in figure 12. Three pairs of nozzles were used alternately during the testing; one pair for the 44° swept trapezoidal wings, a second pair for the "locked vortex" wings, and a third pair for the canards. Each wing nozzle was made of 0.953 cm-diameter stainless steel tubing, whose inner diameter converged from 0.775 cm to the diameter d of the circular exit shown in the figure. The 44° swept trapezoidal wing nozzles, which rested on the wing upper surface, were extended out through the fuselage and located at approximately 23 per cent of the wing root chord. The "locked vortex" wing nozzles rested on the wing surface and were located at approximately 38 per cent of the wing root chord (flaps retracted). The original sweep angles of the latter nozzles ($\Lambda_n = 44^{\circ}$) were reduced (swept forward) after initial assembly of the model to the angles shown in figure 8(b), which resulted in the nozzles being extended out a greater distance from the fuselage. Each canard nozzle was made of 0.635 cm-diameter stainless steel tubing, whose inner diameter converged from 0.508 cm to the diameter d of the circular exit shown in the figure. The exit diameters of the two nozzles in all three pairs were slightly different. The canard nozzle size was smaller than the wing nozzle size to reflect lower blowing rates needed on the smaller canard

surface. In addition, the canard nozzle size was subject to physical limitations in this area of the fuselage (cover plates and canard mounting pin, for example). The canard nozzle was located at the 50 percent root chord location to enable variation of canard incidence angle, i_c, without changing the nozzle location relative to the canard surface. Due to the canard mounting pin, each canard nozzle was positioned approximately 2.33 nozzle exit diameters above the canard surface. Nozzle geometry, location, and sweep angle are summarized in figure 12.

Instrumentation and Calibration

Six-component force and moment data were recorded by means of the internally-mounted strain-gage balance, designated 737-B. High-pressure air was routed around this balance by means of two 0.635 cm-diameter S-shaped tubes shown in the photograph in figure 13. This air-balance system is unique in that the high-pressure air delivery system is combined with the balance assembly such that the balance interactions are essentially independent of air pressure.

The forward end of the air-balance assembly is connected to the cylindrical plenum chamber by means of two 0.318 cm - 0.635 cm swage-lock fittings. Details of the stainless steel settling chamber, which was hydrostatically tested to 600 psi (4.13×10^6 Pa) prior to installation in the model, are shown in figure 14. The stagnation pressure in the plenum chamber was monitored and recorded by means of a 500 psi (3.45×10^6 Pa) pressure transducer located within the model and connected to a digital voltmeter located external to the tunnel. The pressure transducer was calibrated prior to testing, and plenum chamber total pressure was correlated with the digital voltmeter reading in millivolts (mV).

Also shown in figure 14 are the total pressure probe and the iron-constantine thermocouple (used to monitor plenum total temperature). The total pressure probe, which was constructed of 0.318 cm-diameter stainless steel tubing, and the iron-constantine thermocouple were pre-tested prior to welding of the end cap to the settling chamber in order to ensure proper measurement of total pressure and temperature, respectively. The pressure probe was bent 90° such that the tapered mouth of the probe was located along the centerline of the plenum and facing the two air inlet holes. This was done to account for any flow through the plenum and ensure measurement of the total pressure in the plenum.

The two wing-nozzle assemblies and the canard-nozzle assembly were alternately connected to the plenum chamber by means of 0.635 cm - 0.953 cm swage-lock fittings and 0.318 cm - 0.635 cm swage-lock fittings, respectively, with 90° elbows. Allen head pipe-plugs were used to plug up the pair of tapped holes that were not utilized during a given series of test runs.

Nozzle air weight flow rate was determined by means of a #8 Flow-Dyne venturi flow-meter located external to the tunnel. The temperature and absolute pressure at the flow-meter inlet were monitored as well as the differential pressure across the throat, from which an air weight flow rate was determined.

The jet momentum coefficient, C_{μ}, is defined as

$$C_{\mu} = \dot{w}V_j/gq_{\infty}S \qquad (1)$$

where $\dot{w}$ is the measured air weight flow rate and V_j (British units) is the jet velocity reached by isentropic expansion from the stagnation pressure at the nozzle exit to free-stream pressure, given by

$$V_j = 109.6\sqrt{T_{t,plen}\left(1 - \left(p_\infty/p_{t,plen}\right)^{2/7}\right)} \qquad (2)$$

Since the jet momentum coefficient varied slightly with each data point during a given test run, an average jet momentum coefficient was computed and is designated as $C_{\mu,avg}$.

Each set of nozzles was statically calibrated in the tunnel with all lifting surfaces removed to obtain six-component force and moment data as a function of plenum total pressure. In addition, the right wing nozzle for the 44° swept trapezoidal wing configuration was calibrated in a similar manner with the left nozzle removed and plenum outlet plugged. The resulting data are presented in graphical form in Appendix A along with linear fairings of the calibrations. These linear calibration curves were used with the equations presented in the appendix to correct wind-on data for thrust effects.

Additional static tests were conducted to measure the jet total pressure at the nozzle exit as a function of plenum total pressure. This calibration was performed in order to evaluate the assumption used in deriving equation (2), that the plenum total pressure is equal to that at the nozzle exit. A syringe was used as a total pressure probe and a 300 psi (2.07×10^6 Pa) pressure transducer (pre-calibrated) to measure the pressures. The resulting data are presented in graphical form in Appendix A. A separate static test was conducted for each nozzle and the probe was mounted on the wing or canard and aligned essentially along the jet centerline near the nozzle exit. At the higher plenum total pressures, severe oscillation of the total pressure probe occurred due to curved shock waves in the region of the probe. Prior to onset of oscillation, however, agreement between plenum total pressure was quite good and the correlations for these ranges of total pressures were used to compute V_j in equation (2).

Because of the aerodynamic load, corrections to the model angle-of-attack and side-slip were made for deflections of the balance and sting support system. Wind-off model-weight-tare runs were made in the wind tunnel for each significant configuration change, and wind-on data were corrected accordingly. Fuselage base-cavity pressures were measured during the test and the drag coefficients were corrected to a zero-base-drag condition. Jet boundary and blockage corrections were found to be negligible, and therefore were not applied to the data.

CHAPTER IV

DISCUSSION OF RESULTS

Wind tunnel data which include nozzle thrust components are presented in tabulated form in Appendix B. As discussed in the last section, these data are corrected for the nozzle thrust components in order to obtain the aerodynamic coefficients, which are discussed and plotted in the following figures.

44° Swept Trapezoidal Wing - Flaps Undeflected

The effect of spanwise blowing on the longitudinal aerodynamic characteristics of the 44° swept trapezoidal wing configuration is presented in figures 15 - 21 for $M_{\infty} = 0.30$ and 0.50. Due to the higher free-stream dynamic pressure at the higher Mach number, the jet momentum coefficient at a given plenum total pressure is less than the $C_{\mu,avg}$ at the lower Mach number.

Spanwise blowing results in an increase in lift at $M_{\infty} = 0.30$ and 0.50, particularly at the higher angles-of-attack where the wing without blowing ($C_{\mu,avg} = 0$) experiences partial or complete stall. The data indicate that blowing results in nonlinear lift curves which are characteristic of lift curves obtained on highly-swept wings having a leading-edge vortex (see ref. 3 for example). The data suggest that spanwise blowing provides a favorable spanwise pressure gradient that aids in the formation of a stable leading-edge vortex at the moderate-to-high angles-of-attack. Furthermore, these vortex-induced lift increments increase with increased jet momentum coefficient. At $\alpha = 0^{\circ}$, where there is no leading-edge vortex, even with blowing, the increase in C_L is due to a jet-induced camber effect, which has been observed in refs. 13 and 17.

Because of the nonlinear increase in lift produced by spanwise blowing, the addition of blowing results in large reductions in the high-lift drag coefficient. In addition, increased jet momentum coefficient results in further improvement in the drag polar. These results suggest that one benefit of the spanwise blowing approach is that higher lifts (or load factors) can be provided without the weight penalty which would be associated with the lower wing loadings required to accomplish the same improvement.

Spanwise blowing results in an extension of the linear pitching moment obtained for the blowing-off case to much higher values of lift. This is accomplished without adversely affecting the stability level.

Another way of evaluating the effects of spanwise blowing is presented in figures 17 and 18 which show the effects of α and $C_{\mu,avg}$ on the lift augmentation ratio, $\Delta C_L/C_{\mu,avg}$, and lift effectiveness of blowing, $C_L/C_{L,o}$, for $M_\infty = 0.30$ and 0.50, respectively. ΔC_L is defined as $C_{L,jet\ on} - C_{L,jet\ off}$ and $C_{L,o}$ is defined as $C_{L,jet\ off}$.

The data indicate that increased angle-of-attack increases, in general, the lift augmentation ratio from a minimum value at the lower angles-of-attack (this value would be zero at $\alpha = 0^\circ$ if there were no jet-induced camber effect) to a much higher value at the highest angle-of-attack. The largest lift augmentation ratios of 4.5 and 7.9 were obtained at $M_\infty = 0.30$ and 0.50, respectively, at the lowest jet momentum coefficients, which means that spanwise blowing generates 4.5 and 7.9 times the lift that would be obtained if the jet were vectored downward and perpendicular to the free-stream which would result in a ratio of one. The data also suggest that even higher ratios may be attainable at greater angles-of-attack. At the

moderate-to-high angles-of-attack, increasing the jet momentum coefficient decreases the lift augmentation ratio a trend that is typical of most jet augmentation systems. These data suggest that spanwise blowing exceeds the effect of thrust vectoring at angles-of-attack above about 12° to 14° (depending on $C_{\mu,avg}$ and M_{∞}). These results are typical of other planform configurations featuring spanwise blowing (see ref. 18 for example), although the magnitudes may vary somewhat.

The data indicate that for a given $C_{\mu,avg}$, the percentage increase in lift at the moderate-to-high angles-of-attack that is generated by spanwise blowing, presented as $C_L/C_{L,o}$, increases with increase in angle-of-attack. The largest percentage gains in lift of 45 per cent and 35 per cent were obtained at $M_{\infty} = 0.30$ and 0.50, respectively, at the highest jet momentum coefficients. The data trends also suggest that larger percentage gains in lift may be attainable at higher angles-of-attack.

The effect of $C_{\mu,avg}$ and M_{∞} on the lift augmentation ratio and lift effectiveness of blowing at an angle-of-attack of approximately 21° is presented in figure 19. For the limited range of jet momentum coefficients available for comparison, spanwise blowing is more effective in generating lift at a given jet momentum coefficient at the higher Mach number. Similar results have been obtained for a semi-span, cambered wing-body-horizontal tail configuration in ref. 16, where blowing at $M_{\infty} = 0.75$ was found to be more effective than at comparable blowing rates at $M_{\infty} = 0.30$.

Figure 20 illustrates the effect of C_L and $C_{\mu,avg}$ on the aerodynamic drag reduction ratio, $\Delta C_D/C_{\mu,avg}$, for $M_{\infty} = 0.30$ and 0.50, where ΔC_D is defined as $C_{D,jet\ on} - C_{D,jet\ off}$. The data indicate that at the higher values of lift, spanwise blowing results in a significant

reduction in aerodynamic drag. In fact, at the highest C_L's, spanwise blowing becomes more effective than vectoring the thrust aft and parallel to the free-stream which would result in a drag reduction ratio of one. Figure 21 presents the measured drag-due-to-lift increment due to blowing plotted against the flat-plate, zero-suction drag-due-to-lift increment ($\Delta C_L \tan \alpha$) for $M_\infty = 0.30$ and 0.50 and a range of angle-of-attack and jet momentum coefficient. Spanwise blowing results in drag reductions on the order of 30-40 per cent (depending on M_∞ and $C_{\mu,avg}$) from the zero-suction increment. Part of the improvement in induced-drag characteristics is undoubtedly due to improvement in the lift curve. The data seem to indicate, however, that the wing develops a leading-edge suction force associated with the flow about the round leading-edge.

44° Swept Trapezoidal Wing - Leading and/or Trailing-Edge Flaps Deflected

Leading-Edge Flaps.-

The effect of spanwise blowing on the longitudinal aerodynamic characteristics of the 44° swept trapezoidal wing configuration is presented in figures 22-24 for a range of leading-edge flap deflection angle for $M_\infty = 0.30$ and $\delta_{TE} = 0^\circ$. The $\delta_{LE} = 4^\circ$ data are presented in figure 22, $\delta_{LE} = 8^\circ$ in figure 23, and differential deflections of a segmented leading-edge flap in figure 24. The $\delta_{LE} = 0^\circ$ data presented in these figures are shown for reference.

For all the δ_{LE} values, spanwise blowing induces positive lift increments throughout the angle-of-attack range, particularly at the higher angles-of-attack, the ΔC_L's due to blowing increasing with increased $C_{\mu,avg}$. Nonlinear lift curves result when spanwise blowing is present, similar to the data in figure 15 for $\delta_{LE} = 0^\circ$, indicating the presence of a leading-edge vortex augmented by spanwise blowing, either on the leading-edge flap

of the separated leading-edge flow rather than maintaining attached flow at the higher angles-of-attack.

Figures 28 and 29 are summary plots for the blowing-off and blowing-on cases, respectively, showing the effect of leading-edge flap deflection angle on the longitudinal aerodynamic characteristics for $M_\infty = 0.30$. In both figures the data indicate a slight decrease in lift at the low-to-moderate angles-of-attack due to deflection of the leading-edge flap. At the higher angles-of-attack, with blowing off, the deflected leading-edge flap tends to maintain attached flow near the leading edge, as evidenced by a delay in wing stall. With blowing on, the reduction in lift coefficients due to the deflected flap becomes negligible at the highest angle-of-attack.

The drag polars obtained for the $\delta_{LE} = 0^\circ$ case with blowing off and blowing on are improved by deflecting the leading-edge flap downward. The best drag polars for blowing off and blowing on correspond to the $\delta_{LE} = 8^\circ$ configuration. The data suggest that the augmented vortex system on the cambered leading edge results in a polar having reduced drag at a given lift coefficient, which is most important from a sustained maneuver standpoint.

The effects of leading-edge flap deflection on the lift and drag increments due to spanwise blowing are shown in figure 30 for $M_\infty = 0.30$. The data indicate that favorable lift increments due to blowing occur for the $\delta_{LE} = 0^\circ$ case, but are reduced at the moderate-to-high angles-of-attack when the leading-edge flap is deflected. This reduction in lift is directly reflected in a reduction in the favorable drag benefits due to blowing. The drag results also point out that at the lower angles-of-attack there are small penalties associated with the addition of blowing. These results are similar to the effects observed in ref. 26 for a maneuver strake on the

plain and flapped 44° swept trapezoidal wing. It should be noted that while the favorable lift benefits of spanwise blowing and the maneuver strake for the plain and flapped wing cases are quite comparable, blowing appears to result in more substantial drag improvements at a given value of lift.

Trailing-Edge Flaps.-

Figures 31 and 32 illustrate the effect of spanwise blowing on the wing which has a partial-span trailing-edge flap with deflection angles of 10° and 20°, respectively. The longitudinal aerodynamic characteristics for these configurations are presented for $M_{\infty} = 0.30$ and $\delta_{LE} = 0^{\circ}$, where the blowing-off data for the "clean" wing ($\delta_{LE} = \delta_{TE} = 0^{\circ}$) are shown for reference.

With blowing on, the data indicate the presence of the jet-induced camber effect at the low angles-of-attack. At the moderate-to-high angles-of-attack, nonlinear variation in lift is evident which suggests a strong, leading-edge vortex flow augmented by spanwise blowing. The data also indicate that the vortex-induced lift increments at a given angle-of-attack increase with increased $C_{\mu,avg}$. It is interesting to note that the total lift increment due-to-blowing in combination with the deflected trailing-edge flap is greater than the sum of the increment due to the deflected trailing-edge flap ($C_{\mu,avg} = 0$) and the increment due to blowing on the "clean" wing ($\delta_{LE} = \delta_{TE} = 0^{\circ}$). This effect, which can be seen in the figures by comparing the dashed curves with the data represented by the triangular symbol, becomes more significant with increased δ_{TE}. This is an example of a synergistic effect, which has been discussed in ref. 27 for a canard-wing configuration. The deflected trailing-edge flap increases the camber at the wing trailing edge, which results in increased circulation

at a given angle-of-attack. The upwash at the leading-edge resulting from increased circulation may increase the "effective" angle-of-attack at the leading edge and, as a result, increase the blowing-induced effects at a given angle-of-attack. In addition, blowing may delay flow separation from the trailing-edge flap, hence improving trailing-edge flap effectiveness.

Spanwise blowing in combination with the deflected trailing-edge flap results in large improvements in the drag polar compared to those obtained for the blowing-off case, and additional improvements occur with increased $C_{\mu,avg}$. The synergistic effect noted previously for the lift data is also evident in the drag polars for $\delta_{TE} = 10^{\circ}$ and 20°. That is, the drag polar obtained for the configuration with spanwise blowing in conjunction with a deflected trailing-edge flap is more favorable than the drag polar that would result by summing the effects of each high-lift device acting alone (dashed curve in figures 31 and 32).

Spanwise blowing for a given δ_{TE} extends the linear pitching moment to much higher values of lift without causing an adverse effect on the stability level obtained for the blowing-off case. Furthermore, the data indicate a slight increase in nose-down pitching moment due to blowing.

Figures 33 and 34 illustrate the effect of α and $C_{\mu,avg}$ on the lift augmentation ratio and lift effectiveness of blowing for $\delta_{TE} = 10^{\circ}$ and 20°, respectively. The data indicate that spanwise blowing becomes more effective than thrust vectoring within the range of angle-of-attack from 9° to 12° (depending on $C_{\mu,avg}$ and δ_{TE}). The lowest blowing rate results in the highest lift augmentation ratios and increased $C_{\mu,avg}$ results in greater percentage gains in lift at a given angle-of-attack.

Figure 35 shows the effect of $C_{\mu,avg}$ and δ_{TE} on $\Delta C_L/C_{\mu,avg}$ and $C_L/C_{L,o}$ for α approximately 20.6°. The data reveal that for a given $C_{\mu,avg}$, increasing the trailing-edge flap deflection angle increases the lift augmentation ratio and the percentage gain in lift due to blowing. These results imply that the effectiveness of spanwise blowing is increased by combining blowing with a trailing-edge high-lift device.

The effect of trailing-edge flap deflection angle on the longitudinal aerodynamic characteristics are presented in figures 36 and 37 for the blowing-off and blowing-on cases, respectively. With blowing off, $C_{L,max}$ and $\Delta C_{L,max}$ occur at approximately 18° and 6°, respectively, for both δ_{TE} = 10° and 20°. The data also indicate a slight reduction in the lift increment at the higher angles-of-attack. With blowing on, the data indicate that the flap lift increment is essentially constant throughout the angle-of-attack range. Deflection of the trailing-edge flap shifts the drag polar curves obtained for δ_{TE} = 0° for both blowing off and blowing on such that at the higher values of lift the aerodynamic drag is reduced. In addition, a deflected trailing-edge flap shifts the pitching moment curve such that greater nose-down pitching moment occurs at a given C_L.

Leading-Edge and Trailing-Edge Flaps.-

The data presented in figure 38 show the effect of spanwise blowing on the longitudinal aerodynamic-characteristics of the 44° swept trapezoidal wing with simultaneously-deflected leading- and trailing-edge flaps (δ_{LE} = 8°; δ_{TE} = 10°). The blowing-off data for the "clean" wing are shown in the figure for reference.

The data trends with blowing on are similar to those observed for the configurations with spanwise blowing in combination with a deflected trailing-edge flap only (see figure 31, for example). It should be noted, however, that the synergistic effect discussed previously for the configurations featuring spanwise blowing in combination with a deflected trailing-edge flap, but with $\delta_{LE} = 0^{\circ}$, does not occur when both leading- and trailing-edge flaps are deflected. The deflected leading-edge flap delays the more beneficial effects of blowing to higher angles-of-attack, and this effect is illustrated in figure 38, where the dashed curves represent the lift and drag coefficients that would be obtained by summing the effect due to blowing on the "clean" wing ($\delta_{LE} = \delta_{TE} = 0^{\circ}$) and the effect due to deflected leading- and trailing-edge flaps without blowing ($C_{\mu,avg} = 0$).

The longitudinal aerodynamic characteristics obtained for the configuration with spanwise blowing in combination with leading- and trailing-edge flaps deflected to 8° and 10°, respectively, are compared in figure 39 to the data obtained by blowing on the wing with a trailing-edge flap deflected to 10° ($\delta_{LE} = 0^{\circ}$). The data indicate that with blowing on, the configuration with deflected trailing-edge flap ($\delta_{LE} = 0^{\circ}$) results in higher values of lift up to the highest angle-of-attack. A decreasing lift curve slope is noted, however, at the higher angles-of-attack compared to the increasing $C_{L_{\alpha}}$ obtained for the configuration with both leading- and trailing-edge devices deflected.

The best drag polar was obtained when both flaps were deflected. The data suggest in a manner similar to that discussed in figure 29 for the case with blowing in conjunction with a deflected leading-edge flap only

that the augmented vortex system on the cambered leading-edge results in a polar having reduced drag at a given lift coefficient. These results are encouraging in that spanwise blowing on an advanced fighter configuration employing the variable-camber concept may offer substantial improvement in the drag polars throughout the maneuver envelope.

Figure 40 presents the effect of $C_{\mu,avg}$, δ_{LE} and δ_{TE} on the lift augmentation ratio and lift effectiveness of blowing at α approximately 20.5°. As suggested by the data in figure 38, deflecting the leading-edge flap downward (δ_{TE} fixed) tends to reduce $\Delta C_L/C_{\mu,avg}$ and $C_L/C_{L,o}$ for the range of $C_{\mu,avg}$. A similar effect due to a deflected leading-edge device is seen in the data shown in figure 41, which indicate a delay in the more substantial aerodynamic drag reductions due to blowing to higher C_L's.

Spanwise Blowing as a Roll-Control Device - Blowing on Right Wing Only

In order to evaluate spanwise blowing as a roll-control device, blowing was initiated on the right wing of the 44° swept trapezoidal wing configuration and the resulting longitudinal aerodynamic characteristics are illustrated in figure 42.

The data exhibit trends similar to those observed in figure 15 for the case with blowing on both wings ($\delta_{LE} = \delta_{TE} = 0^{\circ}$). It should be noted, however, that at the higher angles-of-attack, blowing on both wings (figure 15) at a combined jet momentum coefficient of 0.059 results in more favorable lift and drag characteristics than those obtained for blowing on the right wing only for $C_{\mu,avg} = 0.067$. This may be due to the fact that blowing on both wings enables the spanwise jets to act upon more

lifting surface area and to augment the leading-edge vortices on both wings, particularly at the inboard stations where the jet is most effective.

Of most significance is the effect of differential wing blowing on the rolling moment coefficient. The effect of α and $C_{\mu,avg}$ on rolling moment coefficient for the 44° swept trapezoidal wing configuration is shown in figure 43. With blowing off, C_{ℓ} is essentially zero throughout the angle-of-attack range. Spanwise blowing on the right wing results in small positive values of C_{ℓ} at the low angles-of-attack, indicating a right wing-down moment. Despite the jet-induced camber effect on the right wing at low angles-of-attack, the data suggest that blowing has altered the spanwise lift distribution on the right wing such that the center of lift is located more inboard than the center of lift on the left wing. At the moderate-to-high angles-of-attack differential blowing results in large negative C_{ℓ}'s, indicating right wing-up rolling moment. C_{ℓ} becomes increasingly negative with increased angle-of-attack, and increased $C_{\mu,avg}$ at a given angle-of-attack results in greater negative values of C_{ℓ}. These results occur due to the augmentation of the right wing leading-edge vortex with consequent large vortex-induced lift increments, and, in addition, to separated flow conditions on the left wing at the higher angles-of-attack. Simultaneously-deflected ailerons act in much the same manner by deflecting the right aileron down to increase lift and deflecting the left aileron up to spoil the flow on the wing upper surface. The dashed line in figure 43 represents a theoretical estimate of rolling moment coefficient using the method of ref. 28 that would result at a Mach number of 0.30 by deflecting plain trailing-edge flap ailerons on the 44° swept trapezoidal wing with

the following aileron characteristics: $c_f/c = 0.30$; $\eta_i = 0.75$; $\eta_o = 0.95$; $\delta_{left} = -15^o$; $\delta_{right} = +15^o$. The theory predicts a rolling moment coefficient of -0.0105 (independent of angle-of-attack), or right wing-up rolling moment. The experimental data indicate that for the case with blowing on the right wing with $C_{\mu,avg} = 0.034$ a comparable rolling moment occurs at $\alpha \approx 16^o$ and with $C_{\mu,avg} = 0.067$ at alpha approximately 13^o. At the higher angles-of-attack, differential blowing for roll control exceeds the theoretical estimate due to trailing-edge flap ailerons. At α approximately 20.5^o, the rolling moment coefficients that result with $C_{\mu,avg} = 0.034$ and 0.067 exceed the theoretical rolling moment due to trailing-edge flap ailerons by factors of nearly two and four, respectively.

44^o Swept Trapezoidal Wing with Aft Horizontal Tail

The effect of spanwise blowing on the longitudinal aerodynamic characteristics of the 44^o swept trapezoidal wing-horizontal tail configuration is presented in figure 44 for $M_\infty = 0.30$. Data for the wing-alone case with blowing off are shown for reference.

With blowing off, addition of the horizontal tail results in an increase in lift compared with the wing alone case, particularly at the higher angles-of-attack, and an improvement in the drag polar. The tail loading acts well aft of the moment reference center, hence resulting in a large nose-down pitching moment contribution. At the higher values of lift where the wing alone approaches stall, the data indicate a sizeable change in stability level.

With horizontal tail on, the effect of spanwise blowing on the aerodynamic lift and drag characteristics for the total configuration are similar to those observed for configurations featuring wing spanwise blowing with

tail off (see figure 15, for example), hence these data will not be discussed.

Spanwise blowing extends the linear pitching moment obtained for the blowing-off case to higher values of lift. The data suggest that at the higher C_L's, with blowing on, the wing downwash tends to reduce the effective angle-of-attack of the tail, thereby reducing the nose-down pitching moment contribution of the horizontal tail. These results imply that spanwise blowing on the wing may result in more favorable trim characteristics for the wing-horizontal tail configuration.

The effect of angle-of-attack and the addition of the horizontal tail component on the lift augmentation ratio and lift effectiveness of blowing on the wing is presented in figures 45 and 46 for $C_{\mu,avg}$ approximately 0.06 and 0.13, respectively, for $M_\infty = 0.30$. The data indicate that blowing on the wing in the presence of the horizontal tail is less effective at a given angle-of-attack than blowing on the wing alone, as evidenced by lower values of $\Delta C_L/C_{\mu,avg}$ and $C_L/C_{L,o}$. These results suggest that there is an unfavorable interference effect between the wing and horizontal tail, which delays the favorable effects of spanwise blowing to slightly higher angles-of-attack.

44° Swept Trapezoidal Wing-Vertical Tail and Wing-Vertical Tail-Horizontal Tail Configurations

Figures 47 and 48 illustrate the effect of spanwise blowing on the longitudinal aerodynamic characteristics of the wing-vertical tail and wing-vertical tail-horizontal tail configurations, respectively. The discussions pertaining to spanwise blowing on the wing-alone configuration and the wing-horizontal tail configuration presented in figures 15 and 44, respectively, are applicable to the data illustrated in figures 47 and 48,

respectively, hence further analysis is not presented.

Figure 49 illustrates the effect of spanwise blowing on the lateral-directional stability derivatives of the wing-vertical tail configuration for $M_\infty = 0.30$. With blowing off, the wing-vertical tail configuration exhibits lateral stability at the low-to-moderate angles-of-attack, as evidenced by negative values of the effective dihedral parameter, C_{ℓ_β}, but an unfavorable break in C_{ℓ_β} occurs at $\alpha \approx 10^\circ$. The directional stability parameter C_{n_β} is positive, indicating directional stability, and remains relatively constant up to an angle-of-attack of 14°, at which point there is an unfavorable break in C_{n_β}. At $\alpha \approx 20.6^\circ$, C_{ℓ_β} and C_{n_β} are positive and negative, respectively, indicating an unstable condition.

Blowing results in significant stabilizing increments in C_{ℓ_β} and C_{n_β} at the higher angles-of-attack, with little or no effect on the lateral-directional stability at low angles-of-attack. C_{Y_β} remains essentially constant throughout the angle-of-attack range, and independent of blowing.

The factors resulting in more favorable lateral-directional stability characteristics with blowing on are not clear at the present time, hence the following discussion will only attempt to present some possible factors involved. It is noted that investigation of the lateral-directional stability data for highly-swept wings with vortex flow may provide some insight to understanding trends, just as they do for the longitudinal data.

With blowing off, at the low angles-of-attack, stabilizing increments in the directional stability parameter result from the vertical tail and also from the advancing wing which experiences increased drag. Since the model center of gravity is located at approximately 50 per cent of the fuselage length, there may be a de-stabilizing effect due to the fuselage.

In addition, the vertical tail and advancing wing will probably contribute stabilizing increments in the effective dihedral parameter, and the contribution due to the fuselage would appear dependent on whether the side force acts above or below the model center of gravity. At the higher angles-of-attack partial or complete stall occurs on both wings. It would appear that the separated flow conditions on the wings would tend to reduce the effectiveness of the center-line vertical tail. A de-stabilizing effect due to the fuselage may also occur.

With blowing on, factors that may contribute favorable increments in C_{ℓ_β} and C_{n_β} at the higher angles-of-attack include improved flow conditions in the vicinity of the vertical tail, enhancement of the wing leading-edge vortices due to spanwise blowing, particularly on the advancing wing, and wing-induced sidewash effects on the fuselage afterbody. It may be that at the higher angles-of-attack, the adverse flow in the vicinity of the vertical tail, which ref. 29 has suggested is probably due to wing wake effects, may not be as severe with spanwise blowing on the wing, which induces the separated leading-edge flow to reattach to the wing upper surface. On the advancing wing, the leading-edge sweep angle is reduced slightly to 40°, but blowing undoubtedly enables higher lift and drag values to be attained, which will produce favorable increments in C_{ℓ_β} and C_{n_β}, respectively. It is not known what effect the vortex emanating from the fuselage forebody will have on the downwind wing panel, or if the effectiveness of blowing on the downwind wing is reduced due to partial blockage by the fuselage. The C_{Y_β} data suggest that blowing helps to maintain a constant level of side force, and perhaps enhance the wing-induced sidewash effects on the fuselage afterbody at the higher angles-of-attack.

The data in figure 50 indicate that for blowing off, addition of a horizontal tail to the wing-vertical tail configuration prevents the unfavorable stability break in the effective dihedral parameter C_{ℓ_β} that was observed in figure 49 for the configuration with horizontal tail off. Due to wing downwash, the horizontal tail is acting at a lower effective angle-of-attack and the windward tail may be able to generate a more stable increment in C_{ℓ_β} at the higher angles-of-attack. The end-plate effect of the horizontal tail on the vertical tail may also minimize the loss of the C_{ℓ_β} contribution of the vertical tail at higher angles-of-attack. Also the horizontal tail reduces the severity of the unfavorable break in C_{n_β} obtained for the wing-vertical tail configuration. This may result from the increased drag on the windward horizontal tail and also a decrease in loss of vertical tail effectiveness at the higher angles-of-attack due to the presence of the horizontal tail.

The primary effect to note for the case with blowing on is that blowing results in a favorable increment in C_{ℓ_β} throughout the angle-of-attack range, and that increased blowing increases, in general, this favorable increment. Otherwise, the discussion for figure 49 is applicable to the data presented in figure 50.

Close-Coupled Canard-Wing Configuration

Blowing on the wing.-

The longitudinal aerodynamic characteristics that result because of spanwise blowing on the trapezoidal wing of a close-coupled canard-wing configuration are shown in figures 51 and 52 for $M_\infty = 0.30$ and 0.50,

respectively, and $i_c = 0^\circ$. The jet momentum coefficients for $M_\infty = 0.50$ are less than the $C_{\mu,avg}$ for $M_\infty = 0.30$ due to the greater dynamic pressure at the higher Mach number. The blowing-off data for the wing-alone configuration are shown in the figures for reference.

Spanwise blowing on the wing in the presence of a canard in close proximity to the wing results in an increase in the lift coefficient compared to the blowing-off case, particularly at the higher angles-of-attack. Furthermore, the lift increment due to blowing at a given angle-of-attack increases with increased $C_{\mu,avg}$. At the low angles-of-attack, the data indicate a jet-induced camber effect on the wing. At the moderate-to-high angles-of-attack the data suggest that the wing leading-edge vortex flow is enhanced by spanwise blowing but that the canard downwash, which acts to reduce the effective wing angle-of-attack, may be delaying the more beneficial effects of blowing to higher angles-of-attack.

In addition to the lift results, spanwise blowing improves the drag polar compared to the blowing-off case, and additional improvement is attained by increased jet momentum coefficient. Blowing also results in a slight increase in nose-down pitching moment at a given C_L and that increased $C_{\mu,avg}$ results in more negative C_m. Furthermore, the data indicate that blowing does not appreciably affect the stability level obtained for the blowing-off case.

The effect of spanwise blowing is more pronounced when the canard incidence angle, i_c, is increased to 10°, as illustrated in figure 53 for $M_\infty = 0.30$. The favorable lift benefits due-to-blowing are larger at the higher angles-of-attack, but appear to be limited due to canard stall at the higher angles-of-attack. The drag polar improvement due-to-blowing is similar to the results discussed in figure 51 for $i_c = 0^\circ$, while the

pitching moment results show a favorable effect on the stability level compared to the blowing-off case at the higher lift values, but pitch up at the highest C_L's.

The effect of α and $C_{\mu,avg}$ on the lift augmentation ratio and lift effectiveness of blowing are shown in figures 54 and 55 for $i_c = 0^\circ$ and 10°, respectively. The data indicate that for $i_c = 0^\circ$, spanwise blowing is less effective than thrust vectoring up to an angle-of-attack of approximately 19.5° for both values of $C_{\mu,avg}$. The percentage gain in lift due to blowing at the moderate-to-high angles-of-attack remains essentially constant at a given $C_{\mu,avg}$, with a slight increase in lift effectiveness noted at the highest angle-of-attack.

The angle-of-attack at which spanwise blowing exceeds the effect of thrust vectoring is reduced when the canard incidence angle is increased to 10° (fig. 55). The maximum $\Delta C_L/C_{\mu,avg}$ for a given $C_{\mu,avg}$ occurs at alpha approximately 18.7°, with the lower blowing rate resulting in the largest $\Delta C_L/C_{\mu,avg}$. An abrupt decrease in $\Delta C_L/C_{\mu,avg}$ at alpha approximately 21° reflects canard stall. These results suggest as canard incidence angle increases, the canard downwash decreases at the higher angles-of-attack due to canard stall. This causes the wing to act at a higher effective angle-of-attack, hence enabling greater enhancement of the wing leading-edge vortex by spanwise blowing. The data suggest, however, that the increased upwash ahead of the wing may cause premature canard stall.

Another way of evaluating the effect of canard incidence angle is shown in figure 56, where the aerodynamic drag reduction ratio is presented as a function of C_L and $C_{\mu,avg}$ for $M_\infty = 0.30$. For $i_c = 0^\circ$, blowing on the wing is less effective than thrust vectoring for all values of lift coefficient.

For $i_c = 10^\circ$, blowing exceeds the effect of thrust vectoring at the higher lift values and the lower $C_{\mu,avg}$ values. This is further evidence that the canard downwash on the wing limits the beneficial effects of spanwise blowing. The measured drag-due-to-lift increment due-to-blowing for the canard-wing configuration, $\Delta C_{D,L}$, is shown in figure 57 plotted against the flat-plate, zero-suction drag-due-to-lift increment, $\Delta C_L \tan \alpha$, for $M_\infty = 0.30$ and 0.50 and $i_c = 0^\circ$. Drag reductions on the order of 27 per cent and 12 per cent were obtained over the zero-suction increment for $M_\infty = 0.30$ and 0.50, respectively. The data suggest that in addition to the beneficial effects on drag resulting from the improvement in the lift curve, a leading-edge suction force is developed on the wing which results in improved induced-drag characteristics.

The effect of canard incidence angle on the longitudinal aerodynamic characteristics of the canard-wing configuration with blowing off is shown in figure 58 for $M_\infty = 0.30$. Addition of the canard located longitudinally near the leading edge of the wing and in the wing chord plane results in significant lift increments in the moderate-to-high angle-of-attack range, which were shown in figures 51-53, but not discussed. Data from refs. 30-33 have indicated for a close-coupled canard-wing configuration that the canard and wing, when in the presence of each other, generate vortex lift. In the present studies, the nonlinear lift curves shown in figure 58 when the canard is present indicate that vortex lift is generated either on the wing, the canard, or both lifting surfaces. Refs. 30-33 have also shown that the lift on the wing not in the presence of the canard is greater than the lift on the wing in the presence of the canard up to an angle-of-attack of approximately 18°. Beyond an angle-of-attack of 18°, the wing not in the

presence of the canard has stalled, and it produces a **lower** lift than the wing in the presence of the canard which has not stalled. The present data indicate that at angles-of-attack beyond about 18°, the total configuration has not stalled, whereas the wing-alone has experienced partial or complete stall. Earlier studies (ref. 34 for example) have indicated that the wing in the presence of the canard develop a substantial amount of side-edge vortex lift.

Increasing the canard incidence angle from 0° to 10° results in a slight lift increment at the low angles-of-attack, and a reduction in total lift at the higher angles-of-attack. The data at the higher α's indicate, however, that stall for the total configuration has not occurred.

With blowing off, addition of a canard ($i_c = 0^{\circ}$) results in a slight increase in aerodynamic drag at the lower values of lift. The drag polar obtained for the canard-wing configuration, however, is far more favorable than the drag polar obtained for the wing alone. References 18 and 33 have indicated that the favorable interference between the canard and wing in close proximity results in improvement in the drag polar over what would be obtained if the canard-alone and wing-alone contributions were added together. This is a further example of the synergistic effect noted in ref. 18 and discussed previously in figures 31 and 32 for the case with blowing on the wing in combination with a deflected trailing-edge flap. Increasing the canard incidence angle to 10° results in a slightly less favorable drag polar shape.

Since the canard loading acts well forward of the moment reference center, the canard causes a positive pitching moment which counteracts

the negative pitching moment contribution due to the wing. The total configuration exhibits slightly positive C_m up to the higher C_L values for $i_c = 0^\circ$ and C_m does not vary significantly with C_L. Increasing the canard incidence to 10° results in more positive moment and C_m remains positive throughout the C_L range. In addition, a stability break occurs at the moderate values of lift coefficient.

Blowing on the Canard.-

The longitudinal aerodynamic characteristics that result because of spanwise blowing on the canard of the canard-wing configuration are shown in figures 59 and 60 for $i_c = 0^\circ$ and 10°, respectively, for $M_\infty = 0.30$. The reader should note that the jet momentum coefficients obtained for the canard-blowing case are smaller than the $C_{\mu,avg}$ for blowing on the wing due to the canard's smaller converging nozzle size.

The data suggest that spanwise blowing on the canard in the presence of the wing increases the lift coefficient throughout the range of angle-of-attack, and that the positive lift increment increases with increased $C_{\mu,avg}$. The largest lift increments are generated at the highest test angle-of-attack, such that larger ΔC_L's may be attained at even higher angles-of-attack.

The lift increments due to blowing at the higher angles-of-attack may result from a favorable interference between the canard and wing. Similar results have been obtained in ref. 20 for a large-scale, semi-span canard-wing transport model featuring blowing on the canard. This investigation demonstrated that canard blowing results in a net C_L increase which may be a combination of canard lift and a beneficial wing-canard interference.

Smoke studies from ref. 20 have indicated that for a small-scale, canard-wing model, the canard downwash acts to reduce the "effective" wing angle-of-attack, causing the wing at high angles-of-attack to reattach or unstall. This flow phenomenon results in an effective increase in lift. The present data seem to indicate that the canard downwash has a favorable effect on the wing at the moderate-to-high angles-of-attack when blowing is present on the canard, but is a limiting factor on wing lift when the jet is located on the wing, as a result of the decrease in "effective" wing angle-of-attack. Similar results have been obtained in refs. 35 and 36 for a strake-wing configuration. Ref. 35 has indicated that the downwash off the strake decreases the lifting pressure on the upper surface of the wing station behind the strake. In addition, ref. 36 has found that the effectiveness of spanwise blowing from the wing root is limited at the inboard stations behind the strake due to strake downwash.

Spanwise blowing on the canard (figures 59 and 60) improves the drag polar compared to the blowing-off case, and the data indicate that increased blowing rate results in additional improvement in drag-polar shape.

Canard spanwise blowing also has a slight destabilizing effect for the configuration at high lift levels, which results because of the increased canard lift. At the higher values of lift, pitching moment at a given $C_{\mu,avg}$ appears relatively constant with C_L, indicating neutral stability for the canard-wing configuration. In addition, increased blowing rate results in more nose-up pitching moment at the moderate-to-high values of lift.

The effect of α and $C_{\mu,avg}$ on the lift augmentation ratio and lift effectiveness of blowing is illustrated in figures 61 and 62 for $i_c = 0^\circ$ and 10°, respectively, and $M_\infty = 0.30$. Spanwise blowing becomes more

effective than thrust vectoring at an angle-of-attack of approximately $8^\circ - 9^\circ$ (depending on i_C and $C_{\mu,avg}$). $\Delta C_L/C_{\mu,avg}$ increases with increased α and the lower blowing rate results, in general, in the higher $\Delta C_L/C_{\mu,avg}$ values. In addition, the lift augmentation ratio at a given $C_{\mu,avg}$ for $i_C = 10^\circ$ is considerably greater at the moderate-to-high angles-of-attack than the corresponding $\Delta C_L/C_{\mu,avg}$ value obtained for $i_C = 0^\circ$.

The aerodynamic drag augmentation ratio is shown in figure 63 as a function of C_L and $C_{\mu,avg}$ for $i_C = 0^\circ$ and 10° and $M_\infty = 0.30$. Spanwise blowing on the canard exceeds the effect of vectoring the thrust aft and parallel to the free-stream at the higher values of lift for both $C_{\mu,avg}$ values and both canard incidence angles. The data suggest that blowing enhances the canard leading-edge vortex at the moderate-to-high angles-of-attack, hence favorably affecting the drag characteristics of the canard. In addition, the improved canard flow may improve the flow about the wing and thus favorably affect the wing drag characteristics. The measured drag-due-to-lift increment due to spanwise blowing on the canard is shown in figure 64 plotted against the flat-plate, zero-suction drag-due-to-lift increment for a range of angle-of-attack, $M_\infty = 0.30$ and $i_C = 0^\circ$. Drag reductions on the order of 19 per cent are obtained from the zero-suction induced-drag increment. Since the canard has a sharp leading edge, there is no leading-edge suction force on the canard. The wing, however, has a leading-edge radius and the data suggest that suction forces are present that tend to improve the drag characteristics.

One of the problems associated with the design of a close-coupled canard-wing configuration as a highly-maneuverable aircraft is the provision

of an optimum method of longitudinal trim control. Ref. 37 has indicated that if trim is obtained by changing the canard incidence, a more highly-swept canard seems warranted in order to alleviate canard stall at high angles-of-attack. Such configurations, however, tend to exhibit high induced-drag characteristics and would tend to have high trim drag. Spanwise blowing on the canard may offer one means of alleviating this problem. Leading-edge vortex augmentation by spanwise blowing on a moderately-swept canard would alleviate canard stall at high angles-of-attack and also avoid the high induced-drag and trim drag that a highly-swept canard would be expected to exhibit. Ref. 20 has also indicated that a modest amount of spanwise blowing on a canard at low speed would reduce canard size and permit a more optimum canard to be used in cruise.

The longitudinal aerodynamic characteristics obtained for the configuration with spanwise blowing on the wing in the presence of the canard are compared to the longitudinal characteristics obtained by blowing on the canard in the presence of the wing in figures 65 and 66 for $i_c = 0^\circ$ and 10°, respectively. The canard nozzle exit area is less than the wing nozzle exit area, hence the air weight flow rate at a given plenum pressure and consequently the jet momentum coefficient are reduced. This precluded a comparison of the longitudinal characteristics at the same blowing rates.

The data in figures 65 and 66 indicate that blowing on the canard at $C_{\mu,avg} = 0.030$ results in lift and drag characteristics that compare favorably to those obtained for blowing on the wing at $C_{\mu,avg} = 0.058$ throughout the angle-of-attack range. These results imply that spanwise blowing on the canard requires approximately one-half the engine bleed air

required by spanwise blowing on the wing in order to produce comparable benefits on lift and drag for the total configuration. Furthermore, the configuration with blowing on the wing exhibits unfavorable longitudinal stability trends at the moderate-to-high values of lift whereas the configuration with blowing on the canard exhibits essentially neutral stability for the same range of lift coefficients. These latter data suggest that with relaxed static stability, a canard arrangement can be made to provide an all-lifting configuration for trim at higher subsonic maneuvering conditions.

Figure 67 presents the effect of $C_{\mu,avg}$, jet location, and M_∞ on the lift augmentation ratio and lift effectiveness of blowing at alpha approximately 21° for $i_c = 0^\circ$. Considering first the case with the spanwise jet located on the wing, the data indicate for the rather limited range of comparable $C_{\mu,avg}$ values that spanwise blowing is more effective at the higher Mach number ($M_\infty = 0.50$), as evidenced by higher lift augmentation ratios and greater percentage gains in lift than obtained for $M_\infty = 0.30$. These results suggest that the spanwise blowing concept may be an effective means of augmenting maneuvering lift of fighter aircraft at higher subsonic Mach numbers. Ref. 16 has noted, however, that a deterrent to utilization of spanwise blowing at transonic Mach numbers may be the lack of engine bleed air to supply the momentum required for effective vortex augmentation. Blowing on the canard results in higher lift augmentation ratios and greater percentage gains in lift than those obtained for blowing on the wing for the narrow band of comparable $C_{\mu,avg}$ values shown in figure 67 for $M_\infty = 0.30$. Similar trends are shown in figure 68 for $i_c = 10^\circ$. To summarize, these

results suggest that spanwise blowing on the canard is favorably influenced by the upwash generated ahead of the wing, whereas the canard downwash limits the effectiveness of spanwise blowing on the wing.

Comparison of Experimental and Theoretical Longitudinal Characteristics For Selected Configurations

Comparisons of the experimental and theoretical longitudinal characteristics for selected configurations are presented in figures 69-72. Theoretical estimates of the lift, drag, and pitching moment characteristics were obtained by using the methods outlined in refs. 38, 39, and 40. All calculations were made for a Mach number of 0.30 and for a moment reference center location the same as that used for the experimental data.

The first configuration to be examined is the 44° swept trapezoidal wing with $\delta_{LE} = \delta_{TE} = 0^{\circ}$ (see figure 69). Comparison of the experimental lift for the case with blowing off ($C_{\mu,avg} = 0$) with the potential-flow lift for the zero-leading-edge suction condition (solid line), $C_{L,p}$, indicates some degree of nonlinearity, hence, suggesting that the wing develops some leading-edge vortex lift. Vortex breakdown occurs, however, at relatively low angles-of-attack with subsequent loss in lift. Spanwise blowing results in significant vortex-induced lift increments and the data obtained at the highest jet momentum coefficient are predicted reasonably well up to the higher angles-of-attack by the zero-leading-edge suction, full vortex-lift estimate (long-short-dash curve), $C_{L,tot} = C_{L,p} + C_{L,vle} + C_{L,vse}$. The theoretical estimate for full vortex-lift was modified to account for the jet-induced camber effect at $\alpha = 0^{\circ}$ obtained for the highest blowing rate, and the resulting curve (short-dash curve) results in more reasonable agreement with experiment at the low-to-moderate angles-of-attack.

The leading-edge suction analogy, which was developed in ref. 2, was applied to obtain estimates of drag-due-to-lift in figure 69. The expression for the potential flow case, $C_{L,p} \tan \alpha$, overestimates the experimental drag-due-to-lift obtained for the blowing-off ($C_{\mu,avg} = 0$) condition up to the higher C_L values. This is due to the theoretical assumption that the leading-edge suction is zero, but since the experimental wing has a leading-edge radius, then a leading-edge suction force is developed, hence, obtaining a lower drag than estimated. The improvement in drag polar due to spanwise blowing is estimated reasonably well by the theoretical expression $C_{L,tot} \cdot \tan \alpha$, which assumes that the leading-edge suction is zero and that full vortex-lift exists. The leading-edge suction associated with the flow about the round leading edge of the wing results in less drag-due-to-lift, however, than the theoretical estimates. Accounting for the jet-induced camber effect at $\alpha = 0^\circ$ provides a slightly better estimate of the drag polar improvement, but does not account for the leading-edge suction.

The next configuration for which theoretical calculations were made is the 44° swept trapezoidal wing with the leading-edge flap deflected to 8° and with $\delta_{TE} = 0^\circ$ (see figure 70). The potential-flow lift for the 100 per cent leading-edge suction condition (solid line), obtained from theory for cambered and twisted wings from ref. 39, generally gives reasonable estimates of lift for the blowing-off ($C_{\mu,avg} = 0$) case. In addition, the nonlinear C_{L_α} data indicate there is a weak leading-edge vortex on the wing at the moderate-to-high angles-of-attack. The blowing-induced effects at the highest jet momentum coefficient are predicted very well by the theory, which assumes full vortex lift and zero leading-edge suction (long-short-dash curve). One of the theoretical

assumptions in the method from ref. 39 is that the vortex-lift vector is rotated such that it is normal to the leading-edge flap chord; this assumption appears to be justified by the agreement with experiment. Modification of the theoretical estimate to account for the jet-induced effect at $\alpha = 0^\circ$ for the highest $C_{\mu,avg}$ (short-dash curve) results in a more favorable agreement with experiment at the lower angles-of-attack.

The theory for full vortex-lift with zero leading-edge suction (long-short-dash curve) estimates very well the experimental drag-due-to-lift values obtained at the highest jet momentum coefficient. It should be noted that the theoretical drag polar is not defined by the simple relation $C_D = C_{L,tot} \tan \alpha$, as is the case in figure 69 for example, since a different theory was applied in figure 70. These results suggest that blowing in combination with the cambered and twisted leading edge results in some amount of thrust recovery. It should be noted that the experimental induced-drag polar falls between the zero-suction, full vortex-lift polar and the full suction, no vortex-lift polar given by $C_L^2/\pi AR$. This suggests that the leading-edge radius results in additional leading-edge suction.

The theoretical aerodynamic characteristics for the 44° swept trapezoidal wing-horizontal tail configuration are presented in figure 71. The nonlinear C_{L_α} data exhibited by the blowing-off case indicates that the wing-horizontal tail configuration develops vortex-induced lift at the moderate-to-high angles-of-attack. The vortex-induced lift increments obtained at the highest jet momentum coefficient are estimated reasonably well by the full vortex-lift (zero leading-edge suction) theory (long-short-dash curve). Better agreement is provided by the addition of the maximum jet-induced camber effect at $\alpha = 0^\circ$ to the full vortex-lift estimate and this is presented as the short-dash curve in the figure.

The induced-drag expression for the potential-flow case (solid line), $C_{L,p} \tan \alpha$, estimates higher drag levels than those obtained experimentally for the blowing-off case. This may be attributed to the development of leading-edge suction and to the vortex-lift experienced by the wing-tail configuration, which results in improvement in the drag polar. The full vortex-lift estimate (long-short-dash curve), $C_{L,tot} \tan \alpha$, provides good agreement with experimental data obtained at the lower blowing rate. Accounting for the jet-camber effect results in nominal improvement in the theoretical estimate. The experimental induced-drag polar obtained at the highest $C_{\mu,avg}$ falls between the zero-suction vortex-lift polar and the full suction, no vortex-lift polar given by $C_L^2/\pi AR$. The upwash generated ahead of the aft tail may increase the "effective" angle-of-attack at the wing leading edge, hence increasing spanwise blowing effectiveness at a given angle-of-attack. The resulting reduction in angle-of-attack required for a given lift coefficient and the suction force associated with the flow about the round leading edge result in drag values that are less than the estimates provided by the full vortex-lift theory (zero suction).

The comparison between the theoretical and experimental longitudinal characteristics for the close-coupled canard-wing configuration with blowing on the wing is presented in figure 72. Comparison of the blowing-off data with the potential-flow theory (zero leading-edge suction), represented by the solid line, indicates that the canard-wing configuration exhibits nonlinear C_{L_α} data and, hence, experiences vortex lift. The theory which assumes full vortex-lift (zero leading-edge suction), shown as the long-short-dash curve, results in reasonable agreement with the experimental data obtained at the highest $C_{\mu,avg}$ although the experimental

lift is slightly less than the theory at the moderate-to-high angles-of-attack. Addition of the jet-induced effect on the wing at $\alpha = 0^{\circ}$ to the full vortex-lift estimate, shown as the short-dash curve, results in better agreement with experiment at the low angles-of-attack.

The expression for induced-drag for the full vortex-lift case (zero leading-edge suction), $C_{L,tot} \tan \alpha$, gives a reasonable estimate of the experimental drag polars obtained for both the blowing-off and blowing-on cases. Accounting for the jet-induced camber effect improves the theoretical agreement with the blowing-on data, although the experimental data at the highest $C_{\mu,avg}$ indicate less induced-drag than the theoretical estimate.

Theoretical estimates for pitching moment were made for the basic wing, leading-edge flap, horizontal tail, and canard configurations presented in figures 69-72. Comparisons with experiment show that the theory (with and without vortex flow) predicts the stability levels with and without blowing reasonably well.

Spanwise Blowing in the Channel of the "Locked Vortex" Wing

The effects of spanwise blowing on the longitudinal aerodynamic characteristics of the "locked vortex" wing configuration are illustrated in figures 73 and 74 for $M_{\infty} = 0.15$ and 0.20, respectively, for $\delta_{LE} = \delta_{TE} = 20^{\circ}$. The Reynolds numbers corresponding to $M_{\infty} = 0.15$ and 0.20 based on the wing mean aerodynamic chord are 0.845×10^{6} and 1.12×10^{6}, respectively. Due to the higher free-stream dynamic pressure at the higher Mach number, the jet momentum coefficient at a given plenum chamber total pressure is less than the $C_{\mu,avg}$ at the lower Mach number.

The data indicate that spanwise blowing in the wing channel increases, in general, the lift coefficients obtained for the blowing-off case throughout the angle-of-attack range, and that increased $C_{\mu,avg}$ increases the C_L at a given angle-of-attack. At the low angles-of-attack, the data reveal no consistent trend in lift increment with jet momentum coefficient. Similar results were obtained in reference 21 for a semi-span, rectangular wing featuring the unique leading- and trailing-edge flap system. At the moderate-to-high angles-of-attack, large lift increments are attained at all values of $C_{\mu,avg}$. The lift increments at the low angles-of-attack and nonlinearity in the lift curves at the moderate-to-high angles-of-attack suggest the existence of a vortex flow in the channel and possible flow reattachment to the trailing-edge flap.

Flow visualization tests conducted in reference 22 for a "locked vortex" wing of similar planform, have indicated that at sufficient blowing rates, a vortex flow exists within the wing channel at all angles-of-attack and flow reattachment to the trailing-edge flap occurs. Smoke studies conducted during the present test program, for which tunnel RPM was set at minimum and jet blowing was adjusted such that wing upper surface flow could be visualized, have suggested that blowing induces the separated flow off the leading-edge flap to roll up into a vortex ahead of the jet. Blowing also appears to induce flow reattachment to the trailing-edge flap, thus providing a flow situation similar to the flow about a thick, highly-cambered wing. The second, co-rotating vortex behind the jet within the channel, observed for the semi-span rectangular wing in ref. 22, was not observed during the

limited smoke studies of the present test due to extreme turbulence in this region of the wing channel.

The drag polar shape obtained for the blowing-off case is improved by spanwise blowing. The data also suggest that increased blowing rate results in a reduction in aerodynamic drag obtained for the lower $C_{\mu,avg}$ at the moderate-to-high values of lift. At the low-to-moderate values of lift, the configuration with blowing on exhibits higher drag values than those obtained for $C_{\mu,avg} = 0$. With blowing on, the flow situation tends to be similar to the flow about an effective wing possessing a large amount of camber and thickness, and higher drag values would be anticipated for such a wing.

The data also suggest that spanwise blowing does not significantly affect the stability level obtained for the blowing-off case. Increased jet momentum coefficient results, in general, in slightly greater nose down pitching moment, which seems to suggest that the vortex flow in the channel and the flow reattachment to the trailing-edge flap induced by blowing shift the center of lift on the wing slightly aft.

The effects of spanwise blowing on the longitudinal aerodynamic characteristics of the "locked vortex" wing configuration with leading- and trailing-edge flap deflection angles increased to 30° are illustrated in figures 75 and 76 for $M_\infty = 0.15$ and 0.20, respectively. The lift increments induced by spanwise blowing are significantly less at a given $C_{\mu,avg}$ than those obtained for $\delta_{LE} = \delta_{TE} = 20^\circ$ throughout the angle-of-attack range. These results seem to indicate that for the given leading- and trailing-edge flap geometries and nozzle location, increasing the flap deflection angles necessitates correspondingly higher jet momentum coefficients in order to induce lift increments that are comparable to those obtained for smaller

flap deflection angles and to induce flow reattachment to the trailing-edge flap.

The data also indicate that the drag polar shape obtained for the $C_{\mu,avg} = 0$ case is essentially unaffected by spanwise blowing. The aerodynamic drag at a given lift obtained for $C_{\mu,avg} = 0$ is increased with onset of blowing, and increased $C_{\mu,avg}$ results in a slight reduction in drag obtained for the lower $C_{\mu,avg}$ values at the moderate-to-high C_L's.

Spanwise blowing does not appear to affect the longitudinal stability level obtained for the blowing-off case. Pitching moment is slightly less negative with blowing on, indicating a forward shift of the center of lift. A reverse trend was observed for the configuration with $\delta_{LE} = \delta_{TE} = 20^\circ$.

The effects of spanwise blowing on the longitudinal aerodynamic characteristics of the "locked vortex" wing configuration with $\delta_{LE} = 45^\circ$, $\delta_{TE} = 30^\circ$ are shown in figures 77 and 78 for $M_\infty = 0.15$ and 0.20, respectively. At the low angles-of-attack, the data suggest that spanwise blowing has an adverse effect on lift, as evidenced by a reduction in the C_L's obtained for the blowing off-case. Due to the sharp decrease in lift obtained for the blowing-off case in the moderate angle-of-attack range, the lift increments due to spanwise blowing appear largest in this range. There is a slight recovery in lift obtained for the $C_{\mu,avg} = 0$ case at the higher angles-of-attack, and the ΔC_L's due to blowing are consequently decreased.

The drag polar shape acquired with blowing off is improved slightly by blowing, although the aerodynamic drag at a given lift is greater with blowing on than for blowing off for all lift values. The longitudinal

stability level obtained for $C_{\mu,avg} = 0$ appears relatively unaffected by spanwise blowing in the wing channel. The discussion concerning the trend in pitching moment with blowing on for the configuration with $\delta_{LE} = \delta_{TE} = 30^{\circ}$ in figures 75 and 76 is also applicable to the data presented in figures 77 and 78.

The "locked vortex" wings were designed to provide the capability of retracting the flaps to provide a cruise configuration. It is of interest, therefore, to evaluate the effect of spanwise blowing on the "clean" wing for a range of angle-of-attack. The effect of spanwise blowing on the longitudinal aerodynamic characteristics of the "locked vortex" wing configuration with flaps retracted ($\delta_{LE} = \delta_{TE} = 0^{\circ}$) is shown in figures 79 and 80 for $M_{\infty} = 0.15$ and 0.20, respectively. The data indicate that spanwise blowing on the "clean" wing induces larger lift increments at a given jet momentum coefficient than obtained for any of the configurations with flaps extended, shown in figures 73-78, at the moderate-to-high angles-of-attack. This configuration is similar to spanwise blowing on the 44° swept trapezoidal wing with conventional leading- and trailing-edge flaps (fig. 15). At the low angles-of-attack, there is a positive lift increment due to blowing, which is attributable to the jet-induced camber effect, and possibly due to flow separation in the vicinity of the extremely blunt leading-edge, thereby enabling slight beneficial blowing-induced effects. The nonlinear lift curve suggests a leading-edge vortex flow augmented by spanwise blowing.

Drag polar shape obtained for the blowing-off case is improved by spanwise blowing and aerodynamic drag at a given value of lift obtained for the $C_{\mu,avg} = 0$ case is reduced with blowing on. Due to the extremely blunt

leading-edge, it may be reasonable to assume leading-edge suction forces act to reduce drag at a given lift. Blowing extends the linear pitching moment obtained for the blowing-off case to much higher values of lift without adversely affecting the stability level.

The effect of α and $C_{\mu,avg}$ on the lift augmentation ratio and lift effectiveness of blowing is shown in figures 81-83 and 84-86 for the configurations with extended leading- and trailing-edge flaps. The data presented in figures 81-83 for $M_\infty = 0.15$ and figures 84-86 for $M_\infty = 0.20$ indicate that the configuration with $\delta_{LE} = \delta_{TE} = 20^\circ$ exhibits the highest lift augmentation ratios and, in general, the largest percentage gains in lift due to blowing in the moderate-to-high angle-of-attack range. At the low angles-of-attack, large percentage gains in lift are attained at the higher blowing rates. This occurs because the wing without blowing exhibits low C_L values at the low angles-of-attack and the $C_L/C_{L,o}$ becomes quite large as a result. Spanwise blowing in conjunction with leading- and trailing-edge flaps extended to 20° is the only configuration exhibiting lift augmentation ratios exceeding the effect of vectoring the thrust vertically. These results seem to indicate that the optimum converging nozzle location relative to the wing surface is dependent on leading- and trailing-edge flap deflection angles. As the flap deflection angles increase, the data suggest that for a fixed nozzle location a corresponding increase in jet momentum coefficient is required to attain lift increments that are comparable to those obtained for smaller flap deflection angles.

It is of interest to compare the effectiveness of blowing on the "clean" wing ($\delta_{LE} = \delta_{TE} = 0^\circ$) with spanwise blowing effectiveness in conjunction with

extended leading- and trailing-edge flaps. In this regard, figures 87 and 88 present the effect of α and leading- and trailing-edge flap deflection angles on the lift augmentation ratio and lift effectiveness of blowing for $M_\infty = 0.15$ and 0.20, respectively, for $C_{\mu,avg} = 0.34$. As suggested by the data in figures 73-86, spanwise blowing on the "clean" wing results in higher lift augmentation ratios and larger percentage gains in lift due to blowing than were obtained for the configurations with blowing in combination with extended flaps. It should be noted that two distinct vortex flow phenomena are being compared; a leading-edge vortex flow on a relatively thin wing augmented by spanwise blowing, and a vortex flow "locked" by spanwise blowing in a wing channel formed by extended upper surface leading- and trailing-edge flaps.

For completeness, the effect of leading- and trailing-edge flap deflection angles on the longitudinal aerodynamic characteristics of the "locked vortex" wing configuration with blowing off is illustrated in figures 89 and 90 for $M_\infty = 0.15$ and 0.20, respectively. Similar plots are shown in figures 91 and 92 with blowing on for $M_\infty = 0.15$ and 0.20, respectively. In the latter two figures, data for the configuration with $\delta_{LE} = \delta_{TE} = 0^\circ$ are not presented, since it is desired to evaluate blowing in combination with extended flaps only. With blowing off (figs. 89 and 90), extension of the leading- and trailing-edge flaps increase the lift coefficient obtained for the flaps-retracted case ($\delta_{LE} = \delta_{TE} = 0^\circ$) particularly in the low angle-of-attack range (-2° to 6°) and higher angle-of-attack range (18° to 20°). Part of the lift increment is undoubtedly attributable to the deflected portion of the trailing-edge flap below the wing, but it is difficult at the present

time to isolate the effect of leading- and trailing-edge flaps on the aerodynamic lift coefficient. It should be noted that wing stall did not occur for the configurations with extended flaps.

As would be expected, extension of upper surface leading- and trailing-edge flaps increases the aerodynamic drag at a given lift compared to the flaps-retracted case. The data indicated that for $\delta_{LE} = \delta_{TE} = 20^{\circ}$, and $\delta_{LE} = \delta_{TE} = 30^{\circ}$, the drag polar shape obtained for the flaps-retracted case is improved, but relatively unaffected when $\delta_{LE} = 45^{\circ}$, $\delta_{TE} = 30^{\circ}$

Pitching moment, in general becomes more negative with increased leading- and trailing-edge flap deflection angles. This may be due to the portion of the extended trailing-edge flap below the wing and also to the weak vortex system generated in the vicinity of the leading-edge flap, which may tend to shift the center of lift more aft of the moment reference center. The data seem to indicate that the longitudinal stability level obtained for $\delta_{LE} = \delta_{TE} = 0^{\circ}$ is essentially unaffected by extension of the leading- and trailing-edge flaps.

With blowing on, the data shown in figures 91 and 92 for $M_{\infty} = 0.15$ and 0.20, respectively, indicate that the configuration with the smallest flap deflection angles ($\delta_{LE} = \delta_{TE} = 20^{\circ}$) exhibits higher lift coefficients throughout the angle-of-attack range, lower aerodynamic drag at a given lift, and more favorable pitching moment characteristics. Pitching moment is reasonably linear at the low-to-moderate values of lift, beyond which occurs a decrease in stability at the higher C_L's. The data indicate that increased leading- and trailing-edge flap deflection angles ($\delta_{LE} = \delta_{TE} = 30^{\circ}$; $\delta_{LE} = 45^{\circ}$, $\delta_{TE} = 30^{\circ}$) decreases the lift coefficients compared to the

$\delta_{LE} = \delta_{TE} = 20^{\circ}$ case and results in slightly higher C_{L_α} in the low angle of-attack range and lower C_{L_α} at the higher angles-of-attack. Drag polar shape obtained for the $\delta_{LE} = \delta_{TE} = 20^{\circ}$ configuration is essentially unchanged by increased flap deflection angles. The data also indicate several longitudinal stability breaks for the configurations with larger flap settings. These results seem to indicate that as the wing channel volume is increased, the spanwise jet becomes less effective in inducing a stable vortex flow within the channel and flow reattachment to the trailing-edge flap.

Reference 21 has shown that the longitudinal aerodynamic characteristics of a semi-span rectangular "locked vortex" wing at angles-of-attack greater than 20° were highly Reynolds number-dependent for the range of Reynolds numbers from 0.5×10^5 to 1.5×10^5. Data from the current "locked-vortex" wing study are presented in figure 93, which show the variation of lift coefficient with $C_{\mu,avg}$ for two angles-of-attack and the two Reynolds numbers tested (0.845×10^6 and 1.12×10^6) for the "locked vortex" wing configurations. The data indicate that for the three configurations with extended leading- and trailing-edge flaps, there is essentially no effect of Reynolds number on the variation in C_L with $C_{\mu,avg}$. The results shown in figure 93 for two angles-of-attack are representative of the results obtained for all angles-of-attack considered in the present tests. These results appear to be consistent with the data in reference 21, which showed that no significant Reynolds number effects occurred at angles-of-attack less than 20°.

CHAPTER V

CONCLUSIONS

A generalized wind tunnel model has been tested in the Langley high speed 7- by 10-foot wind tunnel to investigate new component concepts utilizing spanwise blowing that will provide improved maneuver characteristics for advanced fighter aircraft with primary emphasis on high angle-of-attack performance, stability, and control at subsonic speeds. Since separation-induced vortex flows have been shown under certain conditions to significantly increase maneuver performance, the investigation was focused on various methods of controlling and delaying the leading-edge vortex breakdown and of optimizing component interactions. In particular, spanwise blowing was utilized on a 44° swept trapezoidal wing to determine the effect of leading-edge vortex enhancement on leading- and trailing-edge flap effectiveness, horizontal and vertical tail loads, and close-coupled canard-wing effectiveness, and to assess the concept as a roll control device. Additional studies were conducted with a trapezoidal wing featuring a unique leading- and trailing-edge flap arrangement which, when combined with spanwise blowing creates a "locked vortex" system for high lift at take-off, approach, and during maneuvering flight.

The data obtained in the tests indicate that spanwise blowing results in substantial improvement in the high angle-of-attack performance of the 44° swept trapezoidal wing configuration. In particular, significant vortex-induced lift increments occur at the higher angles-of-attack with consequent improvement in the drag polar. In addition, spanwise blowing extends the linear pitching moment to higher angles-of-attack without adverse

pitch-up characteristics. Furthermore, the data suggest spanwise blowing is more effective at higher subsonic Mach numbers and, provided sufficient engine bleed air is available, represents a powerful means of enhancing the higher subsonic maneuver performance of fighter aircraft. The results obtained are similar to the favorable benefits of a highly-swept maneuver strake.

Deflecting a leading-edge flap delays the beneficial blowing-induced effects to higher angles-of-attack. The data suggest, however, that a forward rotation of the vortex lift vector occurs and the consequent thrust recovery results in drag-polar improvement. Deflecting a trailing-edge flap increases the camber, and the data suggest that the resulting increase in circulation increases spanwise blowing effectiveness at a given angle-of-attack. These favorable lift benefits at a given angle-of-attack are reduced slightly by simultaneous deflection of leading- and trailing-edge flaps. The drag polars are improved, however, which is very important from a sustained maneuver standpoint.

The data indicate that spanwise blowing is an effective lateral control device at high angles-of-attack and may compare favorably with more conventional roll control devices such as trailing-edge flap ailerons.

Spanwise blowing on the wing reduces horizontal tail loading at the higher angles-of-attack, which may have a favorable effect on trim characteristics.

The lateral-directional stability characteristics of the wing-vertical tail and wing-horizontal tail-vertical tail configurations are improved by spanwise blowing on the wing. In particular, blowing results in stabilizing increments in the effective dihedral and directional stability

parameters and delays the unfavorable break in the directional stability parameter to much higher angles-of-attack.

For the close-coupled canard-wing configuration, the effectiveness of spanwise blowing on the wing is limited due to the canard downwash on the wing. Spanwise blowing on the canard, however, enhances the canard leading-edge vortex and may improve the favorable canard-wing interference at the higher angles-of-attack. In addition, the data indicate that the effect of blowing is more pronounced when the canard incidence is increased. The results suggest that spanwise blowing on the canard may permit the canard size to be reduced, which would enable a more optimum canard to be used in cruise. Furthermore, blowing on a moderately-swept canard may provide a more favorable method of longitudinal trim control.

Spanwise blowing in the channel of the "locked vortex" wing results in large increases in lift for the smaller flap deflection angles, but the data indicate that increased flap deflection angles reduce blowing effectiveness and hence a departure from the desired "effective" wing possessing a large amount of thickness and camber. The technique of "locking" a vortex flow in the channel by blowing appears promising but the interdependence of the parameters involved in the tests precluded additional refinements.

CHAPTER VI

RECOMMENDATIONS

Results of the present studies indicate that further evaluation of the spanwise blowing concept to improve maneuver performance is warranted. In particular, the present tests require extension to higher angles-of-attack since the data indicate in many instances that the maximum blowing effects occur at angles-of-attack beyond those considered in the studies. Evaluation of spanwise blowing at higher subsonic and transonic Mach numbers is necessary to determine if the utilization of blowing is deterred by a lack of engine bleed air to provide momentum required for effective vortex augmentation. Results obtained by spanwise blowing on a cambered wing surface appear very promising and suggest that by designing a wing to take advantage of the enhanced separation-induced vortex flow at high angles-of-attack, substantial drag polar improvement may be possible. The effects that are actively induced by spanwise blowing also suggest the rather exciting possibility of modifying the wing leading edge to passively induce a spanwise flow and thus enhance the leading-edge vortex without the requirement of engine bleed air or ducting to supply air to the wings.

The applications of spanwise blowing to aircraft components are numerous. For example, blowing on a wing trailing-edge flap, on a vertical tail or vertical tail rudder, or on a horizontal tail or elevator may offer substantial improvement in component effectiveness.

Location of a canard above the wing chord plane may alleviate the downwash effects that appear to limit spanwise blowing effectiveness on the wing. The data suggest, however, that blowing on the canard exhibits

more potential to expand flight envelopes, reduce approach speeds and enhance maneuverability. In this regard, investigation of spanwise blowing on canards of various sizes and planforms and a range of canard longitudinal and vertical locations is warranted. Additional configurations include blowing on the canard in combination with a deflected canard trailing-edge flap and canard blowing in the presence of a cambered wing.

Of perhaps greatest significance, however, is a direct comparison of the spanwise blowing concept with alternate devices which are designed to attain the same effects. For example, it would be of benefit to compare the effects of spanwise blowing and a highly-swept maneuver strake on high angle-of-attack performance, to compare spanwise blowing on a canard with a straked-canard configuration, and to evaluate spanwise blowing as a primary means of roll control or in combination with existing lateral control devices.

More efficient design of the "locked vortex" wing flap arrangement and more effective utilization of the spanwise jet may provide more favorable lift and drag characteristics. The data suggest that the wing channel volume may have been excessive and that a nozzle located well above the wing surface may provide substantial improvement in blowing effectiveness. In addition, the tapered wing channel may have adversely affected the vortex-jet system, which suggests that perhaps an untapered channel or some means of alleviating the adverse pressure gradient at the wing tip may result in more efficient aerodynamic performance.

REFERENCES

1. Polhamus, Edward C.: A Concept of the Vortex Lift of Sharp-Edge Delta Wings Based on a Leading-edge Suction Analogy. NASA TN D-3767, 1966.

2. Polhamus, Edward C.: Application of the Leading-edge Suction Analogy of Vortex Lift to the Drag Due to Lift of Sharp-Edge Delta Wings. NASA TN D-4739, 1968.

3. Wentz, William H., Jr.; and Kohlman, David L.: Wind Tunnel Investigation of Vortex Breakdown on Slender Sharp-Edged Wings. Rep. FRL 68-013 (Grant NGR-17-002-043), Univ. of Kansas Center for Research, Inc., Nov. 27, 1969. (Available as NASA CR-98737.)

4. Polhamus, Edward C.: Predictions of Vortex-Lift Characteristics by a Leading-edge-Suction Analogy. J. Aircraft, vol. 8, no. 4, Apr. 1971, pp. 193-199.

5. Hummel, D.: Study of the Flow Around Sharp-Edged Slender Delta Wings With Large Angles of Attack. NASA TT F-15, 107, 1973.

6. Werle, H.: Partage et Recontre d'Ecoulements Fluides. Etude Effectuee a la Cuve a Huile at an Tunnel Hydrodynamic a Visualisation de l'O.N.E.R.A. La Rech. Aeron., no. 79, Nov.-Dec. 1960, pp. 9-26.

7. Cornish, J. J., III: High Lift Applications of Spanwise Blowing ICAS Paper No. 70-09, Sept. 1970.

8. Werle, H.; and Gallon, M.: Flow Control by Cross Jet. NASA TT F-13, 548, 1972.

9. Werle, Henri: Sur l'Ecoulement au Bord d'attaque d'un Profil Portant. La Rech. Aerospatiale, no. 4, July-Aug. 1973, pp. 197-218.

10. Dixon, C. J.: Lift Augmentation by Lateral Blowing Over a Lifting Surface. AIAA Paper No. 69-193, Feb. 1969.

11. Dixon, C. J.: Lift and Control Augmentation by Spanwise Blowing Over Trailing-Edge Flaps and Control Surfaces. AIAA Paper No. 72-781, Aug. 1972.

12. Bradley, R. G.; and Wray, W. O.: A Conceptual Study of Leading-Edge-Vortex Enhancement by Blowing. AIAA Paper No. 73-656, July 1973.

13. Dixon, C. J.; Theisen, J. G.; and Scruggs, R. M.: Theoretical and Experimental Investigations of Vortex Lift Control by Spanwise Blowing. Volume I - Experimental Research. LG 73 ER-0169, Lockheed Aircraft Corp., Sept. 15, 1973.

14. Bradley, R. G.; Wray, W. O.; and Smith, C. W.: An Experimental Investigation of Leading-Edge Vortex Augmentation by Blowing. NASA CR-132415, 1974.

15. Dixon, C. J.; Theisen, J. G.; and Scruggs, R. M.: Theoretical and Experimental Investigations of Vortex Lift Control by Spanwise Blowing. Volume II - Three-Dimensional Theory For Vortex-Lift Augmentation. LG73ER-0169, Lockheed Aircraft Corp., Sept. 15, 1973.

16. Bradley, R. G.; Whitten, P. D.; Wray, W. O.: Leading-Edge Vortex Augmentation in Compressible Flow. AIAA Paper No. 75-124, Jan. 1975.

17. Campbell, J. F.: Effects of Spanwise Blowing on the Pressure Field and Vortex-Lift Characteristics of a 44° Swept Trapezoidal Wing. NASA TN D-7907, 1975.

18. Campbell, J. F.: Augmentation of Vortex Lift by Spanwise Blowing. AIAA Journal of Aircraft, Vol. 13, No. 9, September 1976 (Presented at AIAA Aircraft Systems and Technology Meeting, Los Angeles, CA., AIAA Paper No. 75-993, August 4-7, 1975).

19. Bradley, R. G.; Jeffries, R. R.; Capone, F. J.: A Vectored-Engine-Over-Wing Propulsive-Lift Concept. AIAA Paper No. 76-917, September 1976.

20. Jenkins, M. W. M.; Meyer, R. T.: A Large-Scale Low-Speed Tunnel Test of a Canard Configuration with Spanwise Blowing. AIAA Paper No. 75-994, Aug. 1975.

21. Westesson, R. A.; Clareus, U.: Studier i ett okonventionellt sätt att erhålla lyftkraft. KTH Flygtecknik, 1973.

22. Erickson, G. E.; Campbell, J. F.: Flow Visualization of Vortices Locked by Spanwise Blowing on a Wing Featuring a Unique Leading- and Trailing-Edge Flap System. NASA TM X-72788, 1975.

23. Sviden, O.: Förslag till Höglyft princip för STOL-Flygplan. TP-71:44 edition 3, 1973.

24. Erickson, G. E.; Campbell, J. F.: Flow Visualization of Leading-Edge Vortex Enhancement by Spanwise Blowing. NASA TM X-72702, 1975.

25. Wentz, W. H.: Effects of Leading-Edge Camber on Low-Speed Characteristics of Slender Delta Wings. NASA CR-2002, 1972.

26. Ray, E. J.; McKinney, L. W.; Carmichael, J. G.: Maneuver and Buffet Characteristics of Fighter Aircraft. NASA TN D-7131, 1973.

27. Campbell, J. F.; Gloss, B. B.; Lamar, J. E.: Vortex Maneuver Lift For Super-Cruise Configurations. NASA TM X-72836, 1976.

28. USAF Stability and Control Datcom, Flight Control Division, Air Force Flight Dynamics Laboratory, Wright-Patterson AFB, Ohio.

29. Henderson, W. P.; Huffman, J. K.: Lateral-Directional Stability Characteristics of a Wing-Fuselage Configuration at Angles of Attack up to 44°. NASA TM X-3087, 1974.

30. Gloss, Blair B.; McKinney, Linwood, W.: Canard-Wing Lift Interference Related to Maneuvering Aircraft at Subsonic Speeds. NASA TM X-2897, 1973.

31. Gloss, Blair B.: Effect of Canard Location and Size on Canard-Wing Interference and Aerodynamic-Center Shift Related to Maneuvering Aircraft at Transonic Speeds. NASA TN D-7505, 1974.

32. Gloss, Blair B.: The Effect of Canard Leading-Edge Sweep and Dihedral Angle on the Longitudinal and Lateral Aerodynamic Characteristics of a Close-Coupled Canard-Wing Configuration. NASA TN D-7814, 1974.

33. Gloss, Blair B.: Effect of Wing Planform and Canard Location and Geometry on the Longitudinal Aerodynamic Characteristics of a Close-Coupled Canard Wing Model at Subsonic Speeds. NASA TN D-7910, 1975.

34. Lamar, J. E.: Extension of Leading-Edge Suction Analogy to Wings with Separated Flow Around the Side-Edges at Subsonic Speeds. NASA TR R-428, 1974.

35. Henderson, William P.: Pressure Distributions on a Cambered Wing-Body Configuration at Subsonic Mach Numbers. NASA TN D-7946, 1975.

36. Campbell, James F.; Erickson, Gary E.: Effects of Spanwise Blowing on the Pressure Field and Vortex-Lift Characteristics of a 44° Swept Trapezoidal Wing in the Presence of a Highly-Swept Maneuver Strake. Proposed NASA TN D 1977.

37. McKinney, L. W.; Dollyhigh, S. M.: Some Trim Drag Considerations for Maneuvering Aircraft. J. Aircraft, vol. 8, no. 8, Aug. 1971, pp. 623-629.

38. Margason, Richard J.; Lamar, John E.: Vortex Lattice FORTRAN Program for Estimating Subsonic Aerodynamic Characteristics of Complex Planforms. NASA TN D-6142, 1971.

39. Luckring, J. M.; Lamar, J. E.: Private communication.

40. Lamar, John E.; and Gloss, Blair B.: Prediction of Subsonic Aerodynamic Characteristics on Interacting Lifting Surfaces with Separated Flow Around Sharp Leading and Side Edges Using Vortex-Lattice Methodology. NASA TN D-7921, 1975.

41. Bartlett, C. E.; Vidal, R. J.: Experimental Investigation of Influence of Edge Shape on the Aerodynamic Characteristics of Low Aspect Ratio Wings at Low Speeds. Journal of Aeronautical Sciences, Vol. 22, August 1955, pp. 517-533, 588.

42. Tosti, Louis P.: Low-Speed Static Stability and Damping-in-Roll Characteristics of Some Swept and Unswept Low-Aspect-Ratio Wings. NACA TN 1468, 1947.

43. Aviation Week and Space Technology, June 16, 1975, pg. 23 (Photograph copywrited by AW&ST).

44. Polhamus, E. C.: Charts for Predicting the Subsonic Vortex Lift Characteristics of Arrow, Delta, and Diamond Wings. NASA TN D-6243, April 1971.

TABLE I.- Geometric Characteristics of Model

Body length, cm (in.)	101.05 (39.78)
44 swept trapezoidal wing:	
AR	2.56
b/2, cm (in.)	27.18 (10.70)
Λ_{LE}, deg	44
$\bar{c}$, cm (in.)	24.56 (9.67)
c_{th}, cm (in.)	35.75 (14.08)
Longitudinal model station of 1/4 c_{th}, cm (in.)	51.81 (20.40)
Airfoil section:	
Root	64A006
Tip	64A004
S, cm^2 (in^2)	1155.71 (179.14)
Root chord (at wing-fuselage juncture), cm (in.)	29.80 (11.73)
Tip chord, cm (in.)	6.77 (2.66)
"Locked Vortex" wing:	
(All geometric characteristics refer to flaps-retracted case)	
AR	2.49
b/2, cm (in.)	27.18 (10.70)
Λ_{LE}, deg	44
$\bar{c}$, cm (in.)	24.64 (9.70)
c_{th}, cm (in.)	35.17 (13.84)
Longitudinal model station of 1/4 c_{th}, cm (in.)	51.66 (20.34)

TABLE I.- CONTINUED.

Airfoil section	Flat plate; round LE; sharp TE
S, cm^2 (in^2)	1186.26 (183.87)
Root chord (at wing-fuselage juncture), cm (in.)	29.77 (11.72)
Tip chord, cm (in.)	8.48 (3.34)
Maximum thickness, percent chord, at	
Root	6.0
Tip	6.0
Canard:	
Λ_{LE}, deg	51.7
Airfoil section	Circular Arc
S_C, cm^2 (in^2)	226.90 (35.17)
b/2, cm (in.)	17.5 (6.89)
Root chord (at canard-fuselage juncture), cm (in)	15.88 (6.25)
Tip chord, cm (in.)	3.18 (1.25)
Maximum thickness, per cent chord at -	
Root	6.0
Tip	4.0
Horizontal and vertical tails:	
Λ_{LE}, deg	51.7
Airfoil section	Circular Arc
S_T, cm^2 (in^2)	288.39 (44.77)
b/2, cm (in.)	19.03 (7.49)
Root chord (at tail-fuselage juncture), cm (in.)	17.92 (7.05)

TABLE I.- CONCLUDED.

Tip chord, cm (in.)	3.59 (1.41)
Maximum thickness, per cent chord at -	
Root	6.0
Tip	4.0

APPENDIX A

Static Calibration Results

The nozzle thrust components determined from the static calibration tests with all lifting surfaces removed are presented and were used to accordingly modify the total coefficients presented in Appendix B and, hence, to obtain the aerodynamic coefficients. Figures 94 - 97 present the forces and moments due to nozzle thrust components as a function of plenum chamber total pressure. The resulting expressions which were used to obtain the aerodynamic coefficients for each appropriate configuration are also presented in the following pages.

In addition, figures 98 - 100 present correlations between the jet total pressure at the nozzle exit and the plenum total pressure and these results were used to modify the computation of V_j and, hence, C_μ.

Expressions for the forces and moments due to nozzle thrust components as a function of plenum chamber total pressure:

(a) 44° Swept Trapezoidal Wing Nozzles.

$$NF_J\ (lb_f) = 0.002526\ (p_{t,plen}) - 0.64774$$

$$AF_J\ (lb_f) = -0.04345\ (p_{t,plen}) + 0.1$$

$$PM_J\ (in\text{-}lb) = -0.017067\ (p_{t,plen}) + 0.1$$

$$RM_J\ (in\text{-}lb) = 0.00583\ (p_{t,plen}) - 0.15$$

$$YM_J\ (in\text{-}lb) = -0.01214\ (p_{t,plen}) - 0.578$$

$$SF_J\ (lb_f) = -0.001067\ (p_{t,plen}) + 0.14$$

(b) 44° Swept Trapezoidal Wing - Right Nozzle Only.

$NF_J\ (lb_f) = -0.001063\ (p_{t,plen}) + 0.07$

$AF_J\ (lb_f) = -0.019386\ (p_{t,plen})$

$PM_J\ (in\text{-}lb) = -0.013502\ (p_{t,plen})$

$RM_J\ (in\text{-}lb) = -0.0045606\ (p_{t,plen})$

$YM_J\ (in\text{-}lb) = -0.10197\ (p_{t,plen})$

$SF_J\ (lb_f) = -0.023209\ (p_{t,plen}) + 0.1$

(c) Canard Nozzles.

$NF_J\ (lb_f) = 0.002333\ (p_{t,plen}) - 0.120$

$AF_J\ (lb_f) = -0.017433\ (p_{t,plen})$

$PM_J\ (in\text{-}lb) = 0.015367\ (p_{t,plen})$

$RM_J\ (in\text{-}lb) = -0.002967\ (p_{t,plen})$

$YM_J\ (in\text{-}lb) = -0.007833\ (p_{t,plen})$

$SF_J\ (lb_f) = -0.000567\ (p_{t,plen}) + 0.08$

(d) "Locked vortex" Wing Nozzles.

$NF_J\ (lb_f) = -0.003617\ (p_{t,plen}) + 0.120$

$AF_J\ (lb_f) = -0.030045\ (p_{t,plen})$

$PM_J\ (in\text{-}lb) = -0.01451\ (p_{t,plen})$

$RM_J\ (in\text{-}lb) = -0.0015\ (p_{t,plen}) + 0.19$

$YM_J\ (in\text{-}lb) = -0.02067\ (p_{t,plen})$

$SF_J\ (lb_f) = -0.005167\ (p_{t,plen})$

Force and moment coefficients due to nozzle thrust components:

$$C_{L,J} = \frac{NF_J}{q_\infty S} \cos\alpha - \frac{AF_J}{q_\infty S} \sin\alpha$$

$$C_{D,J} = \frac{AF_J}{q_\infty S} \cos \alpha + \frac{NF_J}{q_\infty S} \sin \alpha$$

$$C_{m,J} = \frac{PM_J}{q_\infty S\bar{c}}$$

$$C_{\ell,J} = \frac{RM_J}{q_\infty Sb} + C_{n,J,b} \sin \alpha \quad \text{where} \quad C_{n,J,b} = \frac{YM_J}{q_\infty Sb}$$

$$C_{n,J} = \frac{YM_J}{q_\infty Sb} - C_{\ell,J,b} \sin \alpha \quad \text{where} \quad C_{\ell,J,b} = \frac{RM_J}{q_\infty Sb}$$

$$C_{Y,J} = \frac{SF_J}{q_\infty S}$$

Relationships to obtain aerodynamic coefficients:

$$C_L = C_{L,T} - C_{L,J}$$

$$C_D = C_{D,T} - C_{D,J}$$

$$C_m = C_{m,T} - C_{m,J}$$

$$C_\ell = C_{\ell,T} - C_{\ell,J}$$

$$C_n = C_{n,T} - C_{n,J}$$

$$C_Y = C_{Y,T} - C_{Y,J}$$

APPENDIX B

Tabulated Results

The symbols used in the tabulated data are defined as follows:

QINF	Free-stream dynamic pressure, psf
ALPHA	Angle-of-attack, deg
BETA	Angle-of-sideslip, deg
CLT	Total lift force coefficient, including nozzle thrust components
CDT	Total drag force coefficient, including nozzle thrust components
CPMT	Total pitching moment coefficient, including nozzle thrust components
CRMT	Total rolling moment coefficient, including nozzle thrust components
CYMT	Total yawing moment coefficient, including nozzle thrust components
CSFT	Total side force coefficient, including nozzle thrust components
CMU	Jet momentum coefficient
HPLEN	Stagnation pressure in settling chamber, psi
WTFLO	Air weight flow rate, lb_f/sec

TABLE II.- Experimental Configurations

Table	Wing	Canard	Jet Location	δ_{LE}, deg	δ_{TE}, deg	i_C, deg	Horiz. Tail	Vert. Tail	β, deg
III	44° swept trapezoidal	Off	Wing	range	range	----	Off	Off	0
IV	"	Off	Right Wing	0	0	----	Off	Off	0
V	"	Off	Wing	0	0	----	On	Off	0
VI	"	Off	Wing	0	0	----	Off	On	range
VII	"	Off	Wing	0	0	----	On	On	range
VIII	"	On	Wing	0	0	range	Off	Off	0
IX	"	On	Canard	0	0	range	Off	Off	0
X	"Locked Vortex"	Off	Wing	range	range	----	Off	Off	0

TABLE III.- SPANWISE BLOWING ON THE 44° SWEPT TRAPEZOIDAL WING.

(a) $\delta_{LE} = \delta_{TE} = 0^{\circ}$

$M_{\infty} = 0.30$; $C_{\mu, avg} = 0.059$; $T_{t, plen} = 514^{\circ}R$

QINF PSF	ALPHA DEG	BETA DEG	CLT	CDT	CPMT	CMU	HPLEN PSI	WTFLO LBF/SEC
126.0374	.01	-.00	.0114	-.0043	-.0025	.0595	137.4421	.1777
125.0662	-1.84	-.02	-.0843	-.0043	.0155	.0600	137.4945	.1779
125.9050	.04	-.00	.0121	-.0043	-.0027	.0598	137.5278	.1784
126.2589	1.93	.02	.1113	-.0004	-.0209	.0589	136.3677	.1764
126.2655	3.86	.04	.2158	.0070	-.0425	.0588	135.8499	.1762
125.7485	5.85	.07	.3351	.0215	-.0686	.0590	135.6101	.1761
125.6296	7.88	.09	.4547	.0454	-.0968	.0590	135.5082	.1760
125.3477	9.96	.11	.5726	.0789	-.1224	.0591	135.4278	.1759
125.9394	12.08	.13	.6722	.1214	-.1427	.0589	135.4237	.1762
124.9336	14.25	.16	.8056	.1786	-.1838	.0594	135.3719	.1760
123.3016	16.35	.18	.9430	.2426	-.2206	.0601	135.3837	.1759
123.7521	18.46	.20	1.0499	.3092	-.2441	.0600	135.4139	.1762
124.4137	20.56	.23	1.1256	.3747	-.2607	.0597	135.4307	.1761
126.6979	.01	-.00	.0125	-.0034	-.0018	.0584	135.7039	.1755

$M_{\infty} = 0.30$; $C_{\mu, avg} = 0.128$; $T_{t, plen} = 530^{\circ}R$

QINF PSF	ALPHA DEG	BETA DEG	CLT	CDT	CPMT	CMU	HPLEN PSI	WTFLO LBF/SEC
126.0344	.01	.00	.0424	-.0463	-.0175	.1271	295.3766	.3394
125.9049	-1.84	-.02	-.0557	-.0475	.0015	.1275	296.1869	.3400
126.4871	.05	.00	.0474	-.0473	-.0185	.1274	296.9791	.3406
126.2240	1.94	.02	.1483	-.0427	-.0378	.1278	297.4610	.3408
125.9876	3.86	.04	.2564	-.0352	-.0606	.1285	298.1612	.3415
125.7619	5.86	.07	.3797	-.0198	-.0891	.1288	298.5843	.3413
125.8914	7.89	.09	.5080	.0055	-.1200	.1288	298.8826	.3415
126.0103	9.97	.11	.6449	.0444	-.1518	.1288	299.1272	.3414
125.7700	12.11	.13	.7855	.0948	-.1875	.1286	298.3965	.3401
125.4121	14.29	.16	.9335	.1563	-.2270	.1287	297.6161	.3392
125.0017	16.39	.18	1.0690	.2234	-.2613	.1289	297.0508	.3383
125.6456	18.52	.21	1.1814	.2959	-.2854	.1281	296.7721	.3377
125.3170	20.61	.23	1.2686	.3678	-.3041	.1285	296.5591	.3376
125.7271	.01	-.00	.0427	-.0515	-.0162	.1279	296.3762	.3364

$M_{\infty} = 0.30$; $C_{\mu, avg} = 0$

QINF PSF	ALPHA DEG	BETA DEG	CLT	CDT	CPMT	CMU	HPLEN PSI	WTFLO LBF/SEC
127.3139	-.00	-.00	.0060	.0244	.0016	0.0000	-1.4835	.0659
127.1926	-1.85	-.02	-.0906	.0255	.0201	0.0000	-1.3766	.0660
127.1325	.04	-.00	.0070	.0248	.0017	0.0000	-1.4157	.0672
126.9802	1.94	.02	.1039	.0278	-.0162	0.0000	-1.4566	.0662
127.1898	3.86	.04	.2034	.0345	-.0362	0.0000	-1.5097	.0667
127.0215	5.85	.06	.3146	.0486	-.0602	0.0000	-1.5757	.0669
126.9613	7.88	.09	.4291	.0710	-.0859	0.0000	-1.6627	.0665
127.2190	9.96	.11	.5482	.1040	-.1138	0.0000	-1.7138	.0670
126.6515	12.07	.13	.6416	.1456	-.1327	0.0000	-1.7347	.0656
126.6127	14.23	.16	.7264	.1957	-.1573	0.0000	-1.7765	.0659
127.0426	16.31	.18	.8097	.2494	-.1856	0.0000	-1.7637	.0660
126.9224	18.38	.21	.8435	.3033	-.2183	0.0000	-1.7666	.0658
126.8703	20.44	.23	.8482	.3436	-.2324	0.0000	-1.5034	.0668
127.4086	.00	-.00	.0052	.0264	.0021	0.0000	-1.0291	.0665

TABLE III.- Continued.

(a) Continued.

$M_\infty = 0.50$; $C_{\mu, avg} = 0.023$; $T_{t, plen} = 517^0R$

QINF PSF	ALPHA DEG	BETA DEG	CLT	CDT	CPMT	CMU	HPLEN PSI	WTFLO LBF/SEC
314.9928	.01	-.01	.0052	.0148	.0006	.0228	133.5712	.1715
315.8643	-1.90	-.03	-.0952	.0147	.0200	.0228	133.5928	.1714
315.0022	.03	-.01	.0060	.0153	.0003	.0229	133.7378	.1719
315.9168	2.00	.02	.1090	.0190	-.0197	.0228	133.7874	.1713
315.8909	4.00	.04	.2225	.0263	-.0439	.0229	133.8292	.1720
315.7574	6.08	.06	.3446	.0429	-.0712	.0229	133.8910	.1717
315.6802	8.19	.08	.4680	.0691	-.1003	.0228	133.9505	.1714
316.0139	10.35	.11	.5922	.1072	-.1283	.0229	134.2059	.1720
315.2786	12.54	.13	.6853	.1532	-.1467	.0230	134.1823	.1721
314.8467	14.78	.16	.7881	.2098	-.1780	.0231	134.3417	.1723
314.6210	16.92	.18	.8804	.2672	-.2017	.0231	134.3561	.1723
316.5587	19.07	.21	.9362	.3207	-.2137	.0230	134.5125	.1726
317.4495	21.19	.23	.9813	.3797	-.2299	.0229	134.5027	.1725
315.2974	.01	-.01	.0087	.0151	-.0004	.0232	135.0211	.1729

$M_\infty = 0.50$; $C_{\mu, avg} = 0.050$; $T_{t, plen} = 531^0R$

QINF PSF	ALPHA DEG	BETA DEG	CLT	CDT	CPMT	CMU	HPLEN PSI	WTFLO LBF/SEC
315.3700	.02	-.00	.0198	-.0006	-.0063	.0502	293.7988	.3358
316.1764	-1.92	-.03	-.0873	-.0001	.0144	.0500	293.2435	.3349
315.5332	.04	-.00	.0209	-.0008	-.0067	.0502	293.4420	.3350
315.6654	2.01	.02	.1250	.0035	-.0269	.0503	294.3156	.3356
315.5452	4.02	.04	.2394	.0113	-.0518	.0504	294.6892	.3357
316.1563	6.09	.06	.3625	.0287	-.0808	.0504	294.9946	.3360
315.1373	8.22	.09	.4962	.0568	-.1119	.0506	295.2242	.3359
314.3538	10.37	.11	.6225	.0961	-.1418	.0508	295.5269	.3362
316.8004	12.58	.13	.7397	.1475	-.1689	.0503	295.3315	.3353
315.9290	14.85	.16	.8588	.2067	-.1996	.0504	295.1832	.3350
314.1070	17.02	.19	.9702	.2719	-.2257	.0507	295.0395	.3347
315.4237	19.17	.21	1.0349	.3331	-.2391	.0505	294.7166	.3337
317.3297	21.32	.24	1.0887	.3967	-.2558	.0502	294.7197	.3334
314.9280	.01	-.00	.0221	-.0017	-.0063	.0506	294.7321	.3329

$M_\infty = 0.50$; $C_{\mu, avg} = 0$

QINF PSF	ALPHA DEG	BETA DEG	CLT	CDT	CPMT	CMU	HPLEN PSI	WTFLO LBF/SEC
315.6057	-.00	-.01	.0022	.0262	.0041	0.0000	-2.6578	.0621
317.4770	-1.92	-.03	-.0998	.0281	.0238	0.0000	-2.2903	.0638
316.2612	.04	-.01	.0024	.0276	.0036	0.0000	-2.4276	.0633
315.8571	2.00	.01	.1058	.0308	-.0159	0.0000	-2.5302	.0626
315.7099	4.01	.04	.2162	.0381	-.0391	0.0000	-2.6757	.0641
315.8691	6.07	.06	.3347	.0545	-.0655	0.0000	-2.9626	.0635
315.5892	8.18	.08	.4573	.0812	-.0941	0.0000	-3.1707	.0633
315.6578	10.35	.11	.5793	.1192	-.1222	0.0000	-3.3409	.0635
316.9375	12.52	.13	.6566	.1633	-.1374	0.0000	-3.3809	.0637
315.1503	14.75	.15	.7416	.2158	-.1669	0.0000	-3.4161	.0643
317.2178	16.85	.17	.7961	.2659	-.1953	0.0000	-3.3649	.0640
316.8759	18.90	.20	.7976	.3065	-.2087	0.0000	-2.9917	.0651
320.5601	20.98	.22	.7934	.3393	-.2074	0.0000	-2.6384	.0655
315.7812	.01	-.01	.0050	.0288	.0033	0.0000	-2.1582	.0647

TABLE III.- Continued.

(a) Concluded.

$M_\infty = 0.30$; $\alpha \approx 20.6^0$; $T_{t,plen} = 509^0 R$

QINF PSF	ALPHA DEG	BETA DEG	CLT	CDT	CPMT	CMU	HPLEN PSI	WTFLO LBF/SEC
127.4932	20.42	.22	.8226	.3322	-.2121	.0070	13.7909	.0721
126.7373	20.51	.23	1.0082	.3643	-.2275	.0256	53.7492	.0967
126.6184	20.53	.23	1.0830	.3743	-.2489	.0420	94.8220	.1363
126.6277	20.55	.23	1.1282	.3763	-.2619	.0577	133.8602	.1749
126.6651	20.56	.23	1.1689	.3769	-.2746	.0737	174.5925	.2143
126.6544	20.57	.23	1.2050	.3767	-.2857	.0913	214.8897	.2579
126.5863	20.59	.23	1.2403	.3761	-.2970	.1082	255.0916	.2991
126.3926	20.59	.23	1.2691	.3738	-.3062	.1265	294.8022	.3431
126.6330	20.55	.23	1.1257	.3746	-.2603	.0572	133.2772	.1733

TABLE III.- Continued.

(b) $\delta_{LE} = 4^0; \delta_{TE} = 0^0$

$M_\infty = 0.30;\ C_{\mu, avg} = 0.056;\ T_{t, plen} = 521^0 R$

QINF PSF	ALPHA DEG	BETA DEG	CLT	CDT	CPMT	CMU	HPLEN PSI	WTFLO LBF/SEC
124.8800	.01	-.00	.0099	.0002	-.0076	.0568	137.1857	.1667
125.6694	-1.84	-.02	-.0921	.0024	.0127	.0548	135.0340	.1623
125.5480	.04	-.00	.0070	.0003	-.0072	.0562	136.9933	.1661
125.6347	1.92	.02	.1081	.0023	-.0262	.0558	137.2063	.1648
125.3649	3.85	.04	.2090	.0093	-.0459	.0551	135.0785	.1629
125.3434	5.85	.07	.3195	.0187	-.0694	.0564	137.2480	.1663
125.4675	7.87	.09	.4366	.0361	-.0969	.0561	137.8023	.1654
125.2003	9.94	.11	.5610	.0645	-.1263	.0559	136.3966	.1647
124.9759	12.06	.14	.6784	.1037	-.1543	.0559	135.9041	.1646
125.1535	14.24	.16	.7962	.1553	-.1824	.0563	136.8327	.1657
125.2656	16.35	.18	.9122	.2156	-.2172	.0565	137.5876	.1662
125.0037	18.44	.20	1.0314	.2820	-.2496	.0562	136.8476	.1652
124.9636	20.53	.22	1.1307	.3525	-.2735	.0559	136.2494	.1643
124.9289	-.00	-.00	.0103	.0003	-.0083	.0565	137.3576	.1660

$M_\infty = 0.30;\ C_{\mu, avg} = 0.124;\ T_{t, plen} = 533^0 R$

QINF PSF	ALPHA DEG	BETA DEG	CLT	CDT	CPMT	CMU	HPLEN PSI	WTFLO LBF/SEC
125.2461	.00	.00	.0309	-.0432	-.0187	.1238	296.8163	.3260
124.3924	-1.84	-.02	-.0713	-.0430	.0022	.1245	296.5088	.3255
125.3996	.04	.00	.0336	-.0434	-.0190	.1236	296.5805	.3255
126.4639	1.92	.02	.1316	-.0395	-.0375	.1226	296.7616	.3254
125.5785	3.87	.05	.2395	-.0333	-.0587	.1236	297.1334	.3256
125.1163	5.86	.07	.3531	-.0225	-.0839	.1242	297.4211	.3259
125.0482	7.86	.09	.4787	-.0035	-.1138	.1243	297.6382	.3260
125.6439	9.95	.11	.6054	.0274	-.1431	.1235	297.4120	.3253
124.8572	12.11	.14	.7371	.0702	-.1757	.1235	295.7197	.3234
124.7289	14.28	.16	.8930	.1276	-.2190	.1248	297.7795	.3260
125.0256	16.38	.18	1.0345	.1917	-.2564	.1240	297.6039	.3244
124.9707	18.47	.21	1.1567	.2629	-.2879	.1230	294.4564	.3220
124.7425	20.58	.23	1.2728	.3417	-.3197	.1244	296.5171	.3246
125.4132	.01	.00	.0360	-.0450	-.0205	.1233	296.5402	.3229

$M_\infty = 0.30;\ C_{\mu, avg} = 0$

QINF PSF	ALPHA DEG	BETA DEG	CLT	CDT	CPMT	CMU	HPLEN PSI	WTFLO LBF/SEC
125.1701	-.00	-.00	-.0104	.0339	.0025	0.0000	-.6718	0.0000
124.4112	-1.85	-.02	-.1097	.0365	.0222	0.0000	-.5790	0.0000
125.2102	.02	-.00	-.0098	.0340	.0026	0.0000	-.6733	0.0000
125.8820	1.91	.02	.0858	.0350	-.0149	0.0000	-.7600	0.0000
125.9327	3.86	.04	.1823	.0400	-.0339	0.0000	-.8076	0.0000
125.3864	5.82	.06	.2887	.0495	-.0562	0.0000	-.8588	0.0000
125.5853	7.86	.09	.4033	.0664	-.0822	0.0000	-.9744	0.0000
125.1712	9.93	.11	.5183	.0933	-.1096	0.0000	-1.0612	0.0000
125.1391	12.06	.13	.6304	.1309	-.1358	0.0000	-1.1054	0.0000
125.2433	14.21	.16	.7292	.1771	-.1590	0.0000	-1.1380	0.0000
125.2834	16.30	.18	.8070	.2322	-.1844	0.0000	-1.1723	0.0000
125.5371	18.38	.20	.8768	.2912	-.2118	0.0000	-1.2267	0.0000
125.5076	20.44	.23	.8960	.3464	-.2395	0.0000	-1.1237	0.0000
125.6160	-.00	-.00	-.0060	.0340	-.0005	0.0000	-.4039	0.0000

TABLE III.- Continued.

(b) Concluded.

$M_\infty = 0.30$; $\alpha \approx 20.5^0$; $T_{t,plen} = 530^0 R$

QINF PSF	ALPHA DEG	BETA DEG	CLT	CDT	CPMT	CMU	HPLEN PSI	WTFLO LBF/SEC
125.6322	20.47	.23	.9631	.3502	-.2369	.0032	16.4501	.0535
124.6972	20.50	.23	1.0493	.3562	-.2508	.0256	58.6313	.0910
125.4546	20.52	.23	1.0933	.3553	-.2635	.0400	97.4433	.1256
125.0803	20.53	.23	1.1321	.3513	-.2745	.0564	136.8454	.1653
125.3365	20.55	.23	1.1718	.3493	-.2858	.0728	176.7246	.2049
125.2058	20.55	.23	1.2066	.3462	-.2964	.0901	216.8422	.2457
125.4155	20.57	.23	1.2419	.3442	-.3079	.1058	256.6389	.2824
125.1436	20.58	.23	1.2753	.3413	-.3201	.1240	297.0409	.3236
125.5353	20.54	.22	1.1370	.3510	-.2755	.0560	137.2285	.1634
125.4967	20.44	.23	.9017	.3460	-.2412	0.0000	-1.3273	.0287

TABLE III.- Continued.

(c) $\delta_{LE} = 8^0$; $\delta_{TE} = 0^0$.

$M_\infty = 0.30$; $C_{\mu, avg} = 0.057$; $T_{t, plen} = 507^0 R$

QINF PSF	ALPHA DEG	BETA DEG	CLT	CDT	CPMT	CMU	HPLEN PSI	WTFLO LBF/SEC
124.5860	.00	-.00	-.0016	.0047	-.0091	.0566	136.6714	.1683
124.4589	-1.86	-.02	-.1164	.0102	.0162	.0565	136.7314	.1679
124.9918	.02	-.00	-.0035	.0046	-.0090	.0564	136.7455	.1682
124.9184	1.91	.02	.0994	.0059	-.0293	.0564	136.7676	.1681
124.7768	3.84	.04	.1980	.0110	-.0484	.0566	136.7791	.1683
124.5028	5.83	.06	.3032	.0196	-.0688	.0567	136.8106	.1684
124.7045	7.85	.09	.4105	.0323	-.0926	.0565	136.7939	.1681
124.8714	9.92	.11	.5341	.0536	-.1209	.0565	136.8171	.1680
124.5961	12.05	.14	.6591	.0875	-.1520	.0567	136.8424	.1683
124.6442	14.22	.16	.7693	.1344	-.1751	.0567	136.8510	.1682
124.2555	16.31	.18	.8747	.1896	-.2070	.0569	136.8603	.1683
124.6295	18.42	.20	1.0132	.2596	-.2500	.0566	136.8890	.1678
124.7056	20.52	.22	1.1161	.3276	-.2744	.0567	136.9090	.1681
125.0876	.00	-.00	-.0004	.0037	-.0086	.0564	137.1717	.1676

$M_\infty = 0.30$; $C_{\mu, avg} = 0.130$; $T_{t, plen} = 532^0 R$

QINF PSF	ALPHA DEG	BETA DEG	CLT	CDT	CPMT	CMU	HPLEN PSI	WTFLO LBF/SEC
124.8741	.00	.00	.0286	-.0421	-.0232	.1295	298.1523	.3411
124.7724	-1.82	-.02	-.0849	-.0382	.0023	.1296	298.1014	.3406
124.6573	.01	.00	.0268	-.0429	-.0227	.1293	297.4718	.3391
124.9377	1.91	.02	.1338	-.0400	-.0444	.1290	297.2467	.3388
124.6759	3.85	.04	.2345	-.0345	-.0635	.1293	297.2453	.3388
124.9268	5.83	.07	.3435	-.0251	-.0863	.1296	298.1812	.3395
124.4740	7.85	.09	.4613	-.0105	-.1132	.1300	298.3961	.3392
124.6356	9.94	.11	.5940	.0143	-.1438	.1298	297.9417	.3389
124.6489	12.06	.14	.7243	.0513	-.1750	.1297	297.8961	.3384
124.6316	14.24	.16	.8559	.1007	-.2084	.1298	297.9080	.3382
124.8251	16.33	.18	.9892	.1608	-.2450	.1297	298.1667	.3379
124.1226	18.45	.20	1.1310	.2307	-.2847	.1304	298.2378	.3375
123.4933	20.55	.23	1.2573	.3090	-.3212	.1312	298.4190	.3375
124.8586	.02	.00	.0310	-.0473	-.0223	.1295	297.9213	.3357

$M_\infty = 0.30$; $C_{\mu, avg} = 0$

QINF PSF	ALPHA DEG	BETA DEG	CLT	CDT	CPMT	CMU	HPLEN PSI	WTFLO LBF/SEC
124.4908	-.00	-.00	-.0132	.0330	-.0026	0.0000	-.5619	.0646
124.4374	-1.86	-.03	-.1219	.0392	.0224	0.0000	-.4607	.0653
124.9768	.01	-.00	-.0142	.0335	-.0019	0.0000	-.5490	.0654
124.4733	1.90	.02	.0845	.0340	-.0216	0.0000	-.6312	.0652
125.0983	3.83	.04	.1815	.0381	-.0402	0.0000	-.6780	.0657
124.7497	5.81	.06	.2836	.0462	-.0602	0.0000	-.7717	.0657
124.4986	7.83	.09	.3898	.0588	-.0825	0.0000	-.8504	.0660
124.4479	9.92	.11	.5107	.0796	-.1106	0.0000	-.9435	.0654
124.3891	12.04	.13	.6237	.1118	-.1381	0.0000	-1.0328	.0650
124.7991	14.21	.16	.7300	.1587	-.1631	0.0000	-1.0879	.0639
124.8579	16.29	.18	.8150	.2098	-.1870	0.0000	-1.0923	.0639
124.2715	18.38	.20	.8894	.2704	-.2138	0.0000	-1.1482	.0649
124.5666	20.46	.23	.9482	.3325	-.2386	0.0000	-1.2207	.0647
124.5321	-.01	-.00	-.0100	.0340	-.0043	0.0000	-.4712	.0652

TABLE III.- Continued.

(c) Concluded.

$M_\infty = 0.30$; $\alpha \approx 20.5^0$; $T_{t,plen} = 535^0 R$

QINF PSF	ALPHA DEG	BETA DEG	CLT	CDT	CPMT	CMU	HPLEN PSI	WTFLO LBF/SEC
124.4497	20.47	.22	.9841	.3345	-.2455	.0038	16.1557	.0710
124.6767	20.50	.22	1.0500	.3366	-.2607	.0278	57.0497	.0987
124.6393	20.51	.22	1.0926	.3328	-.2702	.0433	96.8097	.1345
124.8155	20.52	.22	1.1319	.3288	-.2816	.0597	137.0578	.1734
124.7955	20.54	.23	1.1713	.3260	-.2938	.0760	176.9757	.2120
124.6726	20.54	.23	1.2031	.3214	-.3046	.0951	217.8874	.2568
124.6151	20.55	.23	1.2344	.3169	-.3146	.1113	258.5135	.2936
124.8248	20.56	.23	1.2614	.3115	-.3228	.1305	298.8617	.3382
124.7166	20.52	.22	1.1265	.3239	-.2781	.0596	137.1939	.1718
124.5643	20.46	.22	.9481	.3285	-.2371	0.0000	-1.3978	.0638

TABLE III.-Continued.

(d) differentially-deflected leading-edge flap; $\delta_{TE} = 0^0$

$M_\infty = 0.30$; $C_{\mu,avg} = 0.058$; $T_{t,plen} = 521^0R$

QINF PSF	ALPHA DEG	BETA DEG	CLT	CDT	CPMT	CMU	HPLEN PSI	WTFLO LBF/SEC
125.9689	-.00	-.00	-.0094	.0034	.0017	.0590	138.6436	.1747
126.4082	-1.85	-.02	-.1159	.0088	.0250	.0577	135.9817	.1721
126.4323	.03	-.00	-.0089	.0039	.0009	.0582	137.9774	.1732
126.6793	1.92	.02	.0988	.0045	-.0219	.0585	138.0498	.1744
126.7526	3.85	.04	.1995	.0097	-.0420	.0593	140.1899	.1765
126.5042	5.84	.06	.3094	.0188	-.0642	.0594	140.8168	.1763
126.6002	7.86	.09	.4168	.0352	-.0866	.0585	138.4519	.1744
127.0089	9.94	.11	.5371	.0614	-.1125	.0581	137.8430	.1738
126.9342	12.06	.14	.6648	.0983	-.1415	.0580	137.2411	.1733
125.9176	14.25	.16	.7899	.1464	-.1682	.0584	137.0841	.1731
126.3531	16.35	.18	.9084	.2034	-.1979	.0582	137.1436	.1732
125.9791	18.46	.21	1.0247	.2709	-.2263	.0586	137.3817	.1738
126.5041	20.56	.23	1.1247	.3451	-.2531	.0584	137.4892	.1738
126.2288	-.00	-.00	-.0087	.0039	.0008	.0586	137.8060	.1738

$M_\infty = 0.30$; $C_{\mu,avg} = 0.128$; $T_{t,plen} = 533^0R$

QINF PSF	ALPHA DEG	BETA DEG	CLT	CDT	CPMT	CMU	HPLEN PSI	WTFLO LBF/SEC
126.5483	.00	-.00	.0227	-.0383	-.0137	.1278	299.7120	.3412
126.3853	-1.85	-.02	-.0840	-.0356	.0102	.1283	299.8652	.3414
126.5911	.03	.00	.0234	-.0396	-.0140	.1285	300.8356	.3421
126.4027	1.92	.02	.1302	-.0378	-.0374	.1287	301.1158	.3420
126.4655	3.86	.04	.2400	-.0316	-.0596	.1286	300.7020	.3416
126.5334	5.84	.07	.3515	-.0210	-.0828	.1286	301.0976	.3417
126.3384	7.87	.09	.4665	-.0031	-.1063	.1288	301.1761	.3414
126.5759	9.95	.11	.5934	.0258	-.1338	.1281	300.0660	.3400
126.4691	12.07	.14	.7258	.0648	-.1640	.1283	300.0586	.3400
126.3357	14.27	.16	.8624	.1162	-.1964	.1286	300.2915	.3402
126.2449	16.37	.18	.9931	.1769	-.2288	.1289	300.6511	.3403
126.2634	18.47	.21	1.1320	.2519	-.2663	.1289	300.9175	.3402
125.9507	20.58	.23	1.2578	.3329	-.2994	.1292	300.9051	.3399
126.7068	.01	-.00	.0249	-.0416	-.0142	.1279	299.8101	.3381

$M_\infty = 0.30$; $C_{\mu,avg} = 0$

QINF PSF	ALPHA DEG	BETA DEG	CLT	CDT	CPMT	CMU	HPLEN PSI	WTFLO LBF/SEC
126.5813	-.01	-.01	-.0219	.0343	.0087	0.0000	-.9092	0.0000
126.3424	-1.86	-.03	-.1286	.0404	.0322	0.0000	-.7807	0.0000
126.5175	.02	-.00	-.0218	.0358	.0084	0.0000	-.8772	0.0000
126.4359	1.91	.02	.0834	.0359	-.0139	0.0000	-.9657	0.0000
126.5280	3.84	.04	.1814	.0401	-.0331	0.0000	-1.0587	0.0000
126.2235	5.83	.06	.2821	.0490	-.0528	0.0000	-1.1229	0.0000
126.0951	7.85	.09	.3874	.0640	-.0730	0.0000	-1.2308	0.0000
125.8708	9.92	.11	.4946	.0880	-.0947	0.0000	-1.3127	0.0000
126.6026	12.05	.13	.6099	.1229	-.1207	0.0000	-1.4243	0.0000
126.7562	14.23	.16	.7203	.1674	-.1443	0.0000	-1.4589	0.0000
126.4864	16.31	.18	.8243	.2207	-.1705	0.0000	-1.4450	0.0000
126.4798	18.40	.21	.9112	.2844	-.2034	0.0000	-1.5243	0.0000
126.2126	20.44	.22	.9561	.3576	-.2641	0.0000	-1.5671	0.0000
126.3692	-.01	-.00	-.0204	.0370	.0069	0.0000	-.8796	0.0000

TABLE III.- Continued.

(e) $\delta_{LE} = 8^0$; $\delta_{TE} = 10^0$

$M_\infty = 0.30$; $C_{\mu,avg} = 0.057$; $T_{t,plen} = 507^0R$

QINF PSF	ALPHA DEG	BETA DEG	CLT	CDT	CPMT	CMU	HPLEN PSI	WTFLO LBF/SEC
128.3415	.02	-.00	.1699	.0082	-.1149	.0571	139.1252	.1746
128.0838	-1.84	-.02	.0657	.0072	-.0935	.0573	139.0341	.1749
128.4417	.04	-.00	.1697	.0082	-.1147	.0570	139.0494	.1745
128.6406	1.93	.02	.2715	.0140	-.1346	.0569	139.0313	.1746
128.4763	3.86	.04	.3720	.0229	-.1542	.0570	139.0210	.1746
128.4348	5.83	.07	.4744	.0355	-.1746	.0570	138.9737	.1744
128.1382	7.88	.09	.5946	.0544	-.2020	.0572	138.9933	.1747
128.9769	9.94	.11	.7189	.0834	-.2339	.0570	138.9984	.1752
128.2224	12.06	.14	.8458	.1259	-.2665	.0571	138.8863	.1746
127.9804	14.25	.16	.9541	.1784	-.2912	.0572	138.9604	.1745
128.1487	16.33	.18	1.0487	.2433	-.3165	.0571	138.8165	.1743
127.2481	18.43	.20	1.1728	.3164	-.3558	.0576	138.8725	.1746
127.8240	20.53	.22	1.2792	.3913	-.3817	.0573	138.8123	.1746
128.7482	.02	-.00	.1744	.0088	-.1167	.0569	139.0961	.1745

$M_\infty = 0.30$; $C_{\mu,avg} = 0.127$; $T_{t,plen} = 522^0R$

QINF PSF	ALPHA DEG	BETA DEG	CLT	CDT	CPMT	CMU	HPLEN PSI	WTFLO LBF/SEC
128.2205	.02	.00	.2089	-.0335	-.1360	.1274	304.1055	.3472
128.1884	-1.82	-.02	.1004	-.0360	-.1134	.1275	304.4200	.3471
128.4529	.05	.00	.2101	-.0337	-.1362	.1270	304.0302	.3463
128.3834	1.94	.02	.3141	-.0266	-.1560	.1268	303.4985	.3456
128.2136	3.87	.04	.4191	-.0164	-.1770	.1270	303.5539	.3455
128.3672	5.86	.07	.5277	-.0019	-.1994	.1267	303.2542	.3450
128.1789	7.88	.09	.6520	.0191	-.2293	.1270	303.4038	.3452
127.9612	9.97	.11	.7824	.0513	-.2632	.1272	303.3782	.3450
128.3219	12.09	.14	.9131	.0971	-.2974	.1270	303.6079	.3452
128.9789	14.27	.16	1.0512	.1566	-.3330	.1262	303.4635	.3448
127.8716	16.35	.18	1.1816	.2240	-.3685	.1275	303.6263	.3451
127.9689	18.47	.20	1.3210	.3039	-.4105	.1273	303.5619	.3447
127.8407	20.58	.23	1.4516	.3886	-.4479	.1276	303.8039	.3449
128.1279	.03	-.00	.2148	-.0356	-.1369	.1276	304.3983	.3451

$M_\infty = 0.30$; $C_{\mu,avg} = 0$

QINF PSF	ALPHA DEG	BETA DEG	CLT	CDT	CPMT	CMU	HPLEN PSI	WTFLO LBF/SEC
128.2663	.03	-.01	.1659	.0391	-.1105	0.0000	-.8127	.0377
128.3719	-1.84	-.03	.0545	.0398	-.0857	0.0000	-.6824	.0408
128.8607	.04	-.01	.1586	.0398	-.1072	0.0000	-.7880	.0434
128.3691	1.93	.02	.2545	.0446	-.1260	0.0000	-.8894	.0418
128.0057	3.87	.04	.3564	.0526	-.1461	0.0000	-.9271	.0459
127.6289	5.84	.06	.4606	.0646	-.1670	0.0000	-1.0533	.0424
128.1832	7.87	.09	.5692	.0822	-.1897	0.0000	-1.1526	.0430
128.6627	9.93	.11	.6823	.1087	-.2155	0.0000	-1.2541	.0420
128.6626	12.07	.13	.7963	.1479	-.2420	0.0000	-1.3268	.0426
128.0562	14.23	.16	.8978	.1958	-.2638	0.0000	-1.3358	.0435
127.6167	16.31	.18	.9528	.2571	-.2783	0.0000	-1.3497	.0424
128.6706	18.39	.20	1.0143	.3215	-.3013	0.0000	-1.4334	.0446
128.5851	20.45	.23	1.0679	.3867	-.3251	0.0000	-1.5211	.0419
128.0562	.02	-.01	.1608	.0411	-.1095	0.0000	-.7229	.0427

TABLE III.- Continued.

(e) Concluded.

$M_\infty = 0.30$; $\alpha \approx 20.5^0$; $T_{t,plen} = 521^0 R$

QINF PSF	ALPHA DEG	BETA DEG	CLT	CDT	CPMT	CMU	HPLEN PSI	WTFLO LBF/SEC
127.9192	20.47	.22	1.1128	.3868	-.3335	.0058	18.7844	.0565
128.1276	20.50	.22	1.1864	.3930	-.3537	.0244	58.0224	.0907
128.1343	20.51	.22	1.2366	.3929	-.3698	.0402	98.6271	.1301
128.2705	20.53	.22	1.2861	.3921	-.3848	.0576	140.2557	.1745
128.5270	20.55	.22	1.3296	.3909	-.4007	.0741	180.9391	.2159
128.0114	20.56	.22	1.3761	.3904	-.4170	.0922	221.9147	.2595
127.9178	20.57	.22	1.4174	.3891	-.4331	.1096	262.9865	.3011
128.5323	20.58	.23	1.4492	.3859	-.4451	.1271	303.9976	.3441
128.5174	20.53	.22	1.2827	.3883	-.3819	.0567	139.5578	.1711
128.7524	20.45	.23	1.0685	.3844	-.3250	0.0000	-1.6312	.0361

TABLE III.- Continued.

(f) $\delta_{LE} = 0^0$; $\delta_{TE} = 10^0$

$M_\infty = 0.30$; $C_{\mu,avg} = 0.058$; $T_{t,plen} = 515^0 R$

QINF PSF	ALPHA DEG	BETA DEG	CLT	CDT	CPMT	CMU	HPLEN PSI	WTFLO LBF/SEC
127.9874	.04	-.00	.1933	.0101	-.1114	.0588	139.0704	.1781
127.8218	-1.80	-.02	.0958	.0063	-.0943	.0589	139.5922	.1782
128.2331	.07	-.00	.1892	.0104	-.1113	.0585	139.0994	.1776
127.9472	1.95	.02	.2894	.0178	-.1300	.0586	138.7490	.1777
127.8924	3.90	.04	.3981	.0299	-.1536	.0584	138.6457	.1771
127.8630	5.88	.07	.5210	.0508	-.1818	.0584	138.5241	.1769
128.2035	7.92	.09	.6442	.0812	-.2114	.0584	138.4576	.1774
128.5948	9.98	.11	.7441	.1209	-.2291	.0581	138.4918	.1772
128.0086	12.10	.14	.8413	.1688	-.2523	.0584	138.4822	.1771
128.4039	14.28	.16	.9765	.2340	-.2950	.0582	138.4732	.1772
127.1816	16.39	.18	1.1183	.3054	-.3337	.0588	138.5039	.1772
127.3352	18.49	.20	1.2159	.3757	-.3536	.0587	138.5422	.1772
127.1415	20.58	.23	1.2920	.4471	-.3700	.0589	138.4576	.1774
128.0633	.04	-.00	.1963	.0106	-.1132	.0584	138.7469	.1773

$M_\infty = 0.30$; $C_{\mu,avg} = 0.128$; $T_{t,plen} = 527^0 R$

QINF PSF	ALPHA DEG	BETA DEG	CLT	CDT	CPMT	CMU	HPLEN PSI	WTFLO LBF/SEC
127.9805	.04	.00	.2285	-.0307	-.1319	.1273	302.0499	.3456
127.5436	-1.81	-.02	.1289	-.0363	-.1131	.1277	301.8614	.3453
128.1074	.08	.00	.2267	-.0313	-.1313	.1273	302.0631	.3454
128.2221	1.96	.02	.3334	-.0228	-.1524	.1273	302.3423	.3455
127.7959	3.91	.05	.4533	-.0093	-.1797	.1278	302.6719	.3455
127.9269	5.89	.07	.5740	.0128	-.2081	.1276	302.3403	.3450
128.3610	7.92	.09	.7037	.0463	-.2395	.1272	302.3458	.3449
127.6785	10.00	.11	.8327	.0913	-.2710	.1279	302.2946	.3447
127.4556	12.12	.14	.9731	.1475	-.3103	.1283	302.3084	.3448
128.0258	14.34	.16	1.1378	.2201	-.3567	.1276	302.4188	.3444
127.3873	16.42	.18	1.2771	.2945	-.3919	.1283	302.5172	.3444
127.4181	18.54	.21	1.3821	.3722	-.4147	.1283	302.6258	.3444
127.6492	20.63	.23	1.4548	.4488	-.4280	.1282	302.9308	.3445
128.2530	.05	-.00	.2316	-.0342	-.1327	.1276	302.9630	.3438

$M_\infty = 0.30$; $C_{\mu,avg} = 0$

QINF PSF	ALPHA DEG	BETA DEG	CLT	CDT	CPMT	CMU	HPLEN PSI	WTFLO LBF/SEC
127.8618	.04	-.01	.1762	.0412	-.1027	0.0000	-1.0296	0.0000
128.2210	-1.82	-.03	.0825	.0385	-.0844	0.0000	-.9465	0.0000
127.7843	.07	-.00	.1766	.0416	-.1023	0.0000	-1.0323	0.0000
128.2410	1.96	.02	.2725	.0480	-.1200	0.0000	-1.1400	0.0000
127.9004	3.88	.04	.3766	.0590	-.1415	0.0000	-1.1919	0.0000
127.9256	5.87	.06	.4901	.0783	-.1658	0.0000	-1.3020	0.0000
128.0165	7.90	.09	.6031	.1069	-.1906	0.0000	-1.3852	0.0000
127.2203	9.96	.11	.6986	.1449	-.2079	0.0000	-1.4852	0.0000
127.5862	12.07	.13	.7759	.1896	-.2234	0.0000	-1.5352	0.0000
128.7214	14.25	.16	.8608	.2430	-.2460	0.0000	-1.5686	0.0000
129.2995	16.33	.18	.9350	.3008	-.2722	0.0000	-1.6020	0.0000
127.7091	18.39	.20	.9802	.3605	-.3005	0.0000	-1.6711	0.0000
127.8827	20.43	.23	.9589	.3982	-.3037	0.0000	-1.5155	0.0000
128.2301	.03	-.00	.1798	.0424	-.1050	0.0000	-.9790	0.0000

TABLE III.- Continued.

(f) Concluded.

$M_\infty = 0.30$; $\alpha \approx 20.6^0$; $T_{t,plen} = 524^0 R$

QINF PSF	ALPHA DEG	BETA DEG	CLT	CDT	CPMT	CMU	HPLEN PSI	WTFLO LBF/SEC
128.0498	20.47	.23	1.0342	.4108	-.3135	.0025	16.3214	.0662
127.5449	20.53	.23	1.1686	.4330	-.3318	.0270	58.5553	.0994
128.0407	20.56	.23	1.2381	.4418	-.3535	.0425	98.7366	.1369
127.8430	20.57	.23	1.2914	.4453	-.3714	.0588	139.2730	.1773
128.0073	20.59	.23	1.3361	.4475	-.3869	.0743	178.7604	.2151
127.9753	20.60	.23	1.3803	.4489	-.4020	.0925	220.4381	.2592
127.7068	20.61	.23	1.4198	.4495	-.4150	.1101	261.2609	.3009
128.4747	20.63	.23	1.4552	.4490	-.4281	.1279	303.3574	.3450
127.8978	20.58	.23	1.2901	.4415	-.3683	.0585	140.0516	.1750
127.7414	20.43	.23	.9576	.3942	-.3021	0.0000	-1.6187	.0557

TABLE III.- Continued.

(g) $\delta_{LE} = 0^{0}$; $\delta_{TE} = 20^{0}$

$M_{\infty} = 0.30$; $C_{\mu, avg} = 0.058$; $T_{t, plen} = 510^{0}R$

QINF PSF	ALPHA DEG	BETA DEG	CLT	CDT	CPMT	CMU	HPLEN PSI	WTFLO LBF/SEC
127.2801	.08	-.00	.3717	.0306	-.2193	.0578	138.5010	.1752
127.1728	-1.73	-.02	.2811	.0222	-.2047	.0580	138.5973	.1756
127.1622	.12	-.00	.3693	.0307	-.2198	.0580	138.5942	.1754
127.2075	2.00	.02	.4672	.0424	-.2373	.0577	138.2171	.1746
126.9843	3.94	.04	.5825	.0610	-.2632	.0577	137.9170	.1744
127.0337	5.93	.07	.7085	.0889	-.2936	.0577	137.8845	.1746
126.7117	7.95	.09	.8186	.1245	-.3193	.0579	137.8222	.1748
127.4000	10.02	.11	.9050	.1692	-.3282	.0575	137.8184	.1744
126.8440	12.14	.13	.9944	.2234	-.3506	.0578	137.8561	.1745
127.0490	14.32	.16	1.1285	.2952	-.3951	.0580	137.8607	.1753
126.9413	16.43	.18	1.2736	.3748	-.4364	.0580	137.8569	.1751
127.0086	18.53	.21	1.3543	.4464	-.4501	.0580	138.0597	.1751
127.1179	20.62	.23	1.4109	.5166	-.4585	.0581	138.1490	.1753
127.1652	.09	-.00	.3706	.0291	-.2195	.0576	137.8778	.1740

$M_{\infty} = 0.30$; $C_{\mu, avg} = 0.127$; $T_{t, plen} = 530^{0}R$

QINF PSF	ALPHA DEG	BETA DEG	CLT	CDT	CPMT	CMU	HPLEN PSI	WTFLO LBF/SEC
127.0793	.12	.00	.4287	-.0110	-.2517	.1271	299.6087	.3422
126.9657	-1.75	-.02	.3262	-.0220	-.2325	.1274	299.9675	.3421
127.6126	.12	.00	.4268	-.0117	-.2513	.1267	300.2063	.3417
127.2945	2.01	.02	.5341	.0025	-.2750	.1269	300.0058	.3412
127.1686	3.95	.05	.6601	.0245	-.3059	.1272	300.1136	.3412
127.1832	5.94	.07	.7826	.0548	-.3350	.1271	300.0473	.3408
127.6648	7.96	.09	.9082	.0957	-.3633	.1266	299.7803	.3404
126.8921	10.04	.11	1.0264	.1485	-.3922	.1274	299.9799	.3403
126.9857	12.17	.13	1.1770	.2146	-.4365	.1273	300.0703	.3400
127.1206	14.38	.16	1.3430	.2957	-.4860	.1270	299.7356	.3391
126.6424	16.48	.18	1.4718	.3768	-.5193	.1274	299.5727	.3386
126.6478	18.57	.21	1.5622	.4579	-.5345	.1274	299.4726	.3384
127.4520	20.66	.23	1.6111	.5343	-.5377	.1268	299.9115	.3380
127.7221	.09	.00	.4321	-.0153	-.2523	.1264	300.0280	.3368

$M_{\infty} = 0.30$; $C_{\mu, avg} = 0$

QINF PSF	ALPHA DEG	BETA DEG	CLT	CDT	CPMT	CMU	HPLEN PSI	WTFLO LBF/SEC
127.9229	.08	-.00	.3587	.0588	-.2107	0.0000	-1.1862	0.0000
126.7318	-1.78	-.03	.2612	.0515	-.1925	0.0000	-1.0889	0.0000
126.9254	.11	-.00	.3545	.0596	-.2085	0.0000	-1.2094	0.0000
127.1910	2.00	.02	.4476	.0702	-.2252	0.0000	-1.3041	0.0000
127.5140	3.92	.04	.5538	.0868	-.2471	0.0000	-1.3897	0.0000
127.1466	5.92	.06	.6706	.1128	-.2734	0.0000	-1.5045	0.0000
127.3521	7.93	.09	.7845	.1484	-.2979	0.0000	-1.6160	0.0000
127.3936	10.01	.11	.8567	.1895	-.3035	0.0000	-1.6776	0.0000
127.5552	12.12	.13	.9144	.2368	-.3115	0.0000	-1.7064	0.0000
126.6895	14.27	.16	.9933	.2949	-.3321	0.0000	-1.6884	0.0000
127.3907	16.36	.18	1.0616	.3576	-.3562	0.0000	-1.7316	0.0000
127.2358	18.41	.20	1.0984	.4197	-.3826	0.0000	-1.8249	0.0000
126.9351	20.46	.23	1.0698	.4567	-.3772	0.0000	-1.6591	0.0000
127.3733	.07	-.00	.3614	.0604	-.2125	0.0000	-1.1314	0.0000

TABLE III.- Concluded.

(g) Concluded.

$M_\infty = 0.30$; $\alpha \approx 20.6^0$; $T_{t,plen} = 527^0 R$

QINF PSF	ALPHA DEG	BETA DEG	CLT	CDT	CPMT	CMU	HPLEN PSI	WTFLO LBF/SEC
127.1163	20.49	.23	1.1584	.4766	-.3967	.0028	16.3639	.0607
127.1475	20.55	.23	1.2876	.5008	-.4181	.0253	57.3899	.0931
127.5002	20.58	.23	1.3597	.5110	-.4416	.0410	97.2719	.1315
127.9266	20.60	.23	1.4185	.5181	-.4633	.0573	137.3839	.1724
126.7601	20.61	.23	1.4809	.5254	-.4865	.0749	178.5465	.2137
127.6537	20.63	.23	1.5246	.5289	-.5046	.0913	219.0126	.2542
127.5254	20.64	.23	1.5686	.5320	-.5218	.1083	260.1321	.2942
127.2702	20.65	.23	1.6089	.5338	-.5370	.1264	299.0018	.3367
127.1858	20.46	.23	1.0662	.4508	-.3747	0.0000	-1.7500	0.0000

TABLE IV.- SPANWISE BLOWING ON THE RIGHT WING ONLY OF THE 44° SWEPT TRAPEZOIDAL WING CONFIGURATION.

$M_\infty = 0.30$; $C_{\mu,avg} = 0.034$; $T_{t,plen} = 514^\circ R$

QINF PSF	ALPHA DEG	BETA DEG	CLT	CDT	CPMT	CRMT	CYMT	CSFT	CMU	HPLEN PSI	WTFLO LBF/SEC
125.4621	.00	.01	-.0012	.0133	.0032	.0024	-.0012	-.0075	.0339	136.8865	.1008
125.4474	-1.85	-.01	-.0958	.0145	.0208	.0019	-.0014	-.0074	.0345	137.3924	.1024
125.1389	.03	.01	.0004	.0133	.0030	.0020	-.0013	-.0071	.0340	136.8826	.1008
125.5716	1.91	.03	.0985	.0160	-.0150	.0025	-.0012	-.0074	.0340	137.5594	.1012
125.3913	3.85	.05	.2022	.0225	-.0361	.0026	-.0012	-.0075	.0340	136.8876	.1010
125.4312	5.83	.07	.3162	.0368	-.0614	.0022	-.0006	-.0082	.0341	136.8700	.1015
125.2522	7.85	.10	.4375	.0611	-.0887	.0019	-.0004	-.0090	.0341	136.7894	.1012
125.6502	9.94	.12	.5494	.0951	-.1127	.0006	.0002	-.0096	.0340	136.7467	.1014
125.6714	12.05	.14	.6453	.1359	-.1355	.0003	.0005	-.0099	.0340	136.7135	.1014
125.6567	14.23	.16	.7541	.1878	-.1671	-.0034	.0028	-.0113	.0341	136.6873	.1016
125.2600	16.31	.17	.8686	.2480	-.2032	-.0134	.0078	-.0124	.0342	136.6247	.1016
124.8591	18.40	.18	.9437	.3083	-.2341	-.0212	.0177	-.0210	.0343	136.6438	.1014
125.2665	20.46	.19	.9981	.3648	-.2555	-.0239	.0255	-.0202	.0343	136.9126	.1018
125.6859	.00	.01	.0039	.0138	.0025	.0018	-.0012	-.0074	.0342	137.4149	.1017

$M_\infty = 0.30$; $C_{\mu,avg} = 0.067$; $T_{t,plen} = 513^\circ R$

QINF PSF	ALPHA DEG	BETA DEG	CLT	CDT	CPMT	CRMT	CYMT	CSFT	CMU	HPLEN PSI	WTFLO LBF/SEC
125.5948	.01	.03	.0116	-.0062	-.0037	.0018	-.0027	-.0278	.0675	298.3566	.1815
125.3570	-1.85	.01	-.0854	-.0057	.0146	.0013	-.0030	-.0279	.0677	298.4375	.1816
125.2915	.03	.03	.0150	-.0066	-.0043	.0014	-.0026	-.0281	.0673	297.5147	.1804
125.7764	1.91	.05	.1121	-.0035	-.0225	.0019	-.0021	-.0276	.0675	297.7004	.1817
125.5813	3.85	.07	.2176	.0035	-.0444	.0019	-.0019	-.0291	.0677	299.3844	.1818
124.8693	5.84	.09	.3324	.0178	-.0708	.0011	-.0010	-.0301	.0675	297.4548	.1802
125.3995	7.86	.12	.4573	.0433	-.0989	.0000	-.0003	-.0310	.0674	296.5921	.1808
125.6346	9.94	.14	.5791	.0793	-.1272	-.0045	.0012	-.0321	.0675	297.8960	.1812
125.1484	12.06	.15	.6966	.1238	-.1571	-.0102	.0040	-.0337	.0677	298.7481	.1808
125.5958	14.24	.17	.8173	.1793	-.1910	-.0197	.0077	-.0324	.0670	296.1899	.1797
125.0481	16.32	.18	.9264	.2393	-.2229	-.0288	.0131	-.0329	.0678	297.6808	.1810
125.4074	18.40	.18	.9949	.2991	-.2522	-.0370	.0248	-.0405	.0677	298.5735	.1812
125.6905	20.48	.18	1.0506	.3575	-.2734	-.0421	.0360	-.0391	.0677	299.3645	.1814
125.1845	.01	.03	.0152	-.0078	-.0039	.0017	-.0024	-.0276	.0676	297.1476	.1804

$M_\infty = 0.30$; $C_{\mu,avg} = 0$

QINF PSF	ALPHA DEG	BETA DEG	CLT	CDT	CPMT	CRMT	CYMT	CSFT	CMU	HPLEN PSI	WTFLO LBF/SEC
124.9611	20.40	.23	.8485	.3474	-.2312	.0028	-.0019	.0009	0.0000	-1.2761	0.0000
125.8761	.00	-.00	-.0030	.0310	.0054	.0007	.0008	.0035	0.0000	-.8665	0.0000
125.6825	-1.85	-.02	-.0981	.0323	.0228	.0002	.0007	.0033	0.0000	-.7885	0.0000
125.6304	.03	-.00	-.0028	.0310	.0053	.0007	.0009	.0031	0.0000	-.8528	0.0000
125.3553	1.91	.02	.0910	.0329	-.0120	.0010	.0011	.0029	0.0000	-.9284	0.0000
125.5517	3.85	.04	.1963	.0391	-.0334	.0009	.0009	.0026	0.0000	-.9994	0.0000
124.7074	5.82	.06	.3088	.0531	-.0580	.0007	.0011	.0017	0.0000	-1.0718	0.0000
125.3993	7.85	.09	.4230	.0767	-.0836	.0013	.0008	.0013	0.0000	-1.1953	0.0000
125.4700	9.93	.11	.5327	.1100	-.1071	.0003	.0007	.0016	0.0000	-1.2801	0.0000
125.1762	12.04	.13	.6283	.1511	-.1306	.0013	.0006	.0015	0.0000	-1.3340	0.0000
125.1320	14.20	.16	.7179	.1984	-.1557	.0007	.0006	.0017	0.0000	-1.3940	0.0000
125.8692	16.29	.18	.8010	.2519	-.1830	.0004	.0007	.0017	0.0000	-1.4491	0.0000
125.6662	18.35	.21	.8441	.3070	-.2160	.0016	-.0003	.0005	0.0000	-1.4722	0.0000
125.1961	20.40	.23	.8465	.3464	-.2303	.0032	-.0028	.0009	0.0000	-1.2395	0.0000
126.0843	-.01	-.00	-.0025	.0311	.0049	.0006	.0008	.0035	0.0000	-.8657	0.0000

TABLE V.- SPANWISE BLOWING ON THE 44^{0} SWEPT TRAPEZOIDAL WING - HORIZONTAL TAIL CONFIGURATION; $\delta_{LE} = \delta_{TE} = 0^{0}$.

$M_{\infty} = 0.30$; $C_{\mu, avg} = 0.06$; $T_{t, plen} = 513^{0}R$

QINF PSF	ALPHA DEG	BETA DEG	CLT	CDT	CPMT	CRMT	CYMT	CSFT	CMU	HPLEN PSI	WTFLO LBF/SEC
124.7715	-.00	-.00	.0085	.0021	-.0040	.0010	.0002	.0026	.0605	137.4561	.1786
124.6297	-1.83	-.02	-.0959	.0031	.0276	.0008	.0001	.0027	.0608	138.1303	.1793
125.0745	.04	-.00	.0122	.0021	-.0051	.0012	.0001	.0023	.0609	138.2485	.1802
124.9128	1.93	.02	.1174	.0058	-.0350	.0013	.0003	.0010	.0608	138.2842	.1798
124.6737	3.85	.04	.2289	.0140	-.0704	.0012	.0007	-.0002	.0608	138.2927	.1794
124.8085	5.83	.07	.3601	.0297	-.1167	.0014	.0013	-.0028	.0608	138.3179	.1797
125.3694	7.85	.09	.4981	.0569	-.1638	.0015	.0014	-.0035	.0605	138.3083	.1796
124.8139	9.92	.11	.6230	.0939	-.2080	.0011	.0015	-.0043	.0608	138.2879	.1797
124.6269	12.03	.14	.7447	.1407	-.2572	.0021	.0012	-.0040	.0610	138.2385	.1799
124.7203	14.21	.16	.8854	.2028	-.3086	-.0007	.0020	-.0036	.0609	138.2205	.1800
124.7322	16.31	.18	1.0483	.2771	-.3809	-.0014	.0020	-.0027	.0609	138.2074	.1798
125.4454	18.39	.20	1.1814	.3551	-.4486	-.0003	.0015	-.0033	.0605	138.1763	.1797
124.5734	20.48	.23	1.2979	.4390	-.5188	.0022	.0007	-.0033	.0609	138.1292	.1796
124.5255	.01	-.00	.0146	.0021	-.0060	.0009	.0009	-.0001	.0609	138.2594	.1796

$M_{\infty} = 0.30$; $C_{\mu, avg} = 0.13$; $T_{t, plen} = 520^{0}R$

QINF PSF	ALPHA DEG	BETA DEG	CLT	CDT	CPMT	CRMT	CYMT	CSFT	CMU	HPLEN PSI	WTFLO LBF/SEC
124.5282	.02	.00	.0169	-.0398	.0115	.0022	.0005	-.0015	.1299	297.2741	.3447
124.6954	-1.82	-.02	-.0949	-.0396	.0529	.0018	.0003	-.0019	.1302	298.5660	.3454
124.9879	.06	.00	.0209	-.0403	.0100	.0023	.0004	-.0020	.1288	296.2380	.3424
125.1638	1.93	.02	.1387	-.0369	-.0300	.0023	.0007	-.0017	.1294	297.4557	.3439
125.1786	3.86	.04	.2555	-.0282	-.0702	.0026	.0006	-.0021	.1296	297.7556	.3442
125.3080	5.84	.07	.3882	-.0116	-.1146	.0028	.0011	-.0037	.1296	298.1601	.3444
124.9314	7.87	.09	.5310	.0173	-.1591	.0027	.0009	-.0045	.1300	298.3234	.3444
124.4144	9.94	.11	.6739	.0573	-.2097	-.0007	.0018	-.0051	.1308	298.5163	.3448
124.3358	12.07	.14	.8325	.1108	-.2688	-.0020	.0018	-.0047	.1309	298.6737	.3446
124.6573	14.25	.16	1.0086	.1803	-.3438	-.0042	.0020	-.0042	.1305	298.6281	.3444
124.4638	16.34	.18	1.1722	.2579	-.4202	-.0038	.0021	-.0039	.1308	298.7739	.3445
124.8577	18.44	.21	1.3145	.3422	-.4907	-.0016	.0012	-.0043	.1305	298.8761	.3444
124.6747	20.52	.23	1.4304	.4293	-.5566	.0009	.0005	-.0044	.1308	298.9141	.3445
124.6885	.02	.00	.0243	-.0434	.0105	.0019	.0005	-.0008	.1287	295.8321	.3389

$M_{\infty} = 0.30$; $C_{\mu, avg} = 0$

QINF PSF	ALPHA DEG	BETA DEG	CLT	CDT	CPMT	CRMT	CYMT	CSFT	CMU	HPLEN PSI	WTFLO LBF/SEC
124.6645	.01	-.00	-.0030	.0327	.0055	.0005	.0011	.0038	0.0000	-.5903	.0702
124.6281	-1.84	-.03	-.1041	.0349	.0325	.0003	.0010	.0037	0.0000	-.4662	.0707
124.3048	.03	-.00	-.0014	.0334	.0051	.0003	.0011	.0038	0.0000	-.5690	.0710
125.2533	1.91	.02	.1009	.0362	-.0232	.0005	.0012	.0039	0.0000	-.6660	.0716
125.1680	3.85	.04	.2157	.0439	-.0604	.0007	.0013	.0032	0.0000	-.7305	.0731
124.8248	5.83	.06	.3398	.0586	-.1048	.0007	.0016	.0016	0.0000	-.8046	.0727
125.2561	7.85	.09	.4726	.0852	-.1525	.0008	.0015	.0002	0.0000	-.9225	.0740
124.8488	9.91	.11	.5911	.1208	-.1958	.0003	.0013	.0003	0.0000	-1.0237	.0740
124.7608	12.02	.13	.7026	.1667	-.2429	.0011	.0010	.0005	0.0000	-1.0728	.0743
124.5457	14.18	.16	.8159	.2227	-.3009	.0007	.0012	.0001	0.0000	-1.1086	.0758
125.0415	16.24	.18	.9205	.2862	-.3640	.0008	.0013	-.0001	0.0000	-1.1498	.0754
125.3592	18.32	.20	1.0004	.3547	-.4287	.0009	.0016	-.0017	0.0000	-1.2486	.0763
125.3178	20.36	.23	1.0409	.4155	-.4905	.0017	.0009	-.0009	0.0000	-1.1657	.0753
125.3394	.01	-.00	.0051	.0342	.0023	.0002	.0015	.0022	0.0000	-.5477	.0750

TABLE VI.- SPANWISE BLOWING ON THE 44° SWEPT TRAPEZOIDAL WING - VERTICAL TAIL CONFIGURATION IN SIDESLIP; $\delta_{LE} = \delta_{TE} = 0^{\circ}$.

(a) $\beta \approx 0^{\circ}$

$M_{\infty} = 0.30$; $C_{\mu,avg} = 0.059$; $T_{t,plen} = 513^{\circ}R$

QINF PSF	ALPHA DEG	BETA DEG	CLT	CDT	CPMT	CRMT	CYMT	CSFT	CMU	HPLEN PSI	WTFLO LBF/SEC
125.0477	.00	-.00	.0117	.0026	-.0079	.0023	-.0040	.0071	.0592	138.2839	.1748
125.1882	-1.85	-.02	-.0871	.0034	.0101	.0022	-.0038	.0069	.0590	138.5265	.1746
125.3323	.04	.00	.0123	.0026	-.0082	.0024	-.0038	.0068	.0593	138.7939	.1754
125.3229	1.92	.02	.1107	.0063	-.0265	.0023	-.0035	.0059	.0587	138.3312	.1741
125.1720	3.85	.04	.2155	.0139	-.0479	.0024	-.0032	.0046	.0586	136.9755	.1737
125.2466	5.84	.07	.3298	.0280	-.0738	.0024	-.0026	.0029	.0590	137.6863	.1749
124.7125	7.87	.09	.4564	.0533	-.1029	.0019	-.0025	.0023	.0585	136.2895	.1730
124.3878	9.95	.11	.5721	.0867	-.1280	.0009	-.0025	.0021	.0587	136.1214	.1732
124.4706	12.06	.14	.6706	.1276	-.1514	.0017	-.0024	.0022	.0588	136.1663	.1736
124.6001	14.25	.16	.8067	.1856	-.1925	-.0017	-.0012	.0015	.0589	136.5392	.1740
124.9981	16.35	.18	.9412	.2496	-.2288	-.0016	-.0013	.0017	.0582	135.8343	.1729
124.7951	18.44	.21	1.0434	.3138	-.2512	-.0009	-.0018	.0018	.0583	135.6417	.1728
125.6083	20.54	.23	1.1331	.3838	-.2722	.0015	-.0026	.0024	.0585	137.0329	.1743
124.7419	.00	-.00	.0108	.0046	-.0079	.0023	-.0036	.0064	.0591	137.0556	.1750

$M_{\infty} = 0.30$; $C_{\mu,avg} = 0.729$; $T_{t,plen} = 512^{\circ}R$

QINF PSF	ALPHA DEG	BETA DEG	CLT	CDT	CPMT	CRMT	CYMT	CSFT	CMU	HPLEN PSI	WTFLO LBF/SEC
125.0039	.01	.00	.0384	-.0343	-.0222	.0029	-.0039	.0041	.1284	297.7664	.3448
125.2417	-1.83	-.02	-.0602	-.0345	-.0037	.0030	-.0040	.0045	.1286	298.7950	.3459
125.1656	.04	.00	.0403	-.0349	-.0226	.0029	-.0039	.0041	.1291	299.4471	.3467
125.0652	1.93	.02	.1419	-.0306	-.0418	.0031	-.0036	.0036	.1287	298.8540	.3452
124.8194	3.86	.05	.2498	-.0229	-.0641	.0031	-.0035	.0030	.1286	297.4909	.3441
125.0985	5.84	.07	.3717	-.0075	-.0931	.0027	-.0032	.0016	.1280	296.9292	.3430
124.4374	7.86	.09	.5040	.0191	-.1235	.0021	-.0033	.0019	.1287	296.9293	.3428
124.0578	9.96	.11	.6347	.0557	-.1550	-.0016	-.0025	.0008	.1291	296.8769	.3426
124.9328	12.09	.14	.7732	.1047	-.1914	-.0025	-.0022	.0008	.1282	296.9068	.3424
124.6776	14.29	.16	.9302	.1666	-.2344	-.0047	-.0012	.0005	.1286	297.0049	.3424
124.9768	16.39	.18	1.0676	.2334	-.2687	-.0032	-.0013	.0004	.1285	297.2143	.3423
124.7431	18.49	.21	1.1771	.3026	-.2924	-.0012	-.0021	-.0002	.1290	297.4643	.3424
124.4290	20.58	.23	1.2665	.3754	-.3127	.0006	-.0023	.0002	.1294	297.6828	.3423
125.0945	.01	.00	.0374	-.0408	-.0209	.0032	-.0039	.0051	.1289	298.4560	.3416

$M_{\infty} = 0.30$; $C_{\mu,avg} = 0$

QINF PSF	ALPHA DEG	BETA DEG	CLT	CDT	CPMT	CRMT	CYMT	CSFT	CMU	HPLEN PSI	WTFLO LBF/SEC
124.9312	-.00	-.00	-.0058	.0347	.0025	.0013	-.0034	.0095	0.0000	-.3073	0.0000
123.8920	-1.85	-.02	-.1023	.0361	.0199	.0015	-.0037	.0098	0.0000	-.2097	0.0000
124.9181	.02	-.00	-.0053	.0347	.0021	.0014	-.0034	.0094	0.0000	-.2878	0.0000
125.0302	1.92	.02	.0912	.0368	-.0154	.0015	-.0033	.0095	0.0000	-.3938	0.0000
125.0942	3.86	.04	.1925	.0429	-.0362	.0014	-.0032	.0095	0.0000	-.4770	0.0000
124.6694	5.83	.06	.2986	.0559	-.0600	.0013	-.0028	.0076	0.0000	-.5402	0.0000
125.0728	7.85	.09	.4195	.0797	-.0871	.0012	-.0028	.0072	0.0000	-.6650	0.0000
124.8711	9.92	.11	.5286	.1124	-.1105	.0006	-.0028	.0069	0.0000	-.7447	0.0000
125.0112	12.04	.13	.6231	.1524	-.1346	.0010	-.0026	.0069	0.0000	-.7818	0.0000
124.9165	14.21	.16	.7147	.1995	-.1596	.0005	-.0021	.0055	0.0000	-.8569	0.0000
125.1006	16.29	.18	.7963	.2517	-.1869	.0002	-.0019	.0054	0.0000	-.8605	0.0000
124.5581	18.36	.20	.8561	.3086	-.2174	.0000	-.0020	.0050	0.0000	-.9614	0.0000
124.5744	20.42	.23	.8602	.3514	-.2357	.0005	-.0019	.0051	0.0000	-.8556	0.0000
124.9647	-.00	-.00	-.0042	.0348	.0008	.0015	-.0033	.0097	0.0000	-.3083	0.0000

TABLE VI.- Continued.

(b) $\beta \approx +4^0$

$M_\infty = 0.30$; $C_{\mu, avg} = 0.058$; $T_{t, plen} = 512^0 R$

QINF PSF	ALPHA DEG	BETA DEG	CLT	CDT	CPMT	CRMT	CYMT	CSFT	CMU	HPLEN PSI	WTFLO LBF/SEC
126.0709	-.04	4.02	.0094	-.0022	-.0051	-.0036	.0129	-.0421	.0584	137.3796	.1748
125.4939	-1.90	3.99	-.0869	-.0014	.0123	-.0024	.0124	-.0411	.0586	137.3817	.1748
126.8042	-.02	4.02	.0082	-.0021	-.0050	-.0037	.0131	-.0420	.0582	137.4050	.1753
126.0563	1.87	4.04	.1089	.0010	-.0239	-.0048	.0135	-.0431	.0583	137.4073	.1748
126.3234	3.81	4.05	.2132	.0080	-.0460	-.0045	.0137	-.0429	.0582	137.4080	.1748
126.2205	5.81	4.06	.3342	.0225	-.0746	-.0051	.0148	-.0459	.0583	137.3887	.1750
125.7542	7.82	4.07	.4566	.0463	-.1036	-.0053	.0152	-.0476	.0586	137.4294	.1749
126.1297	9.92	4.07	.5758	.0800	-.1301	-.0061	.0155	-.0499	.0585	137.4396	.1753
125.6075	12.04	4.07	.6794	.1228	-.1549	-.0031	.0149	-.0503	.0588	137.4863	.1756
126.2033	14.22	4.06	.8102	.1796	-.1937	-.0064	.0146	-.0501	.0585	137.5065	.1752
126.3997	16.32	4.05	.9441	.2437	-.2297	-.0071	.0149	-.0499	.0584	137.5332	.1754
125.8348	18.44	4.03	1.0562	.3109	-.2555	-.0044	.0134	-.0493	.0589	137.5982	.1758
126.4585	20.53	4.01	1.1413	.3800	-.2765	-.0008	.0098	-.0473	.0584	137.5512	.1754
125.8388	-.04	4.02	.0127	-.0025	-.0066	-.0034	.0131	-.0424	.0587	137.8517	.1753

$M_\infty = 0.30$; $C_{\mu, avg} = 0.127$; $T_{t, plen} = 529^0 R$

QINF PSF	ALPHA DEG	BETA DEG	CLT	CDT	CPMT	CRMT	CYMT	CSFT	CMU	HPLEN PSI	WTFLO LBF/SEC
126.4589	-.04	4.02	.0367	-.0464	-.0184	-.0021	.0118	-.0416	.1273	299.3151	.3408
125.9754	-1.90	4.00	-.0632	-.0474	.0003	-.0011	.0112	-.0408	.1278	299.3659	.3402
126.4616	-.02	4.02	.0388	-.0476	-.0188	-.0018	.0119	-.0420	.1272	298.8754	.3395
126.5577	1.88	4.04	.1417	-.0435	-.0382	-.0027	.0126	-.0431	.1272	299.0821	.3396
126.8862	3.81	4.05	.2515	-.0362	-.0618	-.0033	.0128	-.0437	.1269	299.0735	.3393
126.3665	5.82	4.07	.3779	-.0210	-.0926	-.0041	.0135	-.0457	.1276	299.5272	.3395
126.6668	7.85	4.07	.5113	.0069	-.1249	-.0047	.0139	-.0472	.1272	299.3103	.3390
125.4714	9.93	4.08	.6419	.0436	-.1567	-.0064	.0148	-.0501	.1284	299.1067	.3388
126.2261	12.06	4.07	.7841	.0941	-.1945	-.0089	.0149	-.0500	.1276	299.1743	.3387
126.4291	14.25	4.06	.9376	.1569	-.2366	-.0103	.0150	-.0504	.1274	299.1459	.3387
126.3316	16.36	4.05	1.0732	.2245	-.2699	-.0092	.0146	-.0495	.1275	299.1715	.3386
126.3490	18.47	4.03	1.1873	.2958	-.2957	-.0054	.0126	-.0498	.1276	299.3773	.3386
127.0260	20.57	4.01	1.2709	.3685	-.3150	-.0015	.0097	-.0486	.1269	299.3873	.3384
126.6387	-.04	4.02	.0415	-.0494	-.0196	-.0020	.0118	-.0419	.1269	299.1168	.3368

$M_\infty = 0.30$; $C_{\mu, avg} = 0$

QINF PSF	ALPHA DEG	BETA DEG	CLT	CDT	CPMT	CRMT	CYMT	CSFT	CMU	HPLEN PSI	WTFLO LBF/SEC
126.3396	-.05	4.01	-.0024	.0279	.0022	-.0040	.0128	-.0382	0.0000	-.6873	0.0000
126.8525	-1.90	3.99	-.0980	.0311	.0201	-.0031	.0120	-.0382	0.0000	-.5365	0.0000
126.2328	-.03	4.01	-.0019	.0303	.0026	-.0039	.0128	-.0389	0.0000	-.6338	0.0000
126.4345	1.87	4.03	.0956	.0333	-.0154	-.0045	.0131	-.0388	0.0000	-.7094	0.0000
126.4425	3.81	4.05	.1964	.0397	-.0363	-.0053	.0132	-.0392	0.0000	-.7745	0.0000
126.4879	5.79	4.06	.3079	.0528	-.0612	-.0062	.0138	-.0411	0.0000	-.8553	0.0000
126.2594	7.81	4.07	.4241	.0762	-.0877	-.0053	.0155	-.0472	0.0000	-.9641	0.0000
127.0980	9.90	4.07	.5389	.1096	-.1138	-.0054	.0161	-.0492	0.0000	-1.0713	0.0000
126.1579	12.03	4.07	.6349	.1512	-.1382	-.0022	.0157	-.0515	0.0000	-1.1010	0.0000
126.0872	14.19	4.07	.7336	.2014	-.1673	-.0018	.0146	-.0508	0.0000	-1.1393	0.0000
126.2503	16.26	4.05	.8152	.2548	-.1954	-.0009	.0132	-.0483	0.0000	-1.2065	0.0000
126.6895	18.34	4.03	.8709	.3100	-.2227	.0001	.0077	-.0400	0.0000	-1.2749	0.0000
126.9940	20.39	4.03	.8612	.3503	-.2402	.0015	-.0081	-.0273	0.0000	-1.1157	0.0000
126.7031	-.05	4.02	.0061	.0330	-.0016	-.0042	.0130	-.0404	0.0000	-.5875	0.0000

TABLE VI.- Concluded.

(c) $\beta \approx -4^{0}$

$M_{\infty} = 0.30$; $C_{\mu, avg} = 0.057$; $T_{t, plen} = 514^{0}R$

QINF PSF	ALPHA DEG	BETA DEG	CLT	CDT	CPMT	CRMT	CYMT	CSFT	CMU	HPLEN PSI	WTFLO LBF/SE
125.8754	.05	-4.02	.0115	.0005	-.0042	.0081	-.0212	.0565	.0571	137.3140	.1705
126.0877	-1.81	-4.04	-.0869	.0011	.0141	.0072	-.0206	.0559	.0575	137.5394	.1718
125.9461	.08	-4.02	.0130	.0003	-.0048	.0080	-.0212	.0561	.0575	137.3417	.1715
126.3962	1.97	-3.99	.1070	.0042	-.0227	.0089	-.0212	.0550	.0572	137.1361	.1714
125.9608	3.91	-3.96	.2147	.0107	-.0457	.0090	-.0213	.0543	.0573	137.0826	.1712
125.3075	5.89	-3.93	.3281	.0247	-.0734	.0089	-.0211	.0535	.0577	137.0312	.1713
125.4611	7.93	-3.89	.4569	.0508	-.1043	.0088	-.0216	.0545	.0577	137.0816	.1717
125.8244	10.00	-3.85	.5735	.0847	-.1309	.0060	-.0220	.0557	.0576	137.0639	.1718
125.3155	12.12	-3.80	.6747	.1256	-.1540	.0048	-.0209	.0542	.0577	137.0533	.1713
125.5560	14.31	-3.74	.8061	.1827	-.1938	.0039	-.0194	.0552	.0576	137.0912	.1714
125.8673	16.41	-3.68	.9399	.2465	-.2301	.0034	-.0185	.0544	.0575	137.0528	.1716
126.0222	18.52	-3.62	1.0487	.3115	-.2546	.0025	-.0184	.0527	.0584	139.1475	.1738
125.6014	20.61	-3.55	1.1349	.3800	-.2742	.0030	-.0167	.0512	.0577	137.2893	.1715
125.5426	.05	-4.02	.0112	.0006	-.0046	.0078	-.0210	.0561	.0575	137.7369	.1707

$M_{\infty} = 0.30$; $C_{\mu, avg} = 0.127$; $T_{t, plen} = 527^{0}R$

QINF PSF	ALPHA DEG	BETA DEG	CLT	CDT	CPMT	CRMT	CYMT	CSFT	CMU	HPLEN PSI	WTFLO LBF/SE
126.2157	.05	-4.02	.0403	-.0424	-.0194	.0088	-.0204	.0528	.1269	299.3181	.3395
126.0982	-1.78	-4.03	-.0564	-.0434	-.0002	.0079	-.0200	.0532	.1268	298.9512	.3385
125.8803	.09	-4.01	.0399	-.0434	-.0193	.0082	-.0202	.0518	.1267	298.4028	.3375
126.4279	1.98	-3.99	.1447	-.0388	-.0393	.0091	-.0207	.0522	.1263	298.3583	.3374
125.8429	3.91	-3.96	.2508	-.0318	-.0628	.0094	-.0214	.0525	.1270	298.4799	.3374
125.9055	5.91	-3.93	.3770	-.0161	-.0933	.0092	-.0216	.0526	.1271	298.9458	.3373
125.8240	7.94	-3.89	.5080	.0119	-.1241	.0091	-.0222	.0532	.1273	299.2313	.3374
126.1152	10.03	-3.84	.6394	.0491	-.1557	.0040	-.0221	.0536	.1271	299.5596	.3375
125.6517	12.15	-3.79	.7778	.0989	-.1936	.0029	-.0211	.0530	.1268	298.1265	.3354
125.8228	14.34	-3.74	.9288	.1604	-.2355	.0007	-.0192	.0528	.1264	297.0167	.3346
125.5196	16.44	-3.68	1.0629	.2264	-.2686	.0013	-.0181	.0517	.1268	296.9601	.3347
127.2022	18.56	-3.61	1.1785	.2989	-.2954	.0028	-.0185	.0500	.1253	297.6954	.3350
126.0872	20.66	-3.55	1.2704	.3715	-.3159	.0028	-.0164	.0490	.1267	298.4012	.3352
126.8390	.06	-4.02	.0433	-.0463	-.0192	.0088	-.0205	.0536	.1264	299.8011	.3355

$M_{\infty} = 0.30$; $C_{\mu, avg} = 0$

QINF PSF	ALPHA DEG	BETA DEG	CLT	CDT	CPMT	CRMT	CYMT	CSFT	CMU	HPLEN PSI	WTFLO LBF/SE
125.9002	.04	-4.02	-.0027	.0307	.0037	.0068	-.0200	.0600	0.0000	-.6565	0.0000
125.8735	-1.80	-4.04	-.0984	.0328	.0220	.0069	-.0200	.0599	0.0000	-.4869	0.0000
125.9590	.08	-4.02	-.0027	.0326	.0039	.0068	-.0201	.0592	0.0000	-.5859	0.0000
126.4118	1.97	-4.00	.0911	.0353	-.0138	.0074	-.0207	.0616	0.0000	-.6663	0.0000
126.1914	3.90	-3.97	.1933	.0413	-.0351	.0078	-.0207	.0603	0.0000	-.7489	0.0000
126.1673	5.88	-3.93	.3056	.0550	-.0604	.0080	-.0203	.0582	0.0000	-.8214	0.0000
126.3796	7.92	-3.89	.4263	.0801	-.0891	.0080	-.0208	.0585	0.0000	-.9352	0.0000
125.5021	10.00	-3.85	.5379	.1138	-.1152	.0059	-.0213	.0593	0.0000	-1.0170	0.0000
125.6103	12.12	-3.80	.6381	.1549	-.1395	.0037	-.0204	.0600	0.0000	-1.0753	0.0000
125.4620	14.29	-3.74	.7309	.2036	-.1682	.0025	-.0192	.0586	0.0000	-1.1418	0.0000
125.0746	16.36	-3.69	.8122	.2566	-.1959	.0014	-.0169	.0559	0.0000	-1.1622	0.0000
126.7308	18.45	-3.62	.8646	.3096	-.2196	-.0002	-.0107	.0447	0.0000	-1.2422	0.0000
125.8881	20.49	-3.57	.8666	.3535	-.2428	-.0008	.0055	.0306	0.0000	-1.0807	0.0000
125.5035	.05	-4.02	.0043	.0352	.0002	.0068	-.0202	.0601	0.0000	-.5764	0.0000

TABLE VII.- SPANWISE BLOWING ON THE 44° SWEPT TRAPEZOIDAL WING - HORIZONTAL TAIL - VERTICAL TAIL CONFIGURATION IN SIDESLIP; $\delta_{LE} = \delta_{TE} = 0^{0}$.

(a) $\beta \approx 0^{0}$

$M_{\infty} = 0.30$; $C_{\mu, avg} = 0.06$; $T_{t, plen} = 508^{0}R$

QINF PSF	ALPHA DEG	BETA DEG	CLT	CDT	CPMT	CRMT	CYMT	CSFT	CMU	HPLEN PSI	WTFLO LBF/SEC
124.6819	-.00	-.00	.0086	.0051	-.0124	.0019	-.0040	.0079	.0599	138.2049	.1768
125.1239	-1.83	-.02	-.0917	.0070	.0187	.0019	-.0042	.0082	.0594	137.5929	.1765
124.8401	-.01	-.00	.0064	.0062	-.0117	.0018	-.0039	.0073	.0595	137.7207	.1765
125.0123	1.91	.02	.1202	.0102	-.0442	.0018	-.0035	.0062	.0597	137.9507	.1774
125.2310	3.84	.04	.2330	.0182	-.0797	.0019	-.0036	.0059	.0597	137.9778	.1777
124.8946	5.83	.07	.3626	.0342	-.1255	.0019	-.0031	.0047	.0597	137.9941	.1773
125.3380	7.85	.09	.4963	.0611	-.1714	.0016	-.0029	.0041	.0595	138.0510	.1775
124.7288	9.91	.11	.6269	.0985	-.2170	.0008	-.0022	.0023	.0597	138.0687	.1773
124.5233	12.03	.14	.7400	.1441	-.2626	.0020	-.0023	.0026	.0602	138.0779	.1783
124.5845	14.21	.16	.8802	.2057	-.3142	-.0006	-.0013	.0022	.0600	138.0816	.1777
124.3895	16.30	.18	1.0493	.2808	-.3881	-.0020	-.0010	.0024	.0602	138.0015	.1782
124.4242	18.39	.21	1.1775	.3577	-.4536	-.0012	-.0012	.0013	.0602	138.0430	.1783
124.6355	20.47	.23	1.2960	.4423	-.5256	.0019	-.0022	.0021	.0602	138.1074	.1785
124.4338	-.01	-.00	.0148	.0066	-.0137	.0017	-.0039	.0071	.0600	137.9651	.1778

$M_{\infty} = 0.30$; $C_{\mu, avg} = 0.129$; $T_{t, plen} = 516^{0}R$

QINF PSF	ALPHA DEG	BETA DEG	CLT	CDT	CPMT	CRMT	CYMT	CSFT	CMU	HPLEN PSI	WTFLO LBF/SEC
125.1377	.00	.00	.0231	-.0332	.0006	.0031	-.0044	.0063	.1289	297.7795	.3464
124.8397	-1.82	-.02	-.0916	-.0337	.0423	.0033	-.0044	.0059	.1294	298.6589	.3464
124.6326	.04	.00	.0228	-.0352	.0007	.0033	-.0041	.0051	.1296	298.6964	.3459
125.5179	1.92	.02	.1402	-.0309	-.0395	.0030	-.0040	.0054	.1284	297.9493	.3446
125.4992	3.86	.05	.2571	-.0224	-.0798	.0033	-.0041	.0053	.1284	297.6505	.3441
124.7392	5.84	.07	.3888	-.0066	-.1245	.0034	-.0033	.0032	.1292	297.6423	.3440
124.9127	7.87	.09	.5309	.0224	-.1692	.0029	-.0033	.0028	.1288	297.4533	.3431
125.2612	9.94	.11	.6748	.0622	-.2199	-.0003	-.0023	.0007	.1285	297.3457	.3427
124.6057	12.06	.14	.8288	.1143	-.2775	-.0022	-.0022	.0014	.1292	297.3051	.3424
125.5591	14.25	.16	1.0066	.1840	-.3527	-.0053	-.0014	.0015	.1283	297.3978	.3422
125.2969	16.35	.18	1.1680	.2604	-.4267	-.0048	-.0011	.0019	.1286	297.3683	.3418
124.9524	18.45	.21	1.3119	.3445	-.4976	-.0019	-.0016	-.0000	.1290	297.4132	.3416
125.0409	20.53	.23	1.4285	.4322	-.5637	.0008	-.0021	.0003	.1290	297.5021	.3413
124.6295	.01	.00	.0243	-.0423	.0014	.0033	-.0043	.0063	.1296	297.8690	.3401

$M_{\infty} = 0.30$; $C_{\mu, avg} = 0$

QINF PSF	ALPHA DEG	BETA DEG	CLT	CDT	CPMT	CRMT	CYMT	CSFT	CMU	HPLEN PSI	WTFLO LBF/SEC
124.7473	-.00	-.00	-.0028	.0340	-.0023	.0012	-.0031	.0093	0.0000	-.4278	0.0000
126.5936	-1.85	-.03	-.1044	.0366	.0239	.0015	-.0035	.0109	0.0000	-.2797	0.0000
124.8191	.02	-.00	.0019	.0355	-.0039	.0013	-.0034	.0114	0.0000	-.3787	0.0000
125.1756	1.91	.02	.1019	.0383	-.0313	.0012	-.0032	.0104	0.0000	-.4756	0.0000
124.9420	3.84	.04	.2144	.0456	-.0668	.0013	-.0031	.0101	0.0000	-.5660	0.0000
124.7482	5.82	.06	.3369	.0601	-.1114	.0012	-.0026	.0080	0.0000	-.6319	0.0000
125.2197	7.84	.09	.4696	.0865	-.1592	.0009	-.0024	.0072	0.0000	-.7497	0.0000
124.4063	9.90	.11	.5959	.1229	-.2055	.0003	-.0023	.0066	0.0000	-.8405	0.0000
125.4183	12.02	.13	.7029	.1682	-.2499	.0012	-.0023	.0059	0.0000	-.9131	0.0000
124.4875	14.18	.16	.8128	.2231	-.3060	.0005	-.0020	.0057	0.0000	-.9500	0.0000
124.6145	16.24	.18	.9200	.2872	-.3691	.0006	-.0017	.0049	0.0000	-.9731	0.0000
124.7574	18.31	.20	1.0012	.3561	-.4343	.0004	-.0017	.0038	0.0000	-1.0835	0.0000
125.1595	20.36	.23	1.0425	.4173	-.4951	.0012	-.0023	.0048	0.0000	-1.0108	0.0000
124.7416	-.00	-.00	.0030	.0362	-.0046	.0011	-.0032	.0096	0.0000	-.3917	0.0000

TABLE VII.- Continued.

(b) $\beta \approx +4^0$

$M_\infty = 0.30$; $C_{\mu, avg} = 0.057$; $T_{t, plen} = 511^0 R$

QINF PSF	ALPHA DEG	BETA DEG	CLT	CDT	CPMT	CRMT	CYMT	CSFT	CMU	HPLEN PSI	WTFLO LBF/SEC
126.4105	-.05	4.02	.0059	.0030	-.0114	-.0030	.0126	-.0410	.0580	139.4298	.1738
125.8201	-1.90	3.99	-.0976	.0042	.0202	-.0023	.0118	-.0402	.0581	139.1341	.1732
126.0780	-.06	4.02	.0037	.0037	-.0108	-.0029	.0123	-.0404	.0575	137.5929	.1721
126.5681	1.86	4.04	.1147	.0073	-.0433	-.0037	.0132	-.0416	.0572	137.2114	.1721
126.9500	3.79	4.05	.2311	.0151	-.0805	-.0040	.0139	-.0434	.0569	137.0544	.1717
125.8481	5.79	4.06	.3616	.0306	-.1263	-.0051	.0148	-.0467	.0575	137.0427	.1721
126.8136	7.81	4.07	.4991	.0574	-.1742	-.0046	.0151	-.0483	.0571	138.0105	.1720
126.2180	9.89	4.07	.6243	.0944	-.2215	-.0059	.0154	-.0494	.0568	136.1543	.1706
126.1766	12.00	4.07	.7450	.1416	-.2690	-.0038	.0151	-.0505	.0584	139.2353	.1747
125.5073	14.18	4.06	.8853	.2031	-.3163	-.0087	.0147	-.0487	.0575	137.0510	.1715
125.6529	16.27	4.05	1.0367	.2751	-.3842	-.0087	.0153	-.0491	.0573	136.2259	.1714
124.8243	18.37	4.03	1.1763	.3538	-.4556	-.0067	.0131	-.0477	.0590	139.1005	.1748
126.2565	20.45	4.01	1.3000	.4416	-.5307	-.0041	.0102	-.0459	.0583	139.3235	.1745
125.6688	-.05	4.02	.0112	.0034	-.0135	-.0030	.0124	-.0408	.0581	138.3140	.1734

$M_\infty = 0.30$; $C_{\mu, avg} = 0.127$; $T_{t, plen} = 516^0 R$

QINF PSF	ALPHA DEG	BETA DEG	CLT	CDT	CPMT	CRMT	CYMT	CSFT	CMU	HPLEN PSI	WTFLO LBF/SEC
126.3920	-.04	4.02	.0196	-.0372	-.0030	-.0038	.0110	-.0394	.1269	299.0801	.3428
126.0754	-1.87	4.00	-.0938	-.0365	.0371	-.0031	.0105	-.0394	.1271	299.1541	.3424
126.2142	-.04	4.02	.0167	-.0378	-.0020	-.0035	.0113	-.0403	.1271	299.4416	.3426
126.5948	1.86	4.04	.1335	-.0334	-.0413	-.0041	.0115	-.0403	.1266	299.1948	.3421
126.6161	3.80	4.05	.2549	-.0254	-.0822	-.0043	.0124	-.0423	.1265	299.1782	.3419
126.4437	5.80	4.07	.3864	-.0090	-.1270	-.0055	.0131	-.0443	.1267	299.2146	.3418
125.7091	7.83	4.07	.5323	.0197	-.1737	-.0056	.0138	-.0468	.1275	299.3677	.3417
126.4744	9.91	4.08	.6736	.0602	-.2209	-.0068	.0147	-.0495	.1266	299.1343	.3413
125.9082	12.05	4.07	.8327	.1142	-.2798	-.0087	.0148	-.0491	.1270	298.8145	.3408
126.7029	14.23	4.06	1.0032	.1828	-.3516	-.0104	.0153	-.0491	.1263	298.8033	.3407
126.0298	16.32	4.04	1.1606	.2576	-.4249	-.0104	.0146	-.0478	.1269	298.7728	.3403
125.5316	18.42	4.03	1.3084	.3428	-.4990	-.0076	.0128	-.0481	.1273	298.8049	.3400
125.5422	20.51	4.01	1.4267	.4319	-.5678	-.0034	.0098	-.0470	.1274	298.8772	.3400
126.1943	-.02	4.02	.0204	-.0412	-.0027	-.0033	.0114	-.0400	.1266	298.7996	.3384

$M_\infty = 0.30$; $C_{\mu, avg} = 0$

QINF PSF	ALPHA DEG	BETA DEG	CLT	CDT	CPMT	CRMT	CYMT	CSFT	CMU	HPLEN PSI	WTFLO LBF/SEC
126.4443	-.03	4.01	-.0068	.0343	-.0014	-.0033	.0132	-.0391	0.0000	-.2877	0.0000
126.1291	-1.91	3.99	-.1092	.0369	.0252	-.0021	.0122	-.0377	0.0000	-.1601	0.0000
126.1132	-.03	4.01	-.0053	.0352	-.0017	-.0032	.0133	-.0393	0.0000	-.2361	0.0000
126.5846	1.86	4.03	.0983	.0380	-.0301	-.0038	.0138	-.0397	0.0000	-.3327	0.0000
126.5473	3.80	4.05	.2100	.0451	-.0658	-.0039	.0137	-.0392	0.0000	-.3838	0.0000
126.5486	5.78	4.06	.3330	.0596	-.1100	-.0053	.0141	-.0409	0.0000	-.4754	0.0000
125.9328	7.79	4.07	.4634	.0852	-.1567	-.0048	.0152	-.0446	0.0000	-.5765	0.0000
125.9048	9.87	4.07	.5911	.1215	-.2075	-.0049	.0155	-.0468	0.0000	-.6700	0.0000
126.1853	11.99	4.07	.6998	.1676	-.2535	-.0024	.0150	-.0485	0.0000	-.7240	0.0000
126.1199	14.15	4.06	.8195	.2255	-.3133	-.0033	.0142	-.0483	0.0000	-.7844	0.0000
126.6007	16.23	4.05	.9242	.2894	-.3766	-.0036	.0129	-.0456	0.0000	-.8438	0.0000
127.4685	18.30	4.03	1.0066	.3573	-.4391	-.0039	.0089	-.0375	0.0000	-.9402	0.0000
126.8117	20.32	4.02	1.0363	.4165	-.5040	-.0040	-.0043	-.0251	0.0000	-.7899	0.0000
126.0999	-.05	4.01	-.0011	.0364	-.0040	-.0032	.0131	-.0389	0.0000	-.2231	0.0000

TABLE VII.- Concluded.

(c) $\beta \approx -4^0$

$M_\infty = 0.30$; $C_{\mu, avg} = 0.058$; $T_{t, plen} = 510^0 R$

QINF PSF	ALPHA DEG	BETA DEG	CLT	CDT	CPMT	CRMT	CYMT	CSFT	CMU	HPLEN PSI	WTFLO LBF/SEC
126.3917	.05	-4.02	.0095	.0035	-.0096	.0073	-.0225	.0586	.0570	136.5299	.1715
126.3610	-1.83	-4.04	-.0987	.0045	.0244	.0068	-.0220	.0581	.0576	137.8017	.1729
126.5478	.01	-4.02	.0074	.0035	-.0090	.0071	-.0223	.0577	.0572	137.6284	.1723
126.6854	1.94	-3.99	.1164	.0081	-.0413	.0078	-.0226	.0574	.0572	136.8398	.1726
125.9360	3.86	-3.96	.2295	.0149	-.0775	.0078	-.0224	.0558	.0582	138.4304	.1740
126.3314	5.84	-3.93	.3613	.0309	-.1242	.0083	-.0219	.0540	.0575	137.8284	.1727
125.6715	7.87	-3.89	.4937	.0590	-.1691	.0084	-.0222	.0546	.0572	136.3727	.1713
125.3870	9.93	-3.85	.6203	.0956	-.2131	.0061	-.0220	.0547	.0584	138.4369	.1742
126.5907	12.07	-3.80	.7423	.1428	-.2619	.0068	-.0211	.0542	.0580	139.1155	.1744
126.4745	14.24	-3.74	.8836	.2059	-.3210	.0062	-.0183	.0520	.0571	136.5147	.1722
126.0058	16.33	-3.68	1.0425	.2779	-.3918	.0055	-.0179	.0532	.0578	137.5278	.1735
125.8669	18.43	-3.62	1.1809	.3563	-.4605	.0047	-.0176	.0508	.0581	138.2026	.1740
125.7386	20.51	-3.54	1.3033	.4419	-.5325	.0064	-.0171	.0486	.0585	138.8280	.1750
126.5828	.01	-4.02	.0112	.0047	-.0107	.0073	-.0220	.0578	.0573	137.0120	.1727

$M_\infty = 0.30$; $C_{\mu, avg} = 0.127$; $T_{t, plen} = 515^0 R$

QINF PSF	ALPHA DEG	BETA DEG	CLT	CDT	CPMT	CRMT	CYMT	CSFT	CMU	HPLEN PSI	WTFLO LBF/SEC
126.4893	.03	-4.02	.0254	-.0362	-.0046	.0093	-.0221	.0558	.1263	297.7629	.3423
126.9727	-1.82	-4.04	-.0877	-.0356	.0343	.0089	-.0221	.0564	.1257	297.5773	.3420
126.0832	.06	-4.02	.0235	-.0371	-.0044	.0094	-.0221	.0556	.1268	297.9137	.3422
126.6815	1.94	-3.99	.1378	-.0325	-.0420	.0100	-.0220	.0544	.1263	298.2453	.3423
126.8510	3.87	-3.96	.2567	-.0240	-.0827	.0107	-.0219	.0536	.1263	298.5398	.3425
126.0910	5.85	-3.93	.3922	-.0076	-.1289	.0107	-.0218	.0528	.1271	298.8681	.3426
126.5303	7.89	-3.89	.5331	.0227	-.1745	.0106	-.0222	.0530	.1267	298.8815	.3423
126.4182	9.97	-3.84	.6784	.0628	-.2275	.0061	-.0216	.0524	.1265	298.2929	.3415
126.3848	12.09	-3.80	.8291	.1161	-.2852	.0043	-.0211	.0533	.1264	298.0819	.3410
125.8626	14.27	-3.74	.9995	.1836	-.3563	.0011	-.0193	.0528	.1270	298.0288	.3408
125.0396	16.37	-3.68	1.1706	.2611	-.4321	.0016	-.0178	.0527	.1277	297.9774	.3404
125.3255	18.46	-3.61	1.3064	.3426	-.4995	.0040	-.0182	.0502	.1277	298.2045	.3409
126.5224	20.56	-3.54	1.4329	.4346	-.5706	.0052	-.0167	.0474	.1264	298.3454	.3402
126.2645	.03	-4.02	.0248	-.0408	-.0043	.0094	-.0220	.0561	.1268	299.1124	.3398

$M_\infty = 0.30$; $C_{\mu, avg} = 0$

QINF PSF	ALPHA DEG	BETA DEG	CLT	CDT	CPMT	CRMT	CYMT	CSFT	CMU	HPLEN PSI	WTFLO LBF/SEC
126.3326	.01	-4.02	-.0037	.0357	-.0020	.0057	-.0207	.0610	0.0000	-.3199	0.0000
126.6331	-1.84	-4.04	-.1038	.0375	.0253	.0055	-.0207	.0614	0.0000	-.2212	0.0000
126.2044	.01	-4.02	-.0032	.0364	-.0021	.0057	-.0207	.0608	0.0000	-.3100	0.0000
126.3660	1.94	-4.00	.1019	.0392	-.0319	.0067	-.0212	.0616	0.0000	-.3977	0.0000
126.3499	3.86	-3.97	.2115	.0458	-.0667	.0065	-.0210	.0600	0.0000	-.4615	0.0000
126.0627	5.85	-3.93	.3367	.0608	-.1114	.0068	-.0205	.0580	0.0000	-.5500	0.0000
125.3320	7.87	-3.90	.4673	.0880	-.1591	.0072	-.0211	.0592	0.0000	-.6340	0.0000
126.5675	9.94	-3.85	.5945	.1249	-.2065	.0049	-.0212	.0598	0.0000	-.7486	0.0000
125.4055	12.04	-3.80	.7047	.1698	-.2544	.0042	-.0199	.0587	0.0000	-.8167	0.0000
126.0426	14.20	-3.74	.8186	.2271	-.3145	.0046	-.0187	.0571	0.0000	-.8752	0.0000
125.9718	16.28	-3.69	.9251	.2907	-.3779	.0049	-.0168	.0542	0.0000	-.9109	0.0000
125.8195	18.35	-3.62	1.0066	.3572	-.4403	.0043	-.0129	.0444	0.0000	-.9911	0.0000
125.4614	20.38	-3.56	1.0483	.4195	-.5023	.0060	-.0020	.0313	0.0000	-.9062	0.0000
126.1144	.01	-4.02	-.0009	.0372	-.0035	.0059	-.0211	.0619	0.0000	-.3009	0.0000

TABLE VIII.- SPANWISE BLOWING ON THE 44° SWEPT TRAPEZOIDAL WING IN THE PRESENCE OF A CLOSE-COUPLED CANARD; $\delta_{LE} = \delta_{TE} = 0^{\circ}$.

(a) $i_c = 0^{\circ}$

$M_\infty = 0.30$; $C_{\mu, avg} = 0.058$; $T_{t, plen} = 520^{\circ}R$

QINF PSF	ALPHA DEG	BETA DEG	CLT	CDT	CPMT	CMU	HPLEN PSI	WTFLO LBF/SEC
127.1609	.00	-.00	.0058	.0071	-.0027	.0575	133.5962	.1729
126.4049	-1.86	-.02	-.0947	.0087	-.0058	.0582	133.9135	.1740
127.1288	.04	-.00	.0069	.0066	-.0019	.0585	136.0078	.1757
126.8309	1.94	.02	.1107	.0104	.0016	.0579	134.5594	.1738
126.3379	3.90	.04	.2290	.0194	.0063	.0577	133.4256	.1726
127.0190	5.92	.07	.3565	.0374	.0062	.0581	134.2596	.1748
127.1418	7.97	.09	.4931	.0647	.0030	.0582	135.0281	.1749
126.8880	10.07	.11	.6343	.1039	-.0015	.0586	135.5913	.1759
126.3150	12.24	.14	.7741	.1544	-.0043	.0584	134.5711	.1746
126.9467	14.45	.16	.9101	.2170	-.0079	.0576	133.4174	.1733
126.8078	16.57	.18	1.0551	.2906	-.0187	.0586	135.1637	.1759
126.2414	18.71	.20	1.1918	.3743	-.0269	.0593	136.3838	.1771
126.8358	20.83	.22	1.3260	.4730	-.0526	.0580	134.5448	.1744
127.1617	.01	-.00	.0083	.0077	-.0017	.0583	135.4728	.1756

$M_\infty = 0.30$; $C_{\mu, avg} = 0.126$; $T_{t, plen} = 519^{\circ}R$

QINF PSF	ALPHA DEG	BETA DEG	CLT	CDT	CPMT	CMU	HPLEN PSI	WTFLO LBF/SEC
126.6676	.01	-.00	.0362	-.0302	-.0159	.1253	293.8786	.3399
126.6556	-1.85	-.02	-.0713	-.0294	-.0192	.1251	293.0511	.3394
127.2233	.04	.00	.0363	-.0305	-.0161	.1249	293.9119	.3401
126.8735	1.96	.02	.1476	-.0267	-.0136	.1257	294.7337	.3409
127.3849	3.92	.04	.2686	-.0168	-.0107	.1254	295.2655	.3411
126.8908	5.93	.07	.4028	.0021	-.0125	.1259	295.3056	.3409
126.8895	7.99	.09	.5359	.0303	-.0130	.1259	295.4402	.3407
126.4032	10.08	.11	.6727	.0692	-.0139	.1265	295.6810	.3407
126.3138	12.25	.14	.8171	.1207	-.0187	.1268	296.0586	.3406
126.8855	14.46	.16	.9690	.1878	-.0296	.1261	295.9230	.3401
126.8721	16.58	.18	1.1233	.2649	-.0435	.1262	295.9726	.3398
127.3246	18.74	.21	1.2728	.3551	-.0545	.1259	296.0260	.3397
127.0549	20.87	.22	1.4171	.4567	-.0775	.1263	296.1563	.3396
126.3069	.02	.00	.0376	-.0377	-.0145	.1270	296.5088	.3386

$M_\infty = 0.30$; $C_{\mu, avg} = 0$

QINF PSF	ALPHA DEG	BETA DEG	CLT	CDT	CPMT	CMU	HPLEN PSI	WTFLO LBF/SEC
126.8581	-.00	-.00	-.0066	.0327	.0031	0.0000	-.7063	0.0000
126.9635	-1.86	-.03	-.1082	.0352	-.0010	0.0000	-.6806	0.0000
126.9755	.04	-.00	-.0036	.0331	.0040	0.0000	-.6865	0.0000
126.2756	1.94	.02	.0951	.0365	.0085	0.0000	-.7374	0.0000
126.6041	3.90	.04	.2108	.0446	.0138	0.0000	-.7865	0.0000
127.0542	5.93	.06	.3384	.0618	.0159	0.0000	-.8357	0.0000
126.1285	7.97	.09	.4649	.0879	.0167	0.0000	-.8955	0.0000
126.5051	10.07	.11	.5909	.1245	.0156	0.0000	-.9500	0.0000
126.3047	12.23	.13	.7357	.1758	.0110	0.0000	-1.0229	0.0000
125.8638	14.45	.16	.8708	.2367	.0067	0.0000	-1.0919	0.0000
126.7081	16.56	.18	1.0047	.3065	-.0003	0.0000	-1.1874	0.0000
126.3823	18.70	.20	1.1298	.3859	-.0054	0.0000	-1.2755	0.0000
126.7709	20.81	.22	1.2239	.4701	-.0234	0.0000	-1.2125	0.0000
126.7857	.00	-.01	-.0069	.0353	.0042	0.0000	-.5918	0.0000

TABLE VIII.- Continued.

(a) Continued.

$M_\infty = 0.50$; $C_{\mu, avg} = 0.023$; $T_{t, plen} = 533^0R$

QINF PSF	ALPHA DEG	BETA DEG	CLT	CDT	CPMT	CMU	HPLEN PSI	WTFLO LBF/SEC
315.0950	-.00	-.01	.0030	.0189	.0003	.0235	135.7277	.1732
315.7025	-1.96	-.03	-.1061	.0209	-.0033	.0234	135.8213	.1729
316.2226	.04	-.01	.0037	.0186	-.0001	.0235	135.8656	.1735
315.7808	2.05	.01	.1173	.0221	.0029	.0236	135.9590	.1738
315.1810	4.11	.04	.2430	.0322	.0064	.0236	135.9211	.1736
314.7034	6.27	.06	.3839	.0540	.0064	.0236	135.9308	.1732
314.8503	8.43	.08	.5216	.0863	.0020	.0233	133.4946	.1721
313.6629	10.66	.11	.6687	.1326	-.0032	.0234	133.8739	.1716
316.5352	12.96	.13	.8126	.1914	-.0075	.0232	133.5401	.1718
314.9911	15.30	.16	.9526	.2613	-.0150	.0232	133.4642	.1710
314.3251	17.56	.18	1.0960	.3441	-.0237	.0234	134.4878	.1714
315.4496	19.80	.20	1.2182	.4348	-.0423	.0234	134.4530	.1725
319.5236	22.08	.23	1.3366	.5352	-.0476	.0232	135.0583	.1732
315.0404	-.00	-.01	.0072	.0191	-.0007	.0234	133.9875	.1723

$M_\infty = 0.50$; $C_{\mu, avg} = 0.05$; $T_{t, plen} = 541^0R$

QINF PSF	ALPHA DEG	BETA DEG	CLT	CDT	CPMT	CMU	HPLEN PSI	WTFLO LBF/SEC
316.2046	.00	-.01	.0181	.0035	-.0069	.0505	295.5100	.3343
315.3174	-1.96	-.03	-.0930	.0052	-.0098	.0507	295.5357	.3344
314.7397	.04	-.00	.0182	.0033	-.0069	.0509	295.6883	.3344
316.3806	2.05	.02	.1313	.0077	-.0046	.0505	295.2236	.3335
315.9591	4.12	.04	.2577	.0183	-.0024	.0505	294.8053	.3330
316.0650	6.27	.06	.3997	.0406	-.0044	.0504	294.5264	.3327
315.9705	8.44	.09	.5448	.0739	-.0079	.0504	294.2801	.3325
316.6333	10.69	.11	.6903	.1205	-.0103	.0503	294.1045	.3323
314.2142	12.96	.13	.8321	.1785	-.0161	.0507	294.0829	.3323
313.5913	15.32	.16	.9857	.2526	-.0283	.0509	294.4324	.3325
315.7304	17.58	.18	1.1348	.3386	-.0387	.0506	294.8027	.3326
314.5855	19.83	.20	1.2714	.4349	-.0612	.0508	294.8929	.3326
314.7673	22.09	.23	1.3896	.5360	-.0656	.0508	295.1173	.3330
315.2485	-.00	-.01	.0171	.0032	-.0073	.0507	295.5180	.3325

$M_\infty = 0.50$; $C_{\mu, avg} = 0$

QINF PSF	ALPHA DEG	BETA DEG	CLT	CDT	CPMT	CMU	HPLEN PSI	WTFLO LBF/SEC
315.6335	.01	-.01	-.0035	.0340	.0045	0.0000	-.7720	0.0000
315.1557	-1.96	-.03	-.1135	.0363	-.0001	0.0000	-.6858	0.0000
315.4944	.04	-.01	-.0022	.0337	.0044	0.0000	-.7844	0.0000
317.0240	2.05	.01	.1067	.0367	.0079	0.0000	-.8968	0.0000
316.0960	4.12	.03	.2328	.0462	.0111	0.0000	-1.0491	0.0000
315.2946	6.27	.06	.3671	.0663	.0117	0.0000	-1.1719	0.0000
314.4465	8.45	.08	.5082	.0980	.0095	0.0000	-1.4029	0.0000
315.1927	10.69	.11	.6537	.1437	.0061	0.0000	-1.5804	0.0000
315.1217	12.96	.13	.7905	.2000	.0000	0.0000	-1.8154	0.0000
315.3207	15.32	.15	.9375	.2715	-.0092	0.0000	-2.0916	0.0000
315.5652	17.56	.18	1.0715	.3519	-.0157	0.0000	-2.3655	0.0000
314.8509	19.77	.20	1.1746	.4362	-.0307	0.0000	-2.3934	0.0000
314.5331	22.01	.23	1.2809	.5298	-.0323	0.0000	-2.5192	0.0000
319.6099	.00	-.01	-.0038	.0324	.0040	0.0000	-1.2039	0.0000

TABLE VIII.- Continued.

(a) Concluded.

$M_{\infty} = 0.30$; $\alpha \approx 20.8^{0}$; $T_{t,plen} = 527^{0}R$

QINF PSF	ALPHA DEG	BETA DEG	CLT	CDT	CPMT	CMU	HPLEN PSI	WTFLO LBF/SEC
126.9129	20.80	.22	1.2284	.4690	-.0243	.0058	14.5527	.0752
126.7926	20.81	.22	1.2651	.4703	-.0348	.0280	55.7242	.1028
127.0317	20.82	.22	1.2963	.4700	-.0439	.0428	94.8722	.1369
126.8299	20.83	.22	1.3284	.4696	-.0515	.0589	134.9414	.1756
127.1024	20.84	.22	1.3535	.4670	-.0586	.0750	175.4207	.2149
126.8192	20.85	.22	1.3759	.4633	-.0650	.0922	215.1609	.2562
126.5335	20.85	.22	1.3992	.4593	-.0718	.1094	255.7755	.2965
126.9462	20.86	.22	1.4204	.4556	-.0786	.1256	294.4387	.3356
126.8860	20.84	.22	1.3336	.4705	-.0525	.0581	133.5309	.1730

TABLE VIII.- Continued.

(b) $i_c = 10^0$

$M_\infty = 0.30$; $C_{\mu,avg} = 0.058$; $T_{t,plen} = 515^0R$

QINF PSF	ALPHA DEG	BETA DEG	CLT	CDT	CPMT	CMU	HPLEN PSI	WTFLO LBF/SEC
126.6927	.08	-.00	.0349	.0214	.0814	.0578	134.0730	.1739
126.6192	-1.79	-.02	-.0632	.0169	.0748	.0578	134.2370	.1736
127.2308	.11	-.00	.0411	.0218	.0815	.0577	134.3058	.1742
126.8235	2.02	.02	.1396	.0311	.0844	.0577	134.4543	.1739
126.3266	3.97	.04	.2501	.0460	.0840	.0582	134.5319	.1746
126.6605	5.98	.06	.3728	.0693	.0720	.0578	134.5926	.1740
126.8929	8.03	.09	.5162	.1056	.0554	.0577	134.6527	.1741
126.5215	10.14	.11	.6622	.1543	.0414	.0580	134.6821	.1745
125.9885	12.27	.13	.7976	.2114	.0079	.0583	134.7203	.1747
126.3758	14.49	.16	.9550	.2873	-.0163	.0584	134.7828	.1753
128.4908	16.62	.18	1.1105	.3743	-.0362	.0573	134.8097	.1750
127.2478	18.75	.20	1.2147	.4555	-.0298	.0579	134.8372	.1752
126.6135	20.85	.23	1.2333	.5151	-.0010	.0583	134.8493	.1755
126.8380	.09	-.00	.0380	.0207	.0811	.0581	135.1148	.1750

$M_\infty = 0.30$; $C_{\mu,avg} = 0.126$; $T_{t,plen} = 517^0R$

QINF PSF	ALPHA DEG	BETA DEG	CLT	CDT	CPMT	CMU	HPLEN PSI	WTFLO LBF/SEC
126.2197	.09	-.00	.0650	-.0167	.0674	.1261	294.5937	.3418
126.3359	-1.76	-.02	-.0391	-.0223	.0618	.1263	295.2856	.3423
127.0892	.12	.00	.0684	-.0173	.0672	.1257	295.6393	.3424
126.3959	2.02	.02	.1738	-.0079	.0659	.1265	295.7478	.3422
126.5561	3.99	.04	.2961	.0074	.0599	.1264	296.0101	.3418
126.2528	5.99	.07	.4313	.0326	.0458	.1267	295.9915	.3414
126.8138	8.04	.09	.5685	.0692	.0353	.1260	295.5822	.3407
126.6748	10.15	.11	.7189	.1198	.0201	.1262	295.6537	.3406
126.3970	12.29	.14	.8629	.1799	-.0146	.1267	295.8274	.3406
126.7162	14.50	.16	1.0100	.2540	-.0342	.1263	295.8456	.3399
127.1355	16.62	.18	1.1593	.3400	-.0525	.1258	295.8130	.3393
127.0981	18.77	.20	1.2980	.4353	-.0622	.1255	294.9142	.3382
126.3876	20.87	.23	1.3411	.5047	-.0316	.1261	294.5626	.3375
126.6282	.09	-.00	.0655	-.0258	.0673	.1261	295.1399	.3360

$M_\infty = 0.30$; $C_{\mu,avg} = 0$

QINF PSF	ALPHA DEG	BETA DEG	CLT	CDT	CPMT	CMU	HPLEN PSI	WTFLO LBF/SEC
126.8657	.08	-.01	.0276	.0458	.0852	0.0000	-1.1600	0.0000
126.8137	-1.80	-.03	-.0784	.0416	.0787	0.0000	-.5573	0.0000
126.6307	.11	-.01	.0305	.0460	.0854	0.0000	-.6215	0.0000
126.4130	2.01	.02	.1223	.0537	.0880	0.0000	-.6677	0.0000
129.4552	3.98	.04	.2353	.0689	.0900	0.0000	-.7385	0.0000
127.1501	5.98	.06	.3465	.0911	.0839	0.0000	-.7649	0.0000
126.9378	8.02	.08	.4724	.1249	.0749	0.0000	-.8167	0.0000
126.1269	10.12	.11	.6064	.1712	.0647	0.0000	-.8508	0.0000
125.9933	12.26	.13	.7332	.2265	.0348	0.0000	-.7951	0.0000
127.8670	14.48	.16	.8715	.2956	.0176	0.0000	-.7916	0.0000
126.5918	16.57	.18	.9608	.3584	.0252	0.0000	-.8515	0.0000
127.4157	18.67	.20	1.0197	.4213	.0294	0.0000	-.9390	0.0000
126.4248	20.78	.22	1.1026	.4981	.0226	0.0000	-.9882	0.0000
126.6746	.07	-.01	.0271	.0464	.0854	0.0000	-.6476	0.0000

TABLE VIII.- Concluded.

(b) Concluded.

$M_\infty = 0.30$; $\alpha \approx 20.8^0$; $T_{t,plen} = 533^0 R$

QINF PSF	ALPHA DEG	BETA DEG	CLT	CDT	CPMT	CMU	HPLEN PSI	WTFLD LBF/SEC
126.3128	20.79	.23	1.1175	.4992	.0216	.0070	13.7570	.0703
126.5960	20.81	.23	1.1671	.5066	.0138	.0267	54.5703	.0982
126.5678	20.83	.23	1.2027	.5083	.0075	.0414	93.7856	.1317
126.6386	20.84	.23	1.2373	.5093	.0001	.0581	134.6411	.1725
126.5371	20.85	.23	1.2665	.5085	-.0069	.0745	175.0898	.2117
126.1857	20.86	.22	1.3002	.5089	-.0164	.0924	215.6844	.2545
126.9524	20.87	.23	1.3246	.5070	-.0236	.1087	255.3428	.2944
126.6986	20.88	.23	1.3484	.5041	-.0321	.1267	295.0349	.3364
126.4475	20.84	.23	1.2377	.5083	.0007	.0580	133.9299	.1713
126.3540	20.78	.22	1.1032	.4978	.0237	0.0000	-1.0473	0.0000

TABLE IX.- SPANWISE BLOWING ON THE CANARD IN THE PRESENCE OF THE 44° SWEPT TRAPEZOIDAL WING; $\delta_{LE} = \delta_{TE} = 0^{0}$

(a) $i_C = 0^{0}$

$M_\infty = 0.30$; $C_{\mu, avg} = 0.016$; $T_{t, plen} = 526^{0}R$

QINF PSF	ALPHA DEG	BETA DEG	CLT	CDT	CPMT	CMU	HPLEN PSI	WTFLO LBF/SEC
126.2592	.01	-.00	.0003	.0224	.0056	.0160	135.4660	.0952
125.7155	-1.85	-.02	-.1043	.0243	.0016	.0163	135.5433	.0965
126.3922	.05	-.00	.0015	.0221	.0058	.0163	135.5508	.0971
126.3899	1.95	.02	.1045	.0254	.0119	.0160	135.5731	.0954
125.8206	3.91	.04	.2237	.0343	.0165	.0162	135.6220	.0958
126.2042	5.93	.07	.3491	.0521	.0189	.0162	135.6814	.0961
125.6974	7.98	.09	.4850	.0799	.0178	.0162	135.7034	.0962
126.0878	10.10	.11	.6270	.1201	.0167	.0161	135.7368	.0956
126.6767	12.25	.14	.7631	.1714	.0186	.0160	135.7473	.0958
125.5653	14.47	.16	.9074	.2350	.0235	.0162	135.7848	.0956
125.2749	16.60	.18	1.0527	.3083	.0231	.0163	135.8950	.0962
125.9246	18.73	.21	1.1793	.3879	.0192	.0163	135.9470	.0968
125.5781	20.84	.23	1.2978	.4755	.0199	.0161	136.1434	.0954
126.0052	.05	-.00	.0011	.0217	.0058	.0160	135.6073	.0949

$M_\infty = 0.30$; $C_{\mu, avg} = 0.030$; $T_{t, plen} = 524^{0}R$

QINF PSF	ALPHA DEG	BETA DEG	CLT	CDT	CPMT	CMU	HPLEN PSI	WTFLO LBF/SEC
126.2483	.05	.00	.0094	.0052	.0073	.0299	295.9310	.1604
126.3299	-1.87	-.02	-.0996	.0074	.0033	.0300	295.3019	.1606
126.7838	.05	.00	.0106	.0056	.0075	.0298	295.3833	.1603
126.5570	1.95	.02	.1157	.0095	.0129	.0299	295.8276	.1607
126.5567	3.92	.04	.2348	.0189	.0175	.0300	296.1916	.1611
125.7712	5.93	.07	.3635	.0372	.0190	.0302	296.3262	.1612
126.1185	7.98	.09	.5043	.0654	.0190	.0301	296.5735	.1609
125.7921	10.10	.11	.6451	.1060	.0213	.0302	296.7196	.1611
126.1105	12.27	.14	.7845	.1590	.0260	.0301	296.9595	.1610
126.6674	14.49	.16	.9374	.2260	.0286	.0298	294.8839	.1606
125.9329	16.62	.19	1.0873	.3012	.0298	.0302	298.0186	.1613
126.7650	18.77	.21	1.2213	.3847	.0282	.0297	294.5408	.1598
125.6346	20.89	.23	1.3418	.4735	.0310	.0302	296.6019	.1613
126.0154	.01	.00	.0093	.0060	.0070	.0299	294.9077	.1600

$M_\infty = 0.30$; $C_{\mu, avg} = 0$

QINF PSF	ALPHA DEG	BETA DEG	CLT	CDT	CPMT	CMU	HPLEN PSI	WTFLO LBF/SEC
126.2087	-.00	-.00	-.0077	.0348	.0052	0.0000	-.8477	0.0000
126.2633	-1.86	-.02	-.1061	.0368	.0005	0.0000	-.7339	0.0000
126.1204	.04	-.00	-.0052	.0344	.0049	0.0000	-.8190	0.0000
126.1686	1.94	.02	.0964	.0372	.0102	0.0000	-.9112	0.0000
126.3953	3.91	.04	.2125	.0455	.0155	0.0000	-.9959	0.0000
125.9182	5.91	.06	.3392	.0631	.0170	0.0000	-1.0717	0.0000
125.8081	7.97	.09	.4690	.0899	.0173	0.0000	-1.1382	0.0000
125.5121	10.07	.11	.6045	.1286	.0152	0.0000	-1.2182	0.0000
125.5455	12.22	.13	.7387	.1778	.0123	0.0000	-1.3286	0.0000
125.5358	14.44	.16	.8780	.2394	.0068	0.0000	-1.4475	0.0000
126.0858	16.55	.18	1.0042	.3074	.0007	0.0000	-1.6264	0.0000
125.0647	18.70	.21	1.1324	.3884	-.0038	0.0000	-1.8465	0.0000
126.5721	20.81	.23	1.2228	.4704	-.0238	0.0000	-1.7846	0.0000
126.2967	.00	-.00	-.0048	.0334	.0048	0.0000	-.7795	0.0000

TABLE IX.- Continued.

(b) $i_C = 10^0$.

$M_\infty = 0.30$; $C_{\mu, avg} = 0.016$; $T_{t, plen} = 532^0 R$

QINF PSF	ALPHA DEG	BETA DEG	CLT	CDT	CPMT	CMU	HPLEN PSI	WTFLO LBF/SEC
126.3304	.07	-.00	.0268	.0359	.0862	.0162	135.3320	.0959
126.6482	-1.78	-.02	-.0799	.0316	.0780	.0160	135.3641	.0951
126.2195	.07	-.00	.0245	.0358	.0863	.0162	135.4438	.0958
126.4065	2.01	.02	.1252	.0438	.0905	.0161	135.5044	.0956
126.6389	3.96	.04	.2334	.0579	.0948	.0161	135.6025	.0957
126.2596	5.98	.06	.3617	.0839	.0948	.0162	135.6690	.0960
126.0245	8.04	.09	.5070	.1226	.0971	.0163	135.7742	.0966
125.7901	10.16	.11	.6555	.1720	.0938	.0163	135.8991	.0964
125.9932	12.32	.13	.7946	.2334	.0950	.0163	135.9888	.0961
125.7207	14.53	.16	.9291	.3047	.0952	.0162	136.0547	.0956
126.0405	16.66	.18	1.0490	.3813	.0942	.0162	136.1433	.0956
127.0420	18.80	.20	1.1583	.4641	.0918	.0162	136.2110	.0965
126.3157	20.91	.23	1.2559	.5507	.0873	.0163	136.4075	.0963
126.1420	.07	-.00	.0242	.0335	.0812	.0162	135.6080	.0957

$M_\infty = 0.30$; $C_{\mu, avg} = 0.030$; $T_{t, plen} = 527^0 R$

QINF PSF	ALPHA DEG	BETA DEG	CLT	CDT	CPMT	CMU	HPLEN PSI	WTFLO LBF/SEC
126.1810	.07	-.00	.0216	.0160	.0814	.0303	297.4470	.1615
126.5710	-1.79	-.02	-.0800	.0130	.0726	.0302	297.1005	.1615
126.4148	.10	-.00	.0238	.0164	.0816	.0302	297.8741	.1614
126.1897	2.01	.02	.1256	.0248	.0873	.0303	296.3443	.1615
126.7245	3.97	.04	.2356	.0401	.0924	.0300	295.8935	.1607
125.9150	5.99	.06	.3743	.0681	.0986	.0302	295.8055	.1612
125.6894	8.07	.09	.5285	.1094	.1056	.0303	295.8012	.1612
125.8777	10.18	.11	.6721	.1603	.1088	.0302	295.7961	.1610
125.1598	12.34	.13	.8150	.2231	.1134	.0303	295.8930	.1606
126.2357	14.58	.16	.9539	.2977	.1164	.0302	296.1484	.1612
125.8211	16.68	.18	1.0783	.3759	.1146	.0303	296.3412	.1614
126.0033	18.82	.20	1.1923	.4605	.1115	.0303	296.5211	.1614
126.2131	20.95	.23	1.2963	.5513	.1105	.0302	296.7438	.1616
125.5849	.07	-.00	.0219	.0169	.0819	.0304	297.2322	.1616

$M_\infty = 0.30$; $C_{\mu, avg} = 0$

QINF PSF	ALPHA DEG	BETA DEG	CLT	CDT	CPMT	CMU	HPLEN PSI	WTFLO LBF/SEC
125.9710	.06	-.00	.0247	.0469	.0802	0.0000	-.4040	0.0000
126.1522	-1.80	-.02	-.0773	.0427	.0735	0.0000	-.3448	0.0000
125.8332	.09	-.00	.0270	.0467	.0805	0.0000	-.4028	0.0000
126.3002	2.02	.02	.1288	.0547	.0843	0.0000	-.4793	0.0000
126.1030	3.96	.04	.2333	.0684	.0850	0.0000	-.5230	0.0000
126.3716	5.97	.06	.3504	.0920	.0789	0.0000	-.6367	0.0000
126.0630	8.00	.09	.4779	.1266	.0687	0.0000	-.7672	0.0000
126.2780	10.11	.11	.6154	.1738	.0600	0.0000	-.9565	0.0000
125.8104	12.25	.13	.7391	.2282	.0304	0.0000	-.8828	0.0000
125.9144	14.45	.16	.8724	.2950	.0132	0.0000	-.7617	0.0000
125.8954	16.57	.19	.9715	.3607	.0171	0.0000	-.7644	0.0000
126.8399	18.67	.21	1.0252	.4220	.0236	0.0000	-.8176	0.0000
126.1240	20.78	.23	1.1119	.5002	.0170	0.0000	-.8782	0.0000
125.6200	.07	-.00	.0295	.0463	.0806	0.0000	-.3621	0.0000

TABLE IX.- Concluded.

(b) Concluded.

$M_\infty = 0.30$; $\alpha \approx 20.9^0$; $T_{t,plen} = 531^0R$

QINF PSF	ALPHA DEG	BETA DEG	CLT	CDT	CPMT	CMU	HPLEN PSI	WTFLO LBF/SEC
126.1034	20.79	.22	1.1247	.5058	.0255	.0024	14.8814	.0634
126.1615	20.86	.23	1.2032	.5354	.0568	.0097	54.8786	.0711
125.8936	20.89	.23	1.2357	.5449	.0762	.0131	95.6661	.0829
125.8234	20.91	.23	1.2552	.5493	.0882	.0162	135.5597	.0954
126.2715	20.92	.23	1.2647	.5489	.0962	.0193	175.5891	.1098
126.0893	20.93	.23	1.2801	.5512	.1025	.0229	217.3693	.1260
125.6283	20.93	.23	1.2900	.5513	.1079	.0265	256.1552	.1430
126.2768	20.94	.23	1.2921	.5479	.1113	.0301	296.3208	.1605
125.8815	20.91	.23	1.2532	.5504	.0881	.0162	135.7412	.0958
126.5918	20.78	.23	1.1090	.5013	.0170	0.0000	-.9578	0.0000

TABLE X.- SPANWISE BLOWING IN THE CHANNEL OF THE "LOCKED VORTEX" WING CONFIGURATION.

(a) $\delta_{LE} = \delta_{TE} = 20^0$

$M_\infty = 0.15$; $C_{\mu,avg} = 0.154$; $T_{t,plen} = 513^0 R$

QINF PSF	ALPHA DEG	BETA DEG	CLT	CDT	CPMT	CMU	HPLEN PSI	WTFLO LBF/SEC
32.3373	.00	-.00	.1685	.1237	-.1396	.1550	95.3980	.1269
32.3000	-1.81	-.02	.0659	.1191	-.1177	.1549	95.4408	.1267
32.4175	.03	-.00	.1626	.1258	-.1374	.1534	94.5640	.1262
32.4466	1.89	.02	.2787	.1383	-.1682	.1539	94.5179	.1269
32.4065	3.79	.04	.3816	.1531	-.1911	.1536	94.8732	.1264
32.6388	5.75	.07	.4920	.1739	-.2161	.1524	94.3748	.1265
32.5932	7.74	.09	.6046	.1980	-.2420	.1521	94.2746	.1261
32.4148	9.76	.11	.7252	.2257	-.2735	.1566	96.4660	.1285
32.2959	11.87	.14	.8923	.2683	-.3309	.1564	95.8714	.1280
32.1396	14.00	.16	1.0345	.3147	-.3742	.1568	95.7038	.1278
32.8711	16.06	.19	1.1845	.3697	-.4191	.1534	95.6128	.1279
32.4673	18.12	.21	1.2735	.4158	-.4364	.1553	95.5756	.1279
32.4673	20.18	.23	1.3261	.4562	-.4343	.1553	95.5719	.1279
32.1589	.00	-.00	.1516	.1240	-.1338	.1566	95.6990	.1277

$M_\infty = 0.15$; $C_{\mu,avg} = 0.347$; $T_{t,plen} = 517^0 R$

QINF PSF	ALPHA DEG	BETA DEG	CLT	CDT	CPMT	CMU	HPLEN PSI	WTFLO LBF/SEC
32.8213	.01	-.00	.3172	.0616	-.2254	.3427	214.9993	.2493
32.7577	-1.79	-.02	.2221	.0498	-.2090	.3436	215.3258	.2493
32.8711	.05	-.00	.3193	.0611	-.2272	.3431	215.6009	.2497
32.7633	1.90	.02	.4114	.0738	-.2428	.3443	215.8119	.2496
32.7481	3.80	.04	.5040	.0880	-.2547	.3450	215.9796	.2499
32.7052	5.75	.07	.5977	.1043	-.2687	.3457	216.2002	.2499
32.6070	7.73	.09	.7093	.1272	-.2891	.3473	216.3021	.2503
32.5531	9.77	.12	.8382	.1569	-.3204	.3479	216.3848	.2502
32.1492	11.86	.14	.9927	.1987	-.3652	.3527	216.5989	.2502
32.1907	13.99	.16	1.0974	.2353	-.3793	.3524	216.7650	.2502
32.2267	16.05	.18	1.2142	.2833	-.4069	.3524	216.8700	.2504
32.3442	18.11	.21	1.3452	.3422	-.4445	.3513	217.0097	.2505
32.8531	20.18	.23	1.4782	.4118	-.4866	.3461	217.2225	.2505
32.2695	.02	-.00	.3250	.0507	-.2297	.3510	217.3291	.2494

$M_\infty = 0.15$; $C_{\mu,avg} = 0.476$; $T_{t,plen} = 530^0 R$

QINF PSF	ALPHA DEG	BETA DEG	CLT	CDT	CPMT	CMU	HPLEN PSI	WTFLO LBF/SEC
32.6139	.02	-.00	.4055	-.0103	-.2680	.4765	296.7731	.3287
32.6014	-1.80	-.02	.2926	-.0271	-.2437	.4780	297.7158	.3292
32.6042	.06	-.00	.4081	-.0134	-.2675	.4768	296.3055	.3280
32.7328	1.91	.02	.5316	.0046	-.2972	.4749	296.2696	.3277
32.5060	3.80	.04	.6407	.0237	-.3186	.4790	296.2894	.3280
32.5890	5.76	.06	.7542	.0495	-.3423	.4786	296.5676	.3283
32.4064	7.74	.09	.8704	.0781	-.3648	.4820	296.7228	.3285
32.6402	9.78	.11	.9815	.1113	-.3846	.4788	296.8442	.3284
32.4479	11.86	.13	1.0674	.1369	-.3883	.4820	297.1192	.3284
32.2764	14.00	.16	1.1712	.1735	-.4026	.4847	297.3434	.3283
33.2223	16.06	.18	1.2834	.2251	-.4246	.4713	297.3428	.3283
33.0661	18.12	.21	1.4022	.2754	-.4507	.4740	297.4697	.3283
32.9112	20.18	.23	1.5398	.3392	-.4905	.4758	297.4446	.3279
32.2930	.03	-.00	.4224	-.0291	-.2733	.4852	297.9741	.3273

TABLE X.- Continued.

(a) Continued.

$M_\infty = 0.20$; $C_{\mu,avg} = 0.086$; $T_{t,plen} = 526^0R$

QINF PSF	ALPHA DEG	BETA DEG	CLT	CDT	CPMT	CMU	HPLEN PSI	WTFLO LBF/SEC
57.2774	.00	-.00	.1095	.1312	-.1032	.0856	94.1876	.1229
56.9499	-1.83	-.02	.0012	.1269	-.0779	.0859	94.1630	.1227
57.3570	.04	-.00	.1143	.1324	-.1045	.0855	94.1385	.1230
57.3953	1.90	.02	.2217	.1446	-.1308	.0853	94.1347	.1230
57.2706	3.81	.04	.3332	.1602	-.1575	.0855	94.1855	.1230
57.3473	5.78	.06	.4360	.1761	-.1778	.0855	94.2025	.1232
57.3515	7.75	.09	.5256	.1929	-.1919	.0854	94.2249	.1231
57.2583	9.81	.11	.6305	.2170	-.2139	.0861	94.2758	.1239
57.1966	11.90	.13	.7552	.2488	-.2459	.0861	94.3327	.1238
57.3542	14.05	.16	.8563	.2779	-.2649	.0857	94.3200	.1236
57.3761	16.11	.19	1.0142	.3262	-.3186	.0857	94.3291	.1236
56.9429	18.19	.22	1.1270	.3794	-.3541	.0861	94.3348	.1233
56.8333	20.24	.23	1.1319	.4076	-.3270	.0866	94.3296	.1238
56.8333	.02	-.00	.1093	.1347	-.1039	.0865	94.4936	.1237

$M_\infty = 0.20$; $C_{\mu,avg} = 0.197$; $T_{t,plen} = 531^0R$

QINF PSF	ALPHA DEG	BETA DEG	CLT	CDT	CPMT	CMU	HPLEN PSI	WTFLO LBF/SEC
57.4625	.02	-.00	.1789	.0985	-.1448	.1993	218.8662	.2499
57.3035	-1.82	-.02	.0717	.0938	-.1234	.1957	215.7092	.2449
57.4474	.04	-.00	.1683	.0983	-.1392	.1943	214.2458	.2437
57.5927	1.89	.02	.2545	.1058	-.1509	.1937	214.2106	.2435
57.3829	3.80	.04	.3507	.1160	-.1672	.1959	215.7004	.2452
57.2637	5.76	.07	.4520	.1307	-.1840	.1966	216.1224	.2454
57.2294	7.78	.09	.5709	.1547	-.2141	.1971	216.3831	.2458
57.8009	9.81	.11	.7680	.2040	-.2872	.1955	216.6639	.2461
56.8155	11.91	.13	.9413	.2500	-.3406	.1989	216.8869	.2461
57.0581	14.07	.16	1.0824	.2989	-.3786	.1983	217.0722	.2464
56.6797	16.13	.18	1.2084	.3537	-.4163	.1998	217.1628	.2465
57.4117	18.20	.20	1.3223	.4133	-.4503	.1974	217.2800	.2467
57.5186	20.28	.23	1.4263	.4710	-.4772	.1971	217.4598	.2467
57.2432	.01	-.00	.1775	.0972	-.1448	.1982	217.7046	.2469

$M_\infty = 0.20$; $C_{\mu,avg} = 0.274$; $T_{t,plen} = 536^0R$

QINF PSF	ALPHA DEG	BETA DEG	CLT	CDT	CPMT	CMU	HPLEN PSI	WTFLO LBF/SEC
57.4638	.02	-.00	.3004	.0777	-.2127	.2700	295.1401	.3251
57.3186	-1.82	-.02	.2009	.0681	-.1932	.2715	294.8396	.3260
57.4049	.05	-.00	.3035	.0772	-.2130	.2724	296.3097	.3272
57.5570	1.91	.02	.3994	.0892	-.2307	.2723	296.8897	.3278
57.4008	3.80	.04	.4938	.1033	-.2447	.2735	297.4805	.3283
57.3213	5.77	.07	.5819	.1195	-.2545	.2742	297.7330	.3286
57.4515	7.78	.09	.7107	.1483	-.2879	.2738	297.8591	.3288
57.2884	9.83	.11	.8935	.1957	-.3488	.2743	297.7132	.3283
57.4159	11.92	.14	1.0089	.2328	-.3703	.2733	297.3338	.3278
56.8703	14.07	.16	1.1098	.2677	-.3839	.2759	297.1465	.3278
57.0937	16.13	.18	1.2332	.3217	-.4184	.2748	297.1455	.3277
57.1746	18.21	.20	1.3607	.3833	-.4581	.2745	297.1781	.3278
57.3391	20.29	.22	1.4780	.4492	-.4932	.2749	298.2524	.3289
57.0403	.02	-.00	.3061	.0736	-.2151	.2758	298.0711	.3280

TABLE X.- Continued.

(a) Concluded.

$M_\infty = 0.15$; $C_{\mu, avg} = 0$

QINF PSF	ALPHA DEG	BETA DEG	CLT	CDT	CPMT	CMU	HPLEN PSI	WTFLO LBF/SEC
32.2985	.01	-.00	.1478	.1248	-.1238	0.0000	.1381	0.0000
32.4617	-1.81	-.02	.0539	.1274	-.1057	0.0000	.1077	0.0000
32.4963	.03	-.00	.1511	.1261	-.1242	0.0000	.1062	0.0000
32.5544	1.89	.02	.2480	.1295	-.1454	0.0000	.0910	0.0000
32.4631	3.79	.04	.3405	.1382	-.1652	0.0000	.0673	0.0000
32.3373	5.73	.06	.4346	.1482	-.1832	0.0000	.0597	0.0000
32.7411	7.72	.09	.5227	.1615	-.1987	0.0000	.0591	0.0000
32.8558	9.76	.11	.6172	.1829	-.2168	0.0000	.0542	0.0000
32.5696	11.83	.13	.7141	.2115	-.2384	0.0000	.0222	0.0000
32.1934	13.97	.16	.8104	.2505	-.2598	0.0000	.0113	0.0000
32.6913	16.03	.18	.8917	.2953	-.2829	0.0000	.0045	0.0000
32.3469	18.09	.20	.9548	.3437	-.3038	0.0000	.0125	0.0000
32.5060	20.13	.22	1.0005	.3954	-.3202	0.0000	.0118	0.0000
32.7756	.01	-.00	.1521	.1292	-.1242	0.0000	.2602	0.0000

$M_\infty = 0.20$; $C_{\mu, avg} = 0$

QINF PSF	ALPHA DEG	BETA DEG	CLT	CDT	CPMT	CMU	HPLEN PSI	WTFLO LBF/SEC
57.0663	.01	-.00	.1433	.1251	-.1200	0.0000	.1952	0.0000
57.0800	-1.81	-.02	.0498	.1277	-.1015	0.0000	.2442	0.0000
57.4597	.03	-.00	.1471	.1249	-.1204	0.0000	.2009	0.0000
57.4460	1.90	.02	.2413	.1298	-.1411	0.0000	.1626	0.0000
57.1527	3.81	.04	.3368	.1375	-.1601	0.0000	.1290	0.0000
57.1280	5.75	.06	.4271	.1459	-.1770	0.0000	.0866	0.0000
57.0636	7.75	.09	.5155	.1589	-.1936	0.0000	.0652	0.0000
56.9347	9.81	.11	.6113	.1786	-.2119	0.0000	.0389	0.0000
56.7798	11.88	.13	.7124	.2066	-.2336	0.0000	.0093	0.0000
56.3466	14.03	.16	.8075	.2451	-.2545	0.0000	-.0325	0.0000
56.9114	16.11	.18	.8880	.2892	-.2776	0.0000	-.0287	0.0000
57.3445	18.16	.20	.9528	.3381	-.2983	0.0000	-.0455	0.0000
56.6975	20.22	.22	1.0017	.3912	-.3152	0.0000	-.0584	0.0000
57.2143	.01	-.00	.1416	.1249	-.1177	0.0000	.1912	0.0000

TABLE X.- Continued.

(b) $\delta_{LE} = \delta_{TE} = 30^0$

$M_\infty = 0.15$; $C_{\mu, avg} = 0.160$; $T_{t, plen} = 498^0 R$

QINF PSF	ALPHA DEG	BETA DEG	CLT	CDT	CPMT	CMU	HPLEN PSI	WTFLO LBF/SEC
33.1887	-.00	.00	.0991	.1821	-.1082	.1615	95.9438	.1382
33.2149	-1.82	-.02	-.0177	.1776	-.0773	.1608	95.2196	.1380
33.3684	.02	.00	.0908	.1837	-.1050	.1599	94.9630	.1380
33.3878	1.88	.02	.2048	.1935	-.1343	.1593	94.8343	.1376
33.4652	3.79	.04	.3024	.2054	-.1506	.1600	94.8058	.1386
33.3781	5.74	.07	.3830	.2200	-.1611	.1595	94.7613	.1379
33.2730	7.72	.09	.4792	.2388	-.1796	.1601	94.7609	.1380
33.1762	9.76	.11	.5880	.2731	-.2121	.1605	94.7994	.1379
33.0822	11.84	.13	.7008	.3150	-.2491	.1609	94.7917	.1379
33.1223	13.97	.16	.8082	.3560	-.2785	.1616	94.8154	.1387
33.2039	16.03	.18	.8952	.3926	-.3030	.1606	94.7982	.1382
33.0047	18.08	.20	.9858	.4334	-.3282	.1629	94.8435	.1394
32.9978	20.14	.22	1.0947	.4800	-.3623	.1620	94.8403	.1385
33.2786	.00	-.00	.0931	.1838	-.1067	.1615	95.2456	.1392

$M_\infty = 0.15$; $C_{\mu, avg} = 0.346$; $T_{t, plen} = 512^0 R$

QINF PSF	ALPHA DEG	BETA DEG	CLT	CDT	CPMT	CMU	HPLEN PSI	WTFLO LBF/SEC
33.6644	.00	-.00	.1600	.1136	-.1414	.3399	213.4954	.2557
33.3879	-1.82	-.02	.0271	.1053	-.1084	.3428	212.8656	.2557
33.5248	.03	-.00	.1491	.1113	-.1398	.3425	213.6910	.2563
33.6354	1.88	.02	.2879	.1280	-.1796	.3425	214.3425	.2569
33.5027	3.78	.04	.4297	.1520	-.2204	.3445	214.7861	.2573
33.3920	5.74	.07	.5578	.1763	-.2535	.3461	215.0163	.2575
33.4377	7.72	.09	.6721	.2057	-.2806	.3462	215.2859	.2578
33.4114	9.76	.11	.8110	.2508	-.3245	.3468	215.4688	.2580
33.1003	11.84	.14	.9793	.3118	-.3832	.3503	215.6742	.2581
33.2040	13.98	.16	1.0101	.3232	-.3642	.3496	214.7059	.2584
33.4695	16.02	.19	1.0449	.3386	-.3507	.3472	215.9364	.2584
33.4750	18.08	.21	1.0998	.3701	-.3530	.3476	216.1851	.2586
33.7156	20.14	.23	1.1855	.4156	-.3725	.3451	216.3030	.2585
33.5054	.00	-.00	.1730	.1040	-.1452	.3432	213.6807	.2556

$M_\infty = 0.15$; $C_{\mu, avg} = 0.475$; $T_{t, plen} = 528^0 R$

QINF PSF	ALPHA DEG	BETA DEG	CLT	CDT	CPMT	CMU	HPLEN PSI	WTFLO LBF/SEC
33.3520	-.00	-.00	.1892	.0480	-.1512	.4734	293.4639	.3350
33.2040	-1.80	-.02	.0736	.0401	-.1264	.4776	294.6933	.3360
33.3326	.02	-.00	.1827	.0454	-.1480	.4772	295.4070	.3368
33.3105	1.88	.02	.3041	.0584	-.1791	.4783	295.8729	.3371
33.2164	3.78	.04	.4200	.0732	-.2029	.4802	296.2854	.3373
33.5068	5.73	.07	.5349	.0967	-.2260	.4760	296.3881	.3371
33.3478	7.71	.09	.6521	.1266	-.2513	.4769	295.5648	.3361
33.1874	9.75	.11	.8238	.1828	-.3139	.4782	294.9025	.3353
33.3699	11.84	.14	.9791	.2466	-.3632	.4751	294.6729	.3349
33.0048	13.98	.16	1.0997	.2958	-.3904	.4807	294.4739	.3350
33.3824	16.03	.19	1.1884	.3380	-.4079	.4754	294.4274	.3350
33.7682	18.08	.21	1.2164	.3561	-.3931	.4706	294.8575	.3353
33.6299	20.13	.23	1.2678	.3829	-.3955	.4727	295.1625	.3352
33.4031	-.00	-.00	.2099	.0405	-.1609	.4771	296.2304	.3355

TABLE X.- Continued.

(b) Continued.

$M_\infty = 0.20$; $C_{\mu, avg} = 0.095$; $T_{t, plen} = 514^0R$

QINF PSF	ALPHA DEG	BETA DEG	CLT	CDT	CPMT	CMU	HPLEN PSI	WTFLO LBF/SEC
59.0849	-.02	-.00	.0708	.1760	-.0864	.0950	96.6204	.1420
58.6450	-1.85	-.02	-.0309	.1729	-.0645	.0959	95.5921	.1426
58.7985	.00	-.00	.0748	.1784	-.0881	.0936	93.2879	.1404
58.9424	1.87	.02	.1734	.1875	-.1089	.0942	94.4121	.1413
58.9219	3.79	.04	.2774	.2037	-.1319	.0951	95.3743	.1424
58.7231	5.75	.06	.3771	.2238	-.1568	.0950	95.6109	.1417
58.5888	7.73	.09	.4848	.2510	-.1876	.0932	93.1346	.1396
58.3270	9.78	.11	.6193	.2866	-.2335	.0967	95.7099	.1434
58.0652	11.87	.13	.7438	.3213	-.2697	.0952	93.1623	.1415
58.4243	14.02	.16	.8534	.3574	-.2998	.0966	95.4725	.1437
58.1749	16.06	.18	.9442	.3953	-.3250	.0974	96.0531	.1443
57.7047	18.15	.20	1.0406	.4382	-.3537	.0965	94.8800	.1421
58.4312	20.20	.23	1.1460	.4866	-.3903	.0947	93.7389	.1416
59.2686	-.02	-.01	.0719	.1806	-.0888	.0933	93.4747	.1418

$M_\infty = 0.20$; $C_{\mu, avg} = 0.198$; $T_{t, plen} = 519^0R$

QINF PSF	ALPHA DEG	BETA DEG	CLT	CDT	CPMT	CMU	HPLEN PSI	WTFLO LBF/SEC
58.8300	-.01	.00	.1504	.1604	-.1328	.1956	213.2595	.2550
58.5916	-1.85	-.02	.0217	.1506	-.0977	.1973	213.9181	.2560
58.7588	.02	.00	.1518	.1599	-.1328	.1975	214.8174	.2569
58.8670	1.88	.02	.2743	.1766	-.1666	.1971	215.3195	.2567
58.8012	3.79	.04	.3946	.1971	-.1975	.1973	214.8583	.2568
58.5162	5.75	.07	.4904	.2149	-.2129	.1981	214.6602	.2566
58.4997	7.73	.09	.5595	.2293	-.2149	.1981	214.5808	.2565
58.2694	9.78	.11	.6468	.2565	-.2325	.1993	214.7083	.2570
58.6107	11.87	.14	.7602	.2973	-.2681	.1982	214.9297	.2570
58.4394	14.03	.16	.8452	.3302	-.2865	.1992	215.1736	.2575
58.2215	16.07	.18	.9326	.3647	-.3091	.2001	215.5345	.2576
58.6601	18.14	.20	1.0211	.4044	-.3331	.1988	215.7431	.2579
57.6841	20.19	.22	1.1293	.4520	-.3674	.2003	214.1018	.2559
58.4600	-.01	-.00	.1601	.1597	-.1376	.1976	213.7296	.2558

$M_\infty = 0.20$; $C_{\mu, avg} = 0.273$; $T_{t, plen} = 525^0R$

QINF PSF	ALPHA DEG	BETA DEG	CLT	CDT	CPMT	CMU	HPLEN PSI	WTFLO LBF/SEC
58.3257	-.02	-.00	.1178	.1252	-.1129	.2733	295.9975	.3382
58.2105	-1.84	-.02	.0026	.1201	-.0859	.2734	295.5637	.3376
58.4257	.01	-.00	.1210	.1259	-.1143	.2726	295.4615	.3378
58.4408	1.88	.02	.2406	.1408	-.1441	.2725	295.6188	.3377
58.3750	3.78	.04	.3575	.1605	-.1733	.2730	295.7466	.3378
58.1653	5.75	.06	.4725	.1837	-.1998	.2741	295.8445	.3378
58.5230	7.75	.09	.5777	.2091	-.2191	.2725	296.1350	.3378
58.3654	9.79	.11	.7098	.2525	-.2625	.2735	296.0912	.3380
58.0721	11.89	.14	.8163	.2913	-.2910	.2748	296.1730	.3379
58.1913	14.02	.17	.9052	.3279	-.3112	.2741	295.9729	.3376
57.9185	16.08	.19	.9816	.3601	-.3277	.2751	295.8140	.3372
58.3311	18.13	.20	1.0341	.3829	-.3278	.2731	295.6150	.3370
58.1734	20.21	.22	1.1175	.4231	-.3489	.2740	295.6220	.3371
58.6628	-.02	-.00	.1289	.1225	-.1166	.2718	296.1447	.3367

TABLE X.- Continued.

(b) Concluded.

$M_\infty = 0.15$; $C_{\mu, avg} = 0$

QINF PSF	ALPHA DEG	BETA DEG	CLT	CDT	CPMT	CMU	HPLEN PSI	WTFLO LBF/SEC
32.5355	.00	-.00	.2342	.1794	-.1874	0.0000	.2369	0.0000
32.6544	-1.81	-.02	.1280	.1778	-.1607	0.0000	.3126	0.0000
32.6614	.04	-.00	.2359	.1799	-.1868	0.0000	.3204	0.0000
32.6918	1.90	.02	.3422	.1871	-.2151	0.0000	.3256	0.0000
32.5148	3.79	.04	.4441	.1974	-.2420	0.0000	.3396	0.0000
32.5673	5.74	.06	.5333	.2086	-.2640	0.0000	.3292	0.0000
33.2546	7.72	.09	.5837	.2197	-.2692	0.0000	.3301	0.0000
33.0693	9.75	.11	.6353	.2402	-.2735	0.0000	.3451	0.0000
32.7319	11.84	.13	.7048	.2698	-.2865	0.0000	.3357	0.0000
32.6987	13.97	.16	.7883	.3047	-.3063	0.0000	.3141	0.0000
32.8826	16.02	.18	.8822	.3454	-.3324	0.0000	.3128	0.0000
32.9324	18.08	.20	1.0032	.3974	-.3728	0.0000	.2587	0.0000
32.7347	20.14	.22	1.1109	.4572	-.4073	0.0000	.2377	0.0000
32.3391	.02	-.00	.2333	.1824	-.1864	0.0000	.4680	0.0000

$M_\infty = 0.20$; $C_{\mu, avg} = 0$

QINF PSF	ALPHA DEG	BETA DEG	CLT	CDT	CPMT	CMU	HPLEN PSI	WTFLO LBF/SEC
57.1049	.02	-.00	.2278	.1767	-.1819	0.0000	.4091	0.0000
57.2434	-1.81	-.02	.1229	.1761	-.1567	0.0000	.4402	0.0000
57.3969	.04	-.00	.2257	.1767	-.1805	0.0000	.4096	0.0000
57.3243	1.91	.02	.3320	.1823	-.2080	0.0000	.3707	0.0000
57.1653	3.81	.04	.4365	.1909	-.2361	0.0000	.3403	0.0000
57.1242	5.76	.06	.5202	.1998	-.2560	0.0000	.3107	0.0000
57.3394	7.74	.08	.5790	.2120	-.2649	0.0000	.3091	0.0000
57.0694	9.79	.11	.6278	.2320	-.2674	0.0000	.3170	0.0000
56.8102	11.87	.13	.6980	.2607	-.2800	0.0000	.2815	0.0000
57.2969	14.03	.15	.7863	.2973	-.3019	0.0000	.2349	0.0000
57.4065	16.08	.18	.8836	.3376	-.3291	0.0000	.1084	0.0000
56.7910	18.15	.20	1.0075	.3920	-.3722	0.0000	.0154	0.0000
58.2685	20.23	.22	1.1078	.4491	-.4041	0.0000	-.0316	0.0000
57.2201	.01	-.00	.2199	.1763	-.1783	0.0000	.2153	0.0000

TABLE X.- Continued.

(c) $\delta_{LE} = 45^0$; $\delta_{TE} = 30^0$

$M_\infty = 0.15$; $C_{\mu, avg} = 0.342$; $T_{t, plen} = 514^0 R$

QINF PSF	ALPHA DEG	BETA DEG	CLT	CDT	CPMT	CMU	HPLEN PSI	WTFLO LBF/SEC
33.2399	.01	-.00	.2219	.1478	-.1613	.3417	214.2586	.2538
33.0546	-1.80	-.02	.0759	.1316	-.1168	.3439	214.4415	.2538
33.0726	.04	-.00	.2083	.1440	-.1549	.3438	214.5570	.2537
33.1915	1.89	.02	.3644	.1654	-.2008	.3431	214.6404	.2539
33.1846	3.79	.04	.4935	.1899	-.2358	.3433	214.8073	.2538
33.0214	5.74	.07	.6095	.2166	-.2634	.3450	214.8738	.2537
33.3035	7.74	.09	.7431	.2546	-.3051	.3426	214.9011	.2538
33.3188	9.76	.11	.8407	.2914	-.3230	.3422	214.9573	.2535
33.1196	11.84	.13	.9042	.3260	-.3269	.3444	214.9838	.2534
33.2233	13.98	.16	.9705	.3631	-.3398	.3414	213.9401	.2520
33.4391	16.02	.18	1.0759	.4147	-.3771	.3384	213.2551	.2514
33.1307	18.08	.20	1.1684	.4638	-.4036	.3423	213.4201	.2518
33.7363	20.14	.22	1.2488	.5124	-.4245	.3368	213.7643	.2520
33.0491	.02	-.00	.2399	.1307	-.1665	.3450	214.9043	.2523

$M_\infty = 0.15$; $C_{\mu, avg} = 0.472$; $T_{t, plen} = 532^0 R$

QINF PSF	ALPHA DEG	BETA DEG	CLT	CDT	CPMT	CMU	HPLEN PSI	WTFLO LBF/SEC
33.2731	.01	-.00	.2149	.0671	-.1449	.4710	293.2064	.3321
33.1901	-1.80	-.02	.0573	.0511	-.0975	.4770	296.2962	.3347
33.3616	.04	-.00	.1953	.0620	-.1340	.4746	297.2126	.3343
33.4045	1.89	.02	.3509	.0851	-.1820	.4741	296.9269	.3340
33.3090	3.79	.04	.5116	.1148	-.2293	.4747	296.5801	.3330
33.1832	5.75	.06	.6442	.1499	-.2656	.4760	296.2480	.3324
33.5773	7.73	.09	.8150	.2124	-.3301	.4701	296.0714	.3321
33.5054	9.78	.11	.9470	.2630	-.3720	.4712	295.9377	.3320
33.1555	11.86	.14	1.0575	.3072	-.3940	.4763	295.9789	.3319
33.4390	13.99	.16	1.1111	.3387	-.3876	.4717	295.8747	.3314
33.5925	16.02	.18	1.1470	.3753	-.3955	.4697	295.8399	.3314
33.4114	18.10	.20	1.2448	.4321	-.4246	.4725	295.7650	.3314
33.4169	20.14	.22	1.3383	.4892	-.4527	.4702	294.5945	.3299
33.3892	.02	-.00	.2416	.0575	-.1515	.4692	293.8605	.3286

$M_\infty = 0.15$; $C_{\mu, avg} = 0$

QINF PSF	ALPHA DEG	BETA DEG	CLT	CDT	CPMT	CMU	HPLEN PSI	WTFLO LBF/SEC
33.0642	.02	-.00	.3025	.2026	-.2058	0.0000	.0790	0.0000
33.2564	-1.81	-.02	.1887	.2032	-.1720	0.0000	.1224	0.0000
33.1914	.05	-.00	.2926	.2036	-.2015	0.0000	.0974	0.0000
33.3090	1.89	.02	.3999	.2071	-.2353	0.0000	.0835	0.0000
33.2191	3.79	.04	.4717	.2188	-.2566	0.0000	.0949	0.0000
33.2246	5.72	.06	.5035	.2294	-.2562	0.0000	.0912	0.0000
33.2080	7.70	.08	.5437	.2461	-.2533	0.0000	.0873	0.0000
33.0227	9.74	.11	.5996	.2699	-.2608	0.0000	.0650	0.0000
33.2619	11.83	.13	.6834	.3030	-.2812	0.0000	.0472	0.0000
33.5758	13.94	.15	.7762	.3441	-.3068	0.0000	.0263	0.0000
33.0324	15.99	.18	.8660	.3889	-.3340	0.0000	-.0280	0.0000
33.1541	18.05	.20	.9496	.4366	-.3606	0.0000	-.0145	0.0000
33.2163	20.10	.22	1.0307	.4852	-.3860	0.0000	-.0644	0.0000
33.4887	.01	-.00	.2830	.2024	-.1986	0.0000	.1508	0.0000

TABLE X.- Continued.

(c) Concluded.

$M_\infty = 0.20$; $C_{\mu, avg} = 0.194$; $T_{t, plen} = 532^0R$

QINF PSF	ALPHA DEG	BETA DEG	CLT	CDT	CPMT	CMU	HPLEN PSI	WTFLO LBF/SEC
58.0826	.02	-.00	.1956	.1796	-.1366	.1958	214.7904	.2485
58.2389	-1.81	-.02	.0629	.1734	-.1011	.1953	214.9981	.2486
58.5144	.04	-.00	.1805	.1802	-.1278	.1924	213.0770	.2463
58.6268	1.90	.02	.2851	.1905	-.1484	.1923	212.9903	.2466
58.4143	3.81	.04	.3935	.2102	-.1736	.1933	213.2229	.2469
58.3211	5.77	.06	.5170	.2384	-.2123	.1939	213.3792	.2473
58.1032	7.76	.08	.6298	.2689	-.2435	.1945	213.4259	.2472
58.1306	9.81	.11	.7706	.3133	-.2952	.1945	213.5366	.2474
58.0113	11.90	.13	.8731	.3522	-.3222	.1950	213.5896	.2475
58.1909	14.05	.16	.9676	.3936	-.3466	.1943	213.6441	.2473
58.4266	16.09	.18	1.0419	.4334	-.3653	.1935	213.6971	.2473
58.2320	18.16	.20	1.1088	.4744	-.3830	.1945	213.7781	.2477
58.0894	20.21	.23	1.1893	.5253	-.4091	.1948	213.8086	.2476
58.5869	.03	-.00	.2079	.1827	-.1445	.1934	214.1760	.2477

$M_\infty = 0.20$; $C_{\mu, avg} = 0.270$; $T_{t, plen} = 538^0R$

QINF PSF	ALPHA DEG	BETA DEG	CLT	CDT	CPMT	CMU	HPLEN PSI	WTFLO LBF/SEC
58.5582	.03	-.00	.2035	.1650	-.1406	.2692	295.5371	.3304
58.4101	-1.81	-.02	.0543	.1483	-.0950	.2710	297.1447	.3313
58.7130	.04	-.00	.1880	.1640	-.1317	.2686	296.1704	.3301
58.6925	1.92	.02	.3153	.1827	-.1662	.2682	295.6489	.3295
58.6007	3.82	.04	.4472	.2068	-.2055	.2685	295.2204	.3293
58.5980	5.77	.07	.5644	.2317	-.2349	.2682	294.9048	.3289
56.2813	7.77	.09	.7078	.2729	-.2854	.2698	294.7539	.3290
58.5760	9.81	.11	.7780	.2980	-.2948	.2685	295.0364	.3291
58.2443	11.90	.13	.8848	.3371	-.3260	.2703	295.2568	.3293
57.9276	14.05	.15	.9871	.3801	-.3556	.2717	295.2129	.3293
58.3375	16.11	.18	1.0738	.4229	-.3773	.2696	295.1487	.3290
58.0510	18.17	.20	1.1522	.4683	-.3960	.2710	295.0915	.3291
58.4992	20.25	.23	1.2286	.5197	-.4198	.2690	295.0829	.3291
58.2525	.01	-.00	.2166	.1608	-.1484	.2700	295.0872	.3287

$M_\infty = 0.20$; $C_{\mu, avg} = 0$

QINF PSF	ALPHA DEG	BETA DEG	CLT	CDT	CPMT	CMU	HPLEN PSI	WTFLO LBF/SEC
58.5499	.01	-.00	.2635	.1887	-.1883	0.0000	-.2488	0.0000
58.2525	-1.81	-.02	.1635	.1926	-.1624	0.0000	-.1939	0.0000
58.4142	.05	-.00	.2719	.1945	-.1925	0.0000	-.2008	0.0000
58.4910	1.91	.02	.3769	.1975	-.2256	0.0000	-.2145	0.0000
58.3265	3.80	.04	.4469	.2051	-.2457	0.0000	-.1836	0.0000
58.2689	5.75	.06	.4822	.2163	-.2467	0.0000	-.1689	0.0000
58.3361	7.75	.08	.5273	.2335	-.2469	0.0000	-.1781	0.0000
58.2676	9.77	.11	.5854	.2574	-.2537	0.0000	-.1823	0.0000
58.3937	11.86	.13	.6663	.2899	-.2715	0.0000	-.2111	0.0000
57.8289	14.01	.15	.7718	.3351	-.3031	0.0000	-.2269	0.0000
57.9344	16.06	.18	.8615	.3799	-.3299	0.0000	-.2447	0.0000
58.6376	18.12	.20	.9497	.4278	-.3586	0.0000	-.2912	0.0000
58.4567	20.18	.22	1.0170	.4745	-.3770	0.0000	-.3213	0.0000
58.4910	.02	-.00	.2689	.1990	-.1920	0.0000	-.1025	0.0000

TABLE X.- Continued.

(d) $\delta_{LE} = \delta_{TE} = 0^{0}$

$M_{\infty} = 0.15$; $C_{\mu, avg} = 0.342$; $T_{t, plen} = 531^{0}R$

QINF PSF	ALPHA DEG	BETA DEG	CLT	CDT	CPMT	CMU	HPLEN PSI	WTFLO LBF/SEC
33.1692	.01	-.01	.1470	-.1248	-.0605	.3427	213.1698	.2487
33.1318	-1.81	-.03	.0281	-.1272	-.0374	.3423	213.1514	.2482
33.3780	.05	-.01	.1428	-.1227	-.0595	.3401	213.1825	.2485
33.4001	1.90	.02	.2544	-.1123	-.0824	.3396	213.1585	.2483
33.4167	3.80	.04	.3749	-.0957	-.1050	.3397	213.2627	.2485
33.2397	5.76	.06	.5105	-.0727	-.1414	.3414	213.2612	.2484
33.1014	7.73	.09	.6790	-.0359	-.1972	.3428	213.3054	.2485
33.0087	9.77	.11	.8321	.0076	-.2439	.3437	213.3631	.2485
33.3337	11.85	.13	.9834	.0599	-.2907	.3410	213.8882	.2489
33.0571	14.00	.15	1.1582	.1227	-.3507	.3441	213.9627	.2491
32.8995	16.05	.18	1.3430	.1978	-.4223	.3458	213.9707	.2492
33.1498	18.12	.20	1.5285	.2866	-.4948	.3430	214.0670	.2490
32.9548	20.18	.22	1.7061	.3825	-.5591	.3453	214.1503	.2493
33.3019	.00	-.01	.1292	-.1202	-.0551	.3420	214.3347	.2494

$M_{\infty} = 0.15$; $C_{\mu, avg} = 0$

QINF PSF	ALPHA DEG	BETA DEG	CLT	CDT	CPMT	CMU	HPLEN PSI	WTFLO LBF/SEC
33.5412	.01	-.00	.0296	.0536	-.0112	0.0000	.0629	0.0000
33.1844	-1.81	-.02	-.0798	.0537	.0107	0.0000	.0850	0.0000
33.3047	.04	-.00	.0250	.0534	-.0087	0.0000	.0657	0.0000
33.4347	1.88	.02	.1388	.0584	-.0328	0.0000	.0768	0.0000
33.5536	3.79	.04	.2465	.0692	-.0550	0.0000	.0903	0.0000
33.6283	5.73	.06	.3740	.0879	-.0944	0.0000	.0667	0.0000
33.3822	7.72	.08	.5080	.1158	-.1375	0.0000	.0227	0.0000
33.1665	9.76	.11	.6103	.1470	-.1596	0.0000	-.0173	0.0000
33.1222	11.83	.13	.6924	.1806	-.1733	0.0000	-.0739	0.0000
33.1775	13.97	.15	.7743	.2204	-.1887	0.0000	-.1098	0.0000
33.3919	16.01	.18	.8456	.2636	-.2026	0.0000	-.1516	0.0000
33.3006	18.07	.20	.9023	.3115	-.2125	0.0000	-.2093	0.0000
33.2619	20.12	.22	.8665	.3571	-.2307	0.0000	-.2066	0.0000
33.4942	.01	-.00	.0242	.0513	-.0104	0.0000	.0860	0.0000

TABLE X.- Concluded.

(d) Concluded.

$M_\infty = 0.20$; $C_{\mu, avg} = 0.195$; $T_{t, plen} = 529^0 R$

QINF PSF	ALPHA DEG	BETA DEG	CLT	CDT	CPMT	CMU	HPLEN PSI	WTFLO LBF/SEC
58.1439	.02	-.01	.0688	-.0522	-.0308	.1966	214.8791	.2504
58.6195	-1.81	-.03	-.0322	-.0517	-.0137	.1949	214.9048	.2502
58.8689	.04	-.01	.0769	-.0511	-.0332	.1943	214.8679	.2505
58.6483	1.90	.01	.1845	-.0442	-.0548	.1949	214.8254	.2504
58.6812	3.82	.04	.3008	-.0307	-.0787	.1949	214.9370	.2506
59.3266	5.77	.06	.4102	-.0109	-.1004	.1927	214.8928	.2504
58.7977	7.77	.08	.5355	.0173	-.1319	.1946	214.9450	.2507
58.5757	9.81	.11	.6604	.0516	-.1603	.1951	214.9545	.2504
58.3468	11.91	.13	.8228	.0989	-.2107	.1961	215.0283	.2507
58.5346	14.06	.15	1.0013	.1607	-.2755	.1956	215.0500	.2508
58.0946	16.12	.17	1.1928	.2344	-.3542	.1969	215.0604	.2506
58.0301	18.22	.20	1.3770	.3189	-.4232	.1973	215.0724	.2508
58.2741	20.28	.22	1.5168	.4027	-.4675	.1963	215.1270	.2507
58.6552	.03	-.01	.0711	-.0511	-.0321	.1952	215.2536	.2508

$M_\infty = 0.20$; $C_{\mu, avg} = 0$

QINF PSF	ALPHA DEG	BETA DEG	CLT	CDT	CPMT	CMU	HPLEN PSI	WTFLO LBF/SEC
58.3701	.02	-.01	.0281	.0398	-.0127	0.0000	-.3944	0.0000
58.2290	-1.83	-.03	-.0903	.0434	.0121	0.0000	-.2914	0.0000
58.8155	.04	-.01	.0187	.0432	-.0088	0.0000	-.3042	0.0000
59.0156	1.91	.01	.1305	.0487	-.0329	0.0000	-.3059	0.0000
58.9732	3.81	.04	.2435	.0599	-.0545	0.0000	-.3073	0.0000
58.7484	5.76	.06	.3617	.0781	-.0854	0.0000	-.3368	0.0000
58.4647	7.76	.08	.4842	.1050	-.1203	0.0000	-.3929	0.0000
58.5661	9.80	.10	.5671	.1332	-.1289	0.0000	-.4500	0.0000
58.4633	11.88	.12	.6396	.1644	-.1355	0.0000	-.4401	0.0000
58.5195	14.04	.15	.7305	.2053	-.1548	0.0000	-.5047	0.0000
58.6182	16.10	.17	.8205	.2535	-.1810	0.0000	-.5767	0.0000
58.5771	18.15	.20	.8912	.3044	-.2035	0.0000	-.6199	0.0000
58.6127	20.18	.22	.8407	.3459	-.2148	0.0000	-.5448	0.0000
58.7086	.01	-.01	.0259	.0448	-.0120	0.0000	-.1632	0.0000

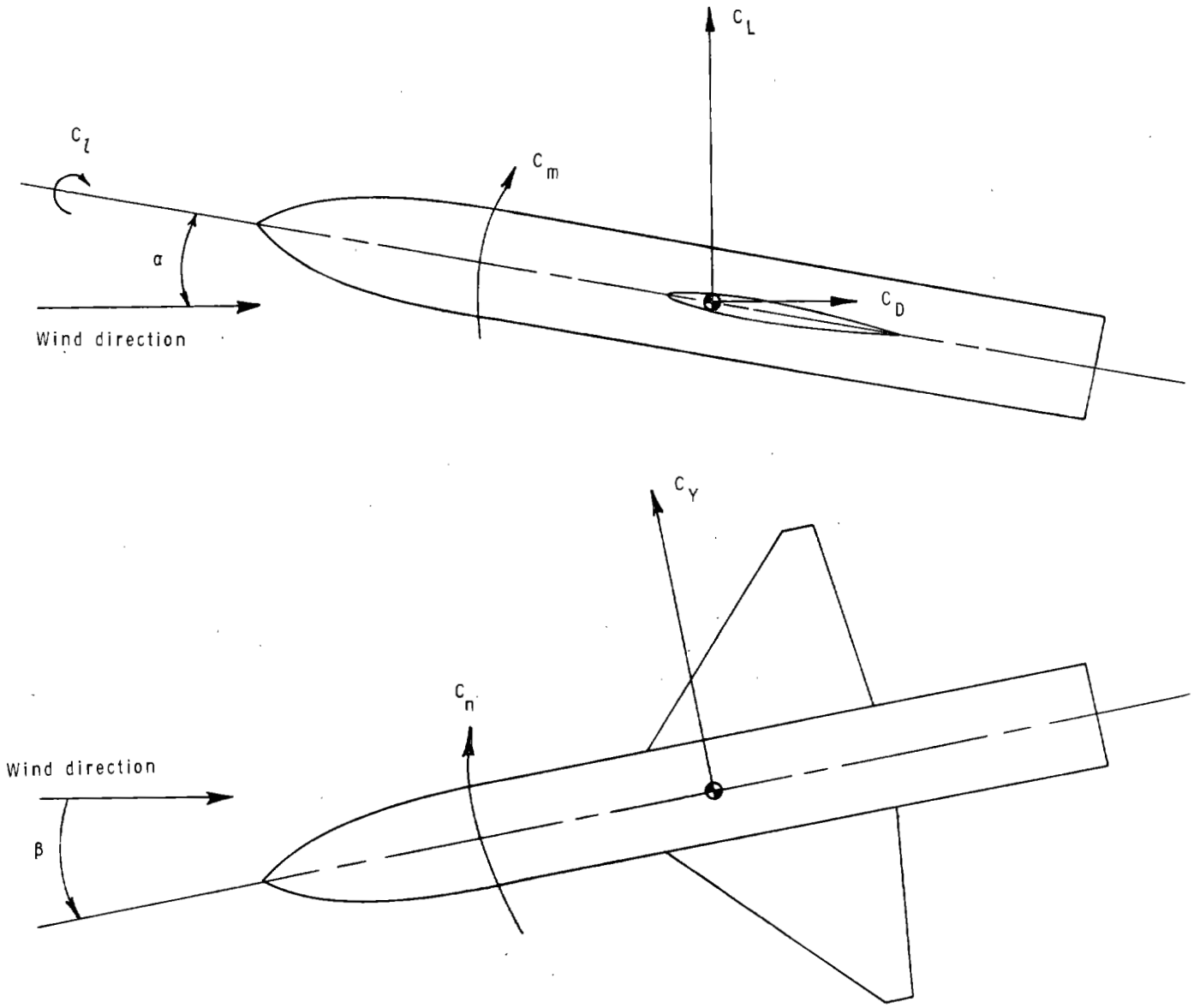

Figure 1.- System of axes used showing positive directions of forces, moments, and angles.

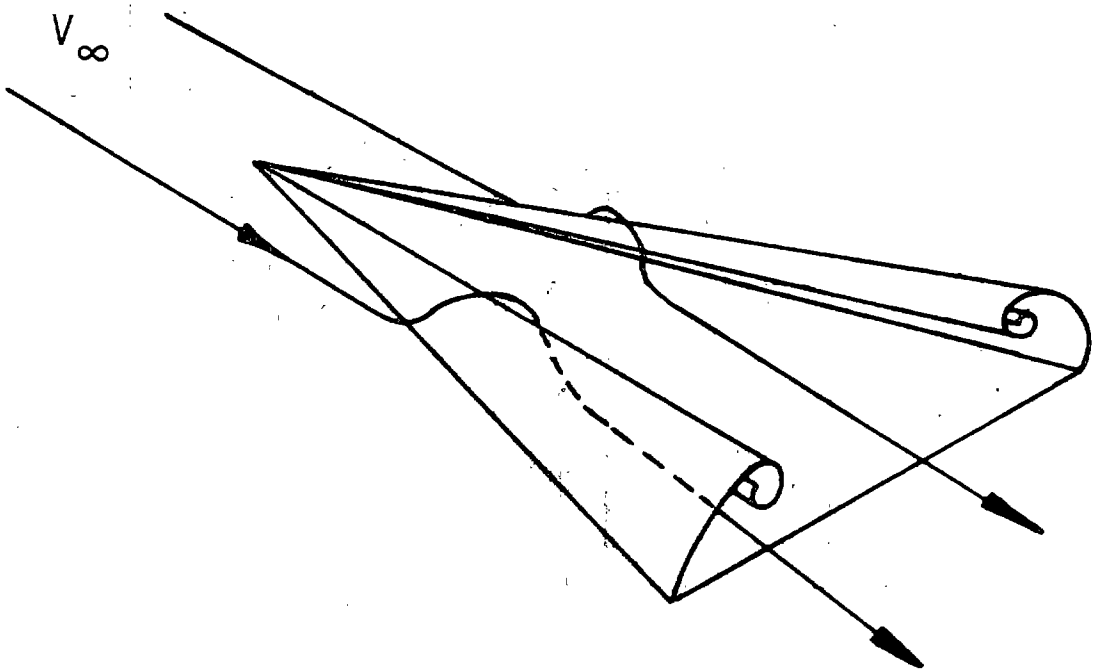

Figure 2.- Stable leading-edge vortices on a slender wing.

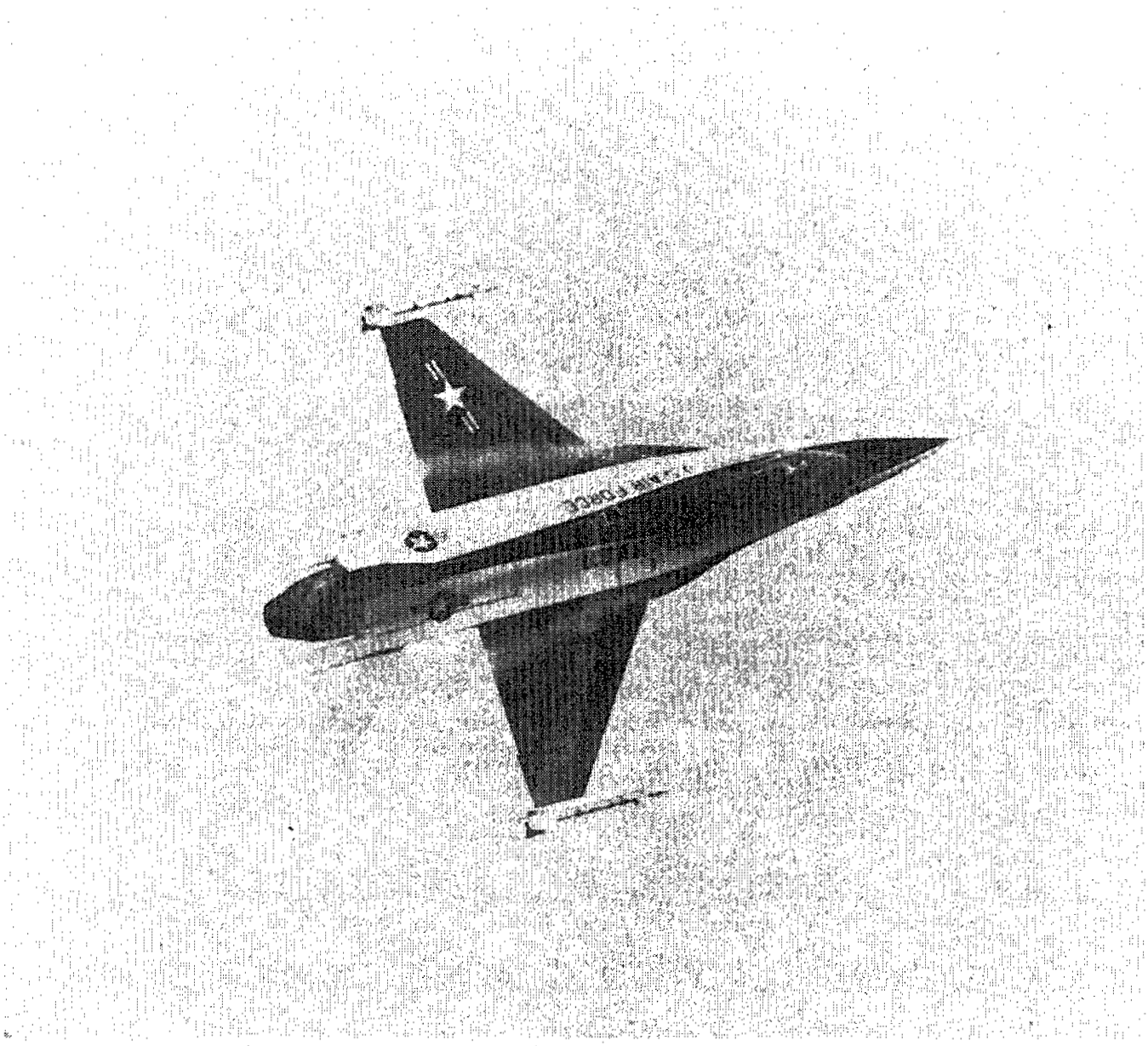

Figure 3.- Vortex flow generated by a highly-swept maneuver strake on the F-16 aircraft (photograph from ref. 43).

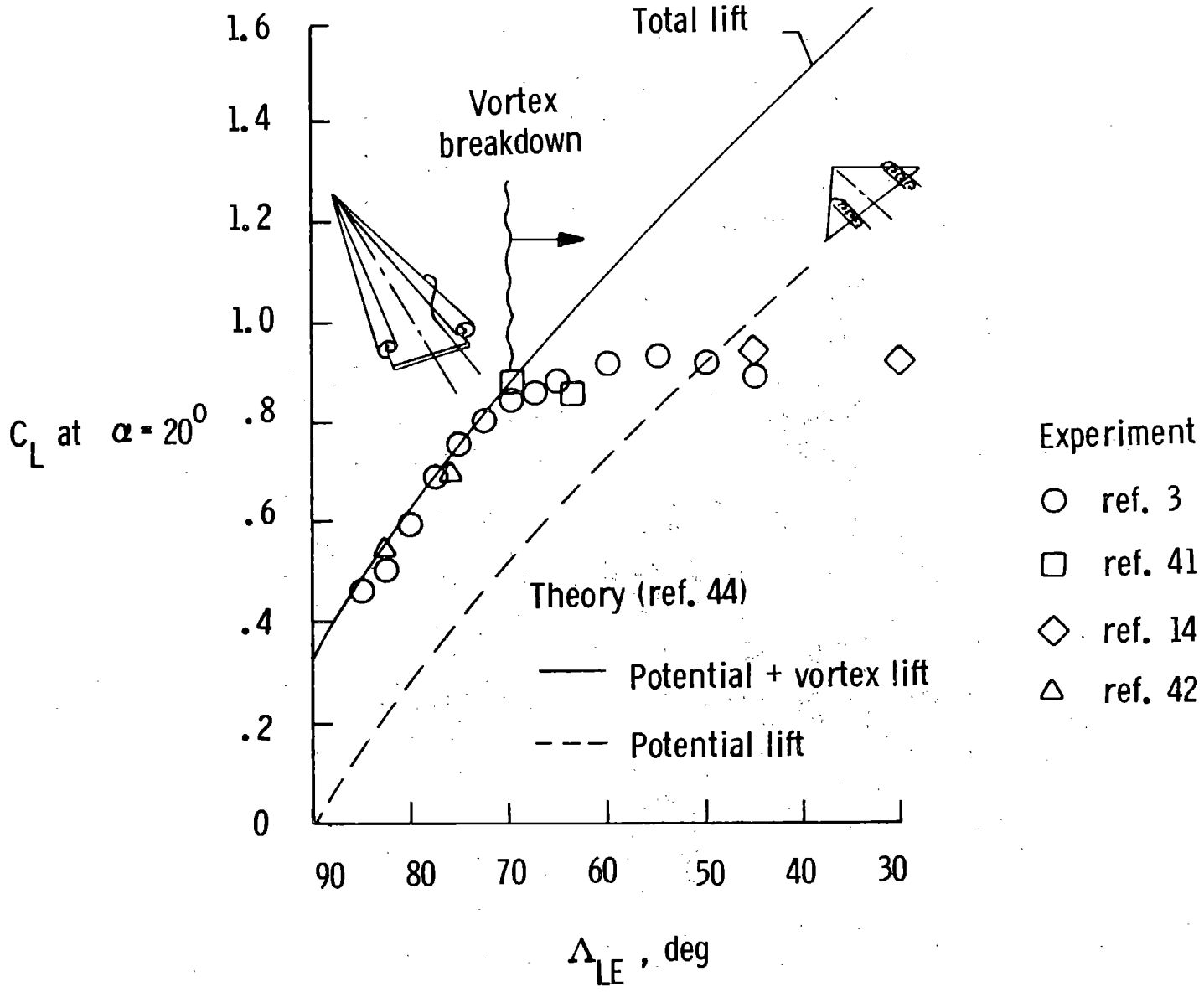

Figure 4.- Vortex-induced lift increments generated by delta planforms. (from ref. 18)

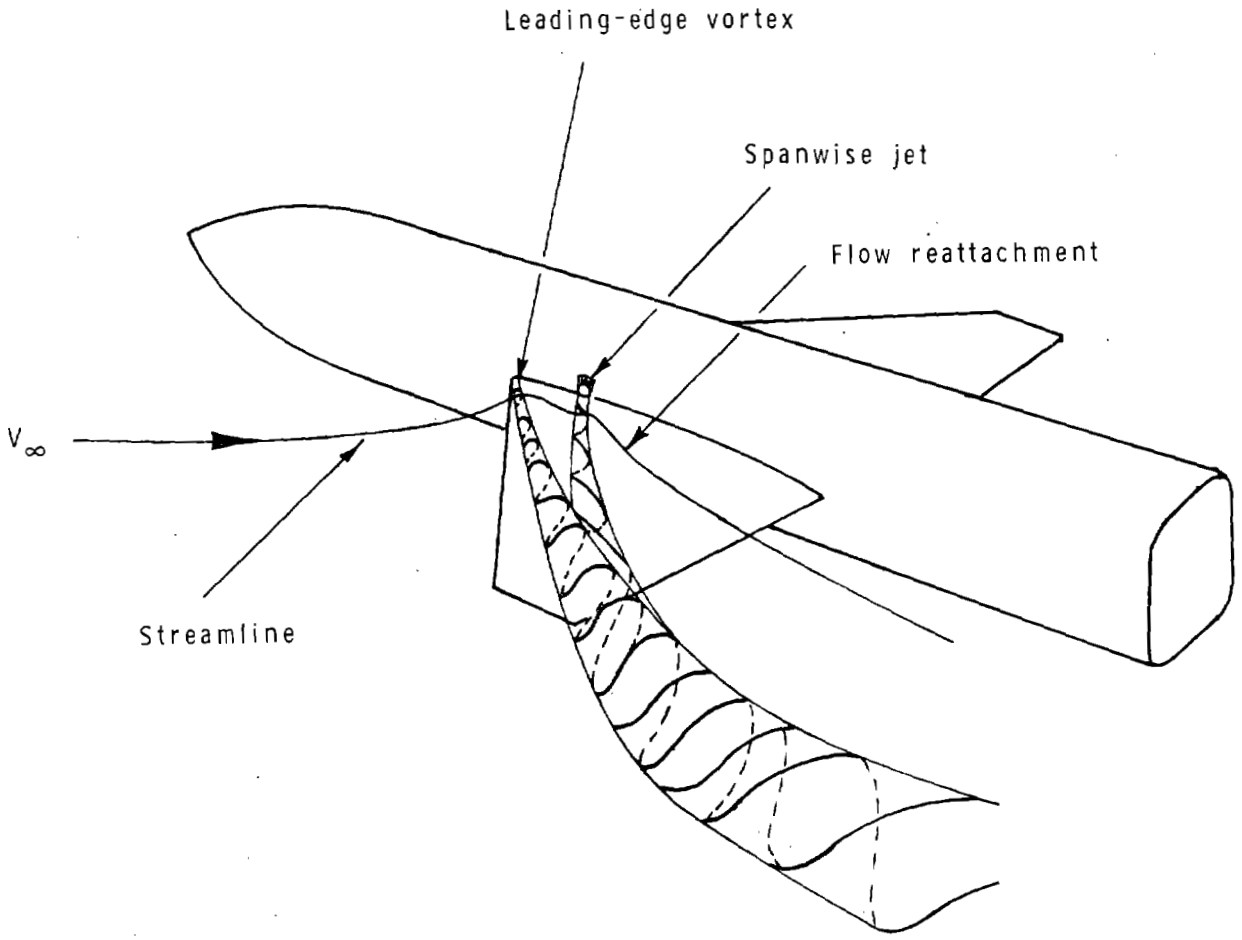

Figure 5 .- Leading-edge vortex enhancement by spanwise blowing.

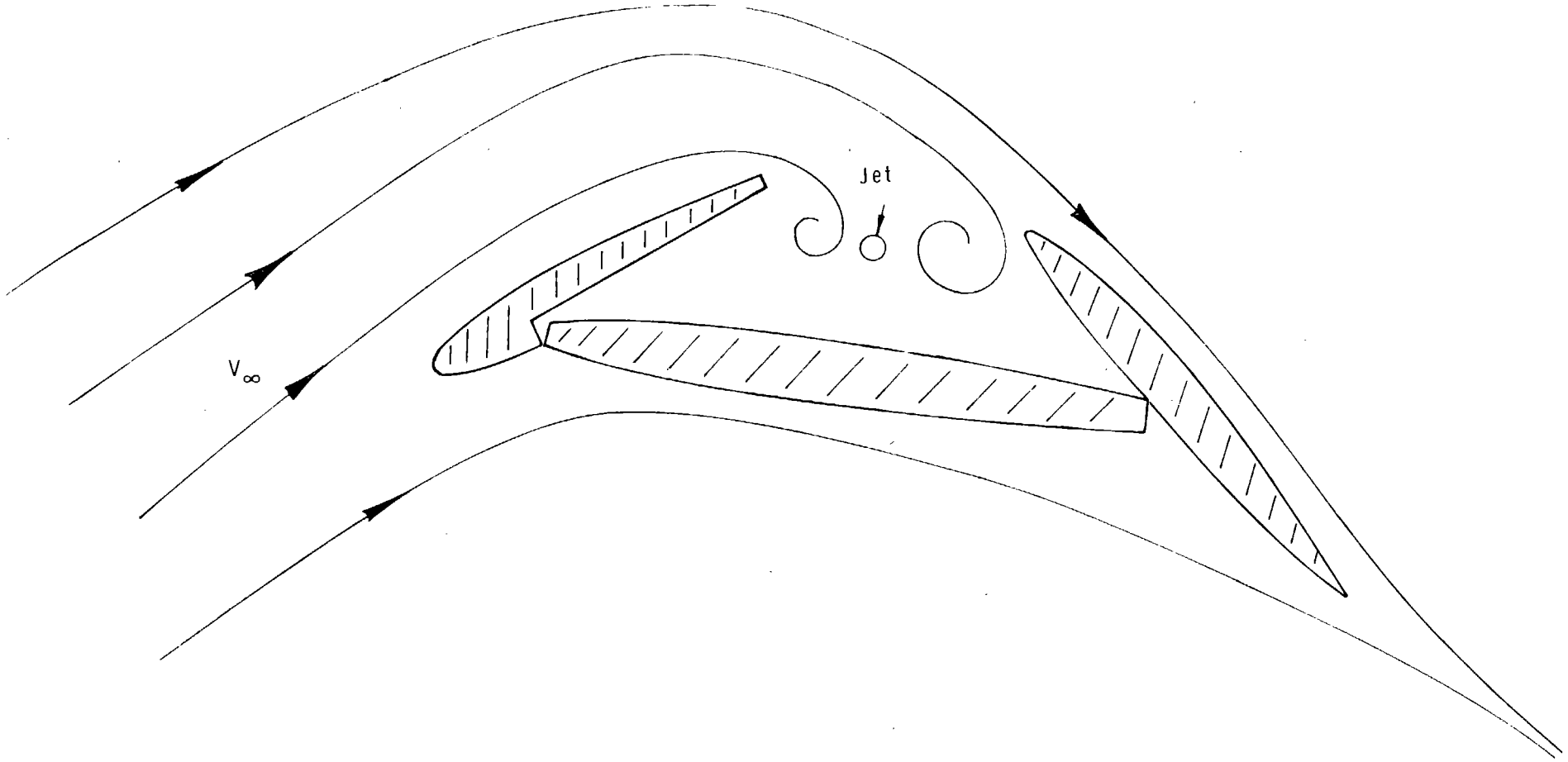

Figure 6 .- Generation of a dual vortex system by spanwise blowing in the channel of a "locked vortex" wing.

(a) Blowing off.

(b) Blowing on.

(c) Blowing on; increased blowing rate.

(a) Leading-edge vortex enhancement by spanwise blowing on a 44° swept trapezoidal wing at $\alpha = 30^{\circ}$ (from ref. 24).

Figure 1. - Flow visualization photographs.

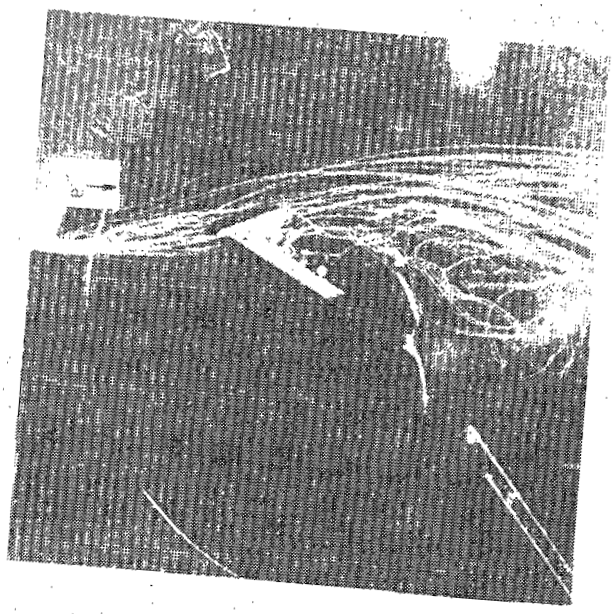

(a) Blowing off.

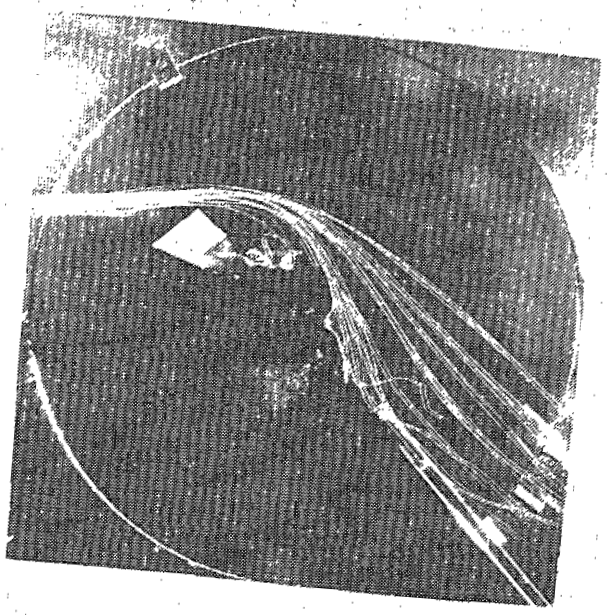

(b) Blowing on.

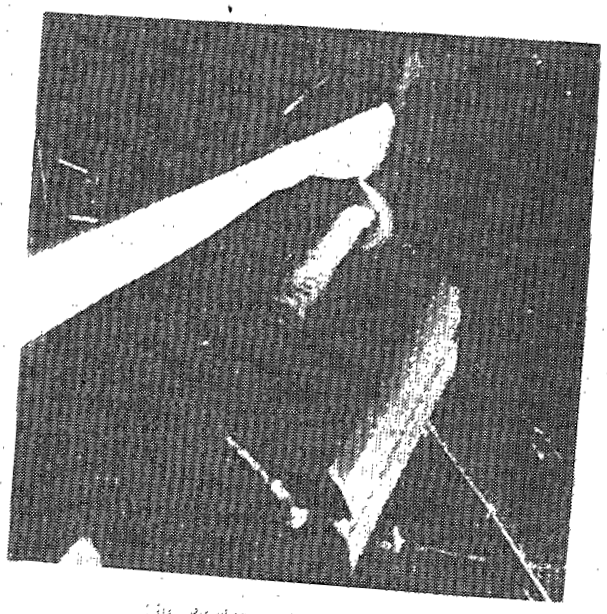

(c) Blowing off, fore vortex.

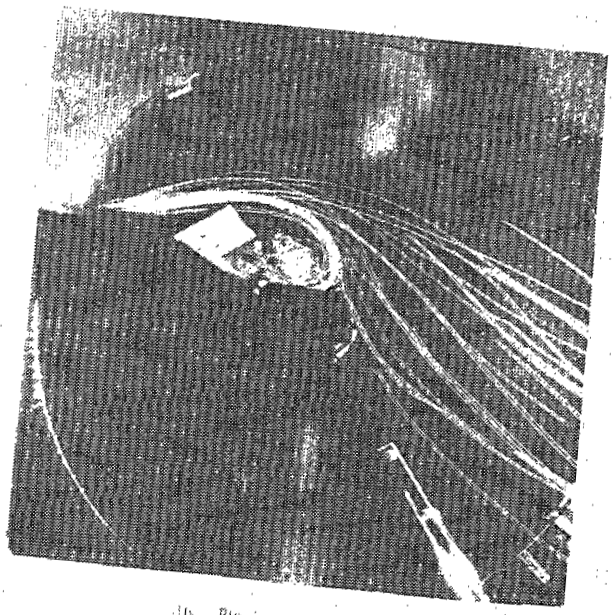

(d) Blowing on, aft vortex.

(e) Spanwise flow in the region of an incipient "forked vortex" axis for $\delta_{LE} = 40^{\circ}$ at $\alpha = 20^{\circ}$ (run 101, 20).

Figure 7.- Concluded.

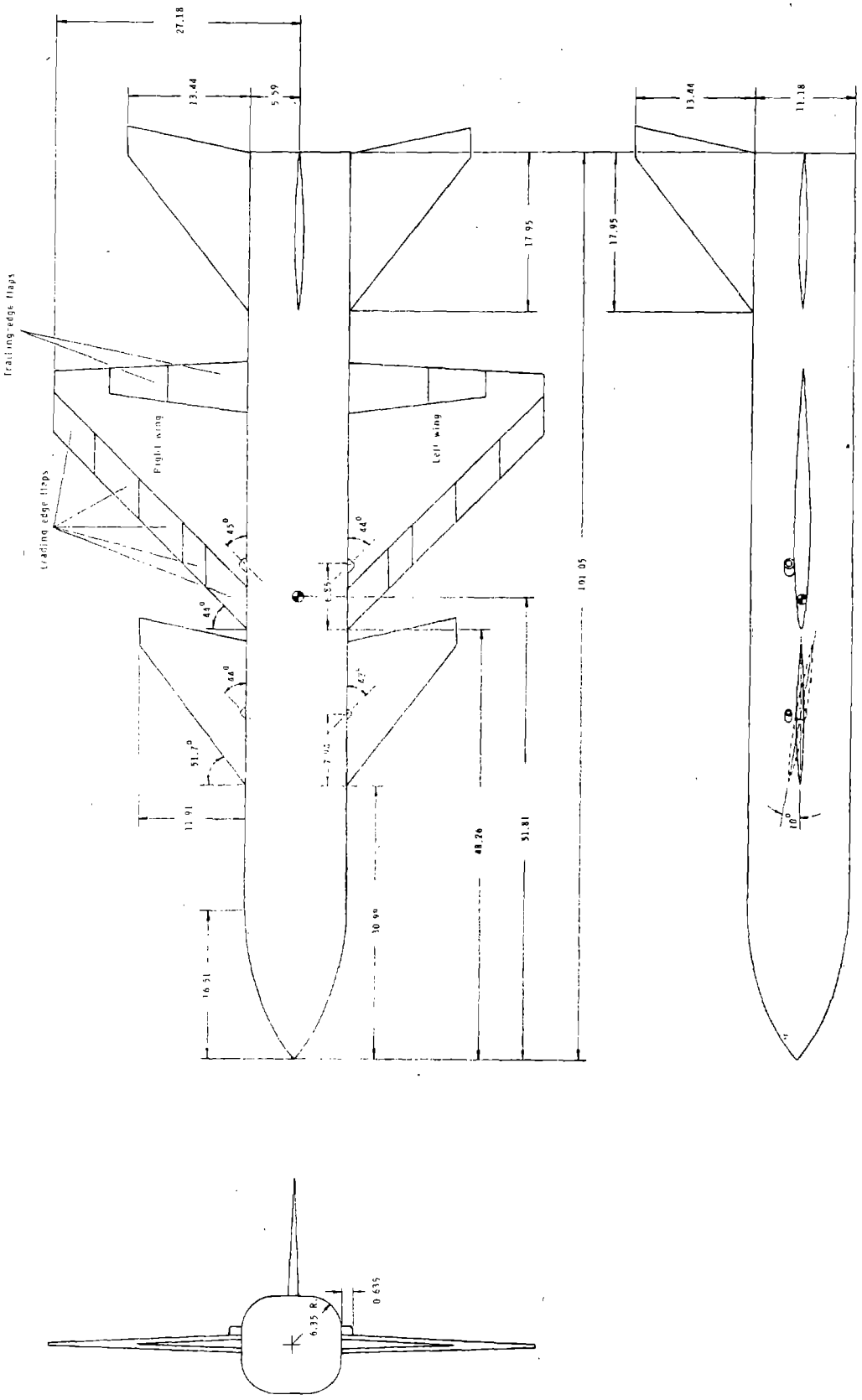

(a) Three-view drawing.

Figure 8.- Details of wind tunnel model. (All dimensions are in centimeters.)

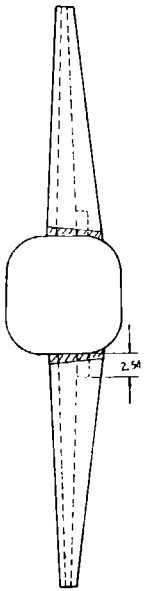

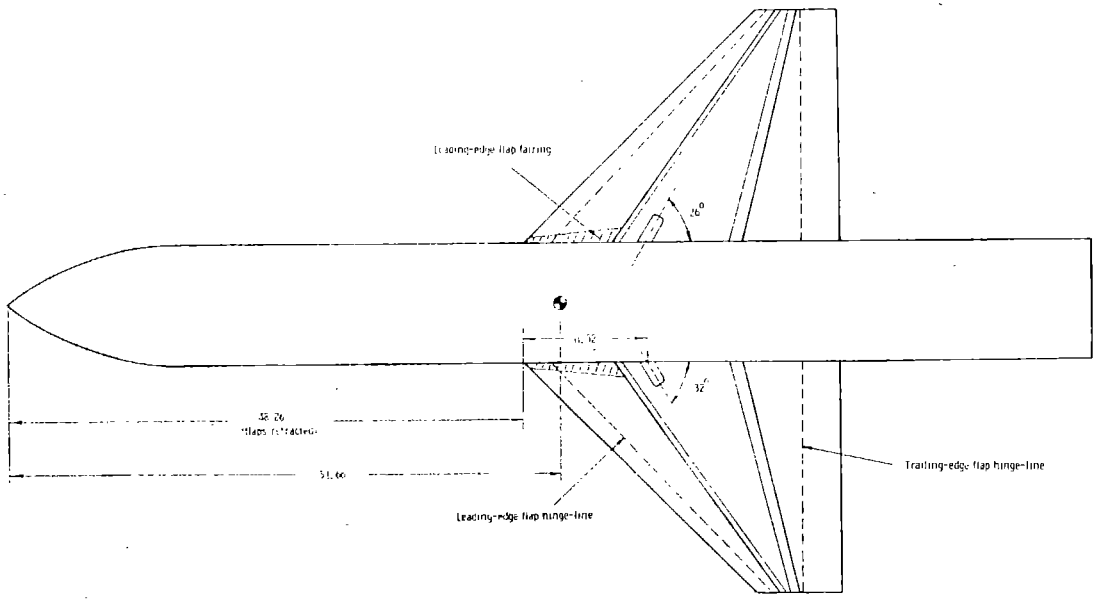

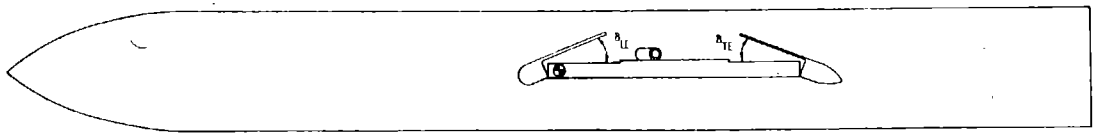

(b) Three-view drawing - "locked vortex" wings.

Figure 8.- Concluded.

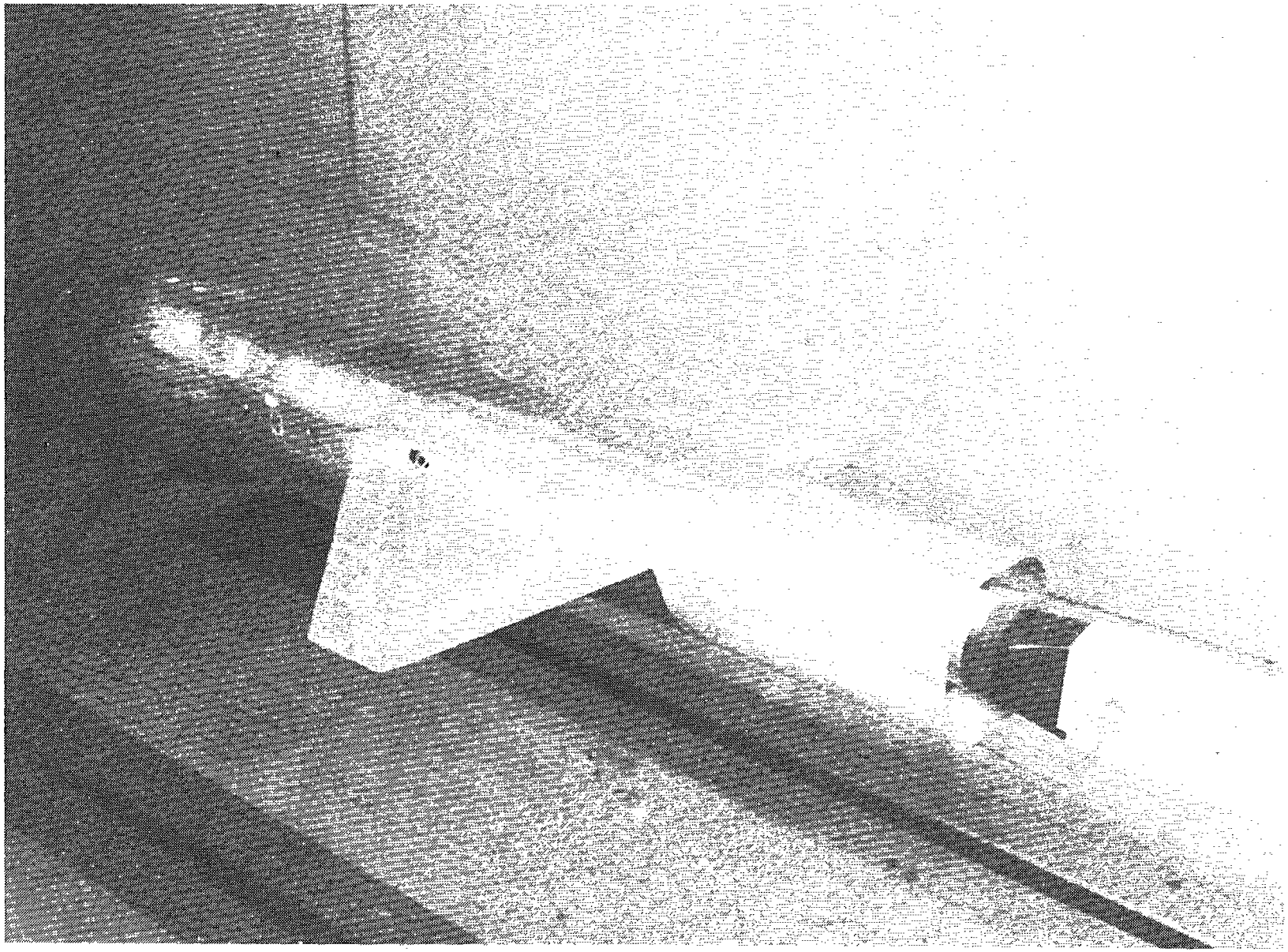

(a) Spanwise blowing on the 44^{o} swept trapezoidal wing.

Figure 9.- Model configurations installed in the wind tunnel.

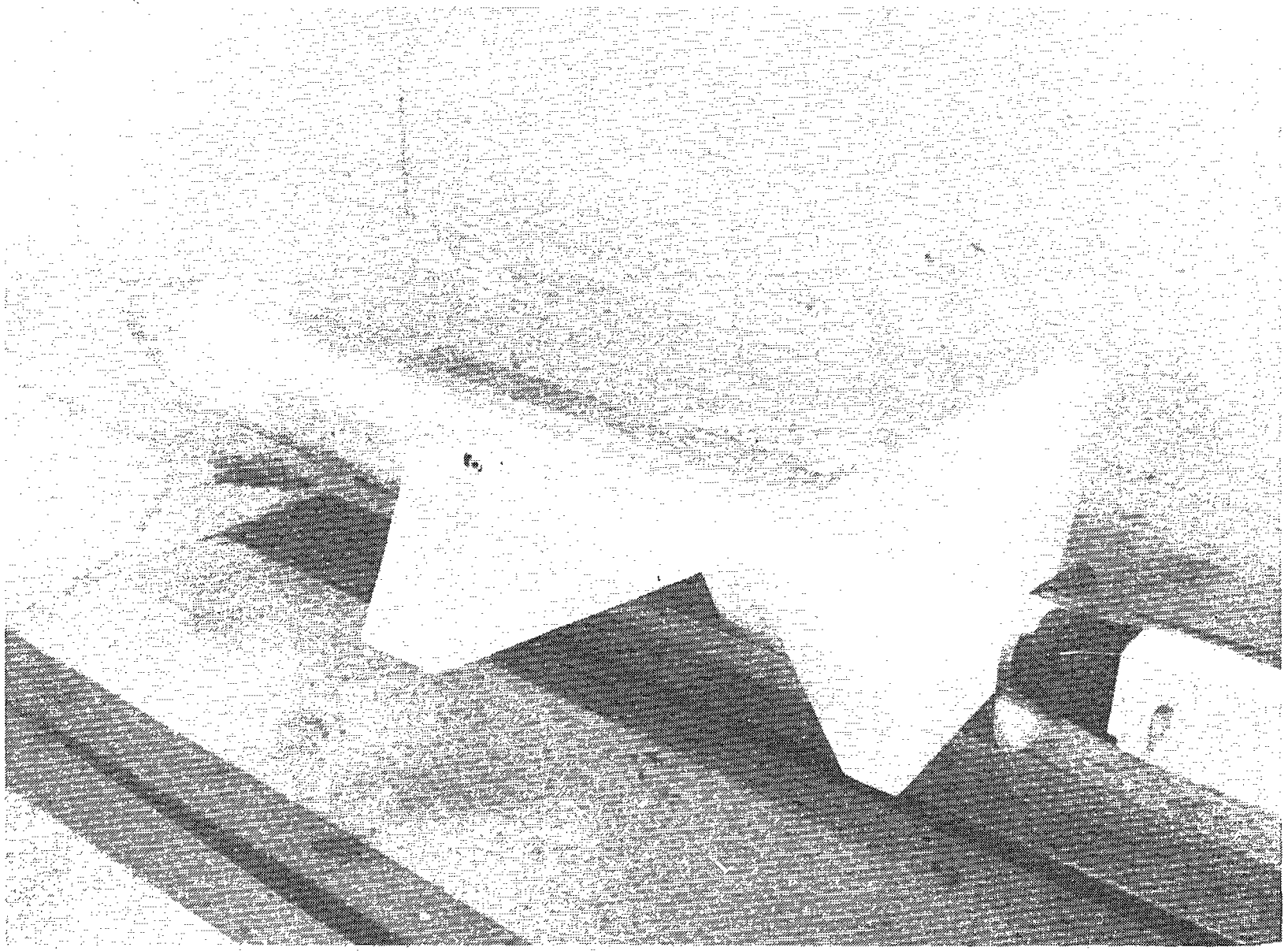

(b) Spanwise blowing on the 44^{o} swept trapezoidal wing with horizontal and vertical tails on.

Figure 9.– Continued.

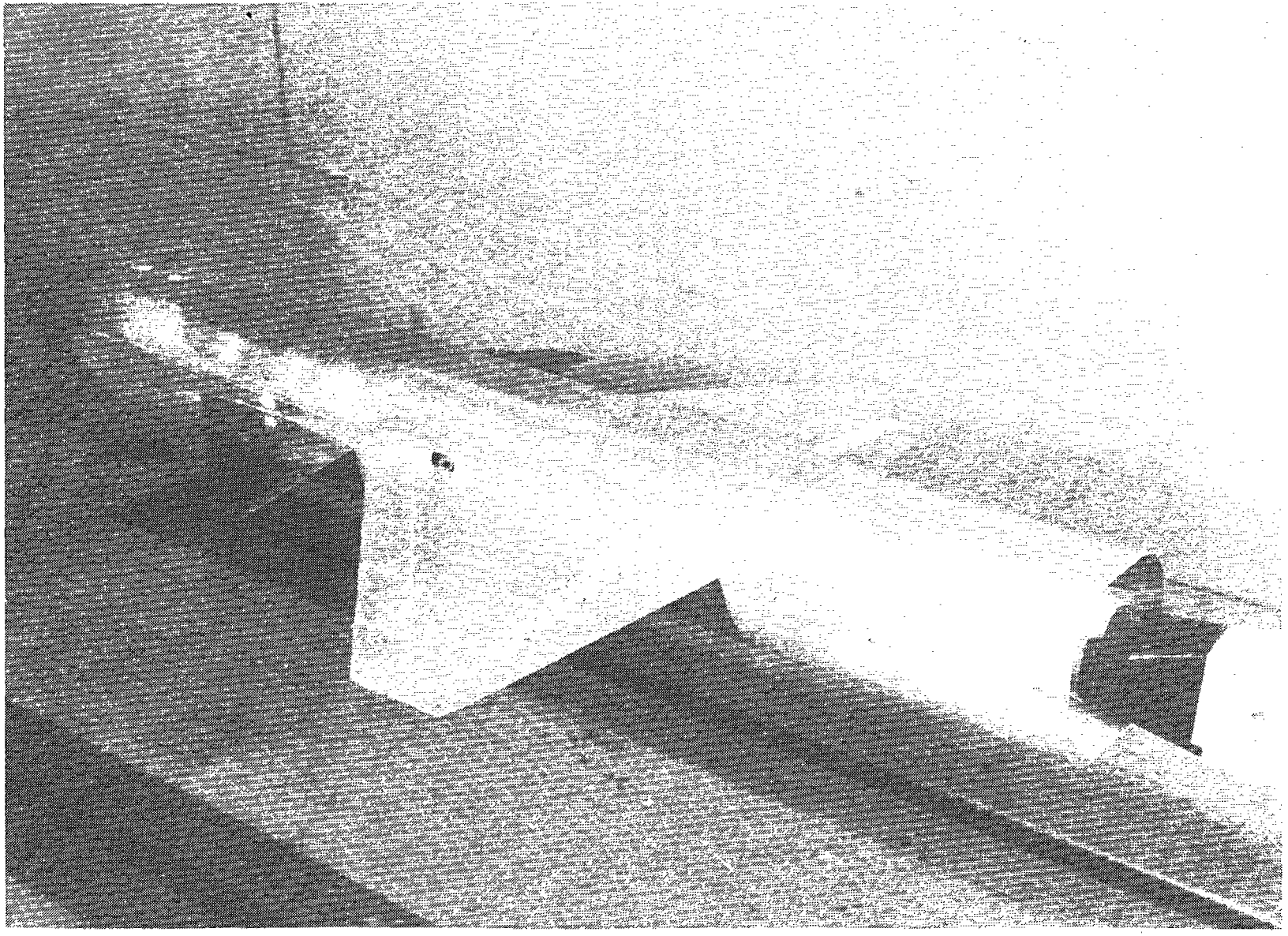

(c) Spanwise blowing on the wing of a canard-wing configuration.

Figure 9.- Continued.

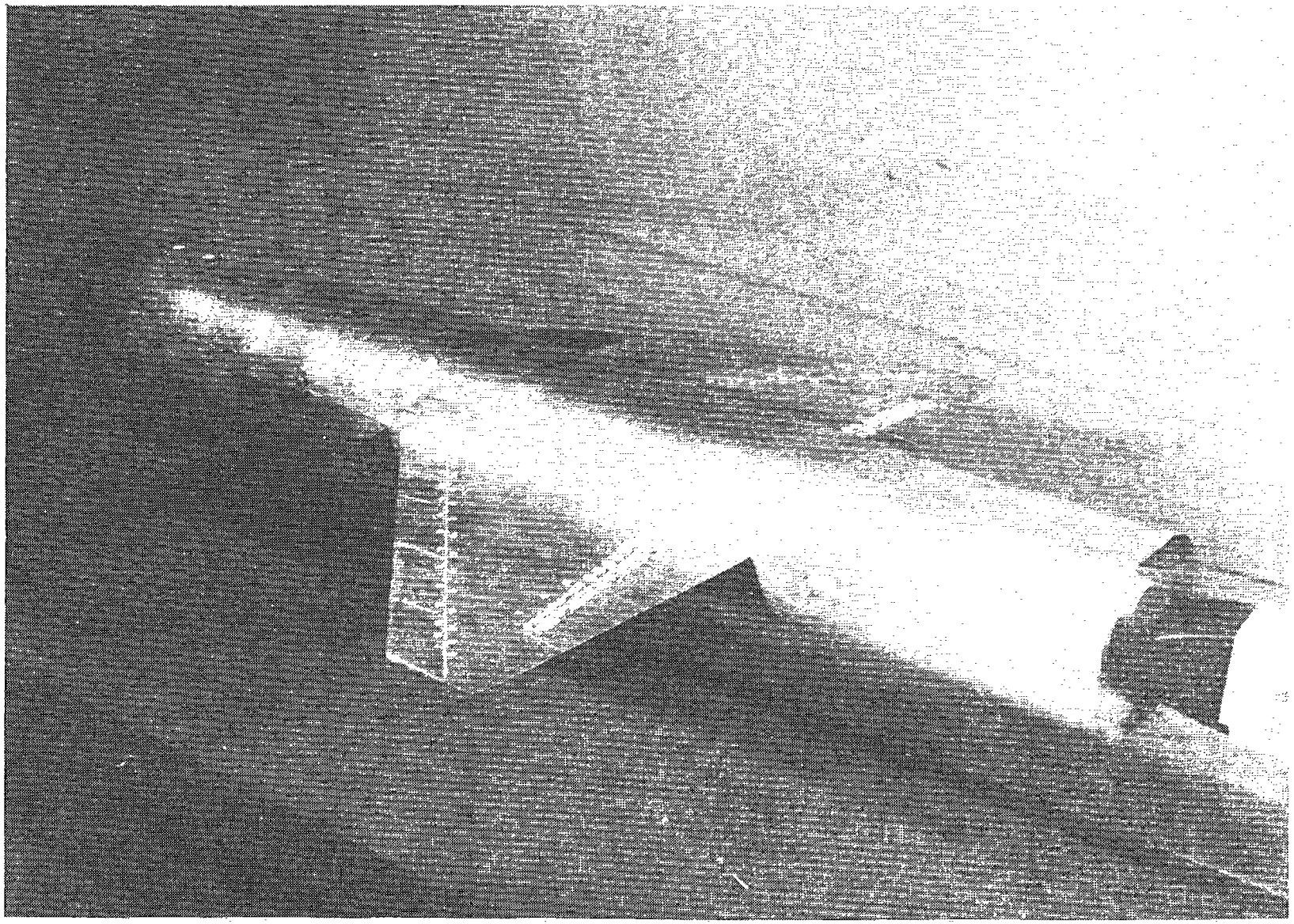

(d) Spanwise blowing on the canard of a canard-wing configuration.

Figure 9.- Continued.

(e) Spanwise blowing in the channel of the "locked vortex" wing.

Figure 9.- Concluded.

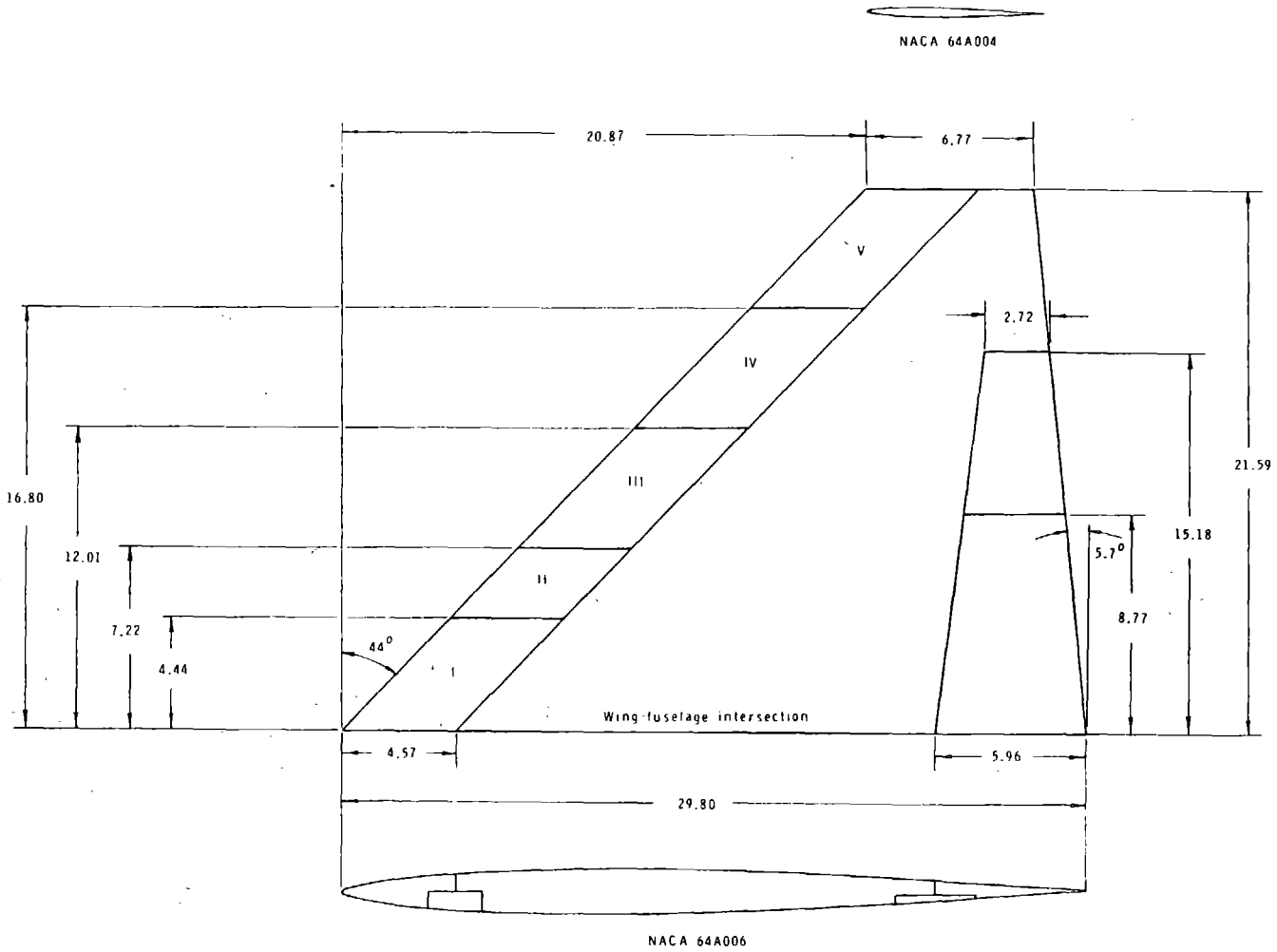

(a) 44° swept trapezoidal wing.

Figure 10.- Details of wing geometries. (All dimensions are in centimeters.)

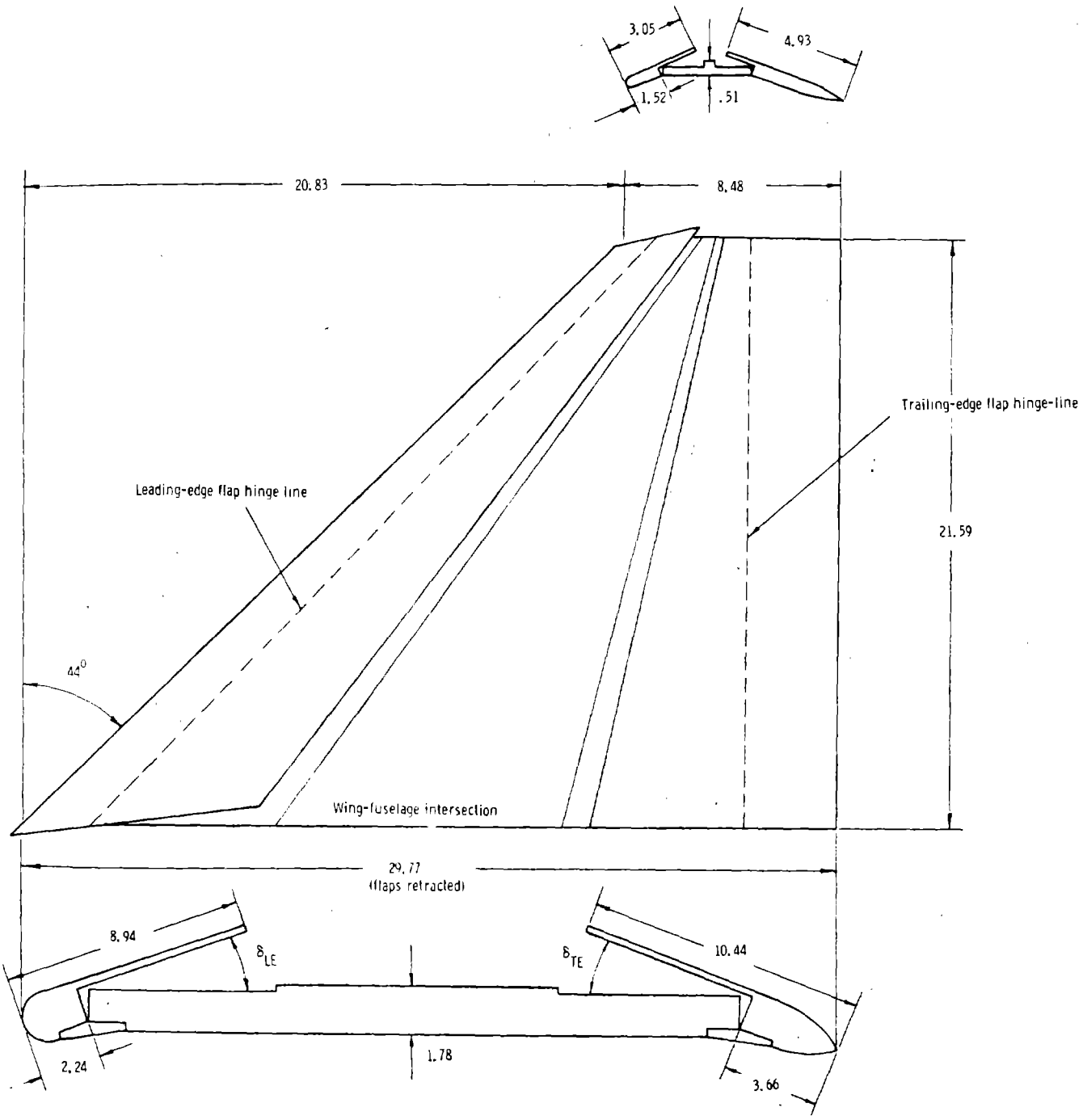

(b) "locked vortex" wing.

Figure 10.- Concluded.

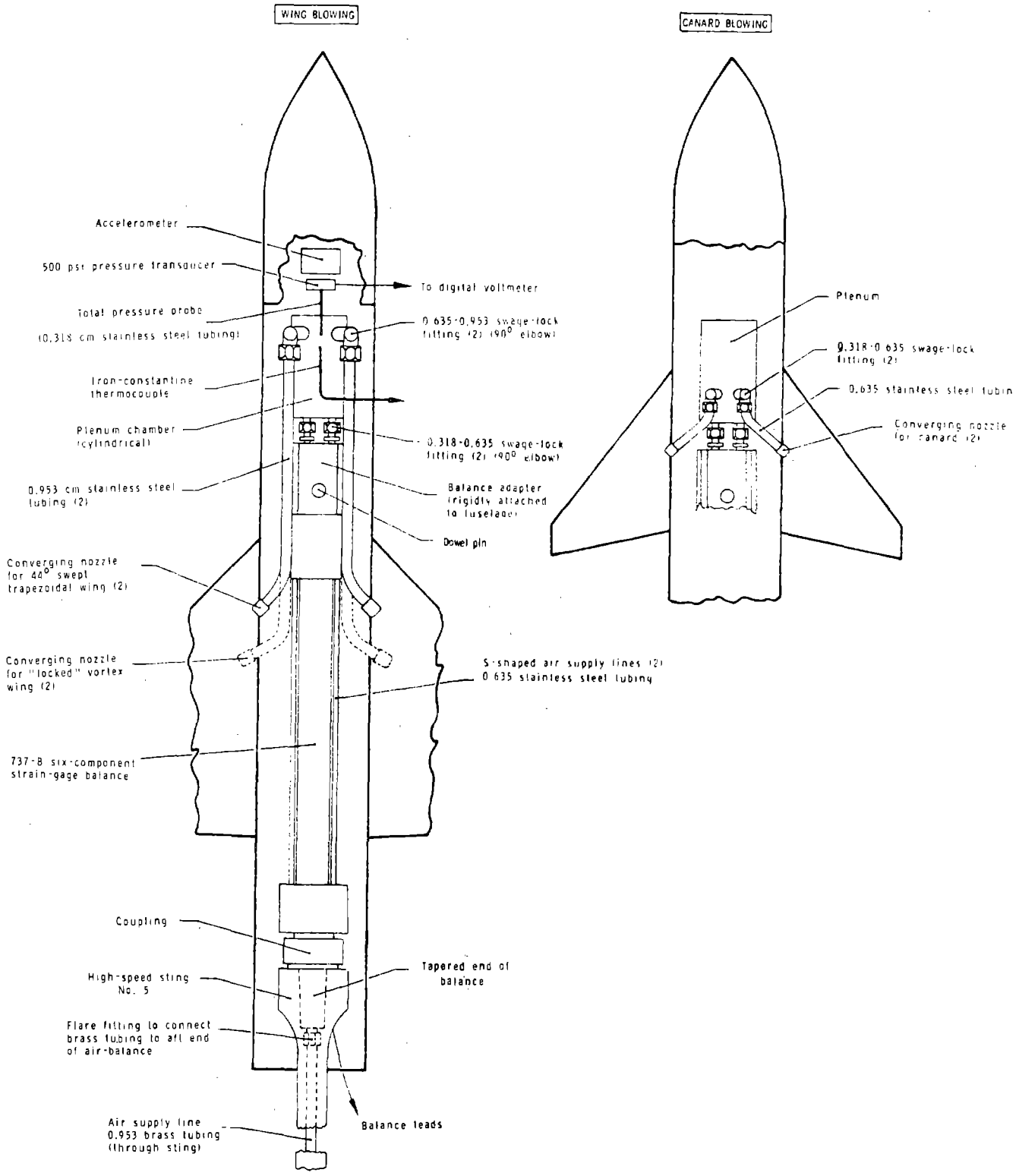

Figure 11.- Planview of air supply system and internal model assembly for the spanwise blowing model. (All dimensions are in centimeters.)

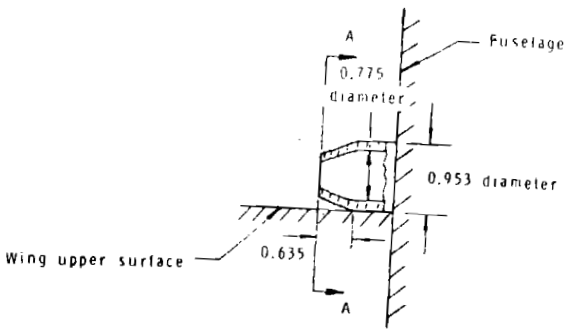

(a) Wing nozzle.

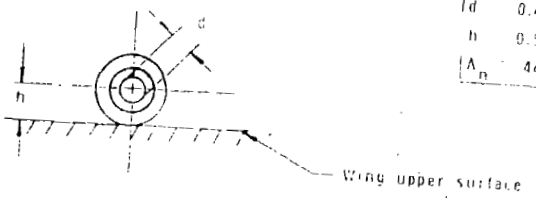

	44° swept trapezoidal wing nozzles		"locked" vortex wing nozzles	
	left	right	left	right
d	0.450	0.462	0.457	0.455
h	0.508	0.508	0.508	0.508
Λ_n	44°	45°	32°	36°

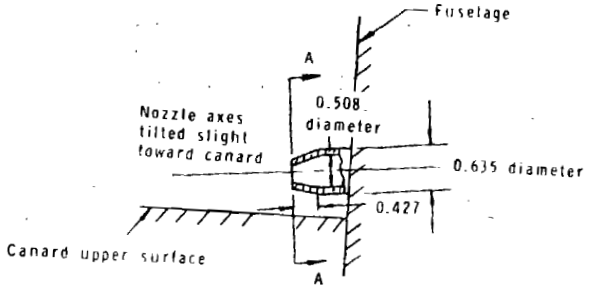

(b) Canard nozzle.

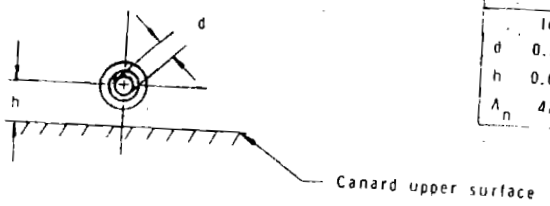

	Canard nozzles	
	left	right
d	0.295	0.318
h	0.698	0.698
Λ_n	42°	44°

Figure 12.- Wing and canard nozzle geometry and vertical location. (All dimensions are in centimeters.)

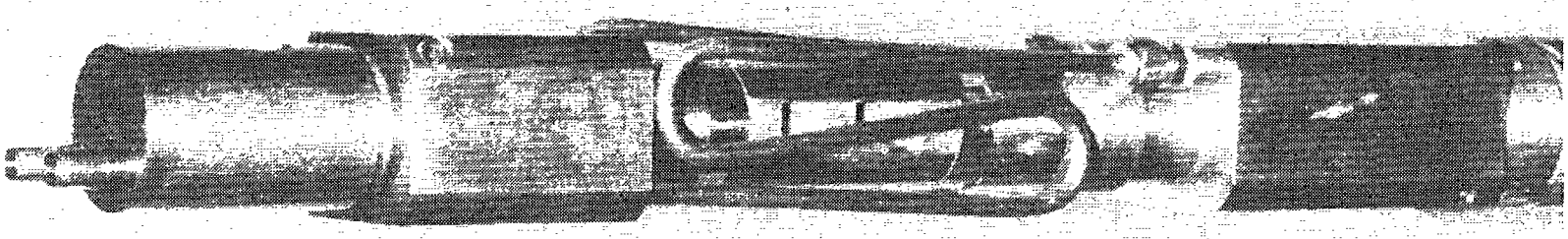

Figure 13.- Photograph of No. 737-B balance - air delivery assembly.

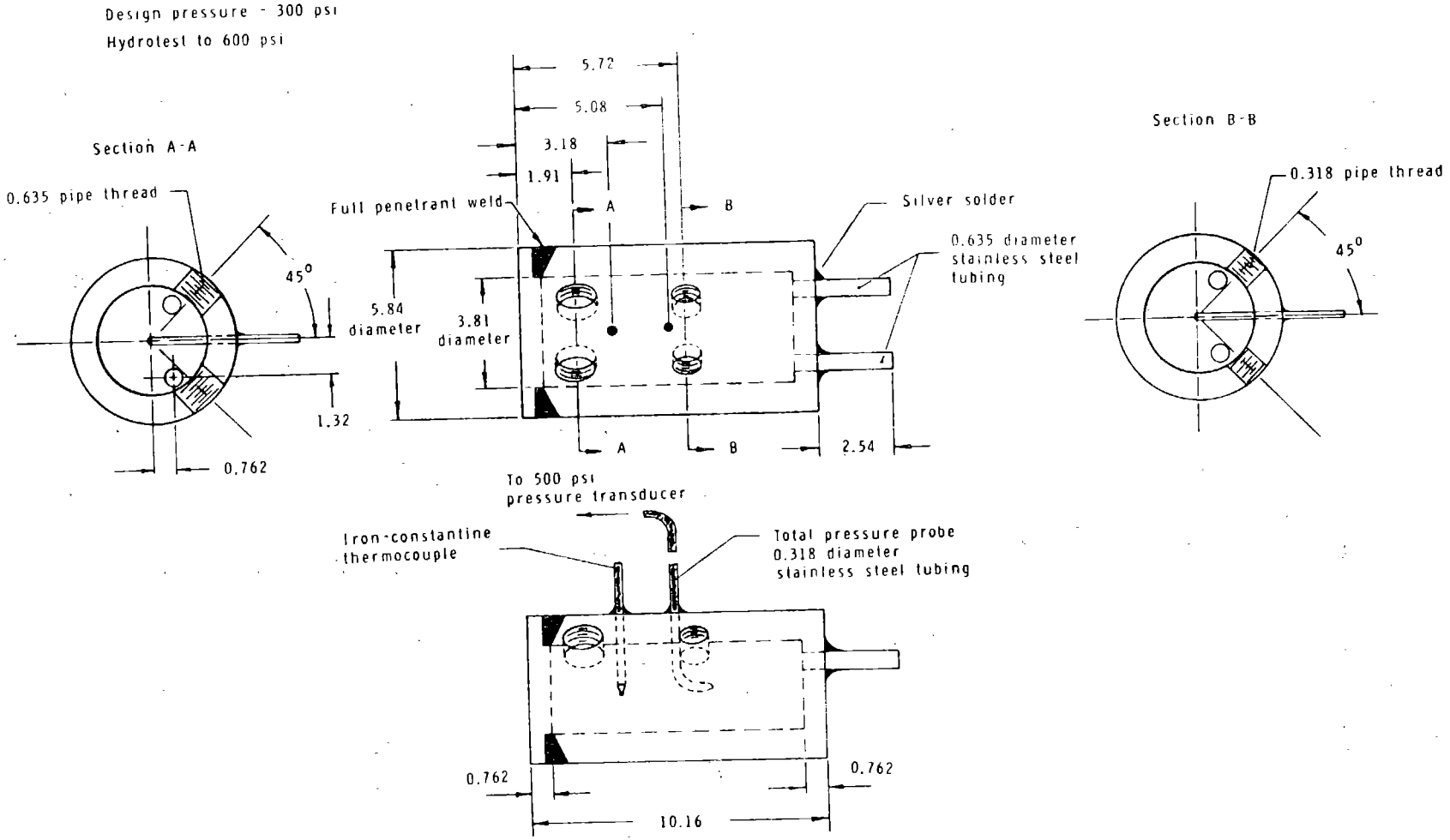

Figure 14.- Details of settling chamber. (All dimensions are in centimeters.)

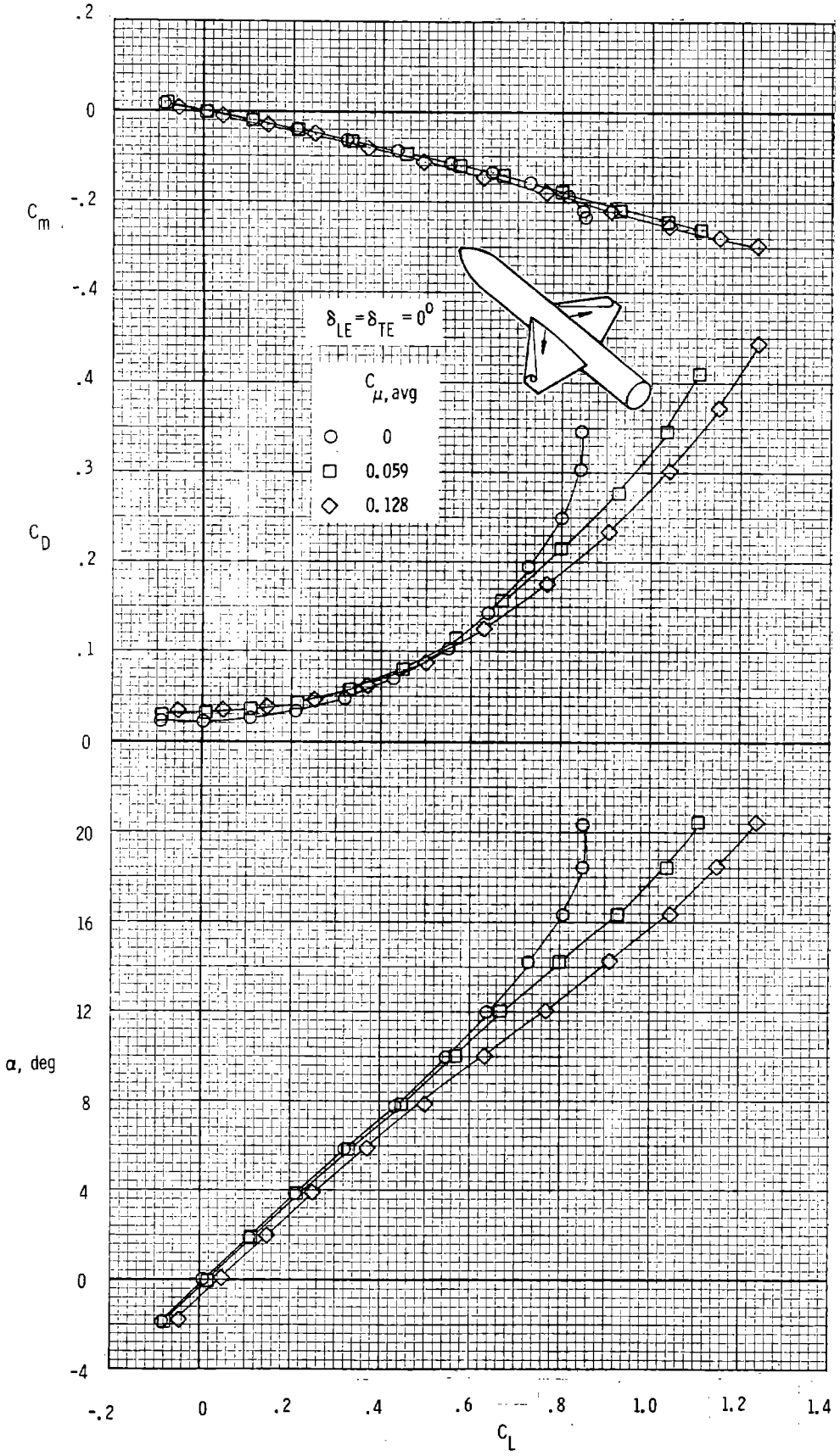

Figure 15.- Effect of spanwise blowing on the longitudinal aerodynamic characteristics of the 44° swept trapezoidal wing configuration; $M_\infty = 0.30$.

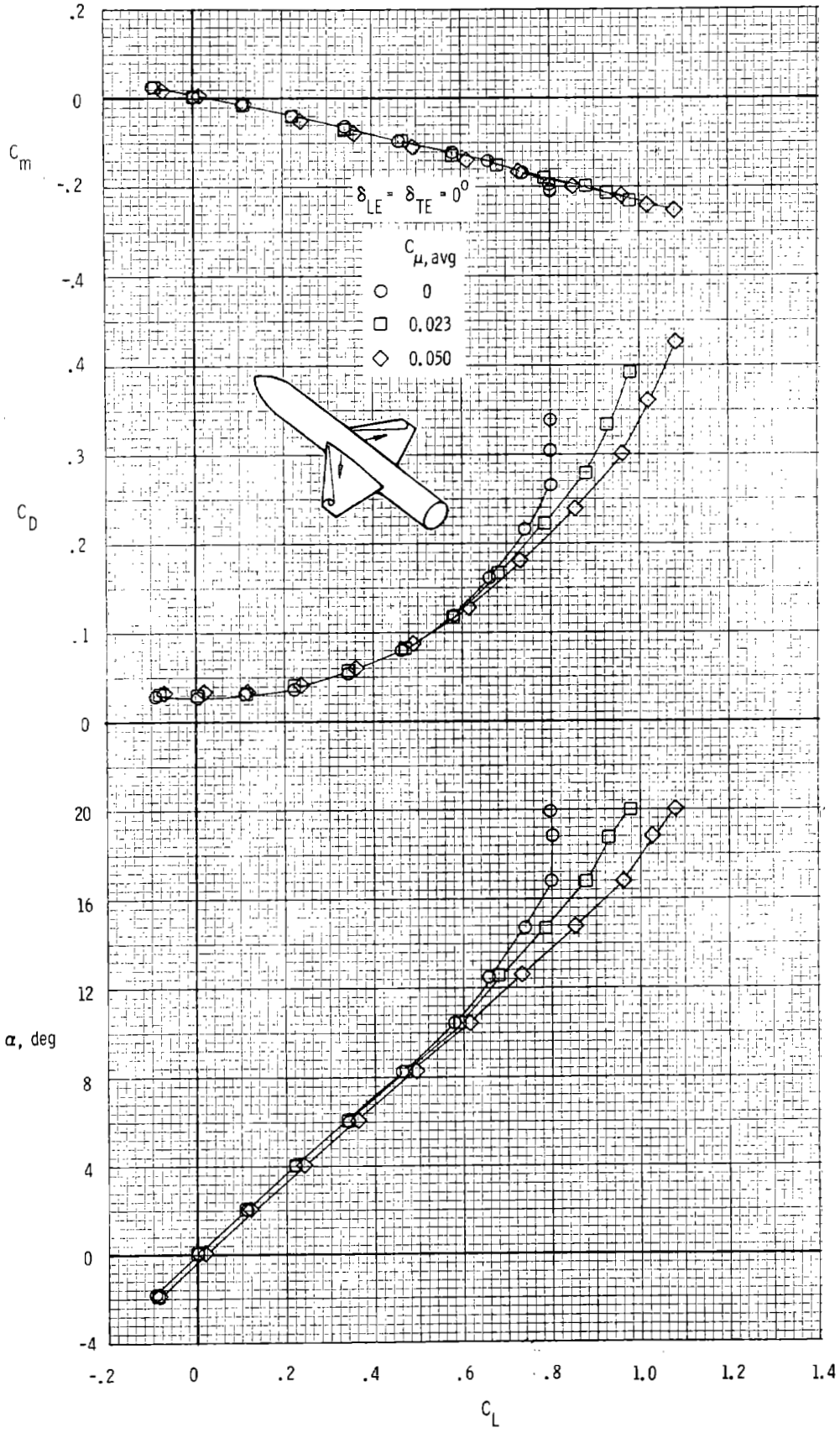

Figure 16. - Effect of spanwise blowing on the longitudinal aerodynamic characteristics of the 44° swept trapezoidal wing configuration; $M_\infty = 0.50$.

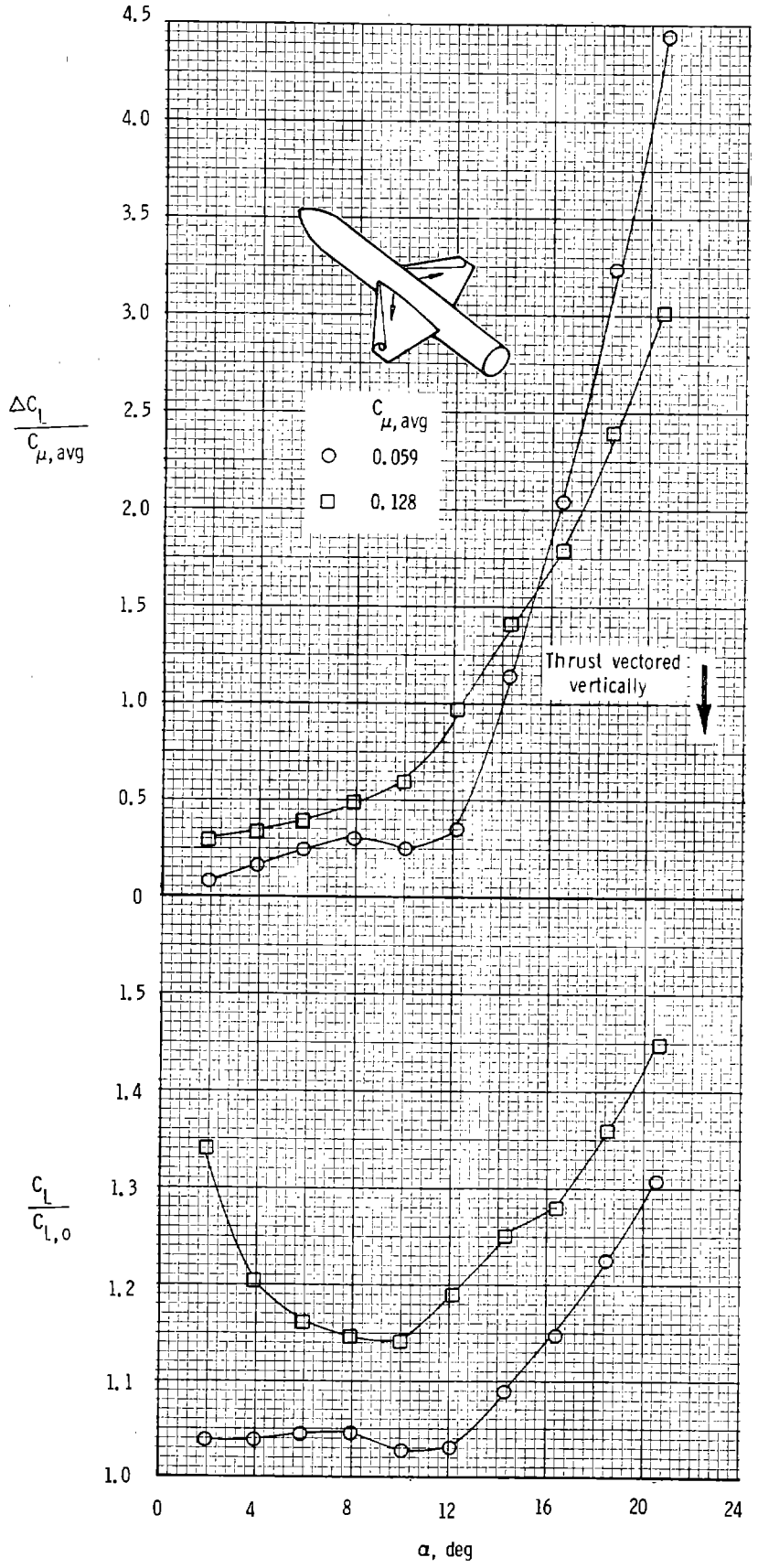

Figure 17.- Effect of α and $C_{\mu,avg}$ on the lift augmentation ratio and lift effectiveness of blowing for the 44° swept trapezoidal wing configuration; $M_\infty = 0.30$.

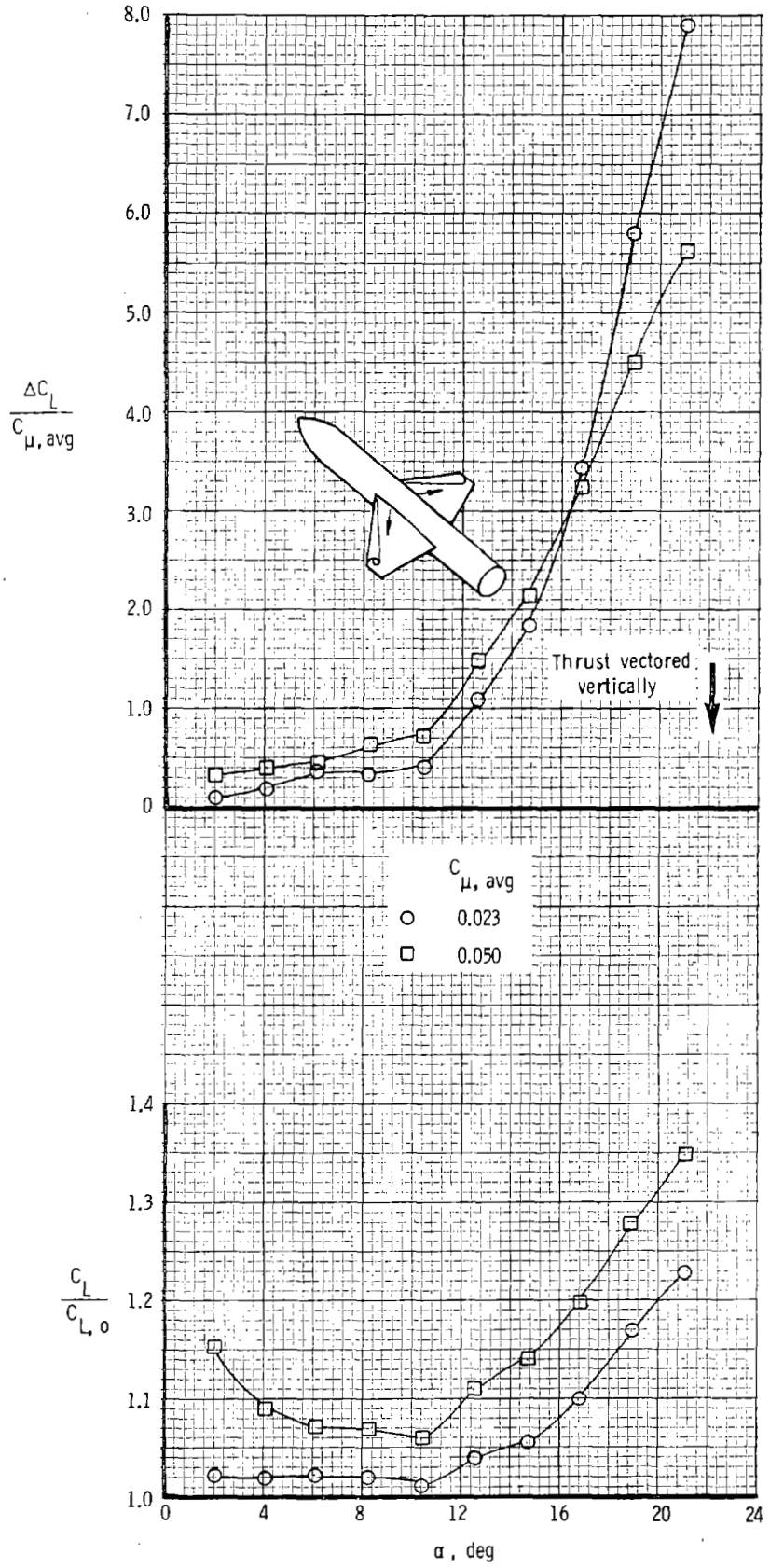

Figure 18.- Effect of α and $C_{\mu,avg}$ on the lift augmentation ratio and lift effectiveness of blowing for the 44° swept trapezoidal wing configuration; $M_\infty = 0.50$.

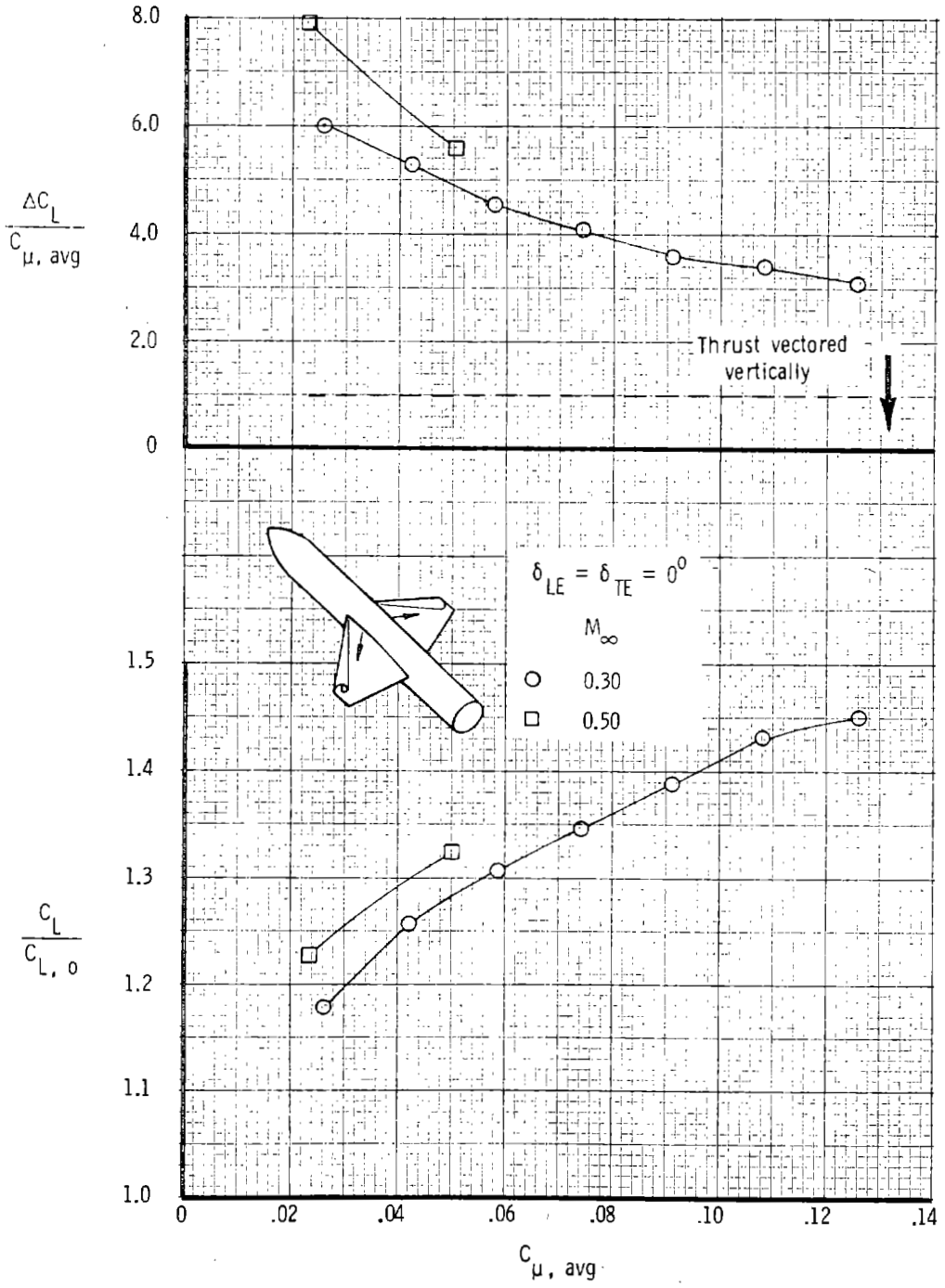

Figure 19.- Effect of $C_{\mu,avg}$ and M_∞ on the lift augmentation ratio and lift effectiveness of blowing for the 44^0 swept trapezoidal wing configuration for $\alpha \approx 21^0$.

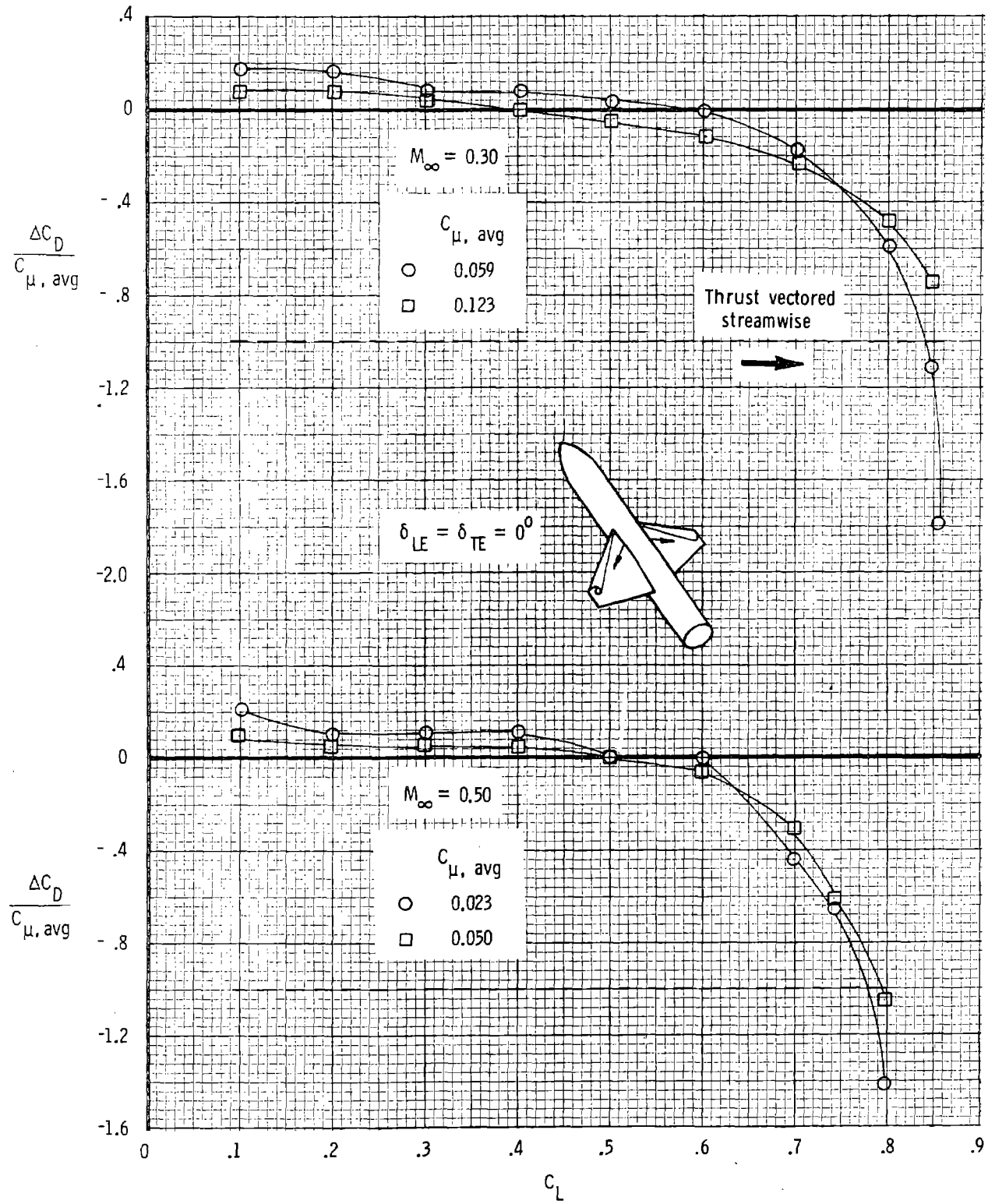

Figure 20.- Effect of C_L and $C_{\mu,avg}$ on the drag reduction ratio for the 44^o swept trapezoidal wing configuration for two Mach numbers.

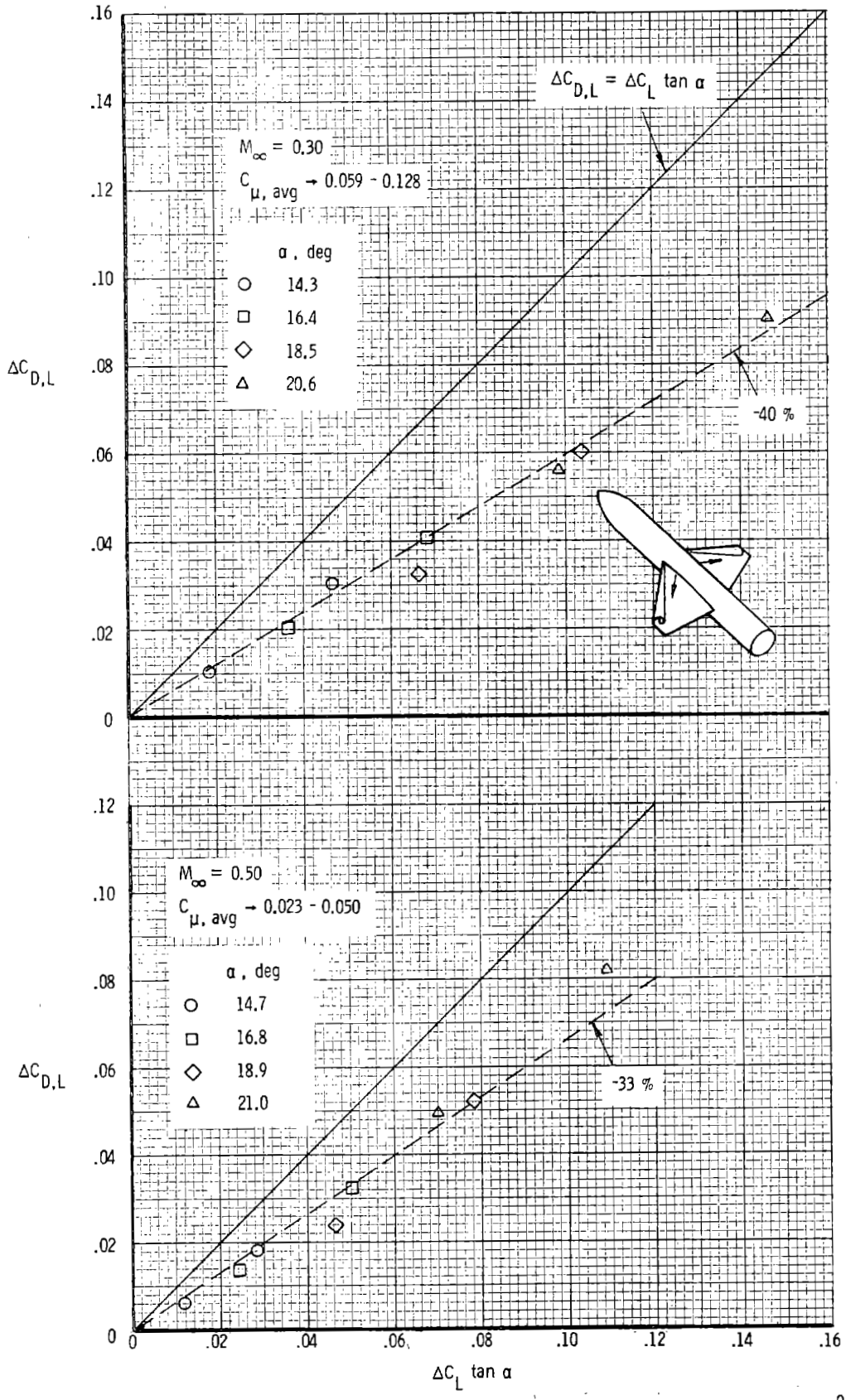

Figure 21.- Drag-due-to-lift increment due to spanwise blowing for the 44° swept trapezoidal wing configuration for two Mach numbers and a range of $C_{\mu,avg}$ and α ; $\delta_{LE} = \delta_{TE} = 0^\circ$.

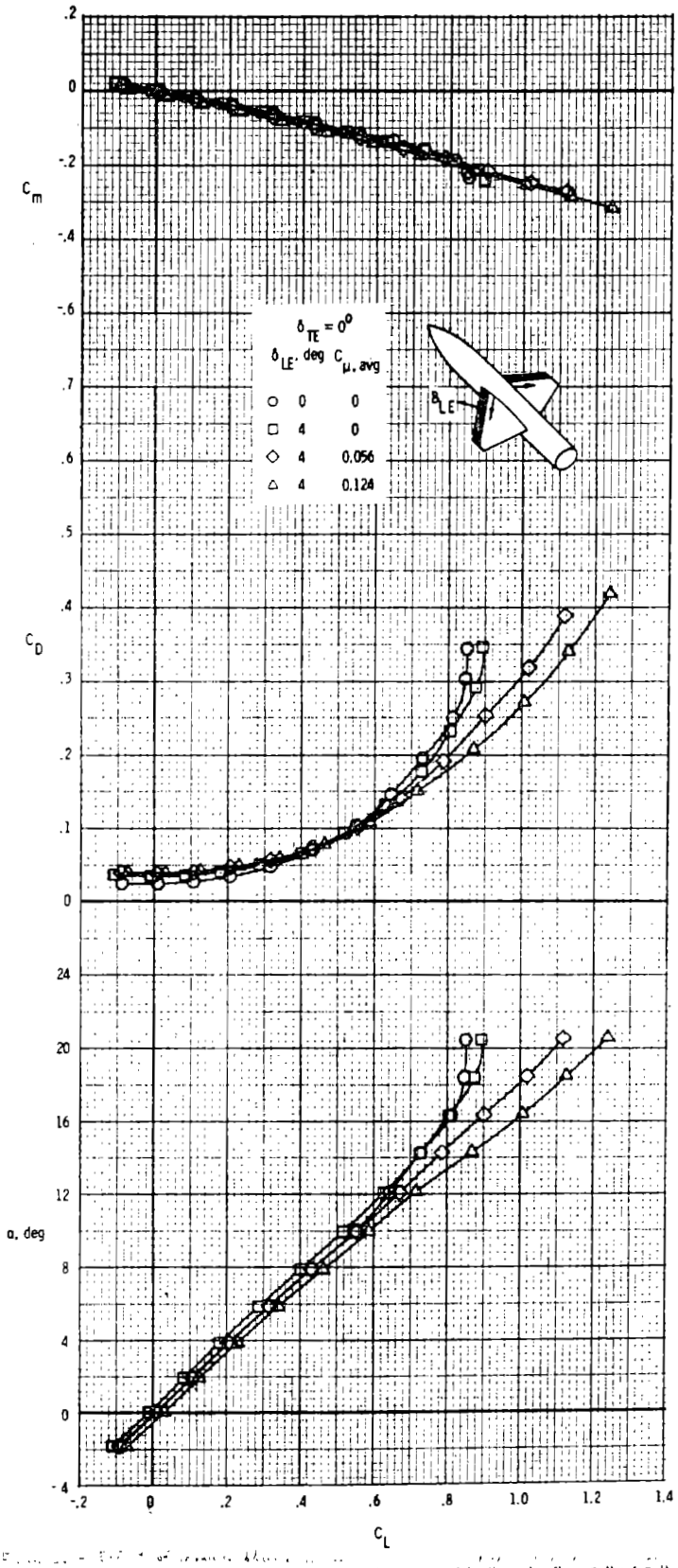

Figure 22.- Effect of spanwise blowing in conjunction with a deflected leading-edge flap on the longitudinal aerodynamic characteristics of the 44° swept trapezoidal wing configuration; $\delta_{TE} = 0^o$; $M_\infty = 0.30$.

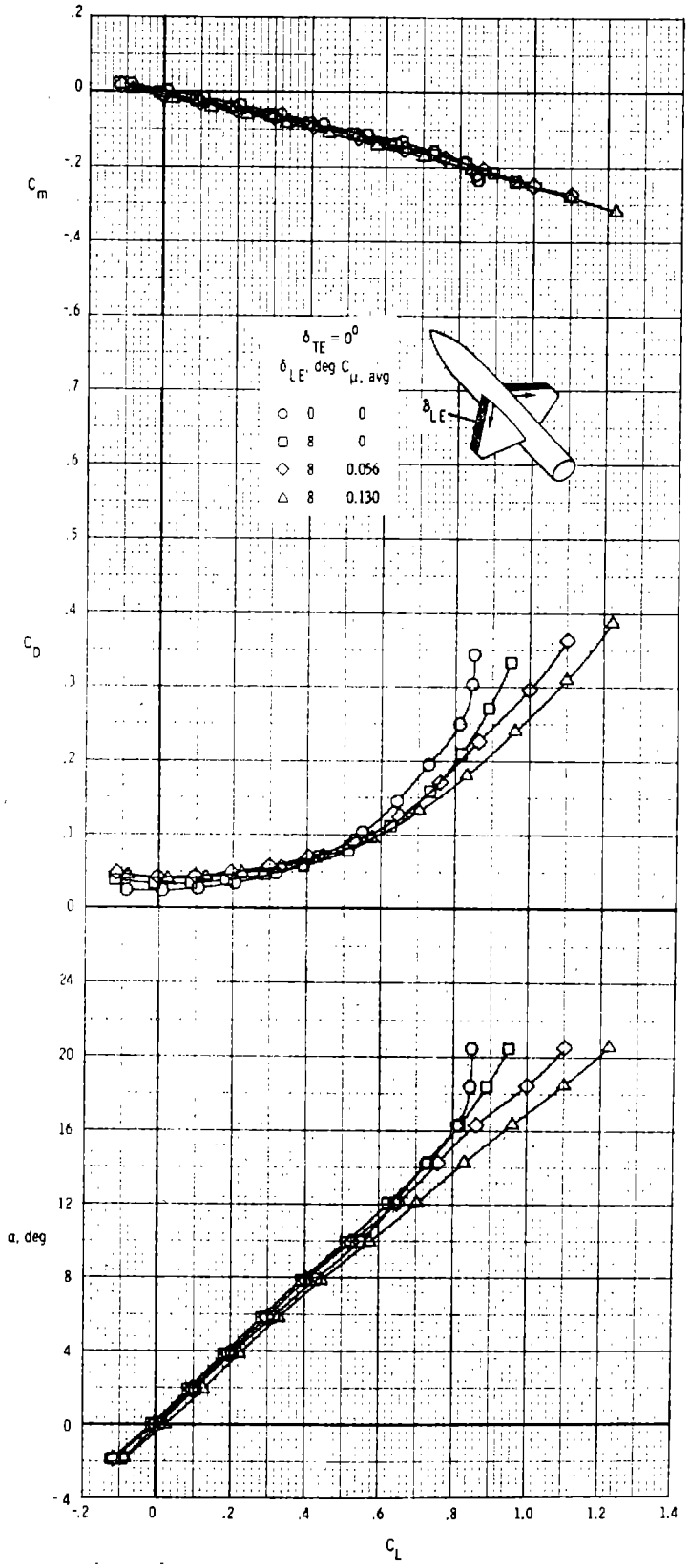

Figure 23.- Effect of spanwise blowing in conjunction with a deflected leading-edge flap on the longitudinal aerodynamic characteristics of the 44° swept trapezoidal wing configuration; $\delta_{TE} = 0^0$; $M_\infty = 0.30$.

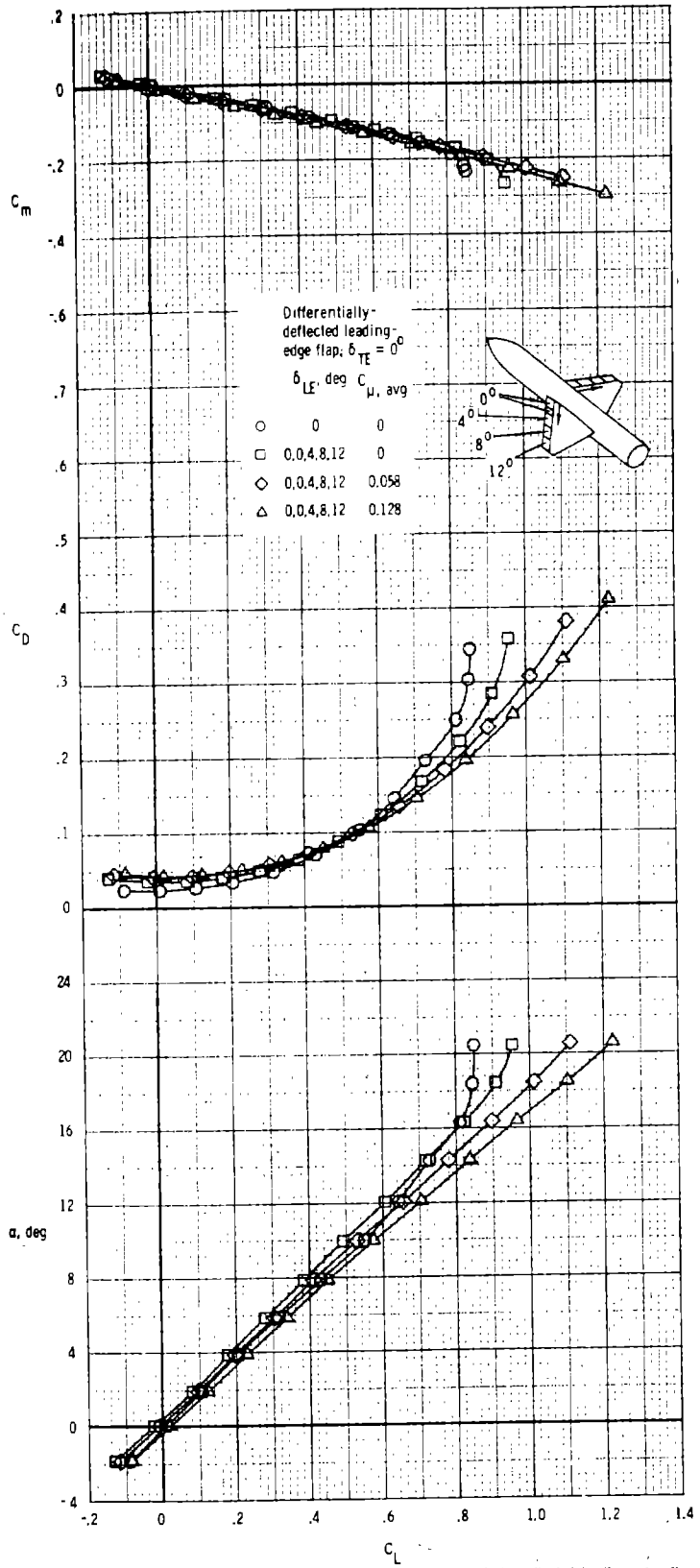

Figure 24.- Effect of spanwise blowing in conjunction with a differentially-deflected leading-edge flap on the longitudinal aerodynamic characteristics of the 44° swept trapezoidal wing configuration; $\delta_{TE} = 0^o$; $M_\infty = 0.30$.

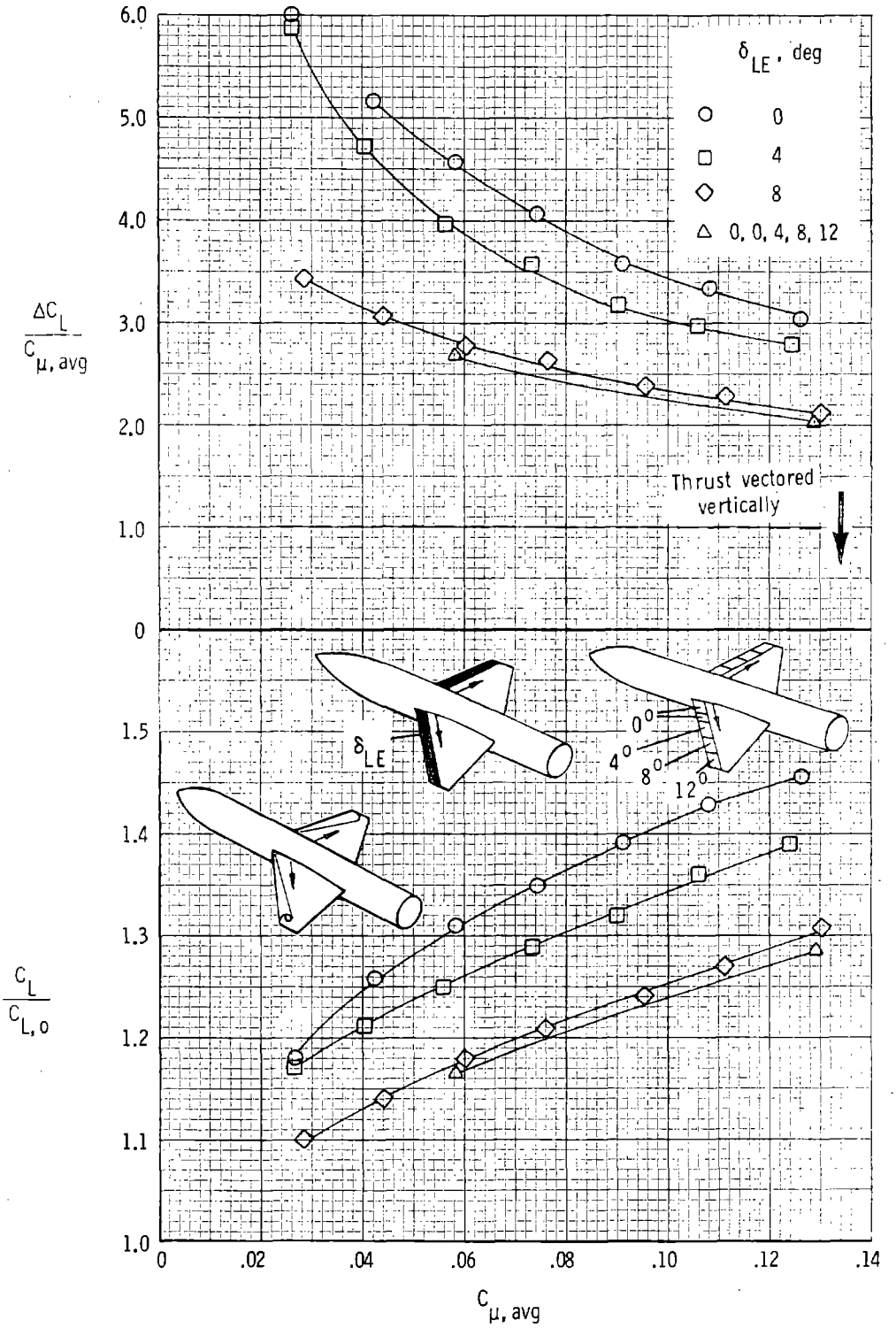

Figure 25.- Effect of $C_{\mu,avg}$ and δ_{LE} on the lift augmentation ratio and lift effectiveness of blowing for the 44° swept trapezoidal wing configuration for $\alpha \approx 20.5^{\circ}$; $\delta_{TE} = 0^{\circ}$; $M_{\infty} = 0.30$.

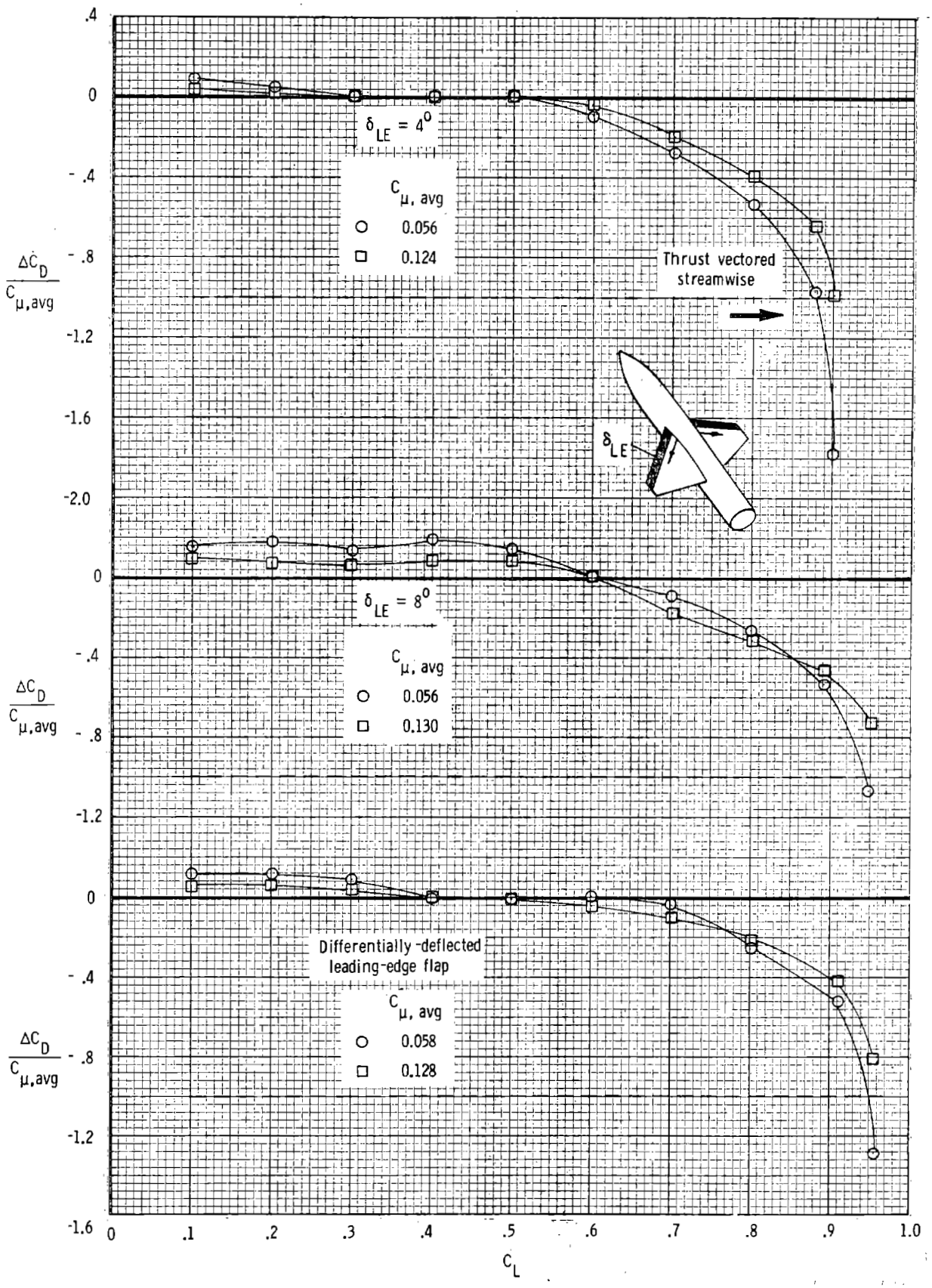

Figure 26.- Effect of C_L and $C_{\mu,avg}$ on the drag reduction ratio for the 44° swept trapezoidal-wing configuration for a range of δ_{LE}; $\delta_{TE} = 0^o$; $M_\infty = 0.30$.

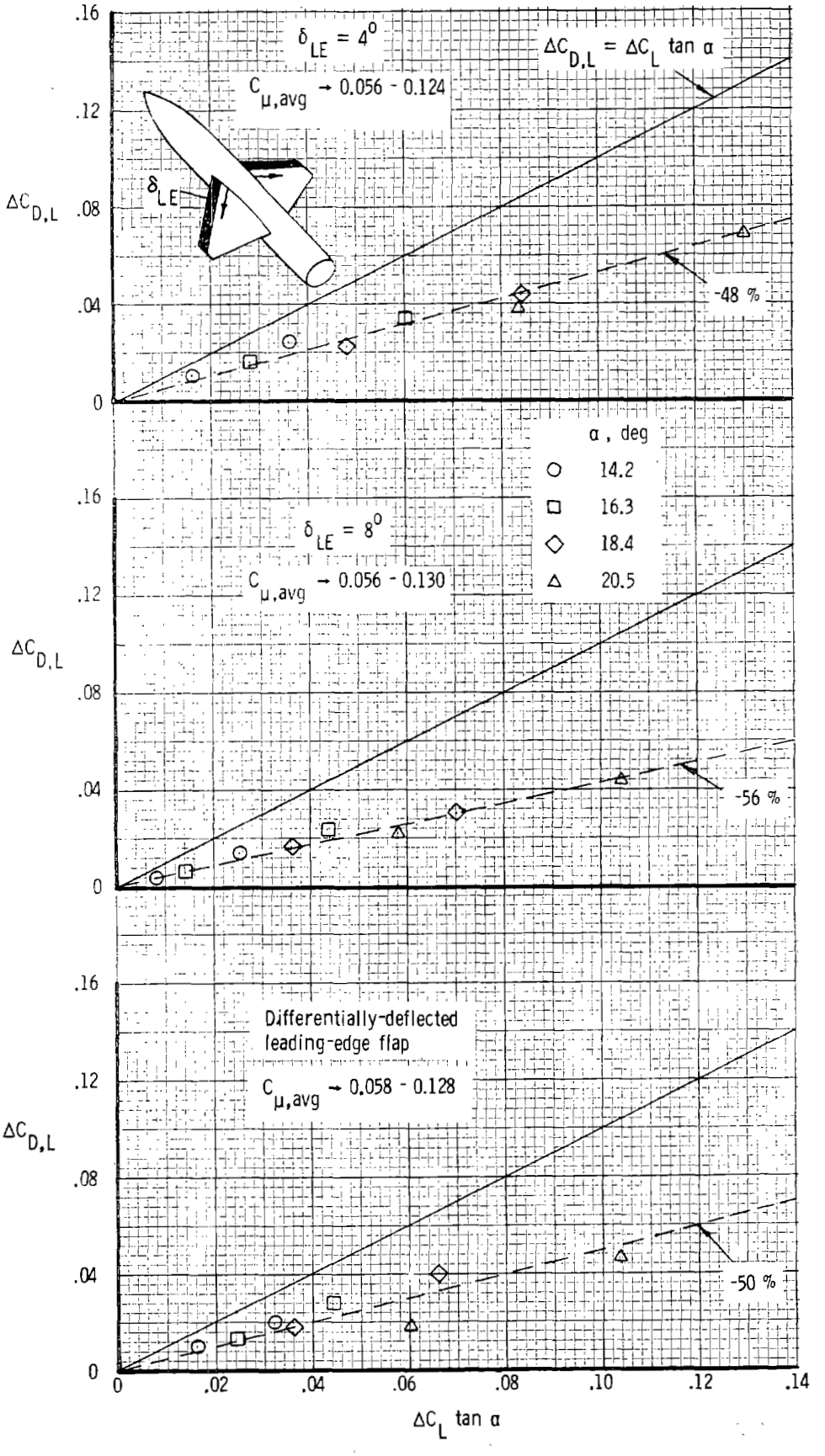

Figure 27.- Drag-due-to-lift increment due to spanwise blowing for the 44° swept trapezoidal wing configuration for a range of δ_{LE}, $C_{\mu,avg}$, and α ; $\delta_{TE} = 0^0$; $M_\infty = 0.30$.

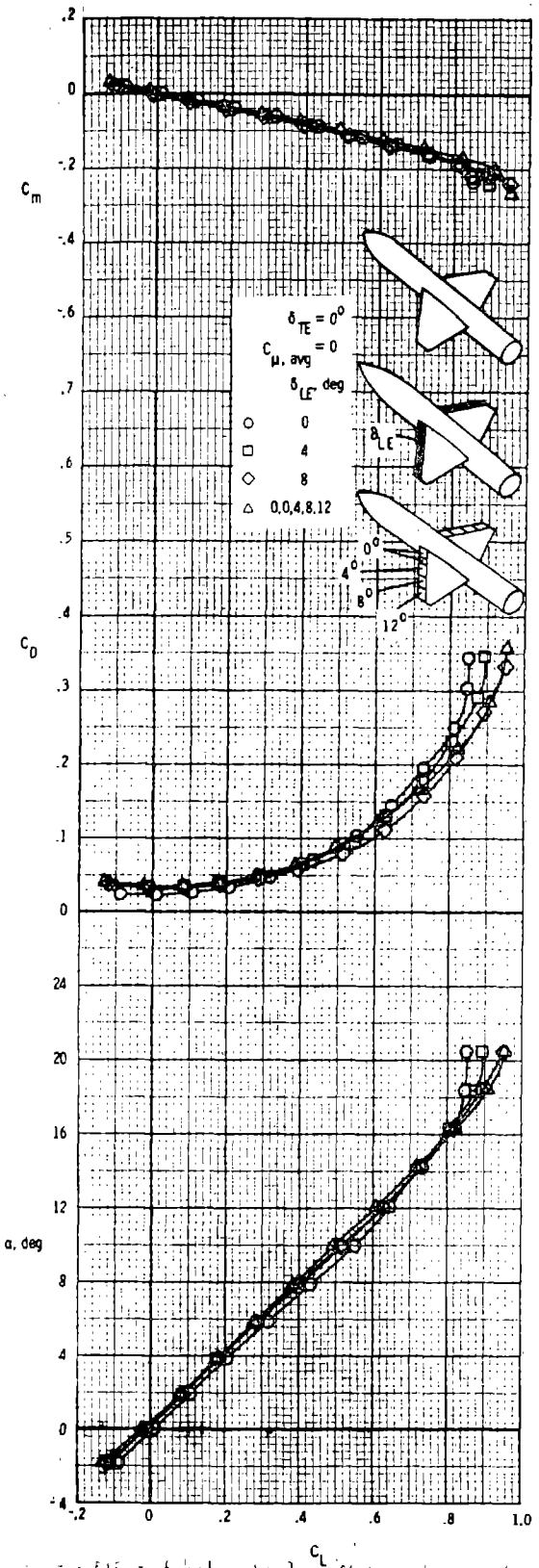

Figure 28.- Effect of leading-edge flap deflection angle on the longitudinal aerodynamic characteristics of the 44° swept trapezoidal wing configuration with blowing off; $\delta_{TE} = 0^o$; $M_\infty = 0.30$.

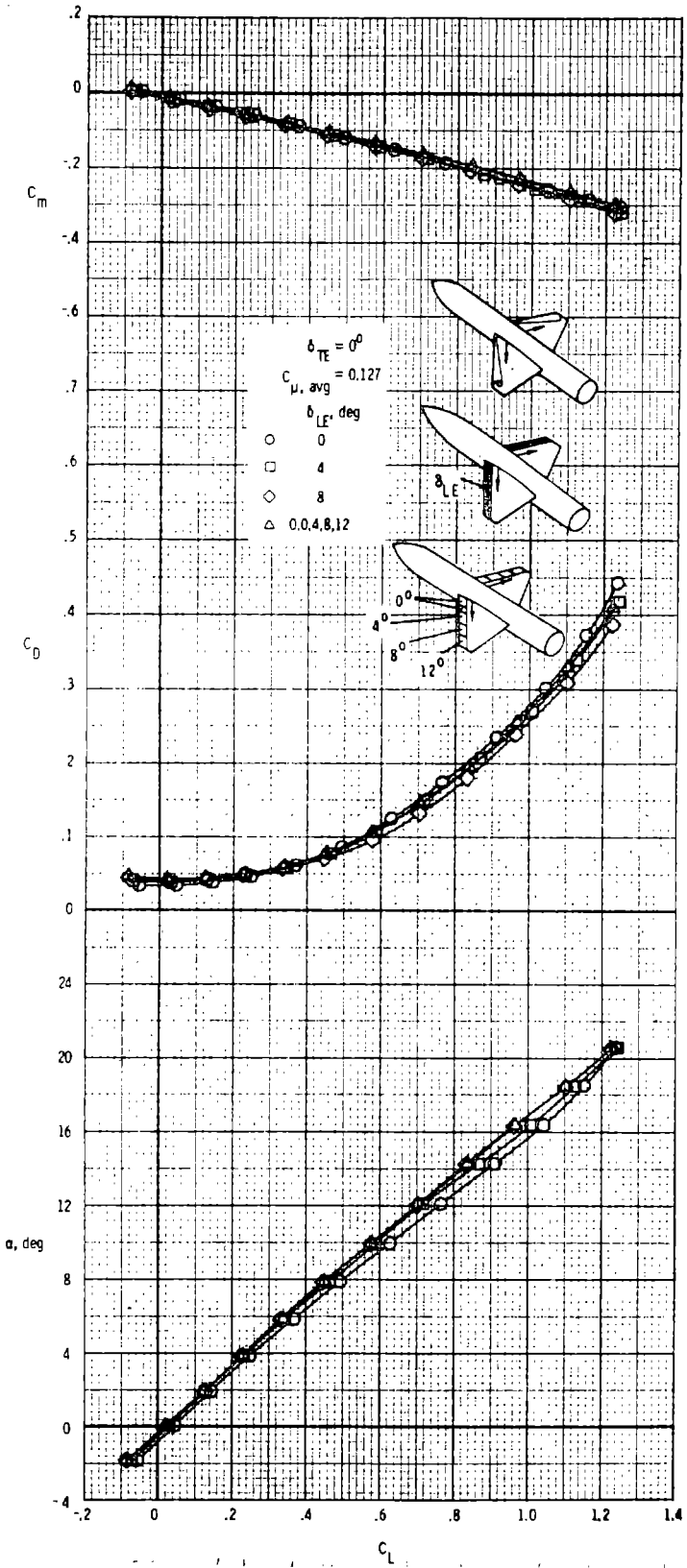

Figure 29.- Effect of leading-edge flap deflection angle on the longitudinal aerodynamic characteristics of the 44° swept trapezoidal wing configuration with blowing on; $\delta_{TE} = 0^0$; $M_\infty = 0.30$.

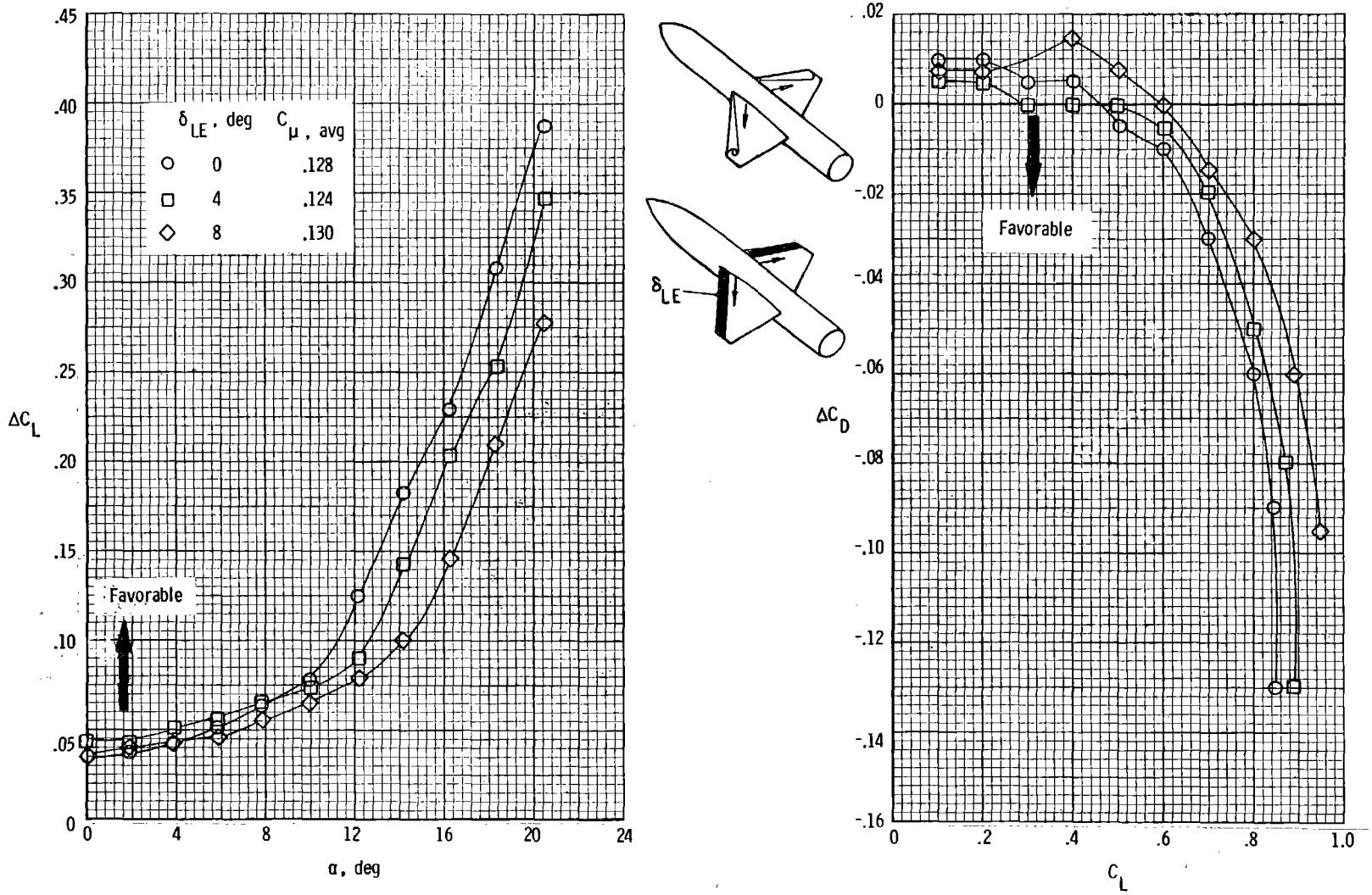

Figure 30.- Effect of leading-edge flap deflection angle on the lift and drag increments due to spanwise blowing on the 44° swept trapezoidal wing configuration; $\delta_{TE} = 0^\circ$; $M_\infty = 0.30$.

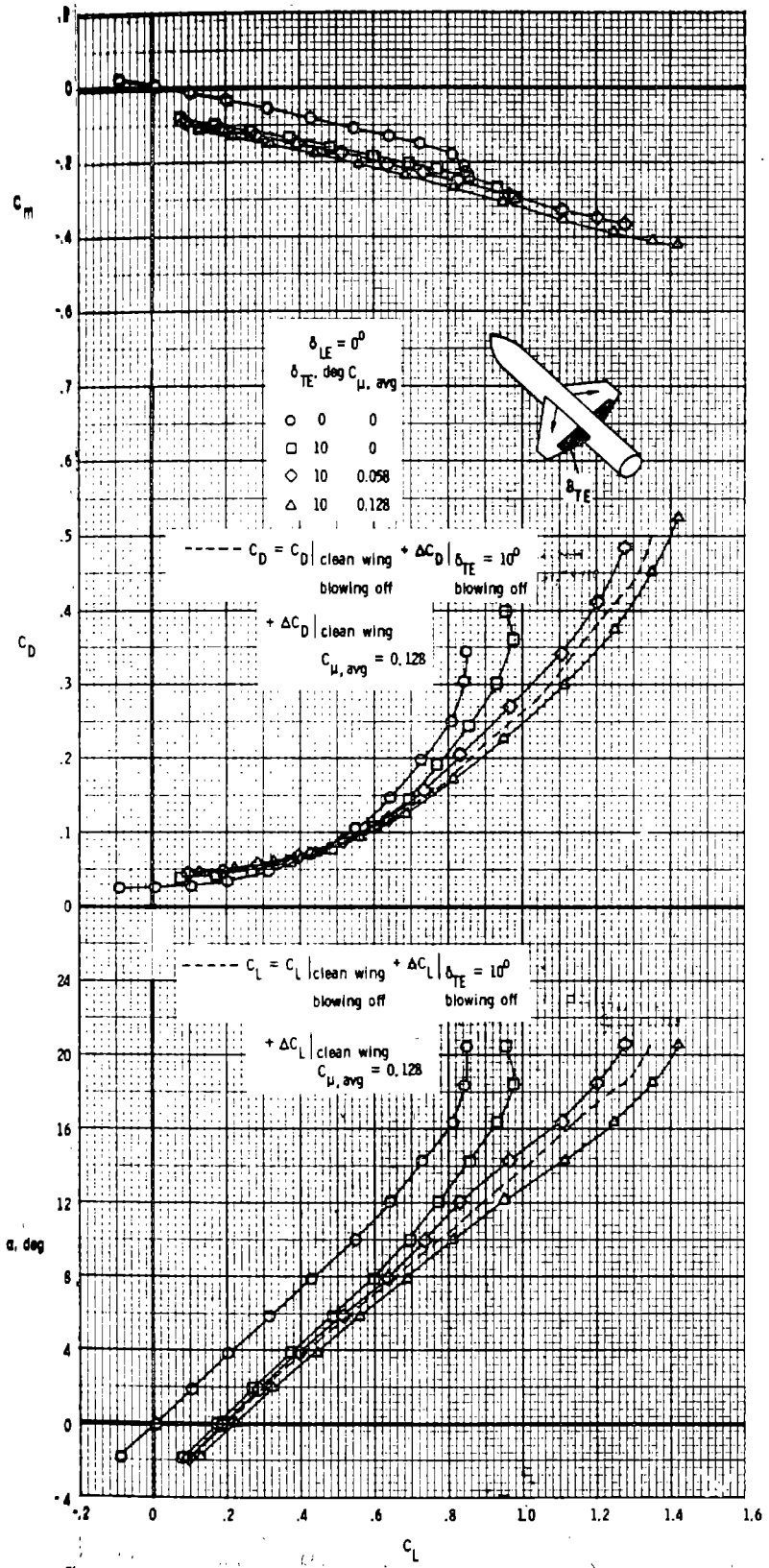

Figure 31.- Effect of spanwise blowing in conjunction with a deflected trailing-edge flap on the longitudinal aerodynamic characteristics of the 44° swept trapezoidal wing configuration; $\delta_{LE} = 0^0$; $M_\infty = 0.30$.

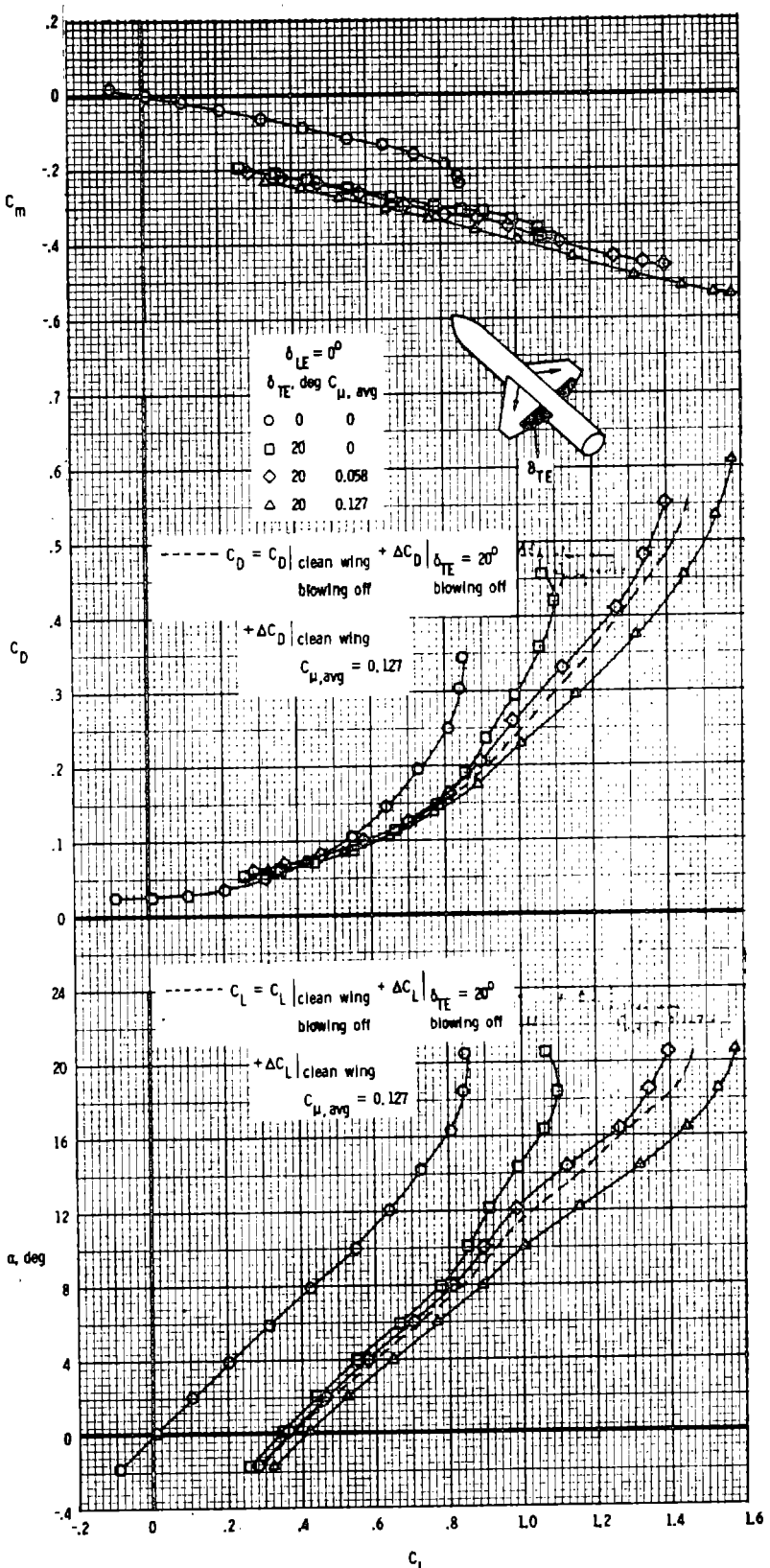

Figure 32.- Effect of spanwise blowing in conjunction with a deflected trailing-edge flap on the longitudinal aerodynamic characteristics of the 44° swept trapezoidal wing configuration; $\delta_{LE} = 0^0$; $M_\infty = 0.30$.

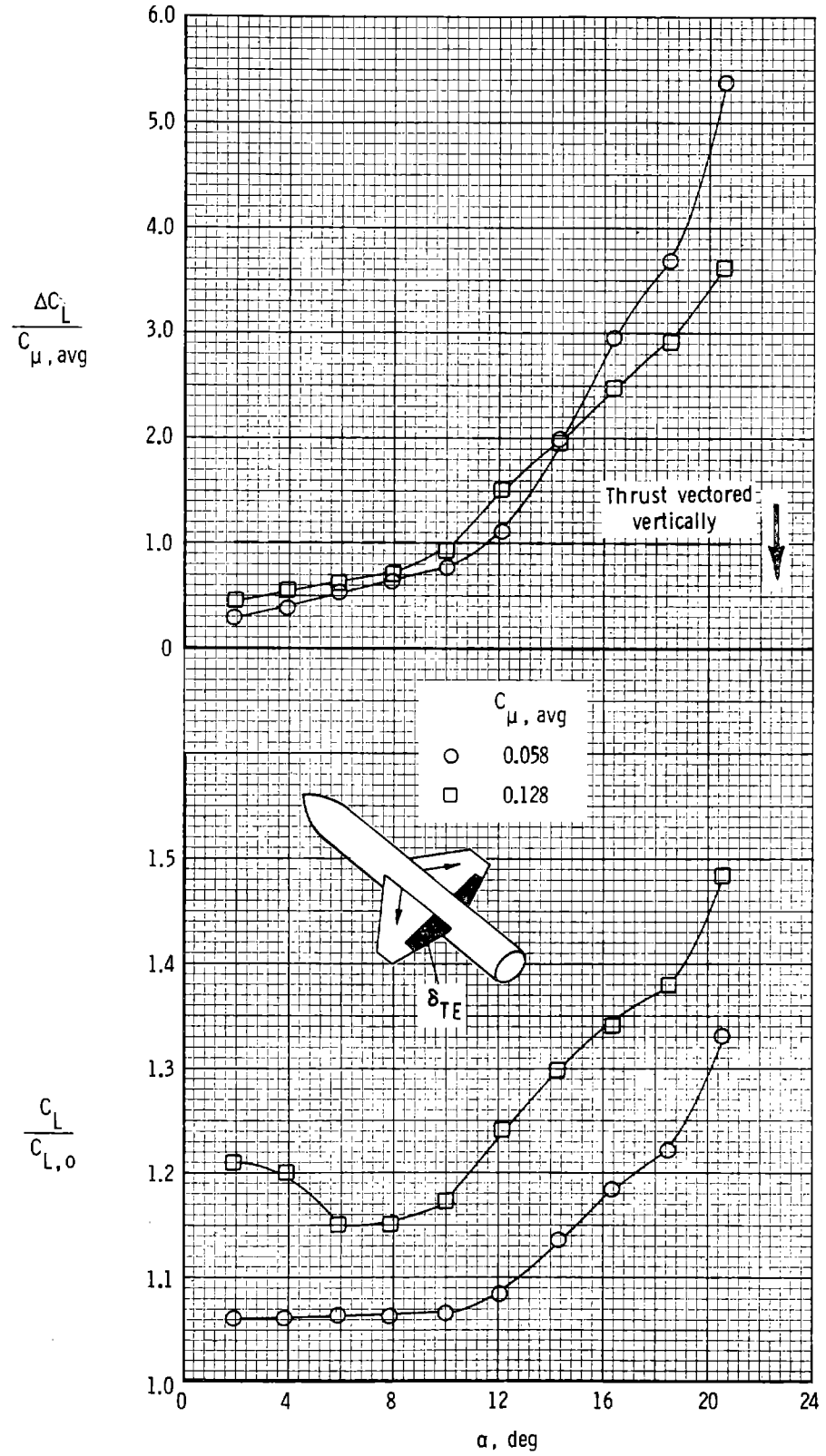

Figure 33.- Effect of α and $C_{\mu, avg}$ on the lift augmentation ratio and lift effectiveness of blowing for the 44° swept trapezoidal wing configuration with $\delta_{TE} = 10^{\circ}$; $\delta_{LE} = 0^{\circ}$; $M_{\infty} = 0.30$.

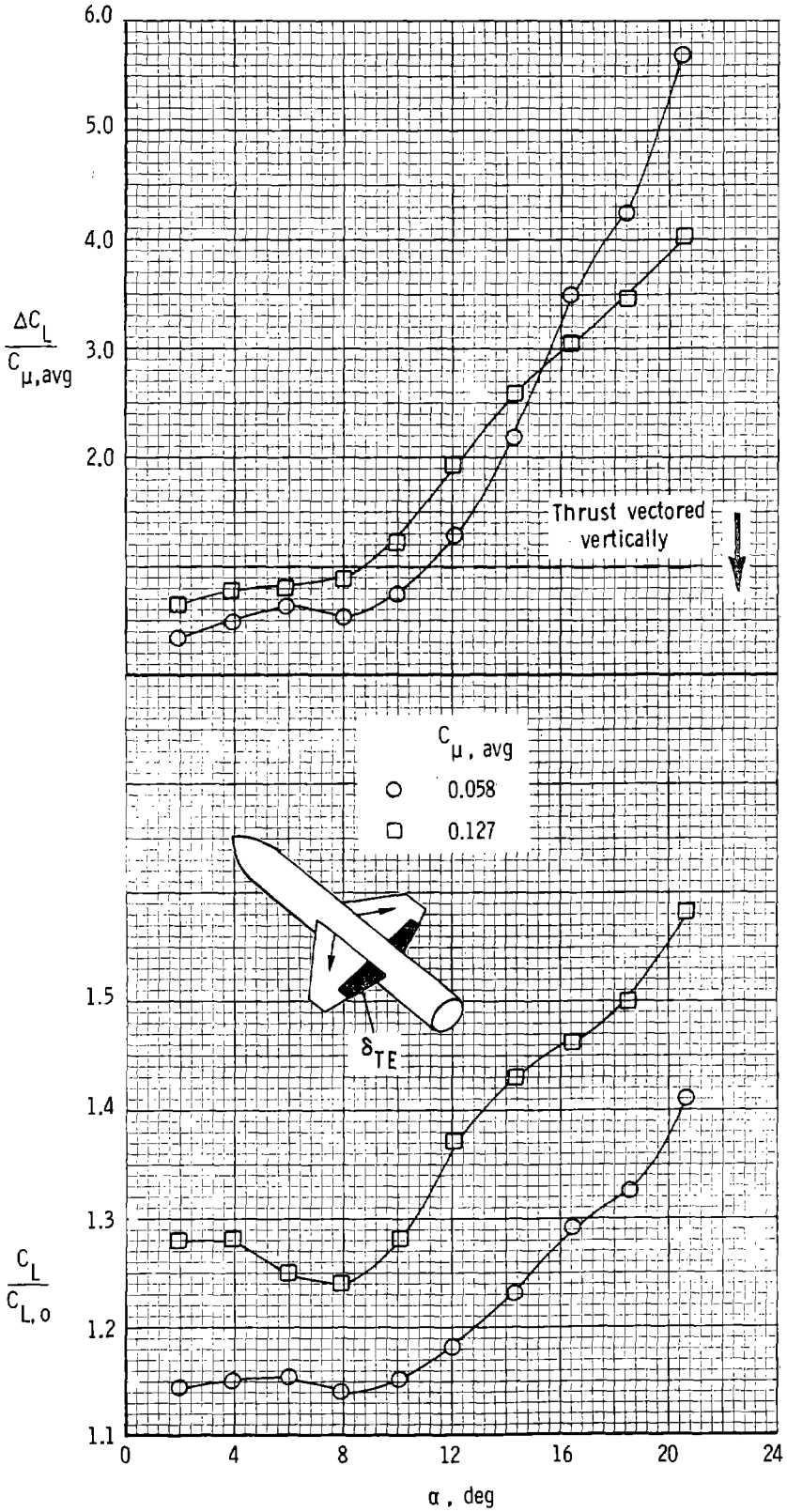

Figure 34.- Effect of α and $C_{\mu_\delta\ avg}$ on the lift augmentation ratio and lift effectiveness of blowing for the 44° swept trapezoidal wing configuration with $\delta_{TE} = 20^\circ$; $\delta_{LE} = 0^\circ$; $M_\infty = 0.30$.

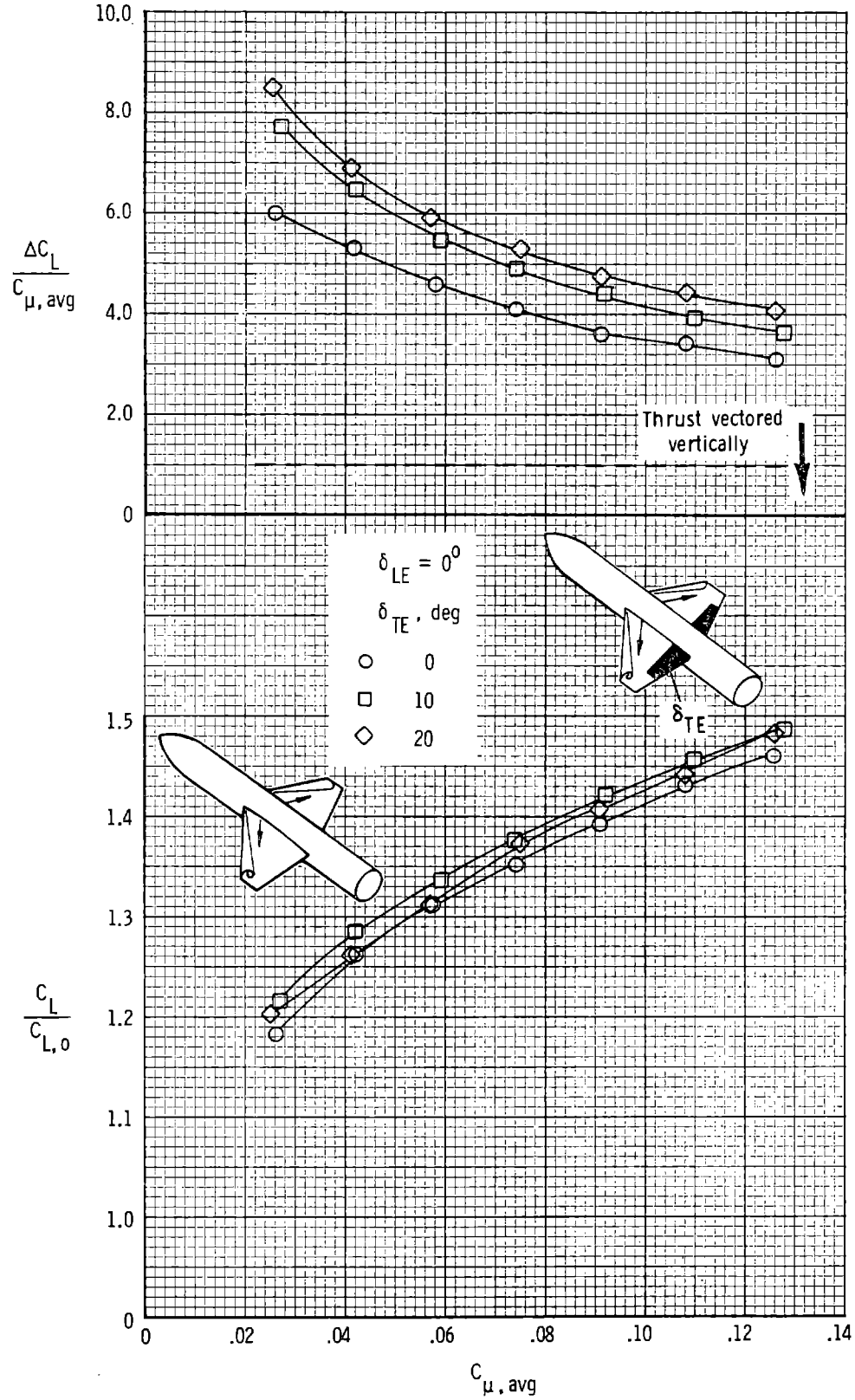

Figure 35.- Effect of $C_{\mu,avg}$ and δ_{TE} on the lift augmentation ratio and lift effectiveness of blowing for the 44^o swept trapezoidal wing configuration; $\delta_{LE} = 0^o$; $M_\infty = 0.30$; $\alpha \approx 21^o$.

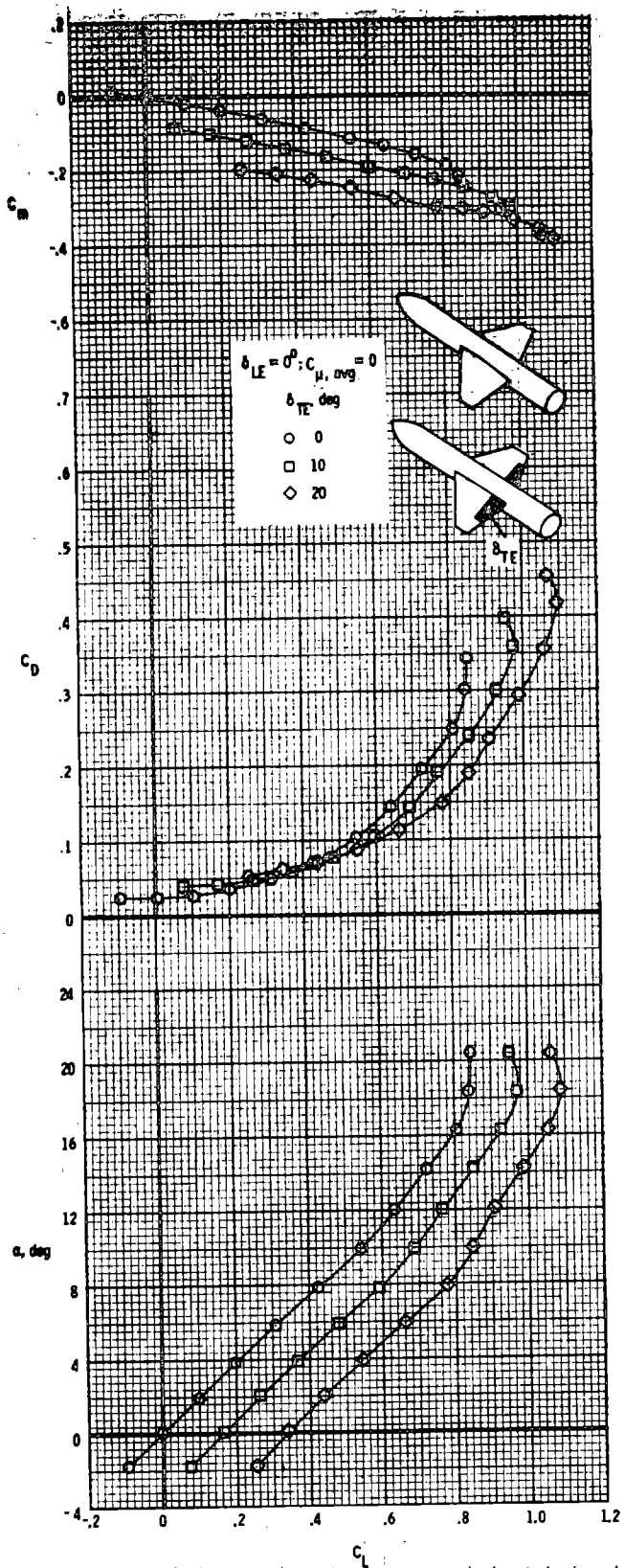

Figure 36.- Effect of trailing-edge flap deflection angle on the longitudinal aerodynamic characteristics of the 44° swept trapezoidal wing configuration with blowing off; $\delta_{LE} = 0^0$; $M_\infty = 0.30$.

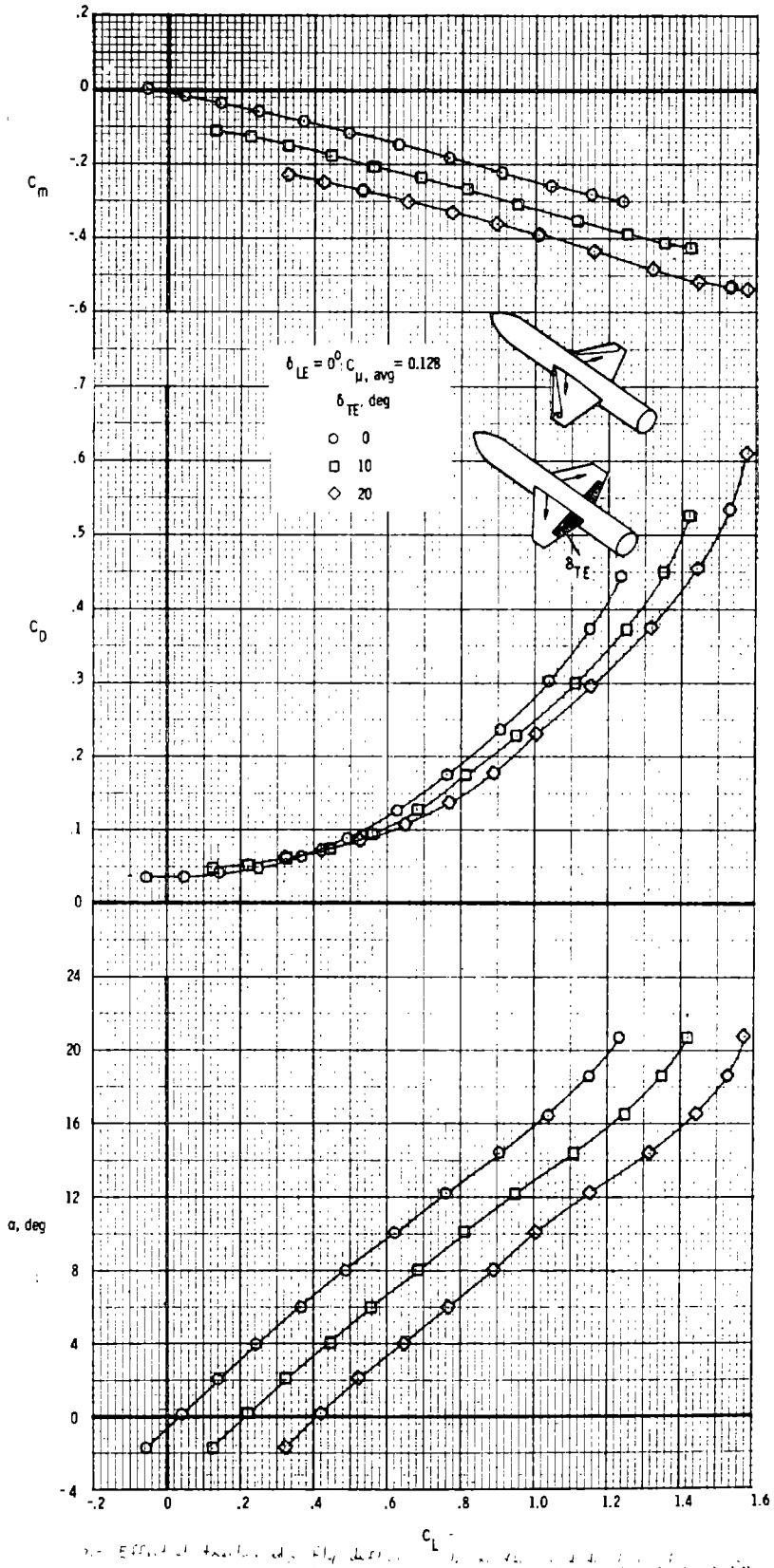

Figure 37.- Effect of trailing-edge flap deflection angle on the longitudinal aerodynamic charcteristics of the 44° swept trapezoidal wing configuration with blowing on; $\delta_{LE} = 0^0$; $M_\infty = 0.30$.

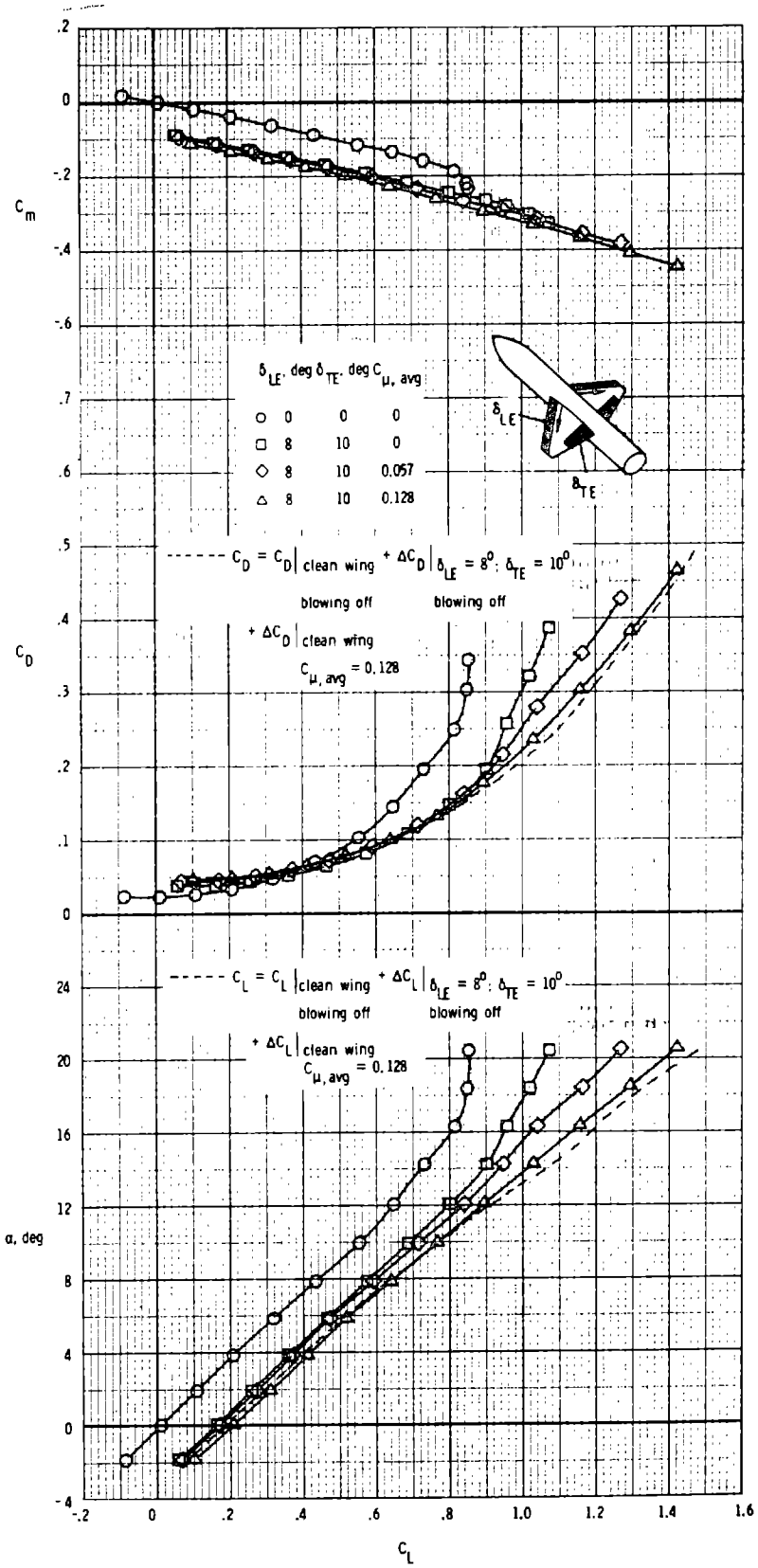

Figure 38.- Effect of spanwise blowing in conjunction with deflected leading- and trailing-edge flaps on the longitudinal aerodynamic characteristics of the 44° swept trapezoidal wing configuration; $\delta_{LE} = 8^0$, $\delta_{TE} = 10^0$; $M_\infty = 0.30$.

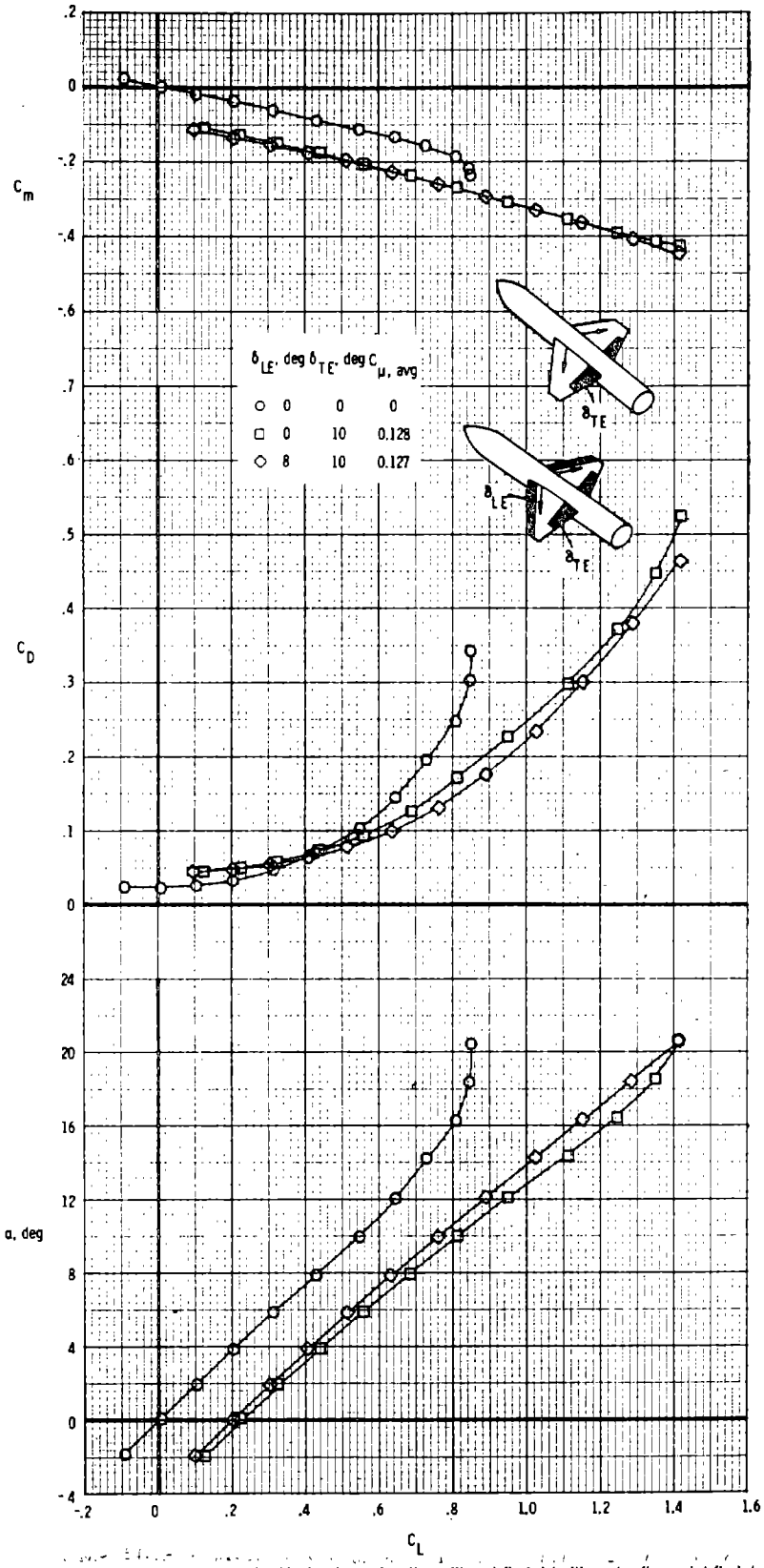

Figure 39.- Effect of spanwise blowing in conjunction with a deflected trailing-edge flap and deflected leading- and trailing-edge flaps on the longitudinal aerodynamic characteristics of the 44° swept trapezoidal wing configuration; $M_\infty = 0.30$.

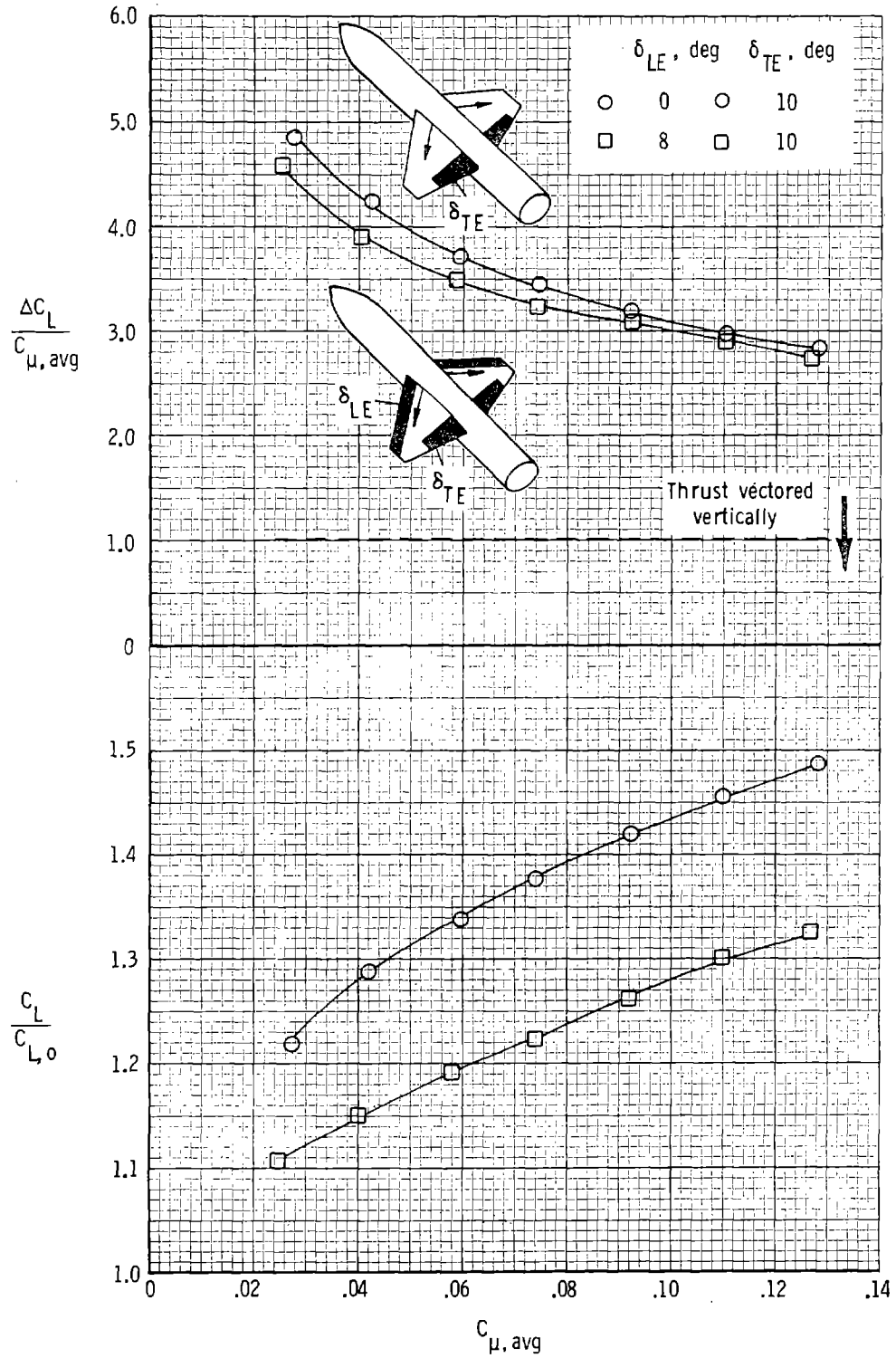

Figure 40.- Effect of $C_{\mu,avg}$, δ_{LE}, and δ_{TE} on the lift augmentation ratio and lift effectiveness of blowing for the 44° swept trapezoidal wing configuration for $\alpha \approx 20.5^{\circ}$.

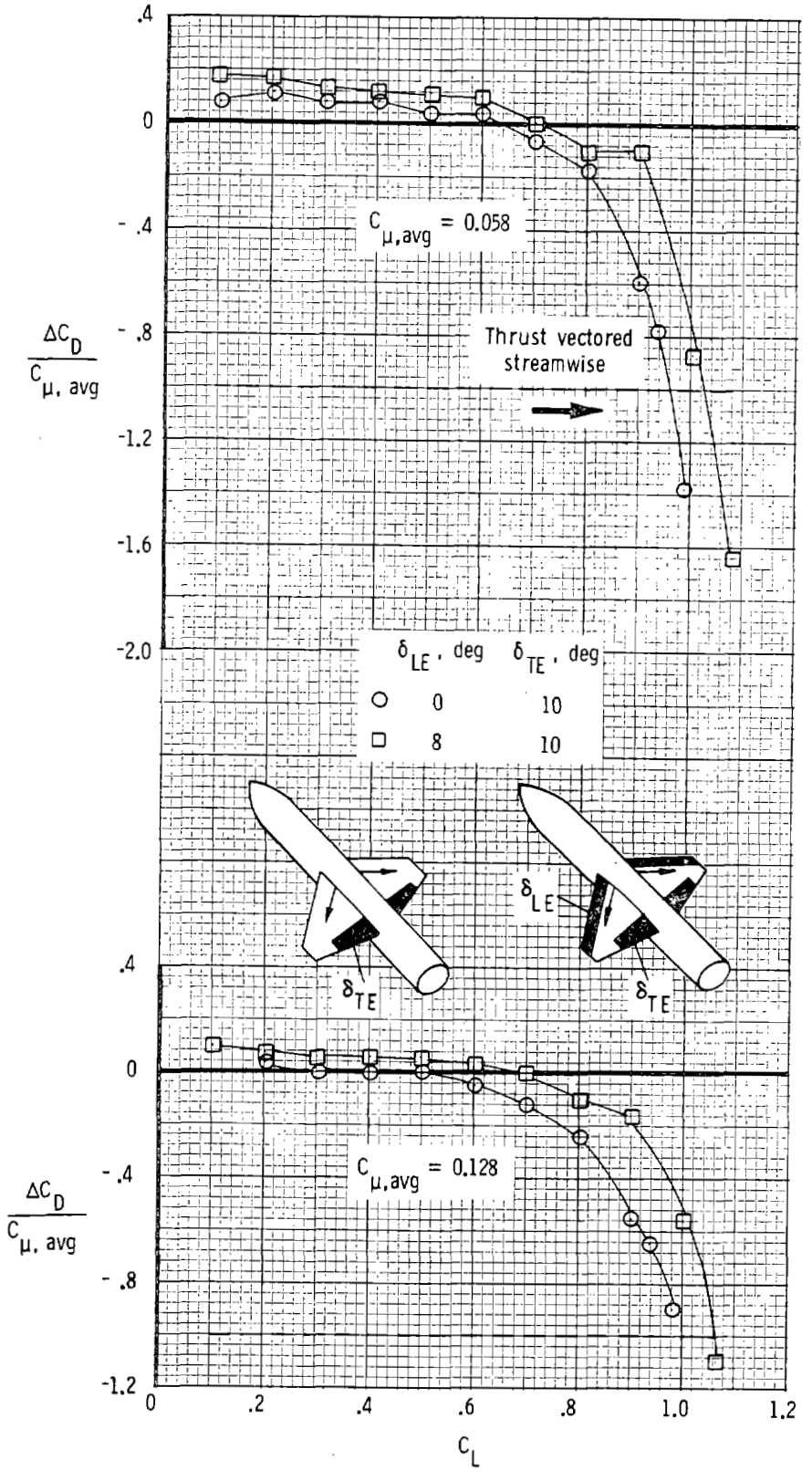

Figure 41.- Effect of C_L and leading- and trailing-edge flap deflection angles on the drag reduction ratio for two jet momentum coefficients; M_∞ = 0.30.

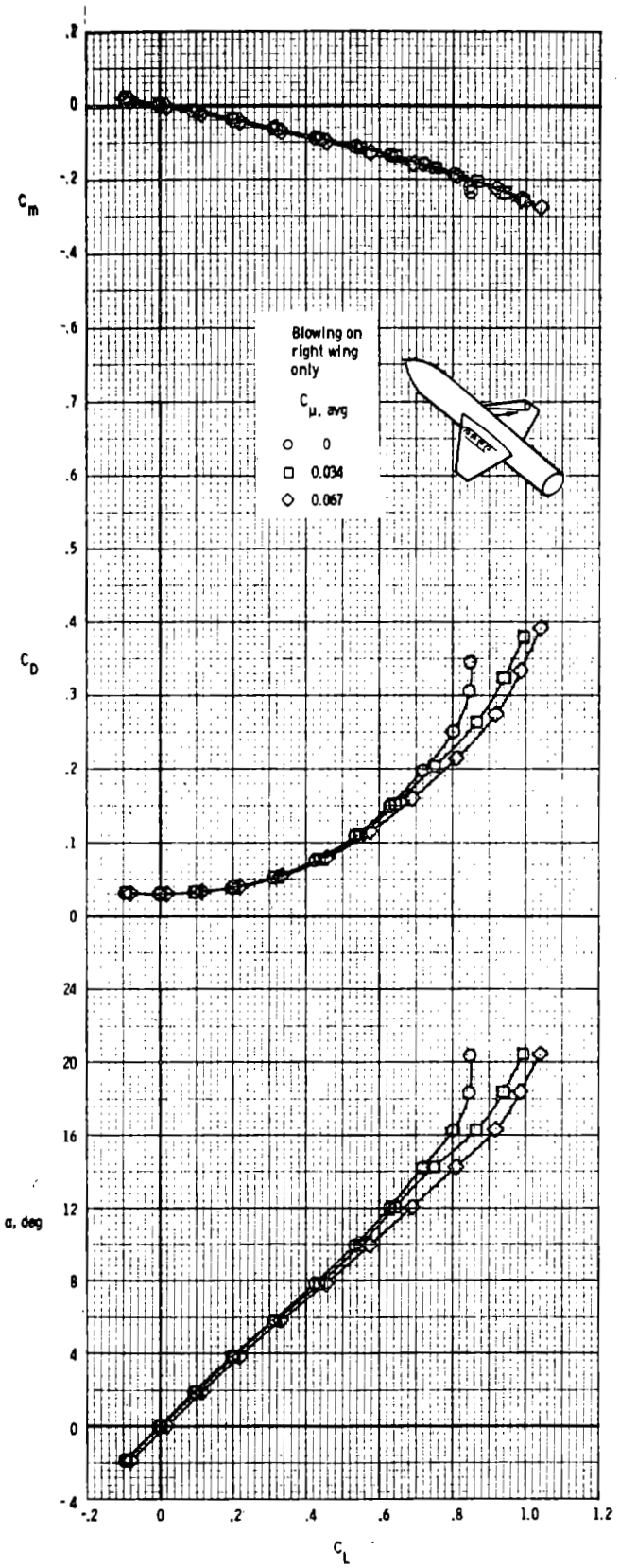

Figure 42.- Effect of spanwise blowing on the longitudinal aerodynamic characteristics of the 44° swept trapezoidal wing configuration with blowing on the right wing: $M_{\infty} = 0.30$.

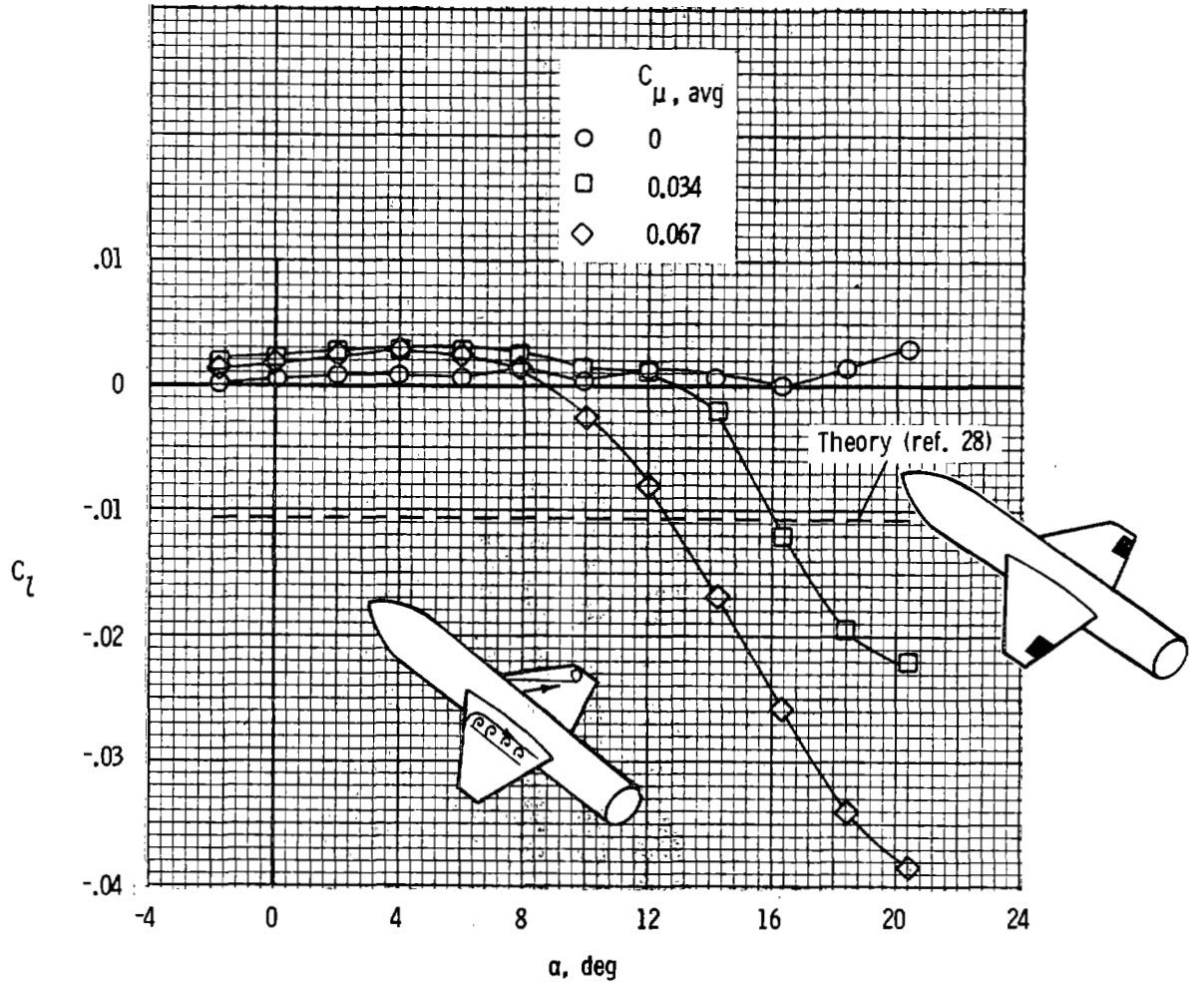

Figure 43.- Effect of α and $C_{\mu,avg}$ on rolling moment coefficient for the 44° swept trapezoidal wing configuration with blowing on the right wing only; M_∞ = 0.30.

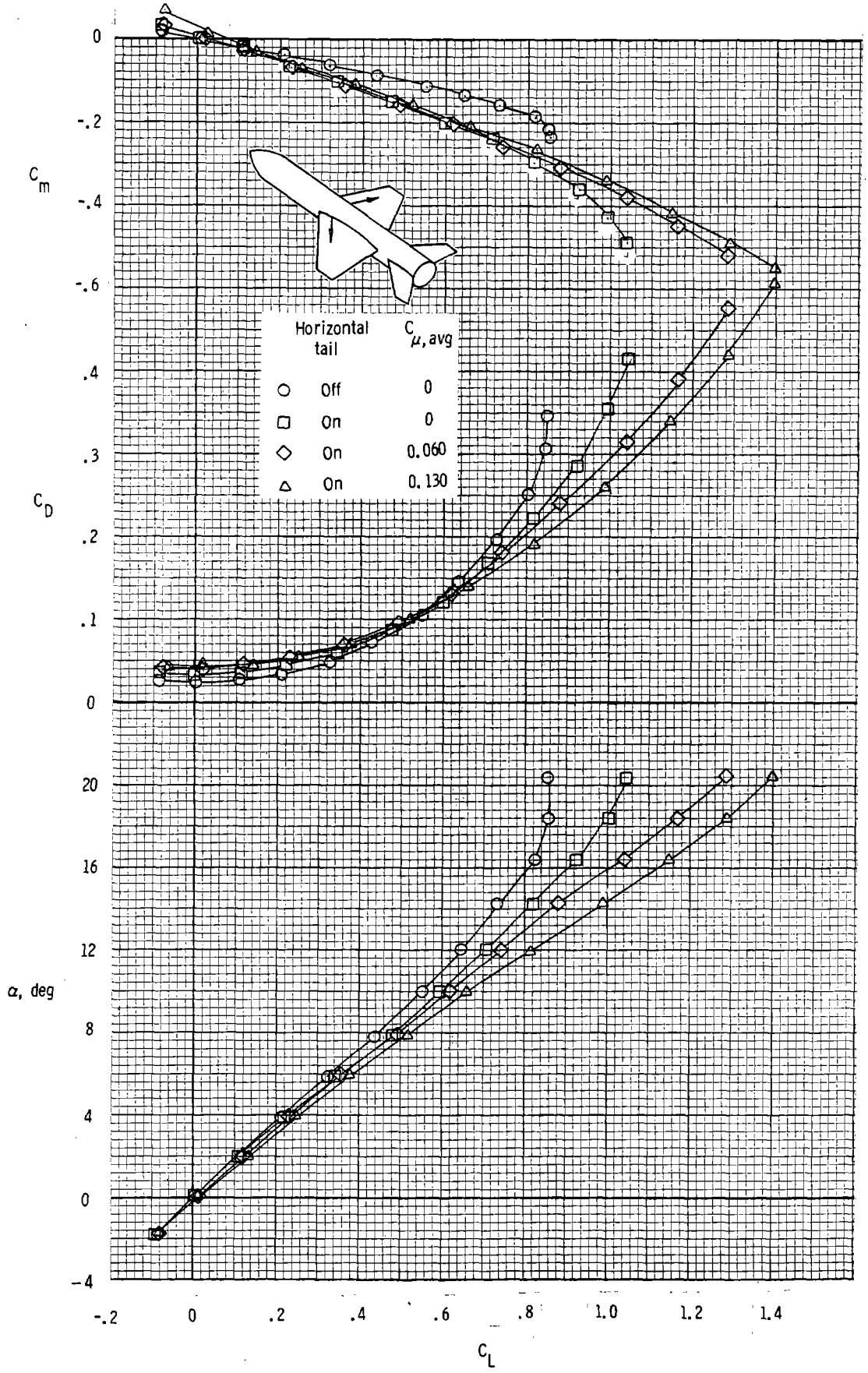

Figure 44.- Effect of spanwise blowing on the 44° swept trapezoidal wing on the longitudinal aerodynamic characteristics of the wing-horizontal tail configuration; $M_{\infty} = 0.30$.

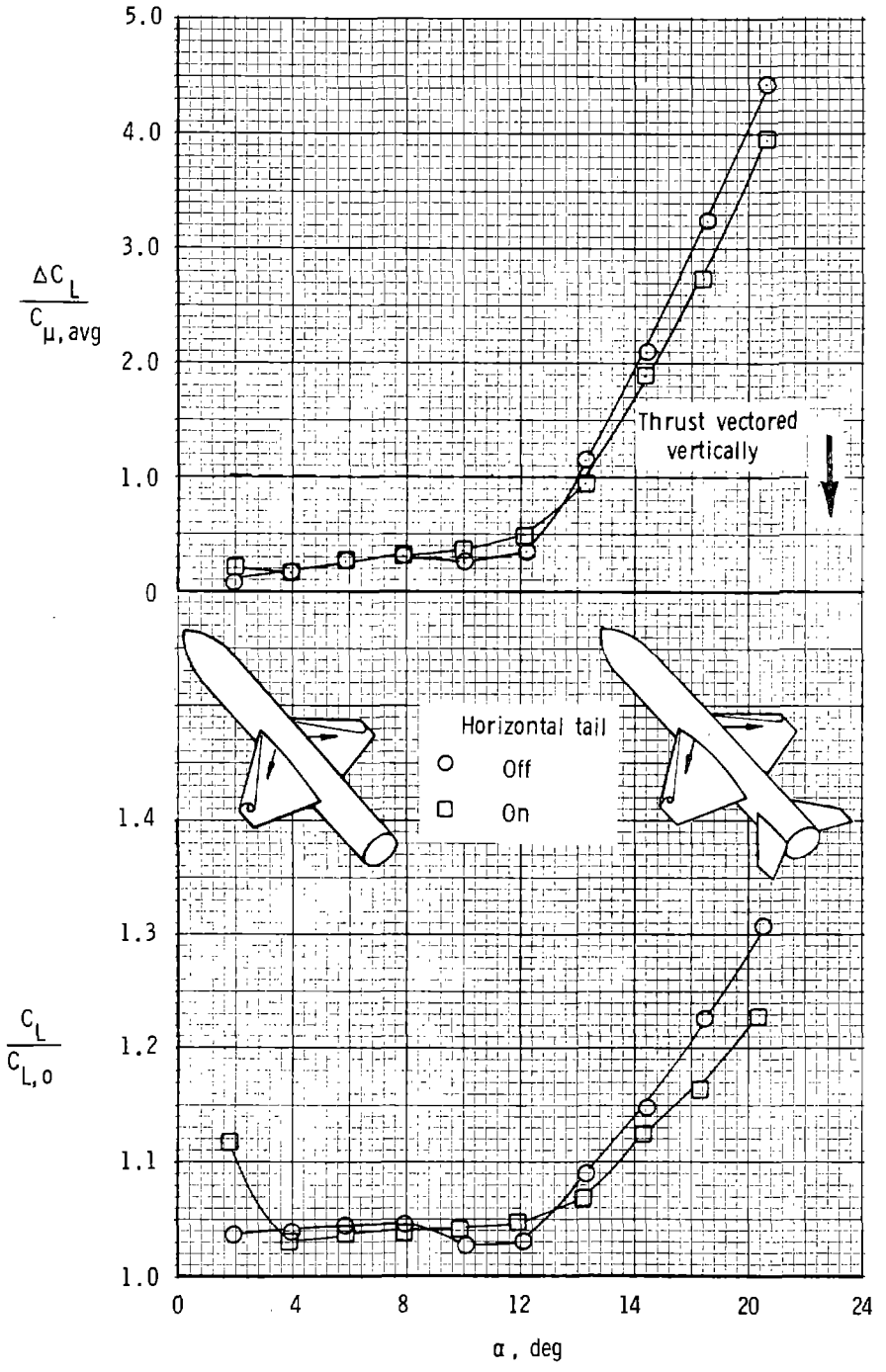

Figure 45.- Effect of angle-of-attack and horizontal tail on the lift augmentation ratio and lift effectiveness of blowing on the 44^0 swept trapezoidal wing for $C_{\mu,avg} = 0.060$; $M_\infty = 0.30$.

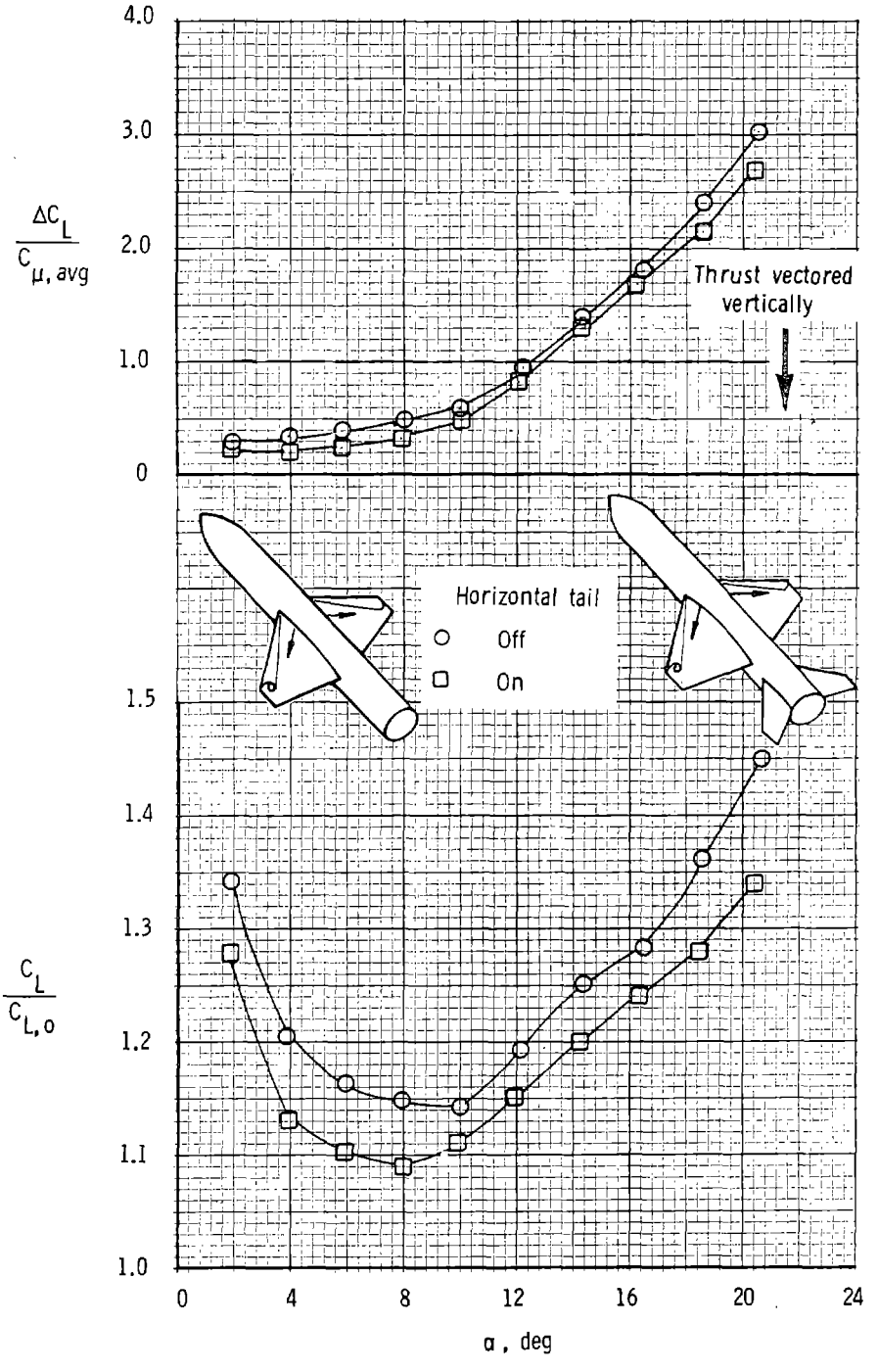

Figure 46.- The effect of angle-of-attack and horizontal tail on the lift augmentation ratio and lift effectiveness of blowing on the 44° swept trapezoidal wing for $C_{\mu,avg} = 0.13$; $M_\infty = 0.30$.

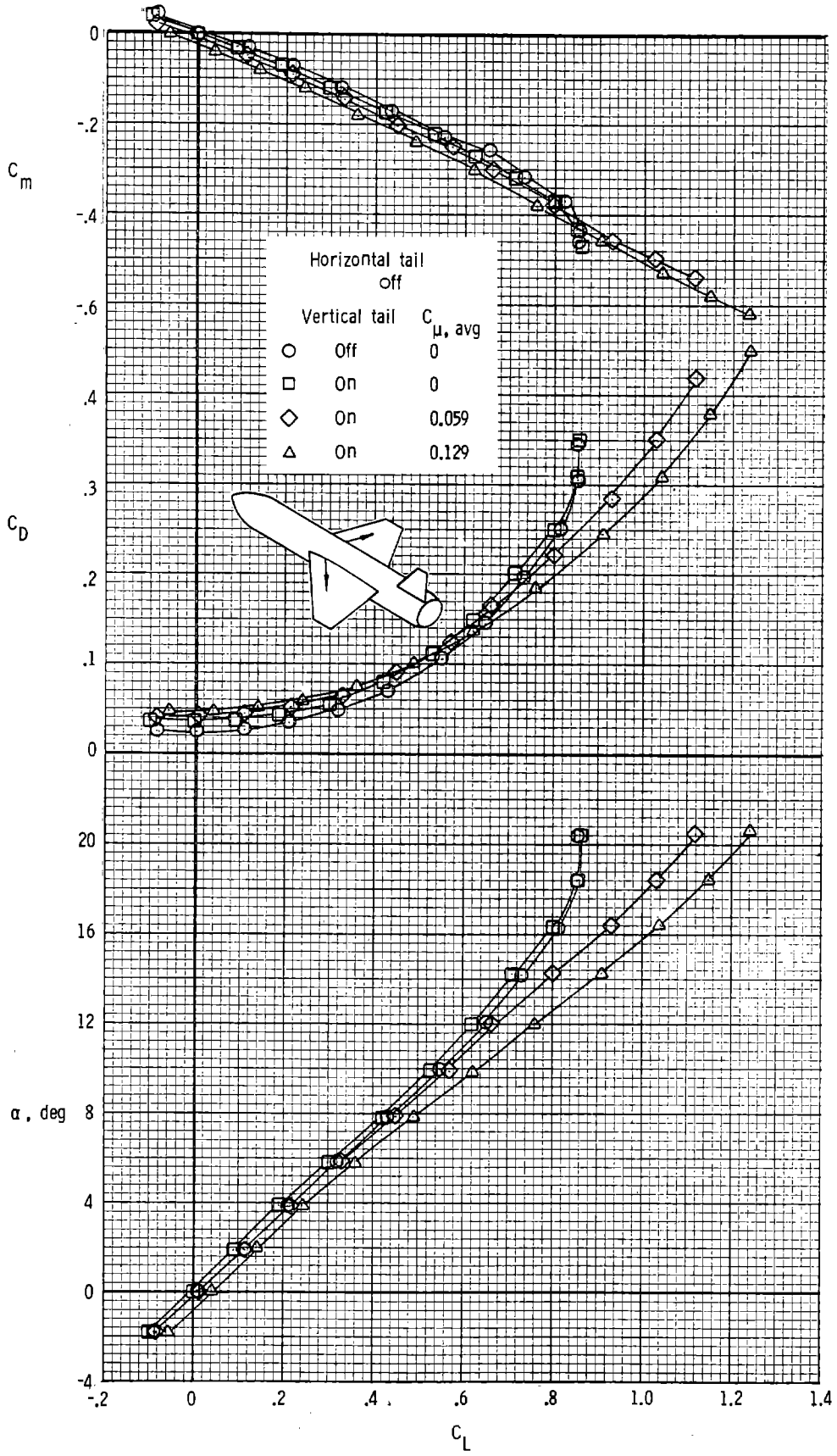

Figure 47.- Effect of spanwise blowing on the longitudinal aerodynamic characteristics of the wing-vertical tail configuration at $\beta \approx 0^0$; $M_\infty = 0.30$.

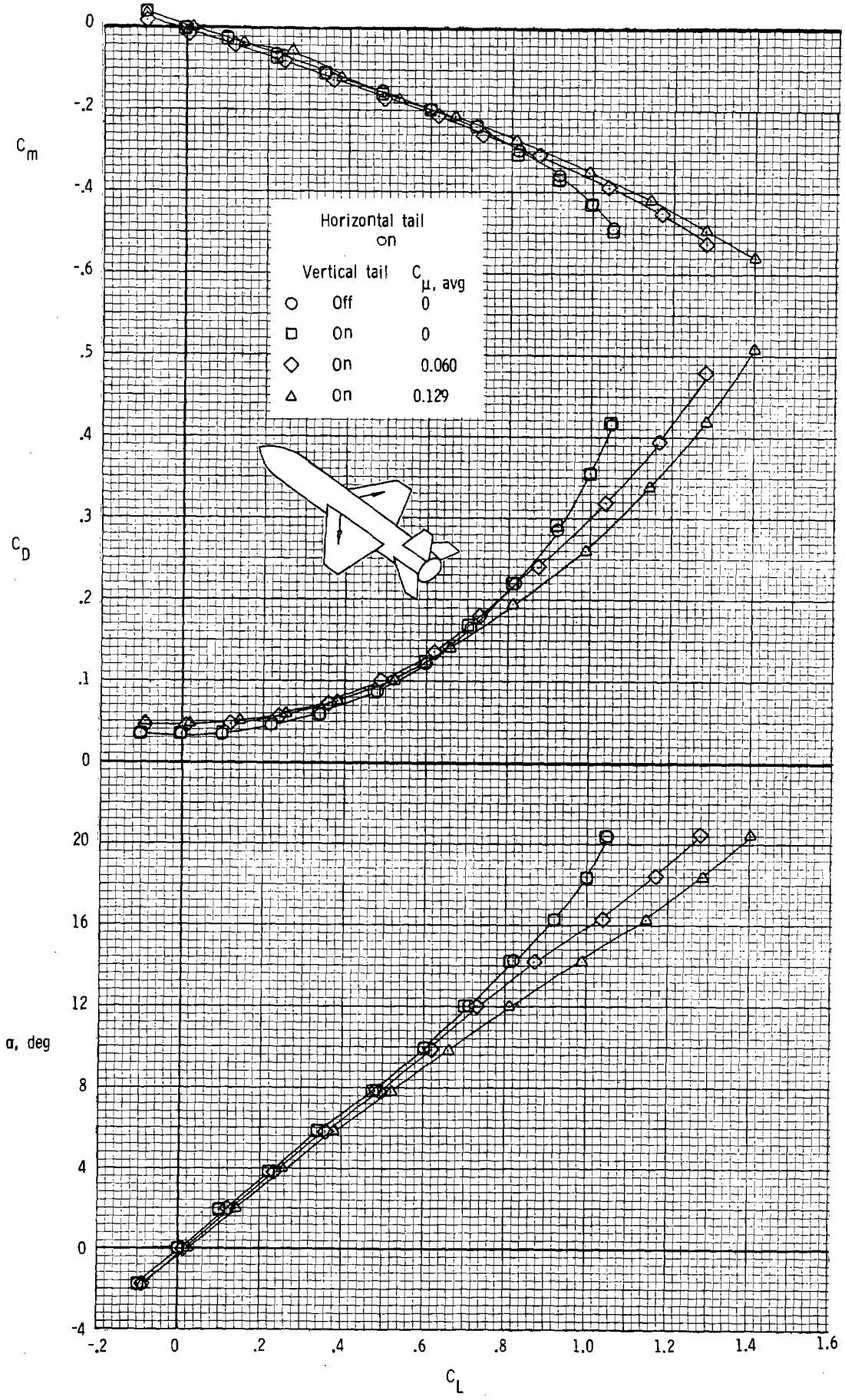

Figure 48.- Effect of spanwise blowing on the longitudinal aerodynamic characteristics of the wing-vertical tail-horizontal tail configuration at $\beta \approx 0^{\circ}$; $M_{\infty} = 0.30$.

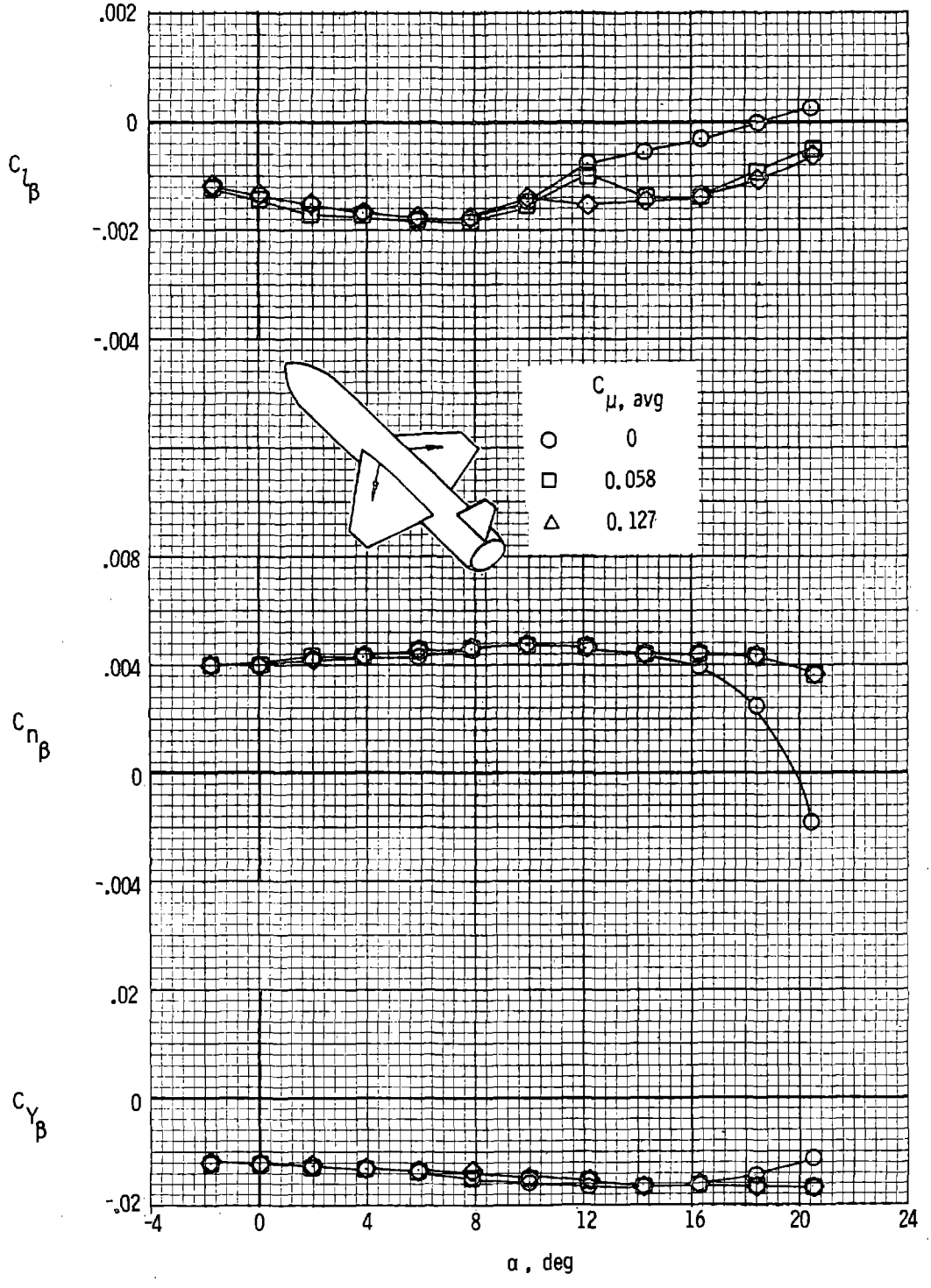

Figure 49.- Effect of spanwise blowing on the lateral-directional stability derivatives of the wing-vertical tail configuration; $M_\infty = 0.30$.

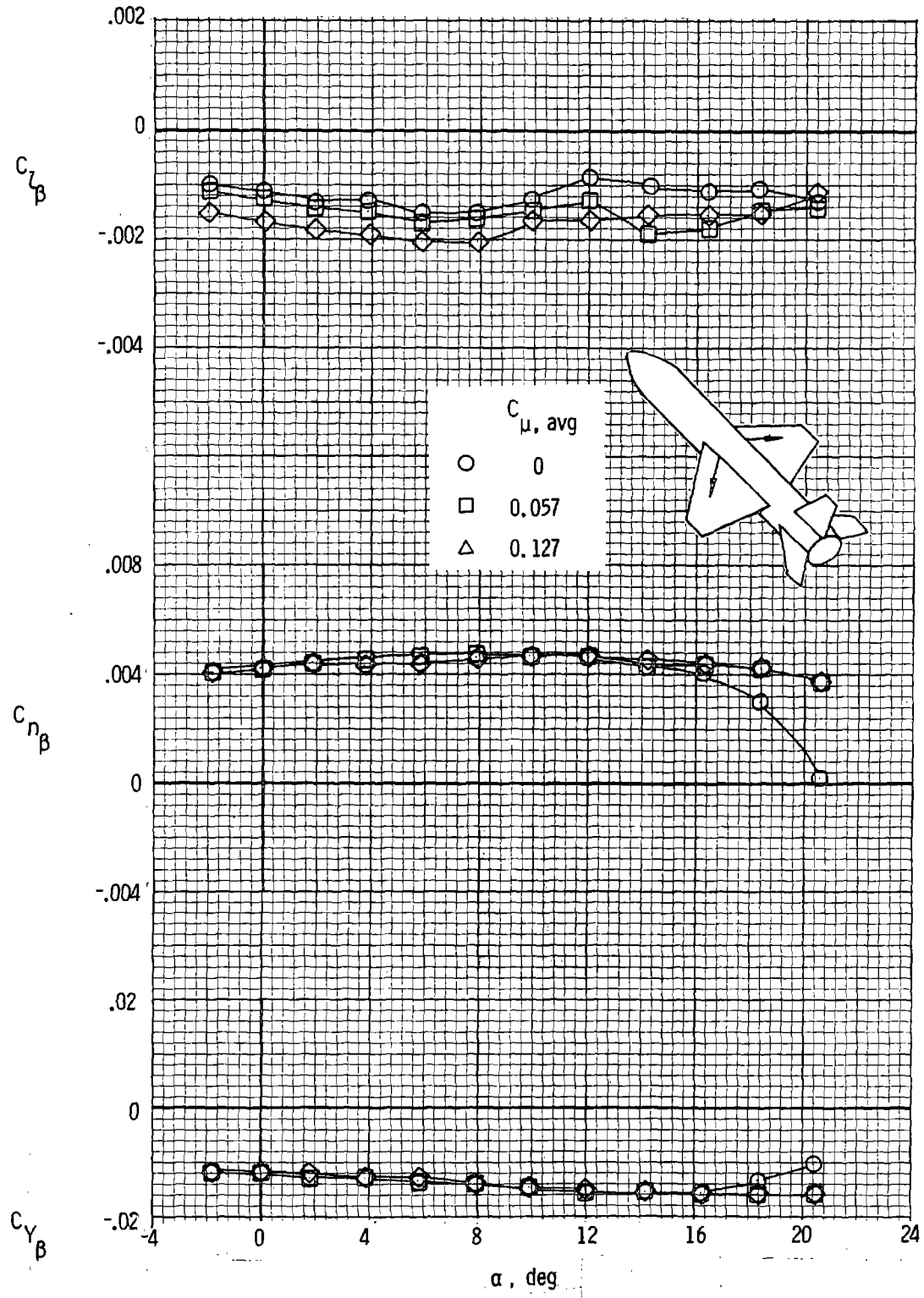

Figure 50.- Effect of spanwise blowing on the lateral-directional stability derivatives of the wing-vertical tail-horizontal tail configuration; $M_\infty = 0.30$.

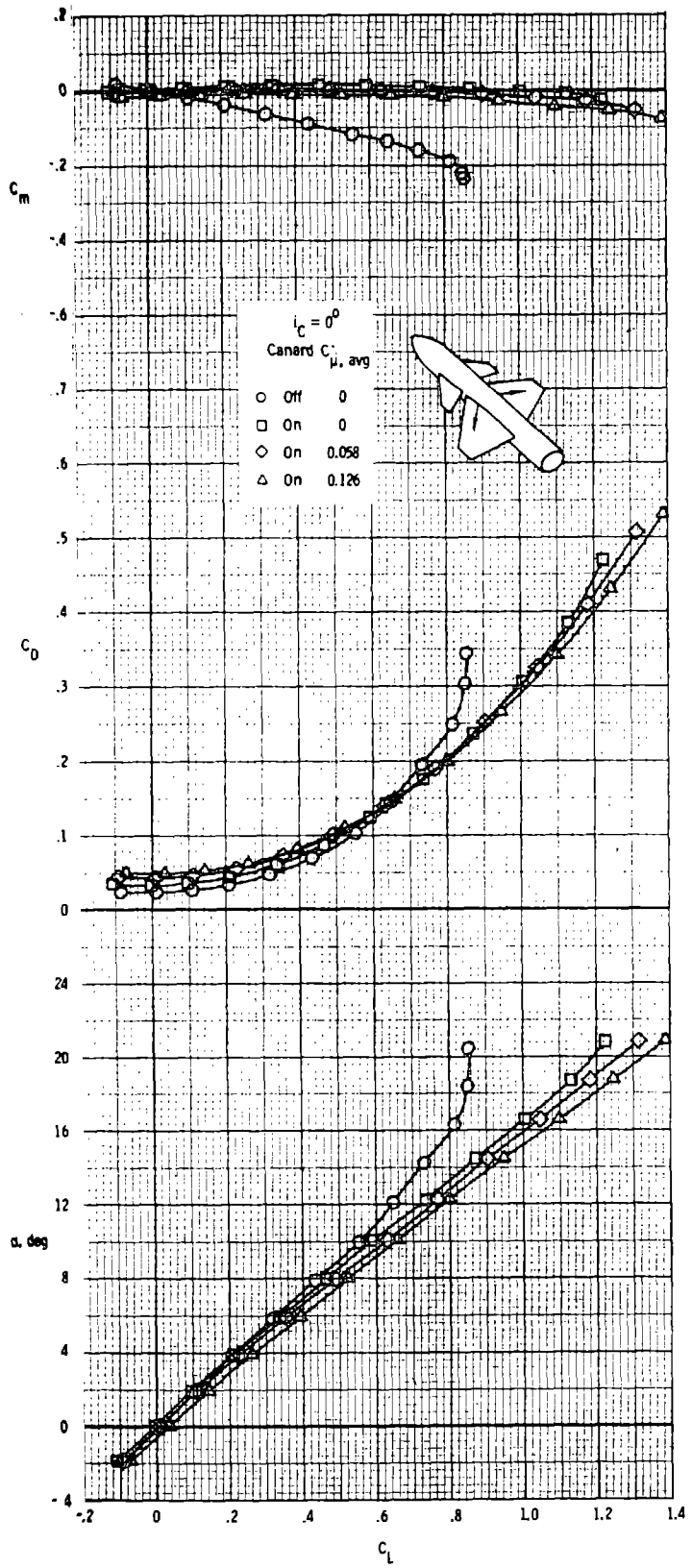

Figure 51.- Effect of spanwise blowing on the 44° swept trapezoidal wing on the longitudinal aerodynamic characteristics of the close-coupled canard-wing configuration for $i_c = 0^o$; $M_\infty = 0.30$.

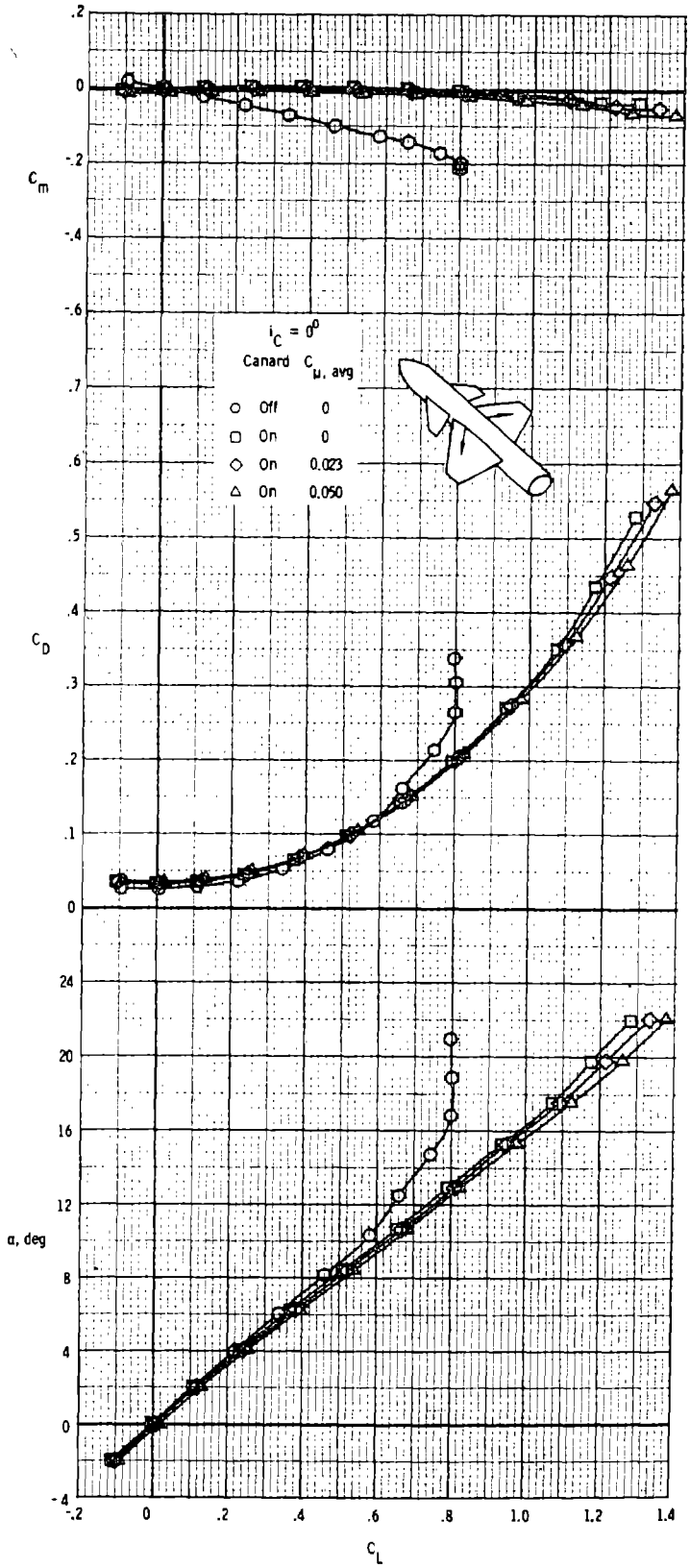

Figure 52.- Effect of spanwise blowing on the 44° swept trapezoidal wing on the longitudinal aerodynamic characteristics of the close-coupled canard-wing configuration for $i_C = 0^0$; $M_{\infty} \approx 0.50$.

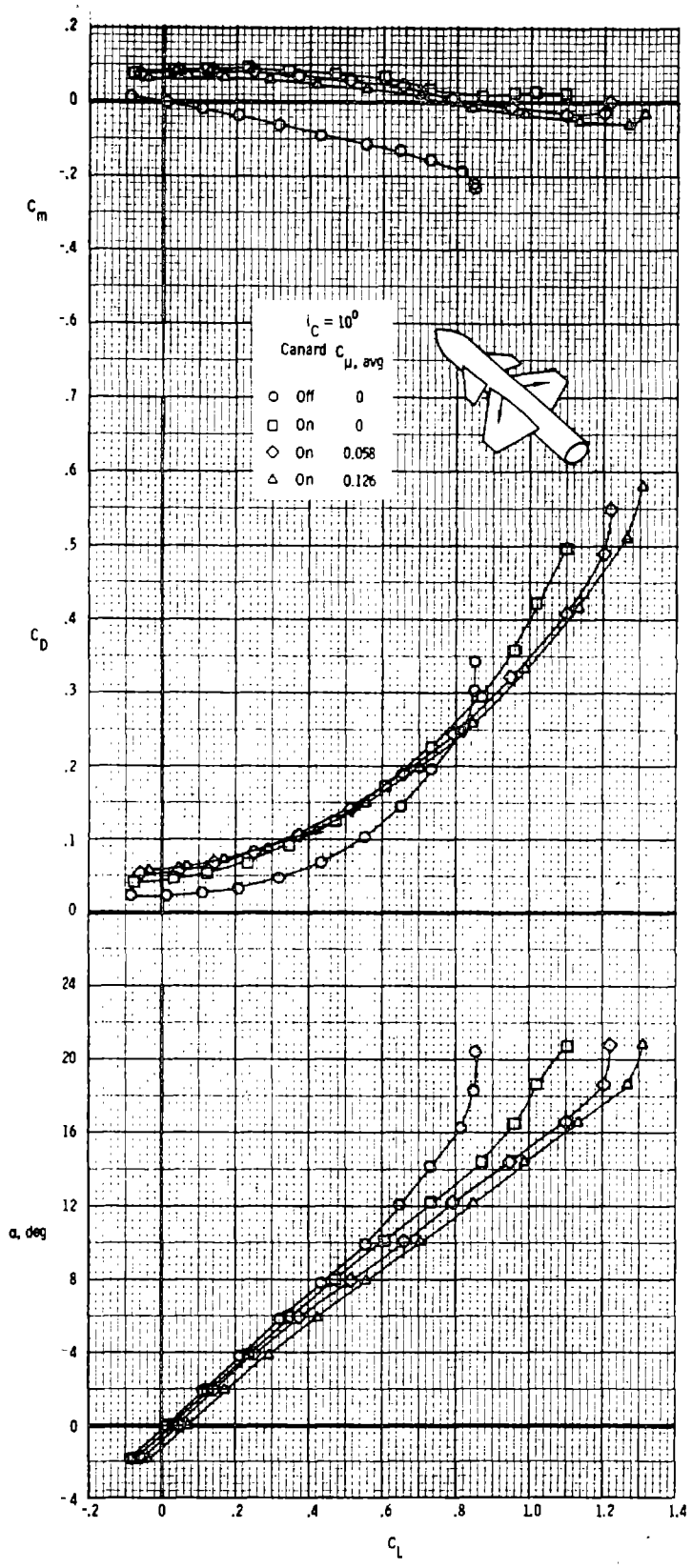

Figure 53.- Effect of spanwise blowing on the 44° swept trapezoidal wing on the longitudinal aerodynamic characteristics of the close-coupled canard–wing configuration for $i_C = 10^0$; $M_\infty = 0.30$.

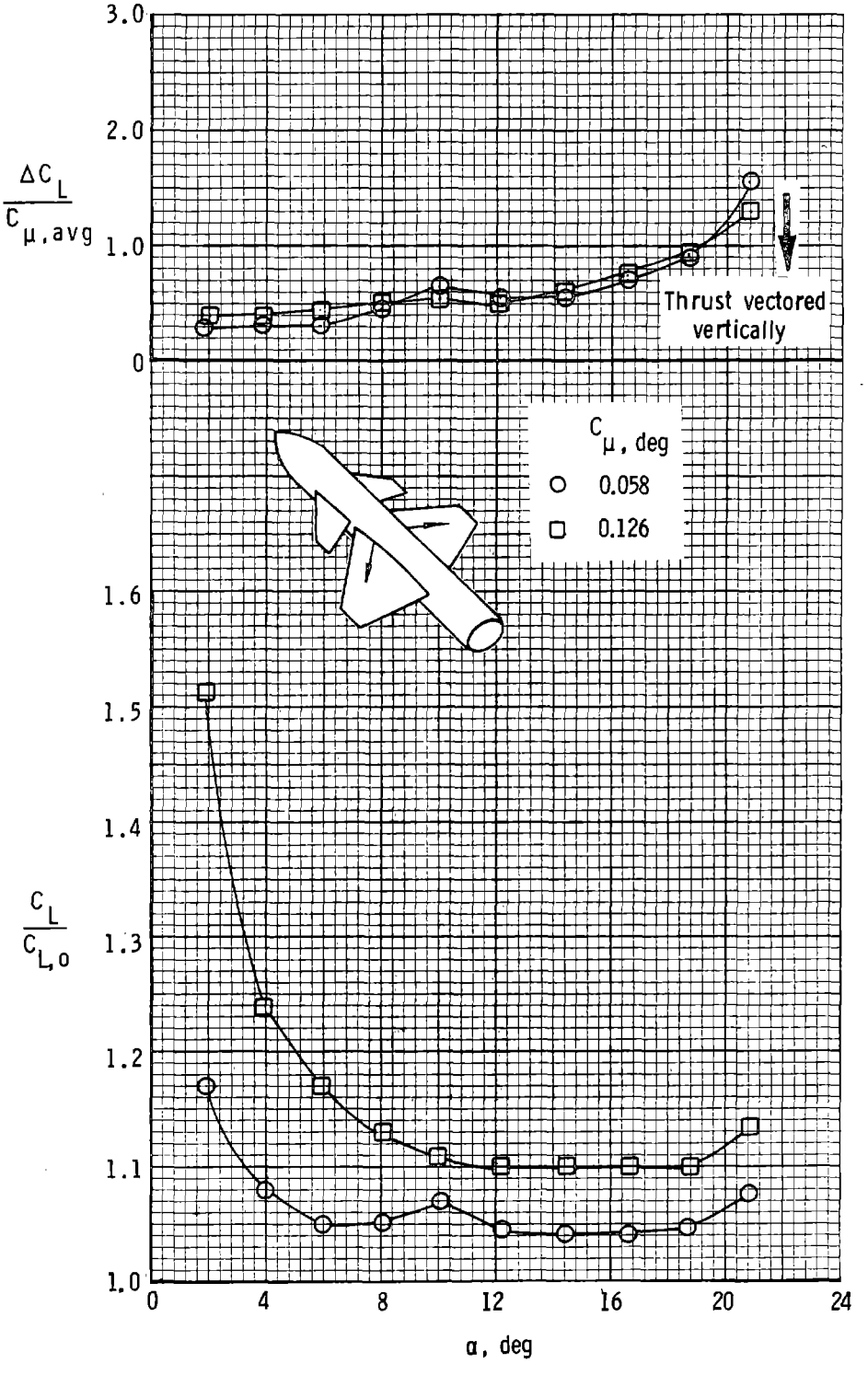

Figure 54. - Effect of α and $C_{\mu,avg}$ on the lift augmentation ratio and lift effectiveness of wing spanwise blowing for the canard-wing configuration; $i_C = 0^o$; $M_\infty = 0.30$.

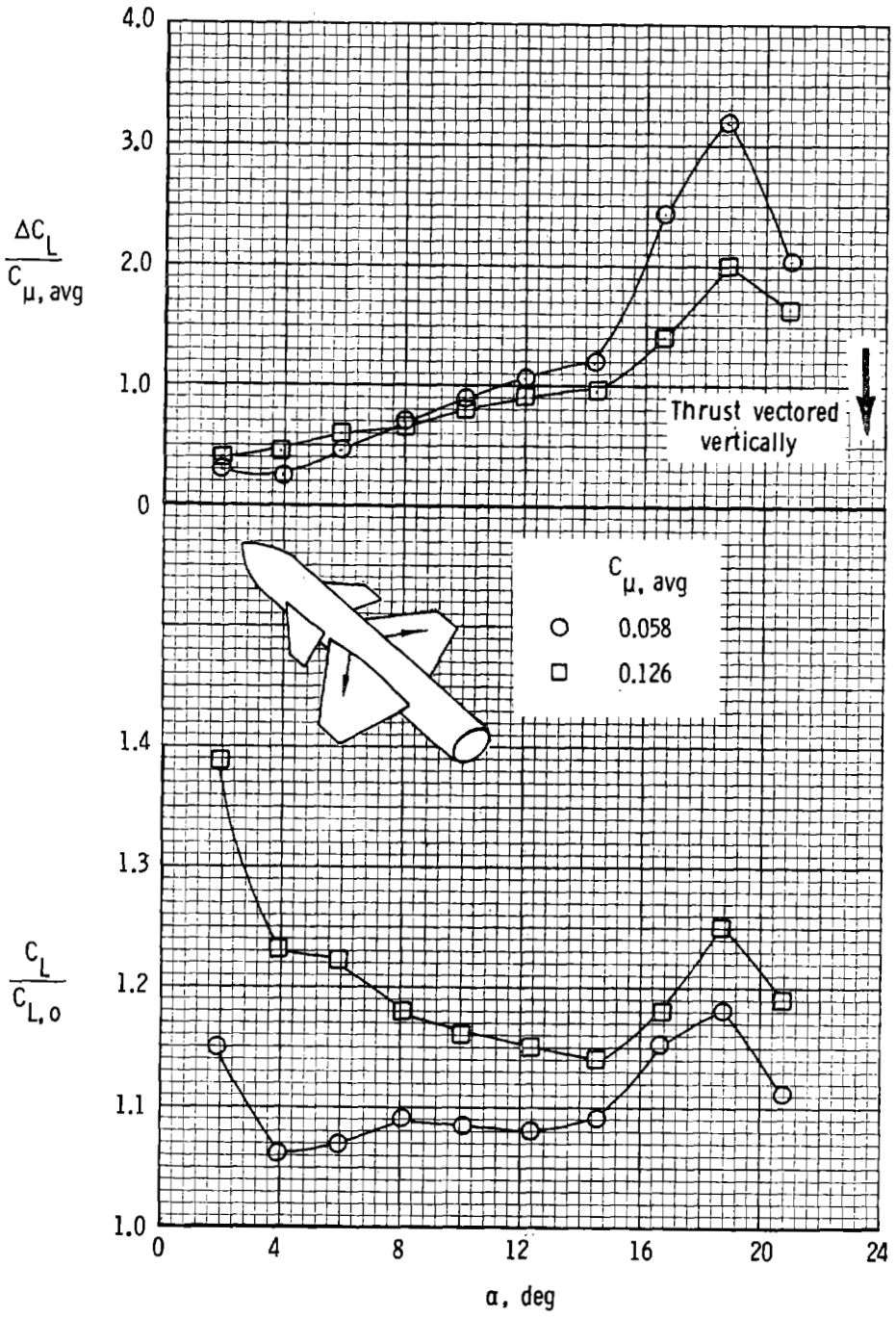

Figure 55.- Effect of α and $C_{\mu,avg}$ on the lift augmentation ratio and lift effectiveness of wing spanwise blowing for the canard–wing configuration; $i_c = 10^0$; $M_\infty = 0.30$.

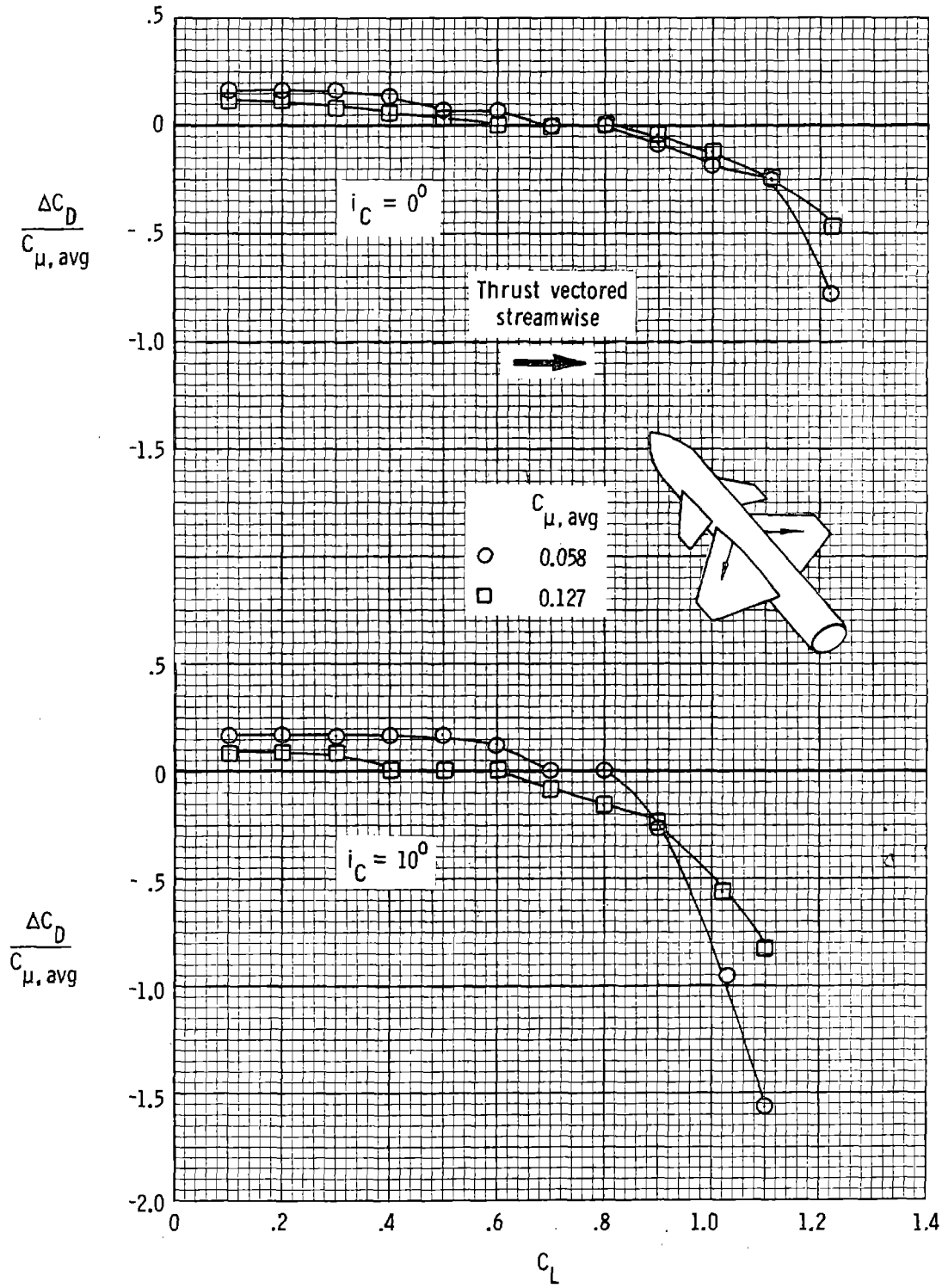

Figure 56.- Effect of C_L and $C_{\mu,avg}$ on the drag reduction ratio for the canard wing configuration for two canard incidence angles with spanwise blowing on the wing; $M_\infty = 0.30$.

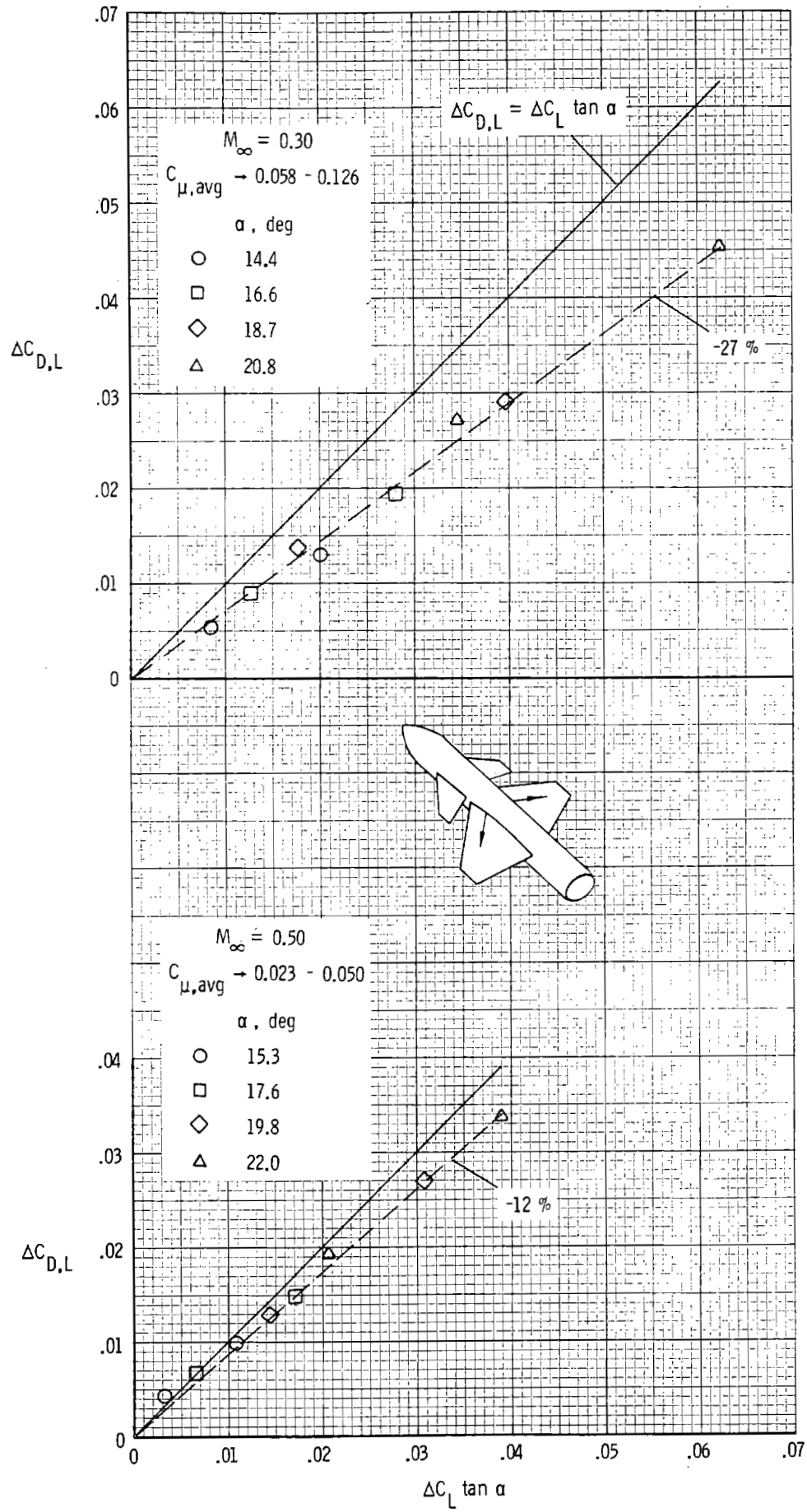

Figure 57.- Drag-due-to-lift increment due to spanwise blowing on the wing of the canard-wing configuration for $i_C = 0^o$.

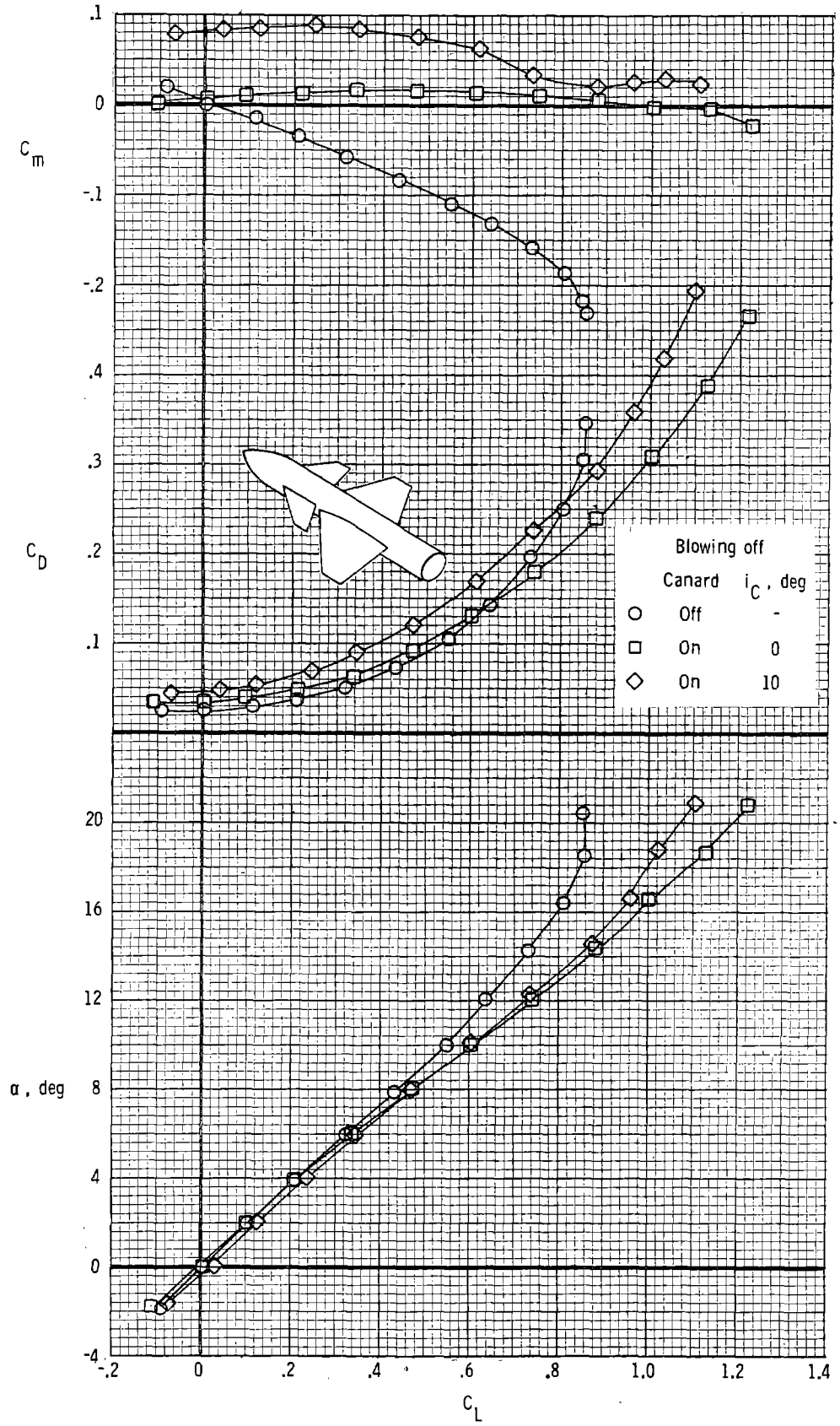

Figure 58.- Effect of canard incidence angle on the longitudinal aerodynamic characteristics of the canard-wing configuration with blowing off; $M_\infty = 0.30$.

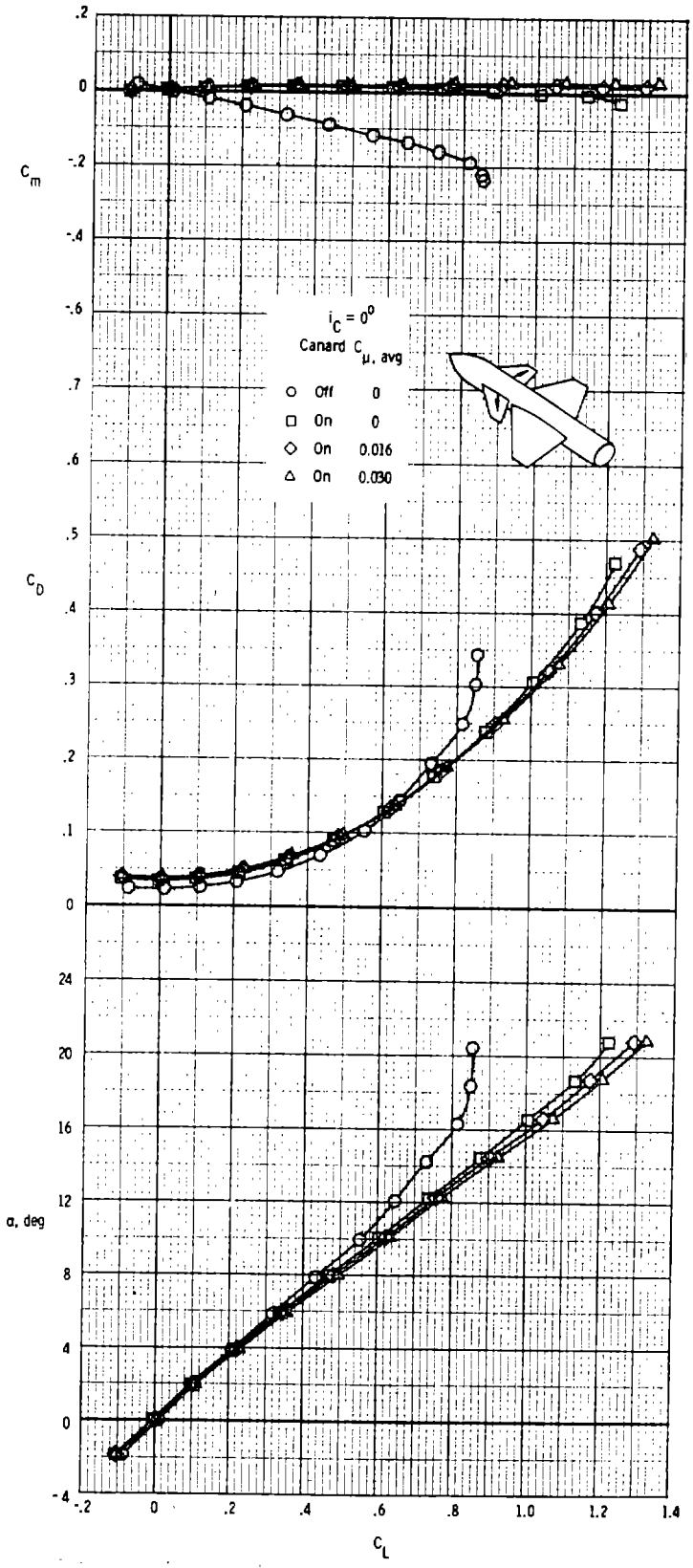

Figure 59.- Effect of spanwise blowing on the canard on the lonitudinal aerodynamic characteristics of the canard-wing configuration for $i_C = 0^0$; $M_\infty = 0.30$.

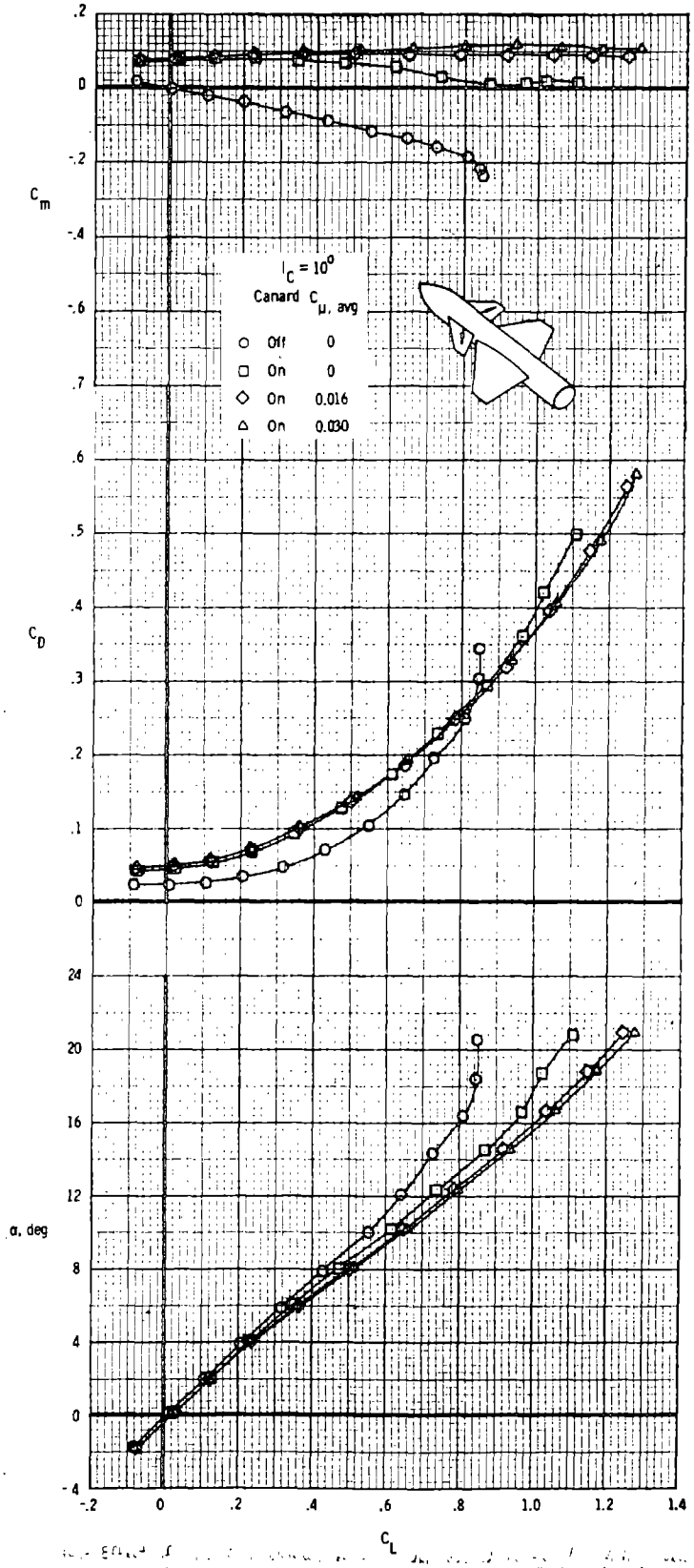

Figure 60. - Effect of spanwise blowing on the canard on the longitudinal aerodynamic characteristics of the close-coupled canard-wing configuration for $i_C = 10^0$; $M_\infty = 0.30$.

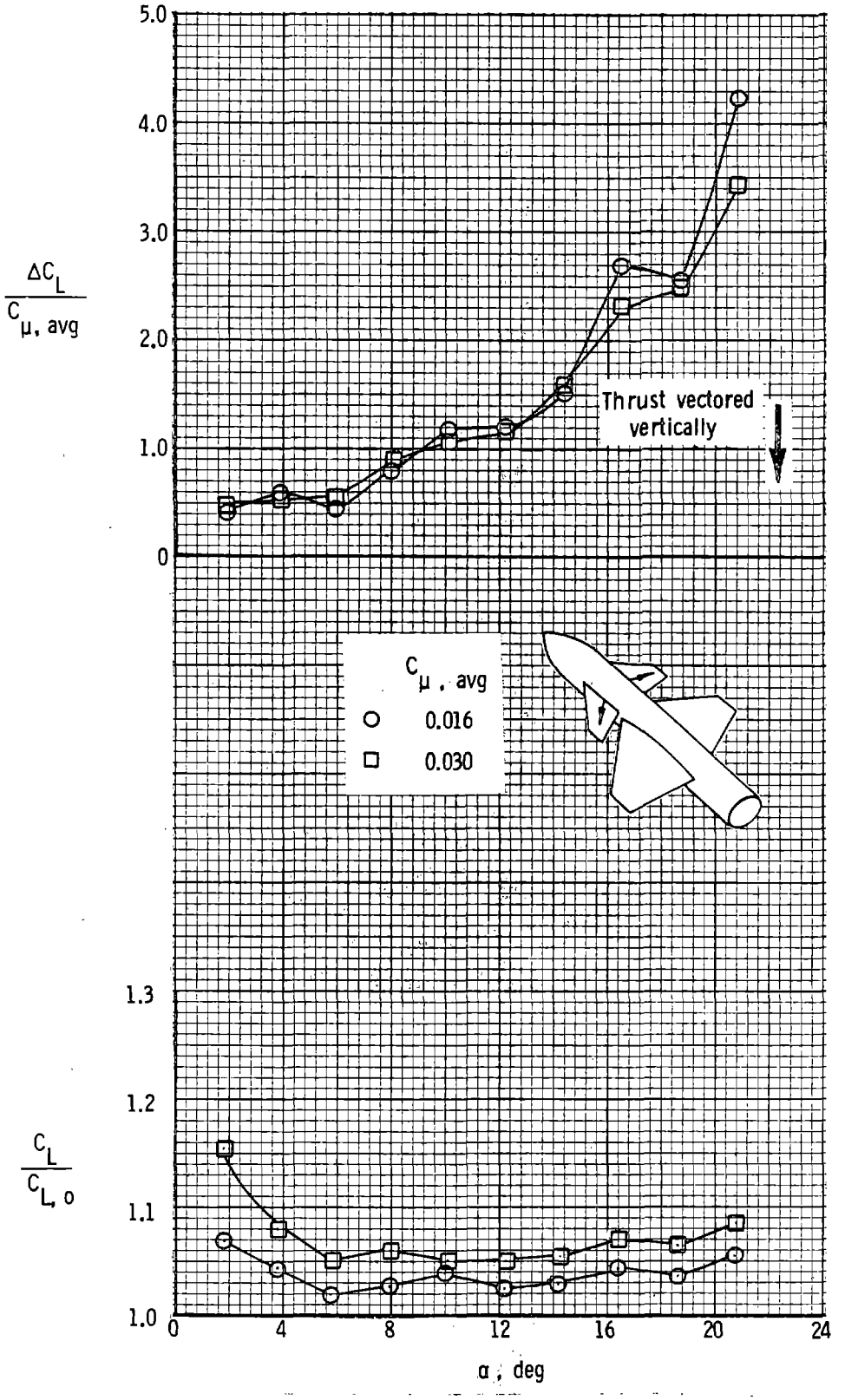

Figure 61.- Effect of α and $C_{\mu,avg}$ on the lift augmentation ratio and lift effectiveness of canard spanwise blowing for the canard-wing configuration; $i_c = 0^o$; $M_\infty = 0.30$.

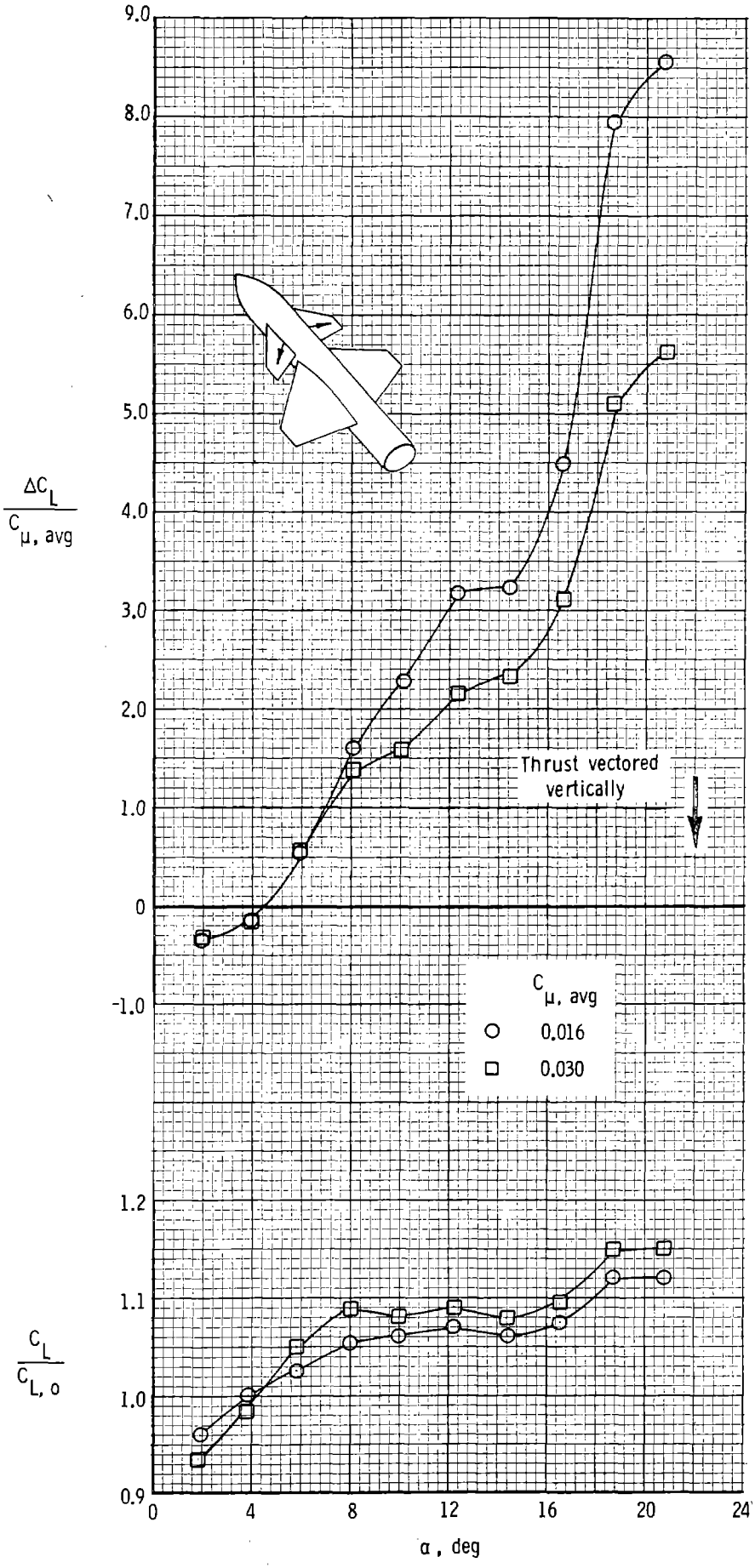

Figure 62.- Effect of α and $C_{\mu,avg}$ on the lift augmentation ratio and lift effectiveness of canard spanwise blowing for the canard-wing configuration; $i_C = 10^0$; $M_\infty = 0.30$.

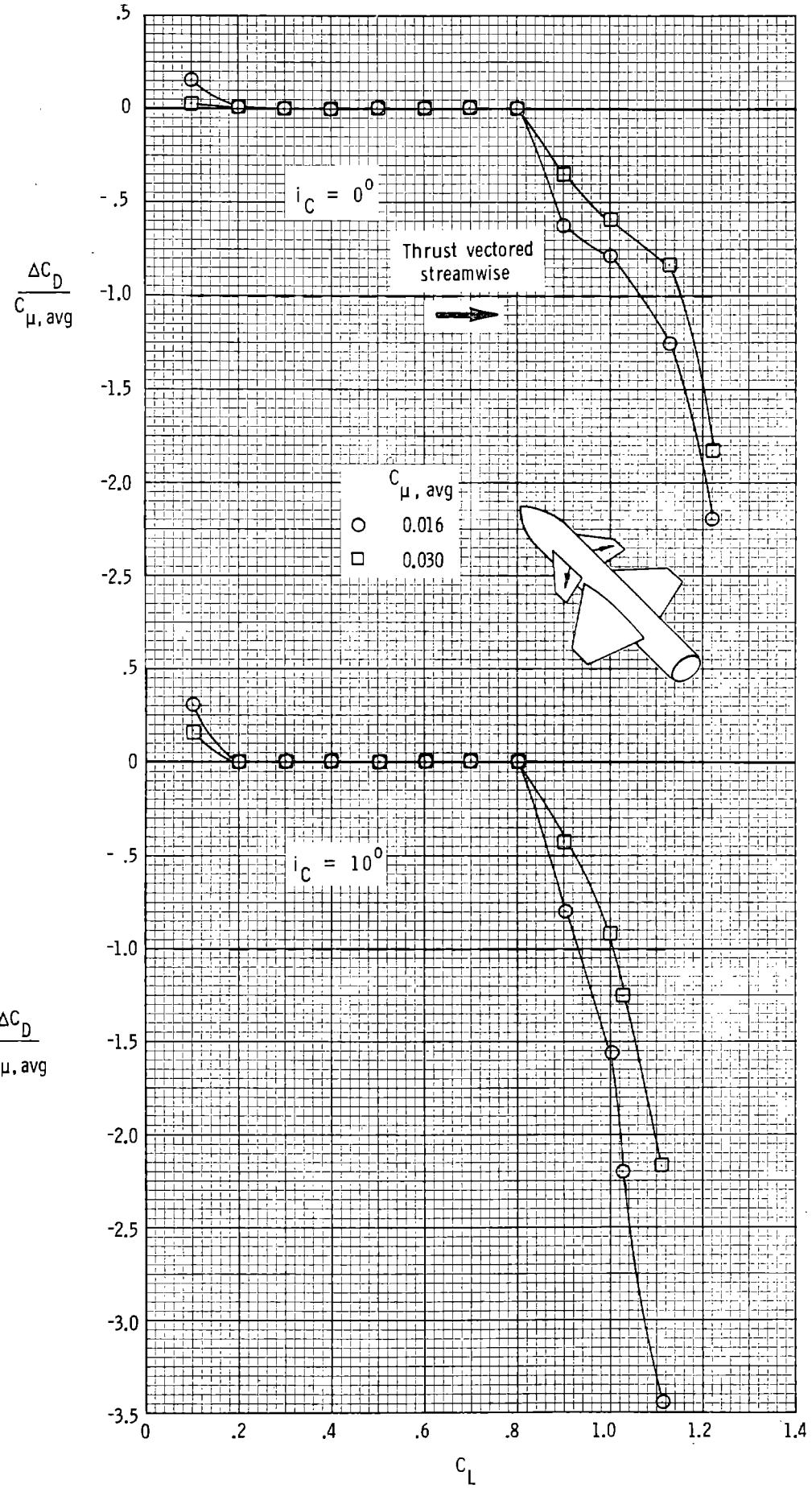

Figure 63.- Effect of C_L and $C_{\mu,avg}$ on the drag reduction ratio for the canard-wing configuration for two canard incidence angles with spanwise blowing on the canard; $M_\infty = 0.30$.

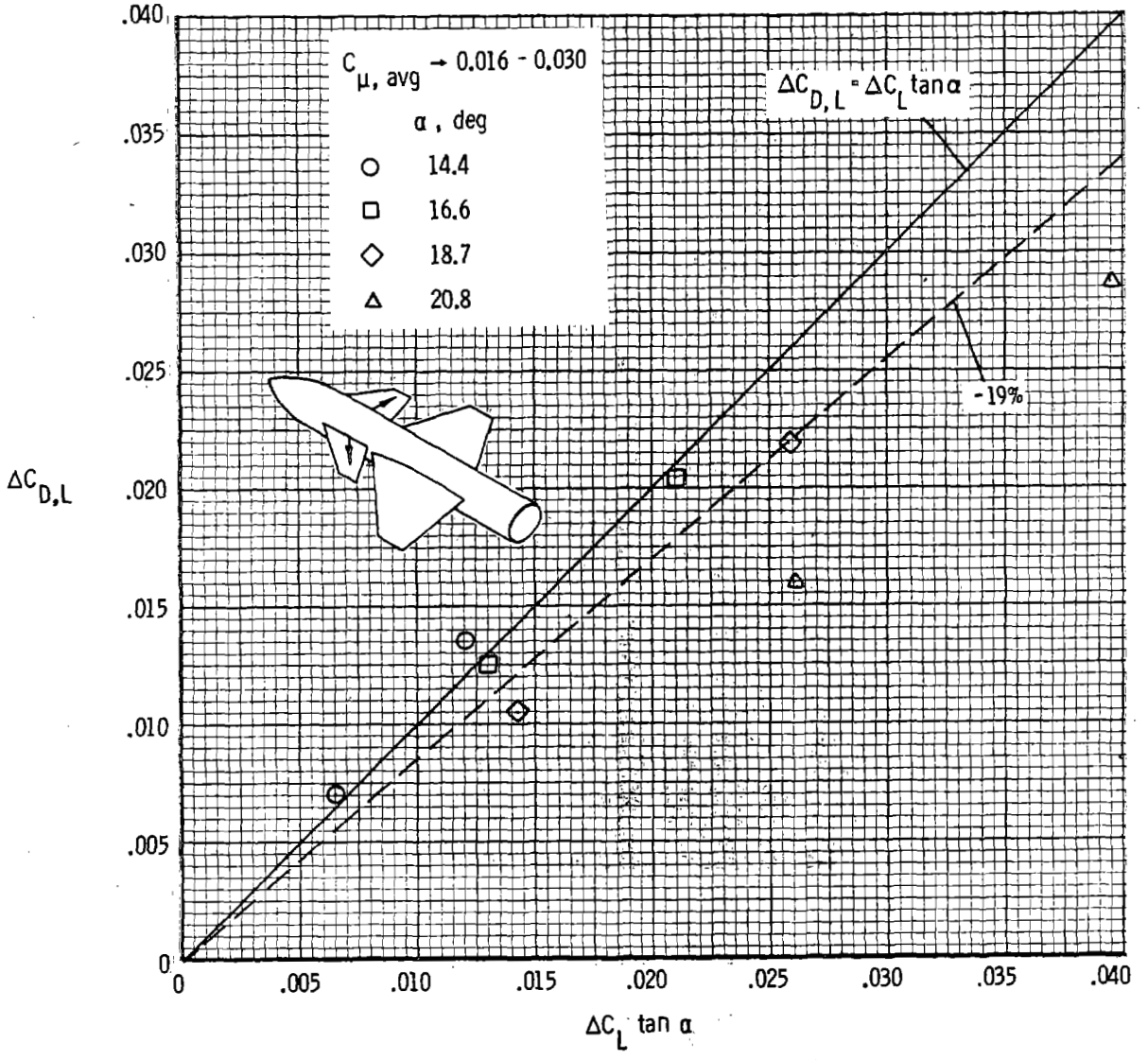

Figure 64.- Drag-due-to-lift increment due to canard spanwise blowing for the canard-wing configuration; $i_C = 0^0$; $M_\infty = 0.30$.

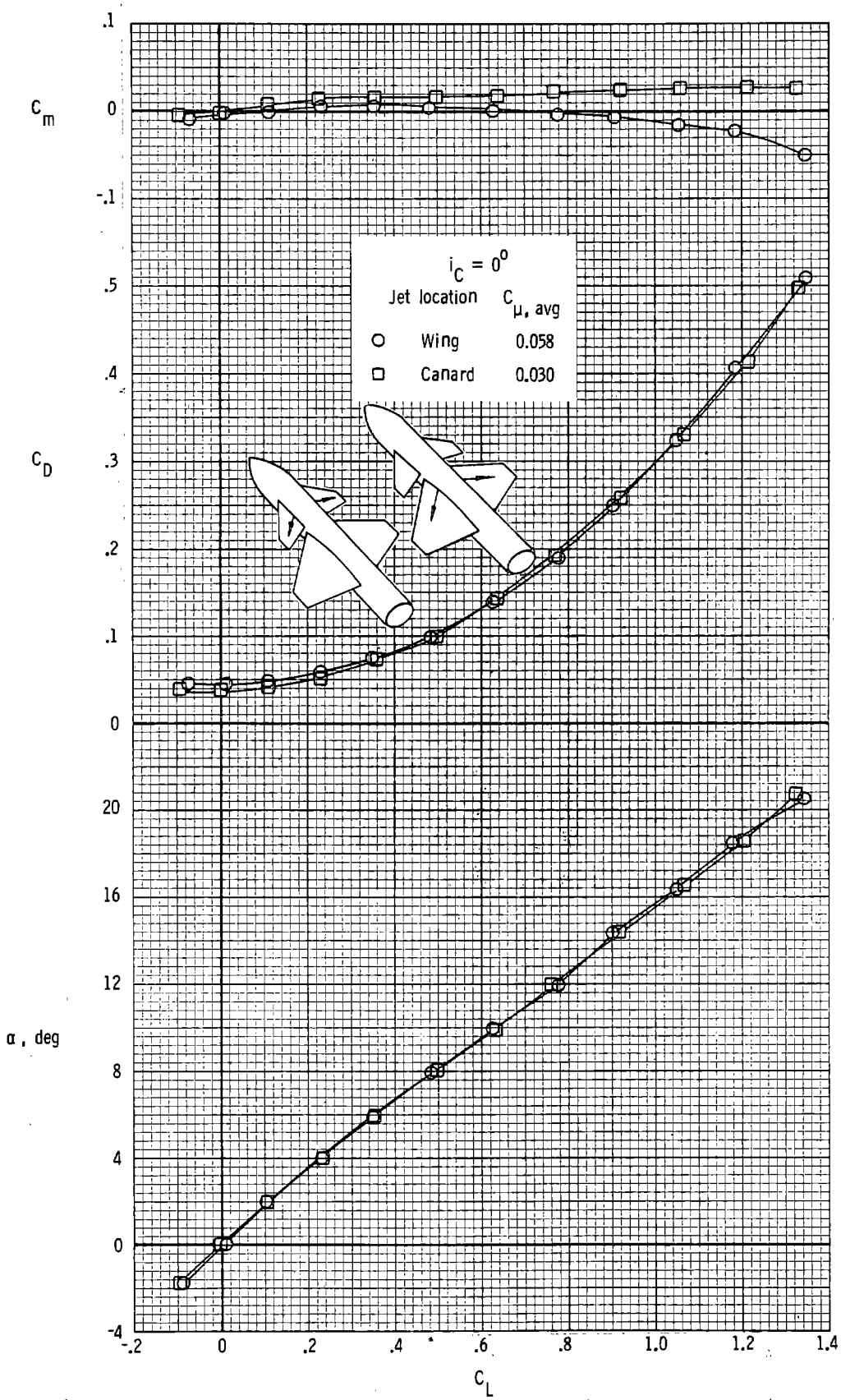

Figure 65.- Comparison of the longitudinal aerodynamic characteristics of the close-coupled canard-wing configuration for spanwise blowing on the wing in the presence of the canard and spanwise blowing on the canard in the presence of the wing; $i_C = 0^0$; $M_\infty = 0.30$.

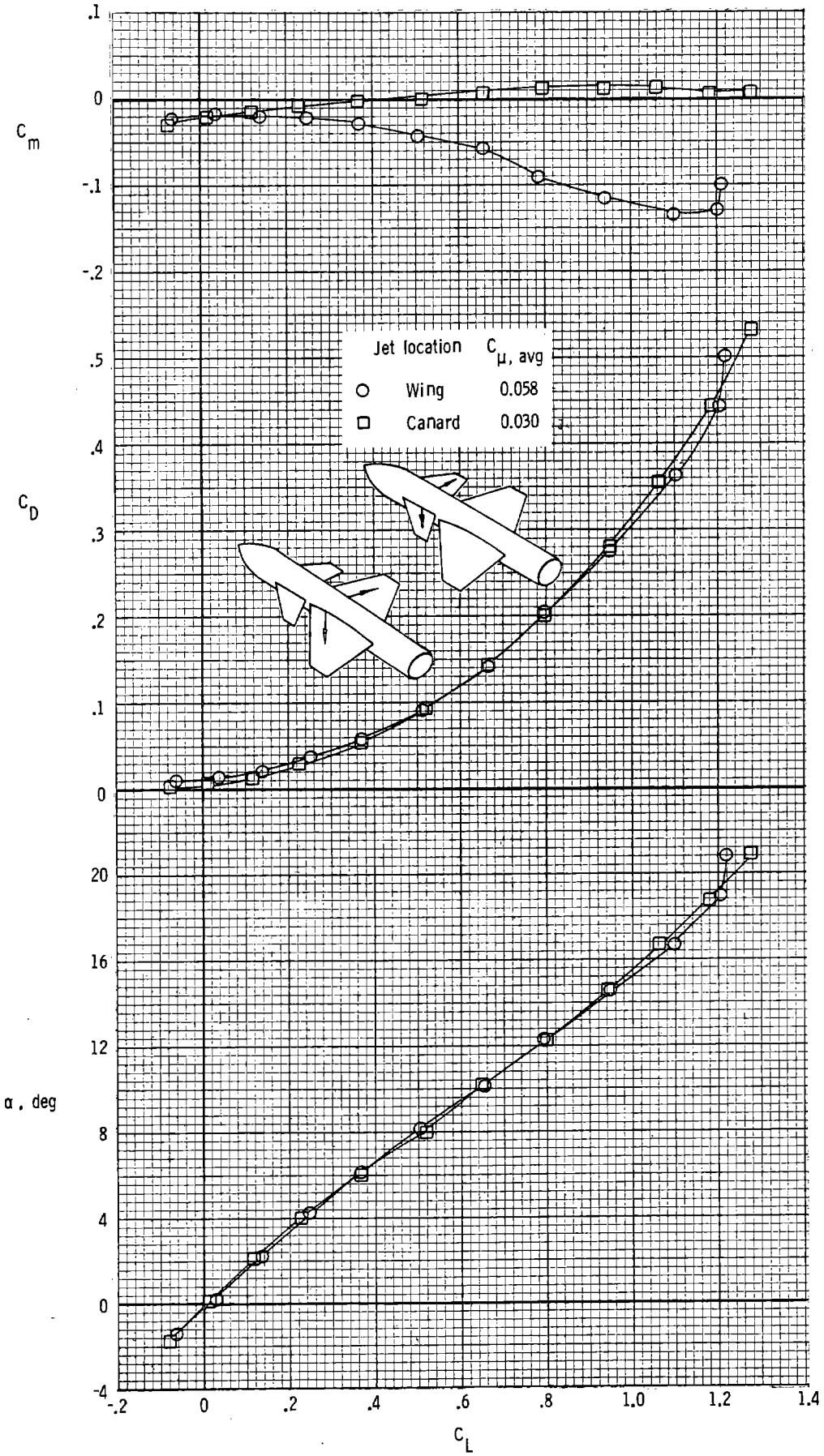

Figure 66 - Comparison of the longitudinal aerodynamic characteristics of the close-coupled canard-wing configuration for spanwise blowing on the wing in the presence of the canard and spanwise blowing on the canard in the presence of the wing; $i_c = 10^0$; $M_\infty = 0.30$.

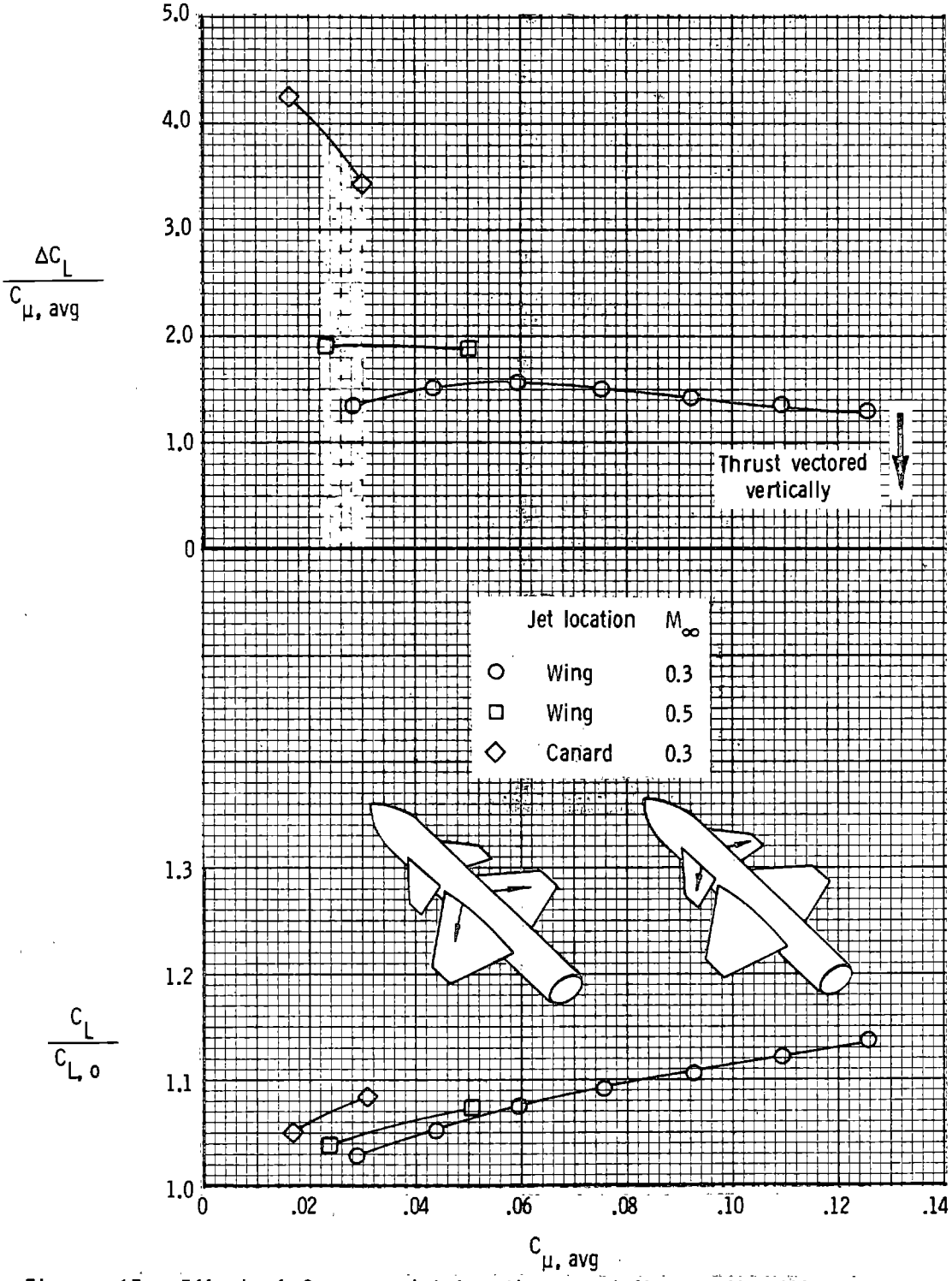

Figure 67.- Effect of $C_{\mu,avg}$, jet location, and M_∞ on the lift augmentation ratio and lift effectiveness of blowing for the canard-wing configuration; $i_c = 0^0$; $\alpha \approx 21^0$.

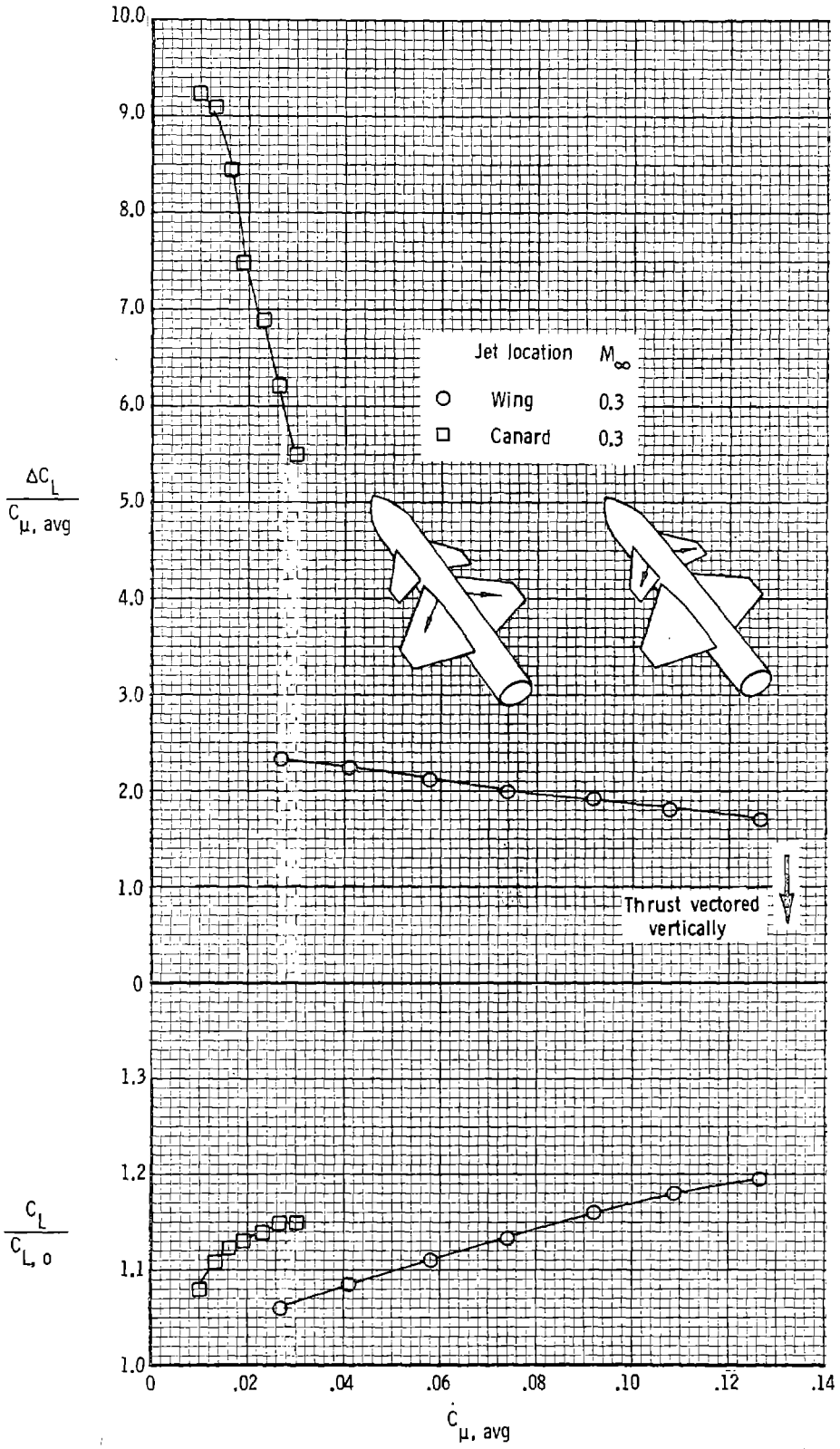

Figure 68.- Effect of $C_{\mu,avg}$ and jet location on the lift augmentation ratio and lift effectiveness of blowing for the canard–wing configuration; $i_C = 10^o$; $\alpha \approx 21^o$.

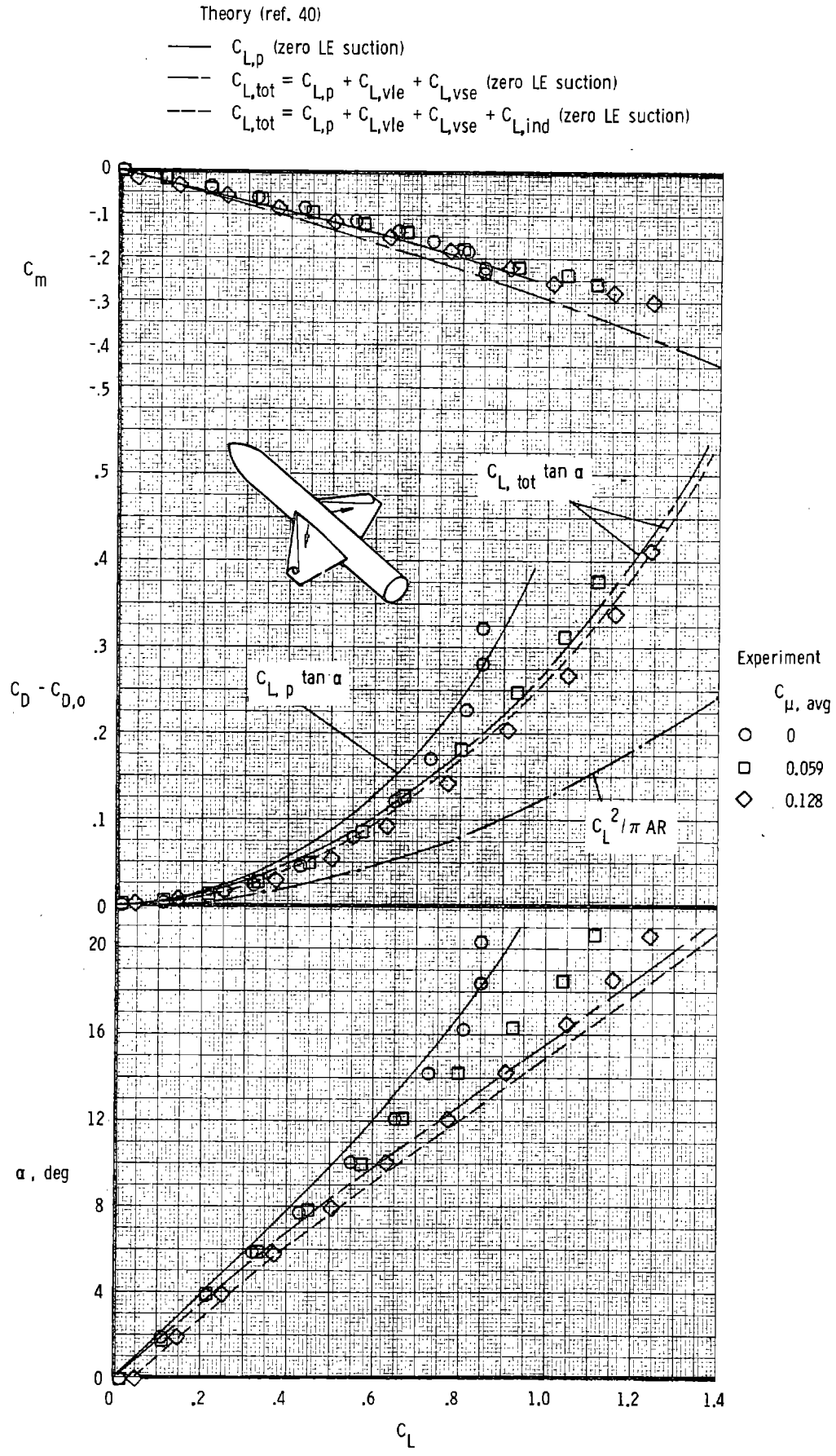

Figure 69.- Comparison of the theoretical and experimental longitudinal aerodynamic characteristics for the 44° swept trapezoidal wing configuration with $\delta_{LE} = \delta_{TE} = 0°$; $M_\infty = 0.30$. (Experimental data from fig. 15)

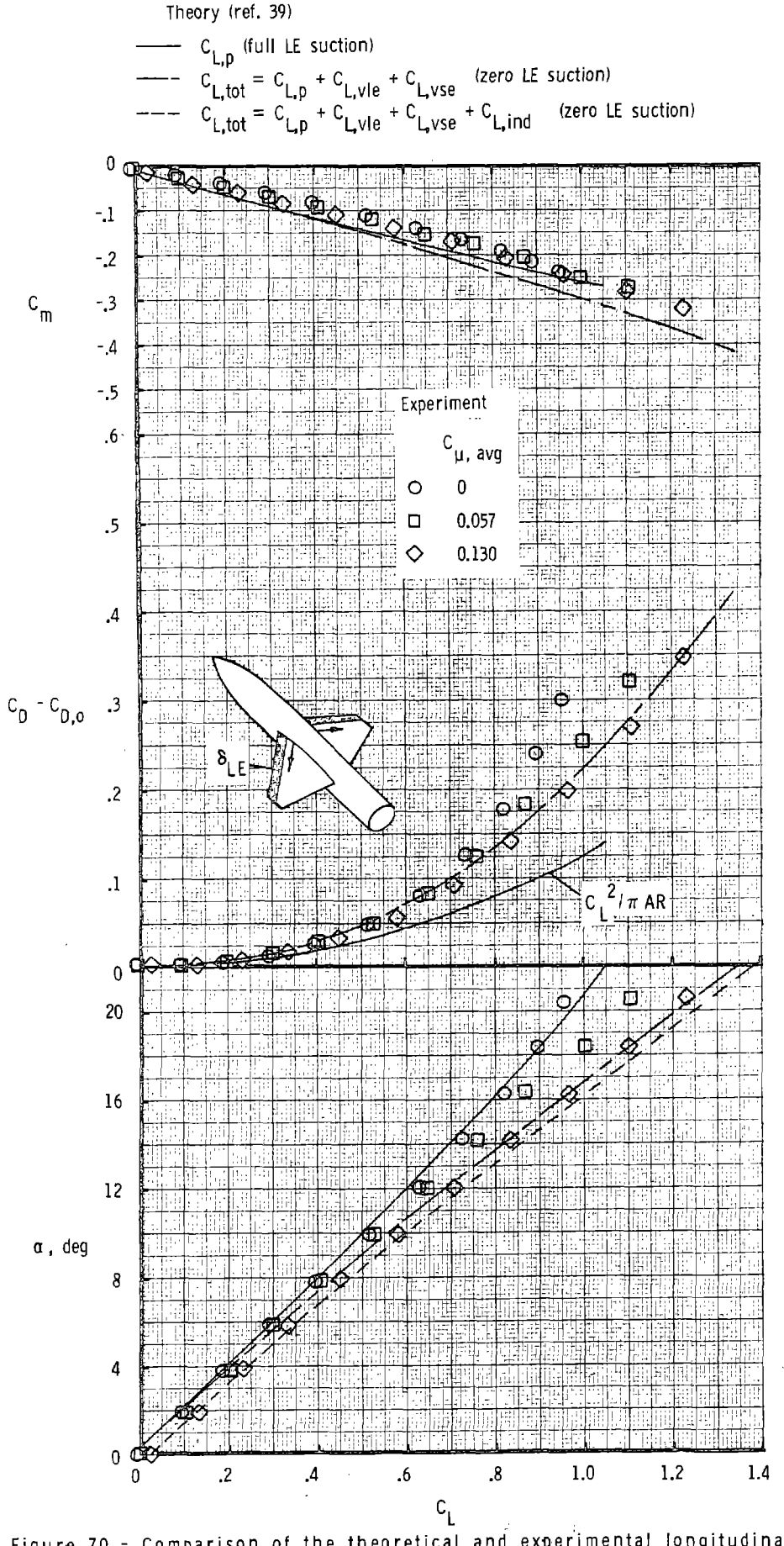

Figure 70.- Comparison of the theoretical and experimental longitudinal aerodynamic characteristics for the 44° swept trapezoidal wing with the leading-edge flap deflected to 8°; $\delta_{TE} = 0°$;

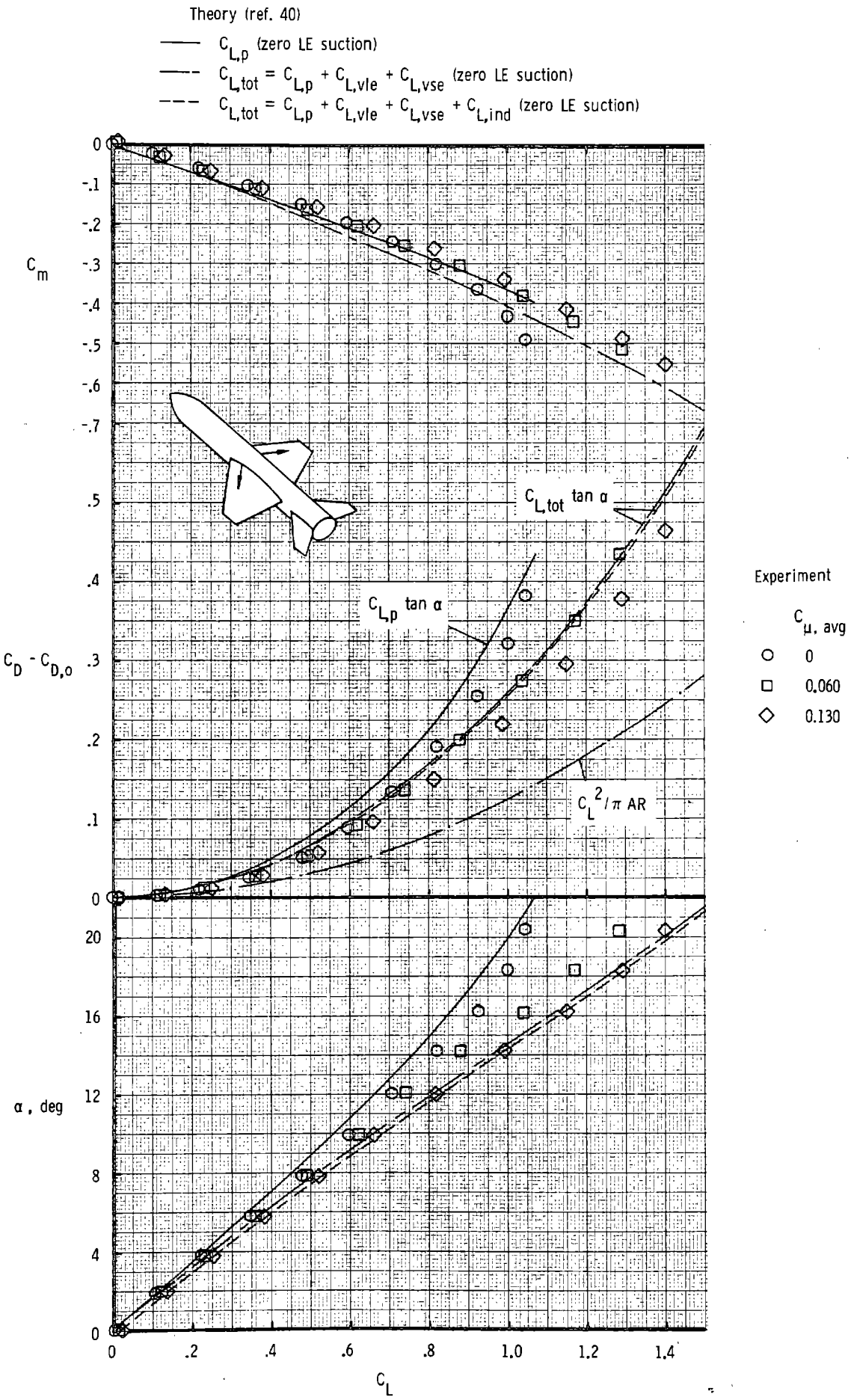

Figure 71.- Comparison of the theoretical and experimental longitudinal characteristics for the wing-horizontal-tail configuration; $M_\infty = 0.30$. (Experimental data from fig. 44)

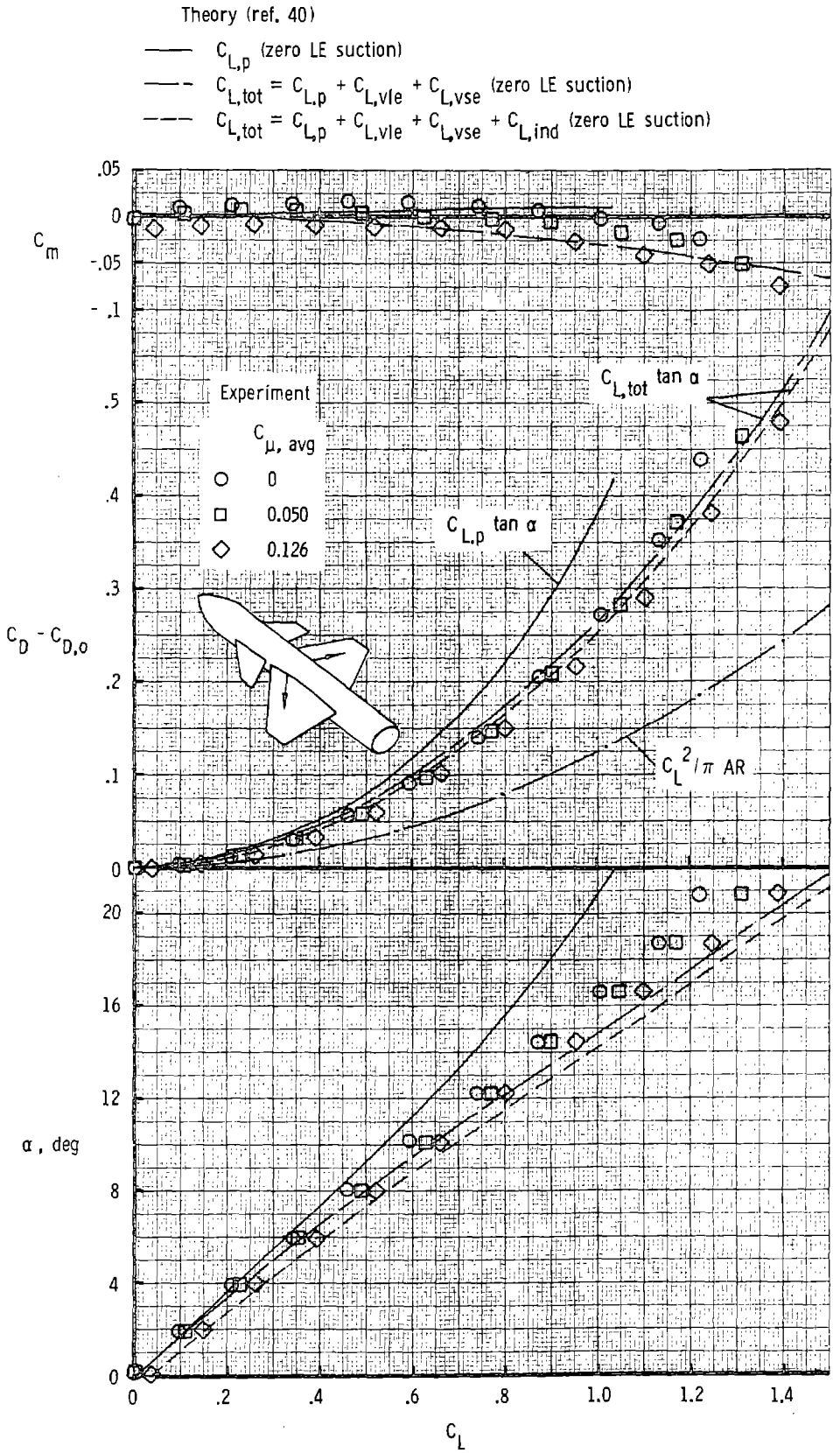

Figure 72.- Comparison of the theoretical and experimental longitudinal aerodynamic characteristics for the canard-wing configuration with blowing on the wings; $i_c = 0^0$; $M_\infty = 0.30$. (Experimental data from fig. 51)

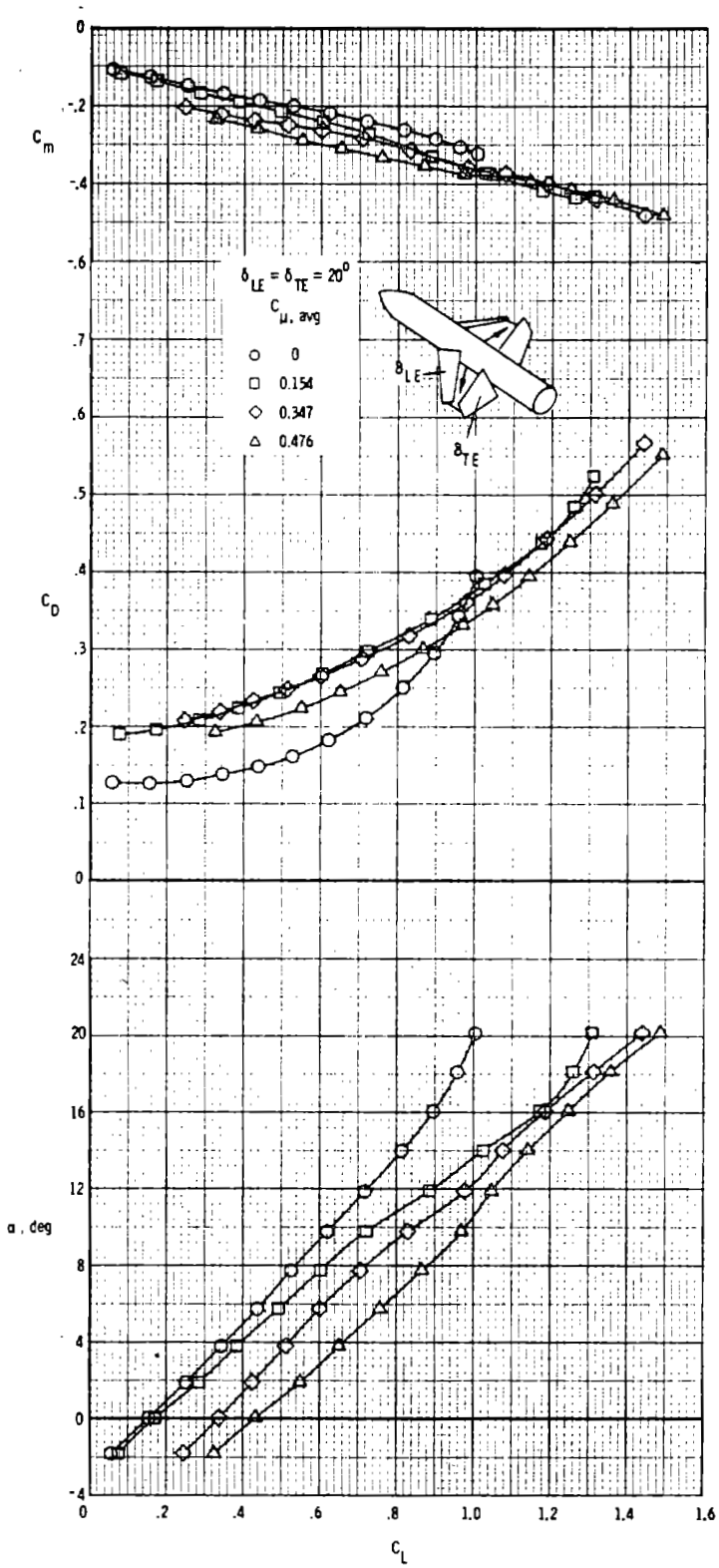

Figure 73.- Effect of spanwise blowing on the longitudinal aerodynamic aerodynamic characteristics of the "locked vortex" wing configuration with $\delta_{LE} = \delta_{TE} = 20^0$; $M_\infty = 0.15$.

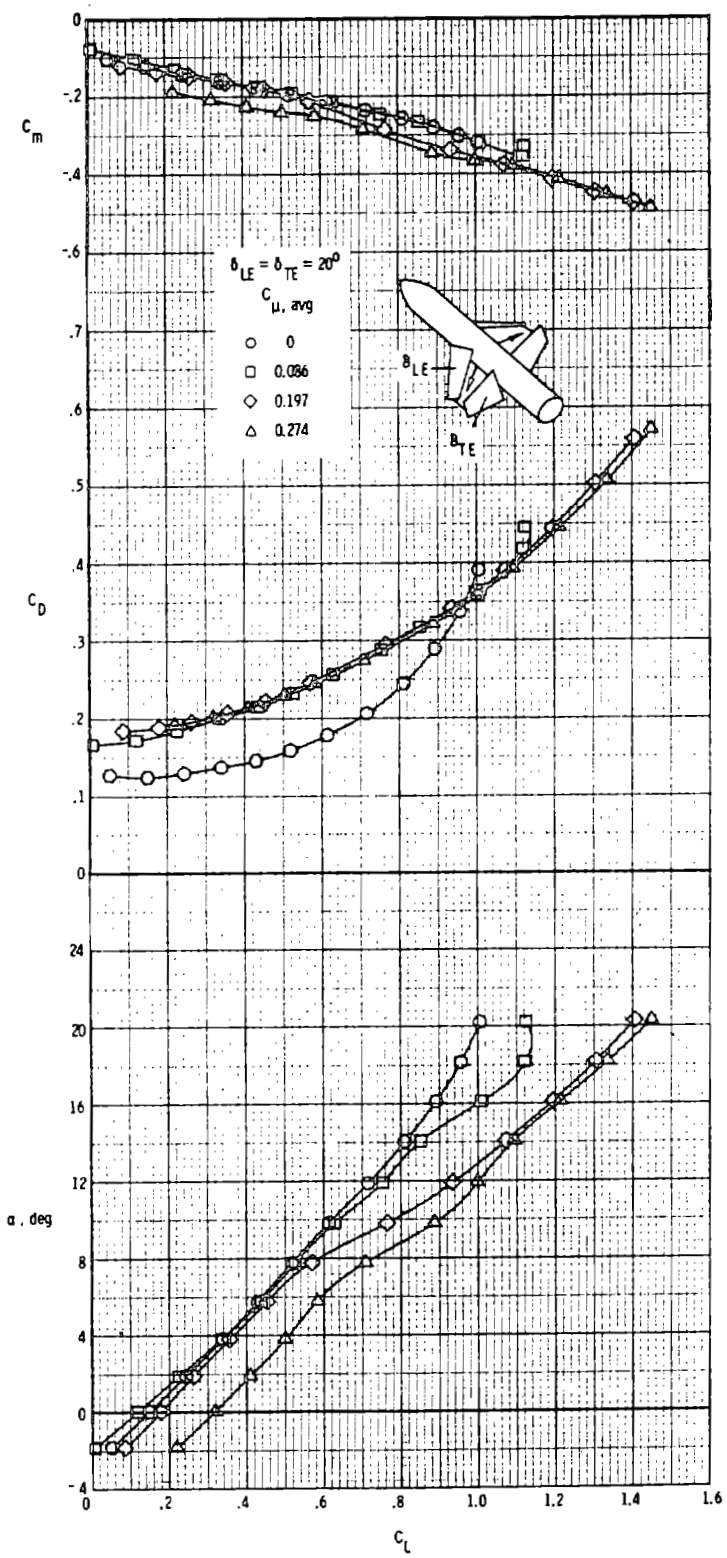

Figure 74.- Effect of spanwise blowing on the longitudinal aerodynamic characteristics of the "locked vortex" wing configuration with $\delta_{LE} = \delta_{TE} = 20^0$; M_∞ 0.20.

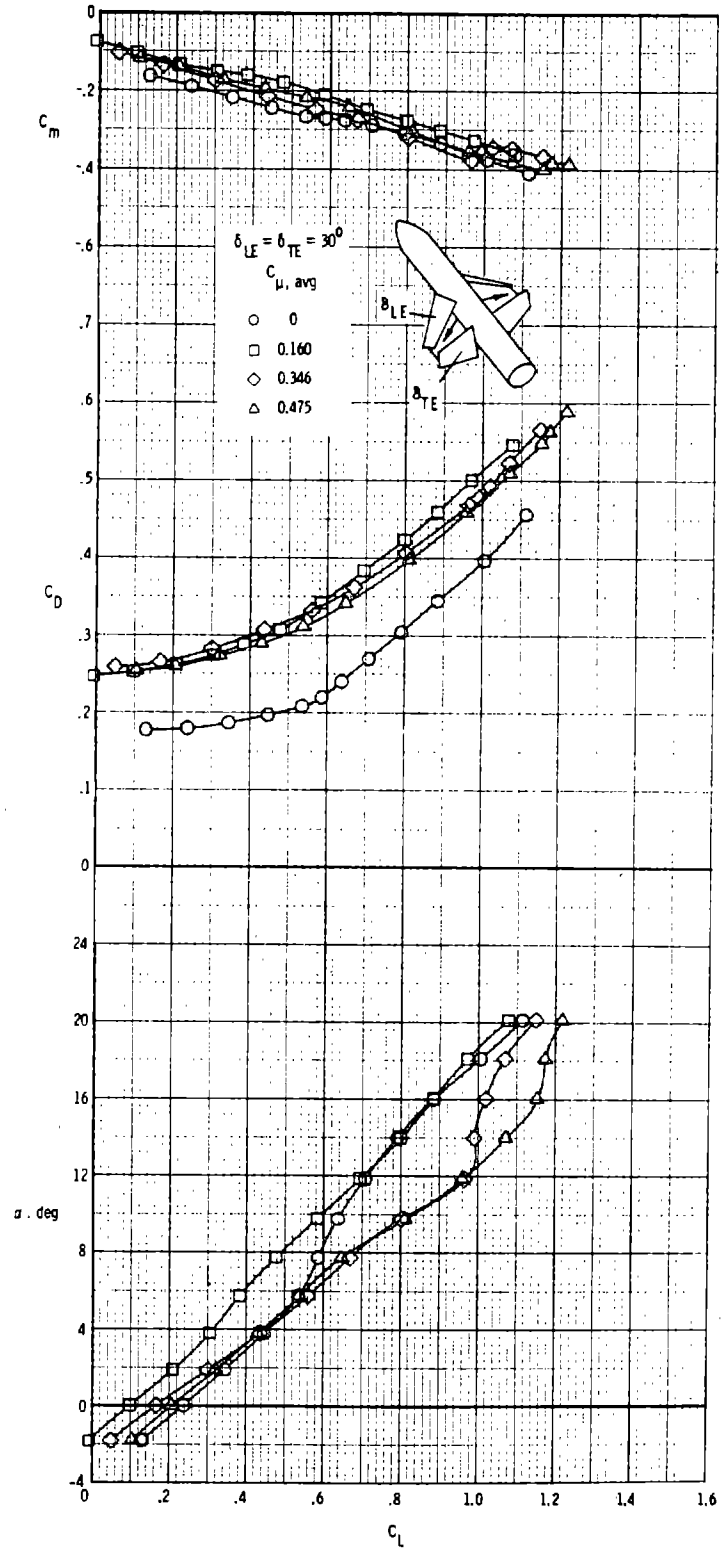

Figure 75.- Effect of spanwise blowing on the longitudinal aerodynamic characteristics of the "locked vortex" wing configuration with $\delta_{LE} = \delta_{TE} = 30^0$; $M_{\infty} = 0.15$.

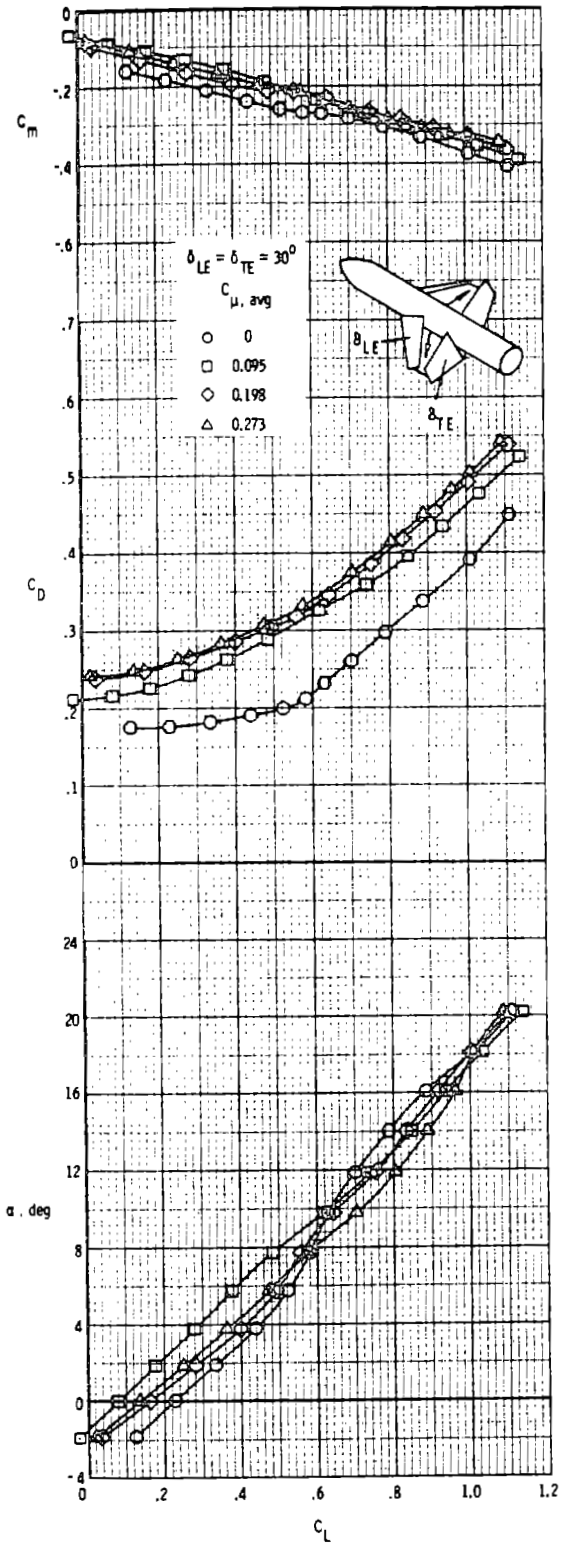

Figure 76.- Effect of spanwise blowing on the longitudinal aerodynamic characteristics of the "locked vortex" wing configuration with $\delta_{LE} = \delta_{TE} = 30^0$; $M_\infty = 0.20$.

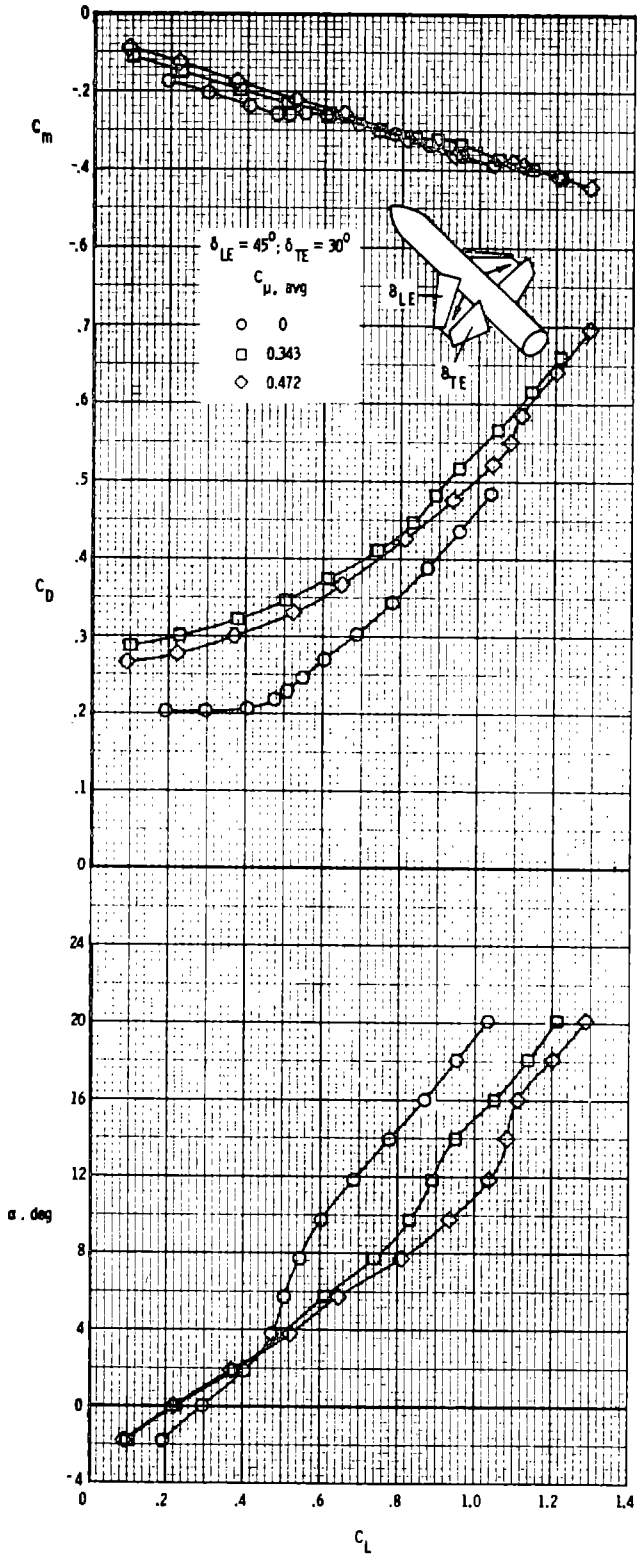

Figure 77.- Effect of spanwise blowing on the longitudinal aerodynamic characteristics of the "locked vortex" wing configuration with $\delta_{LE} = 45^0, \delta_{TE} = 30^0$; $M_\infty = 0.15$.

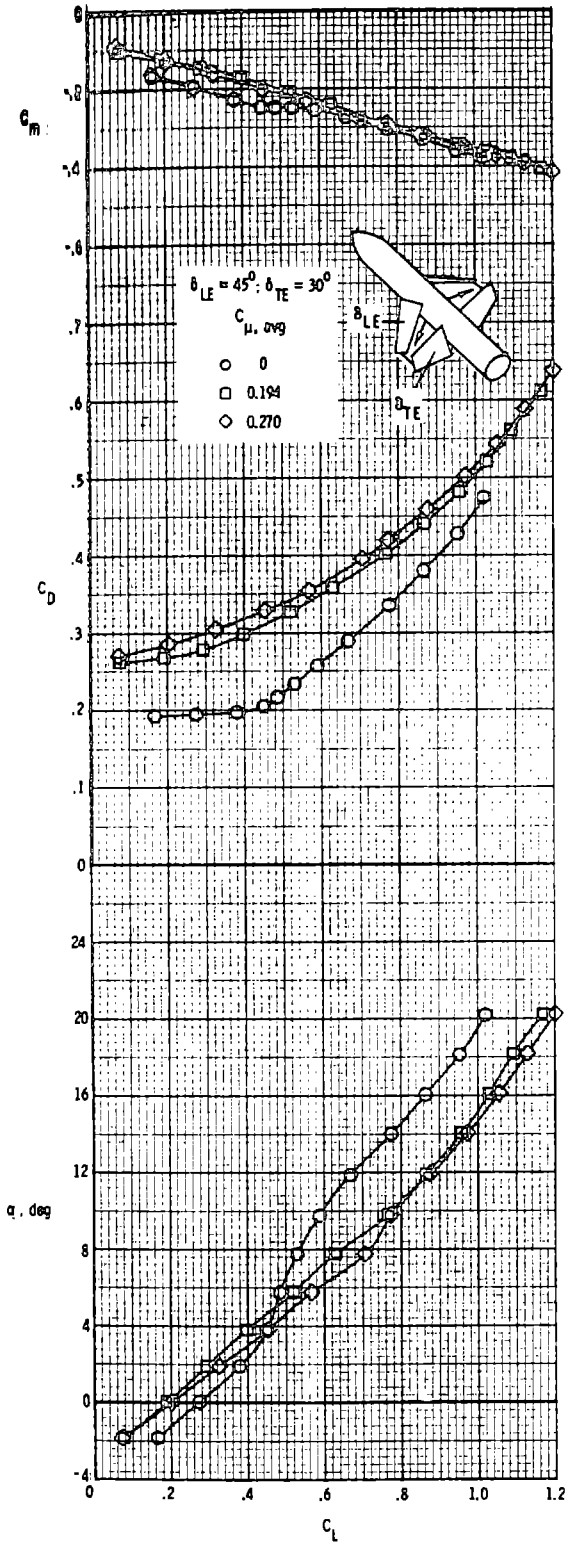

Figure 78.- Effect of spanwise blowing on the longitudinal aerodynamic characteristics of the "locked vortex" wing configuration with $\delta_{LE} = 45^0$, $\delta_{TE} = 30^0$; $M_\infty = 0.20$.

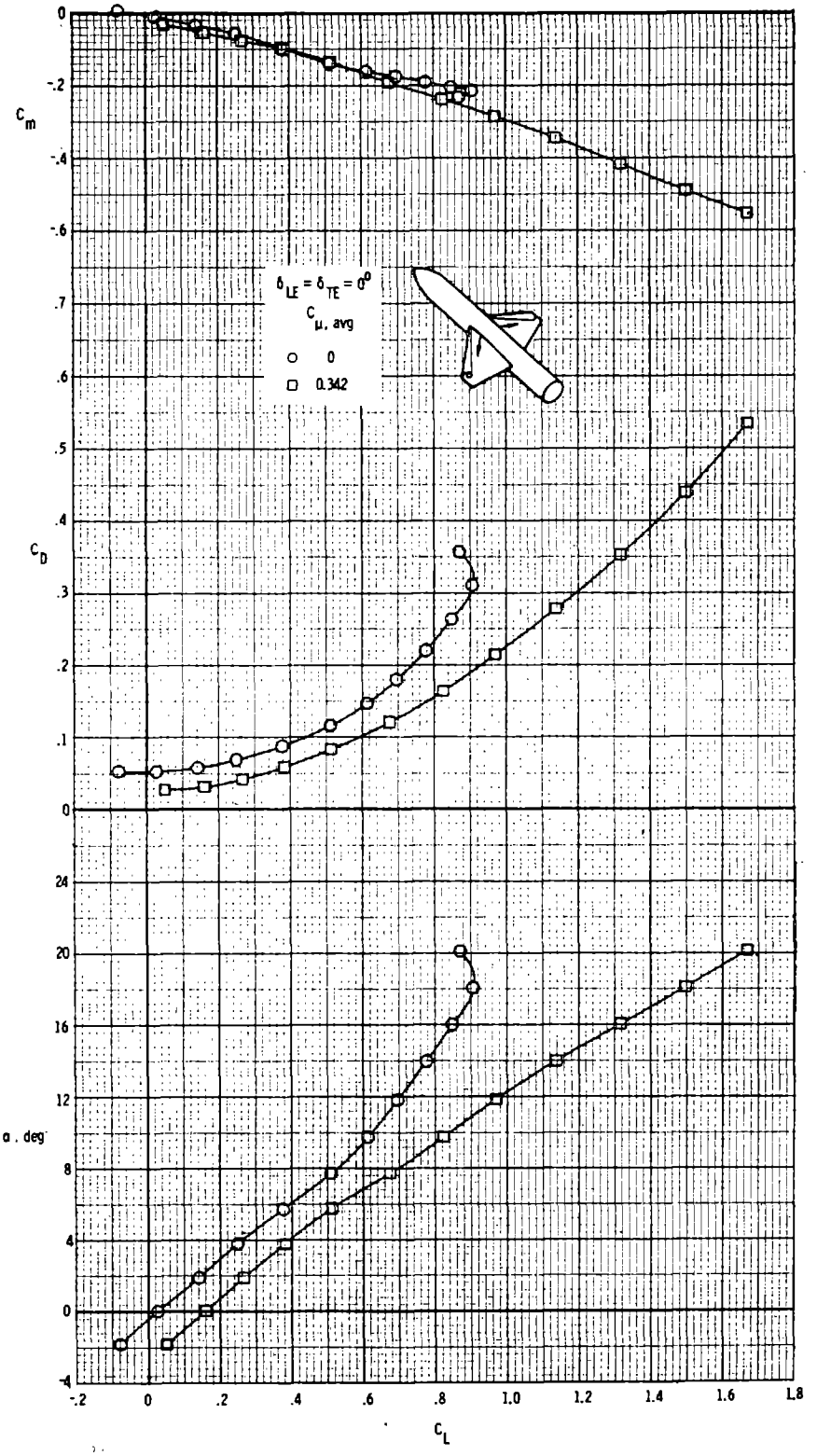

Figure 79.- Effect of spanwise blowing on the longitudinal aerodynamic characteristics of the "locked vortex" wing configuration with $\delta_{LE} = \delta_{TE} = 0^0$; $M_\infty = 0.15$.

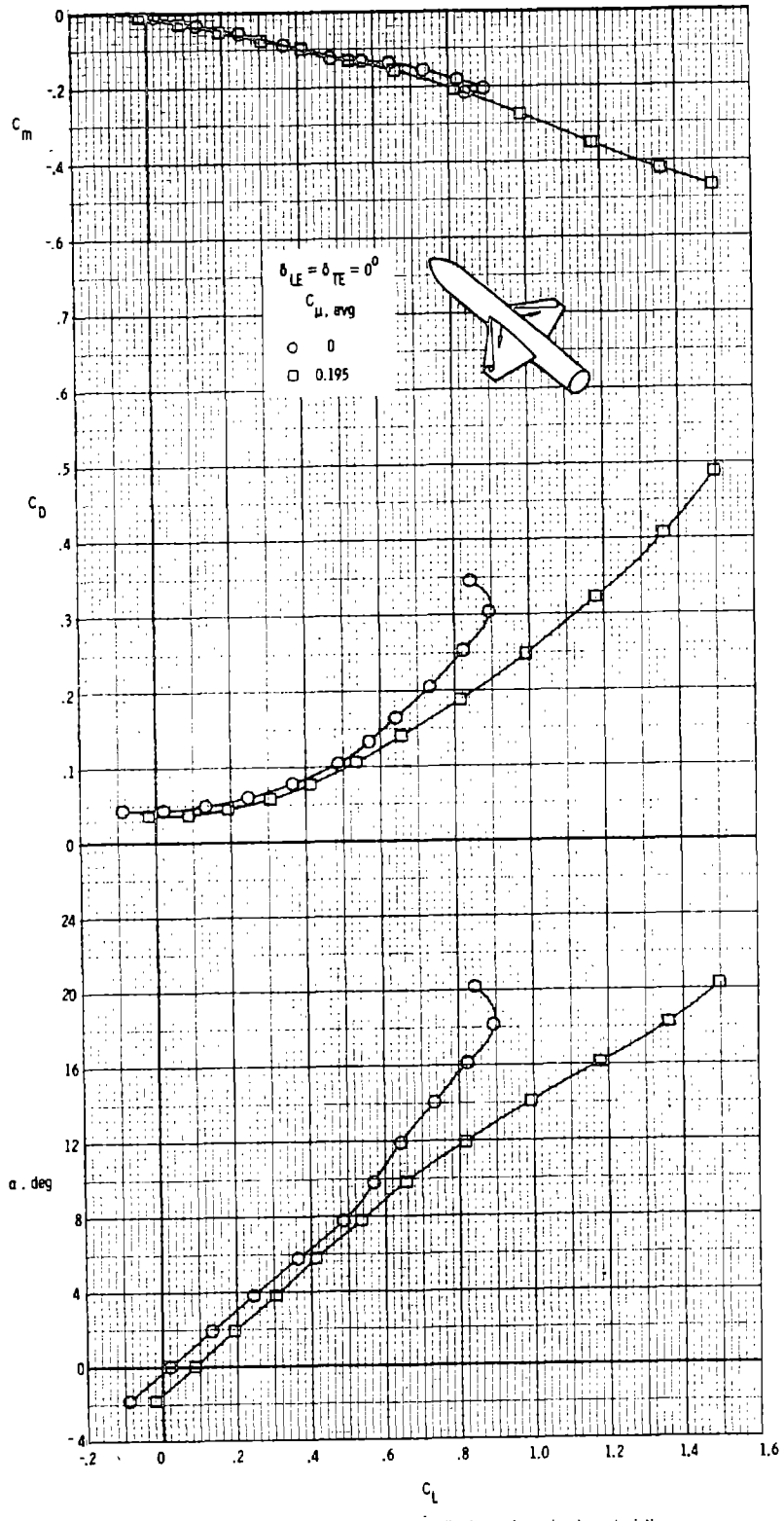

Figure 80.- Effect of spanwise blowing on the longitudinal aerodynamic characteristics of the "locked vortex" wing configuration with $\delta_{LE} = \delta_{TE} = 0^o$; $M_\infty = 0.20$.

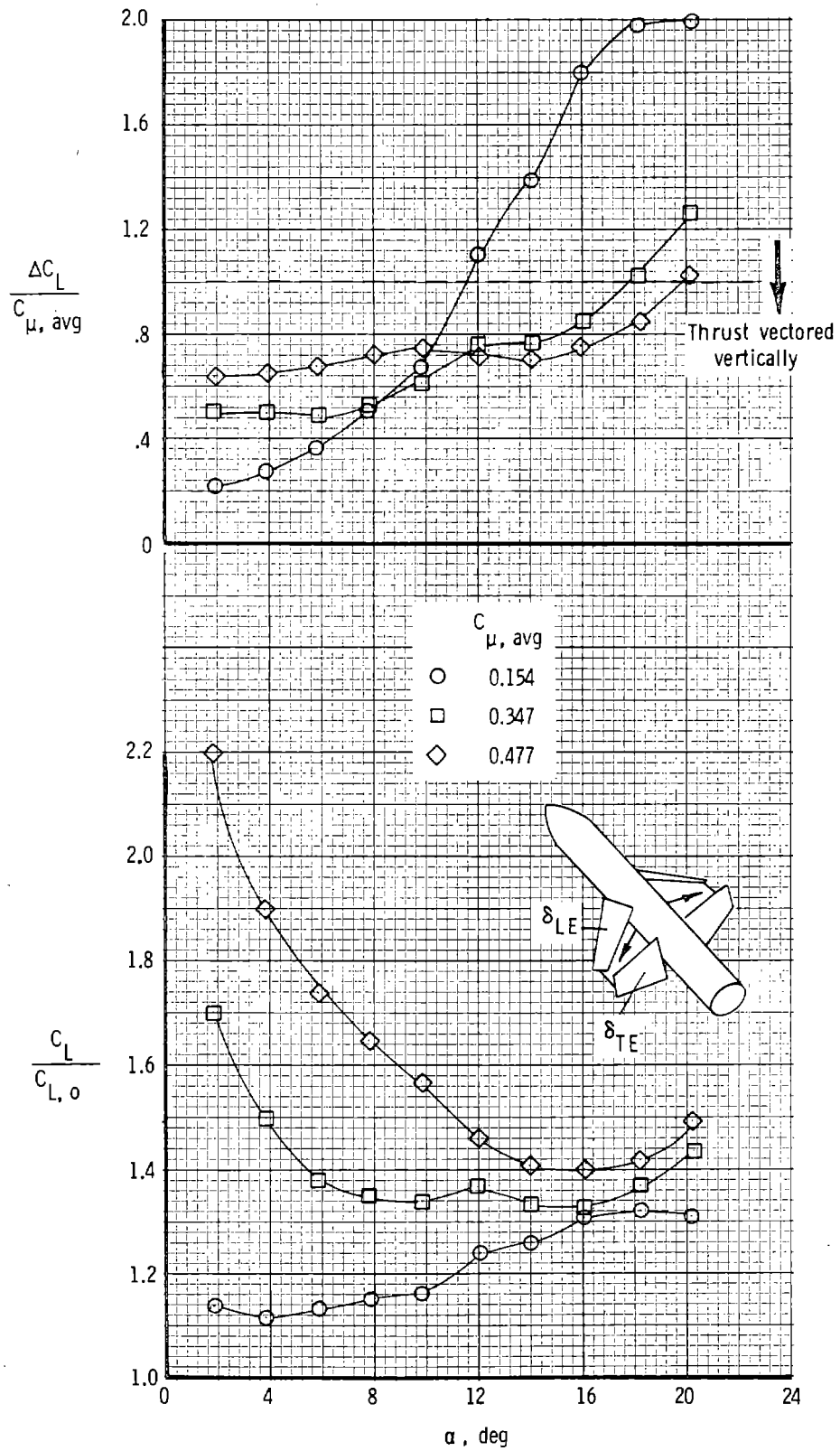

Figure 81.- Effect of α and $C_{\mu,avg}$ on the lift augmentation ratio and lift effectiveness of blowing for the "locked vortex" wing configuration for $\delta_{LE} = \delta_{TE} = 20^{o}$; $M_{\infty} = 0.15$.

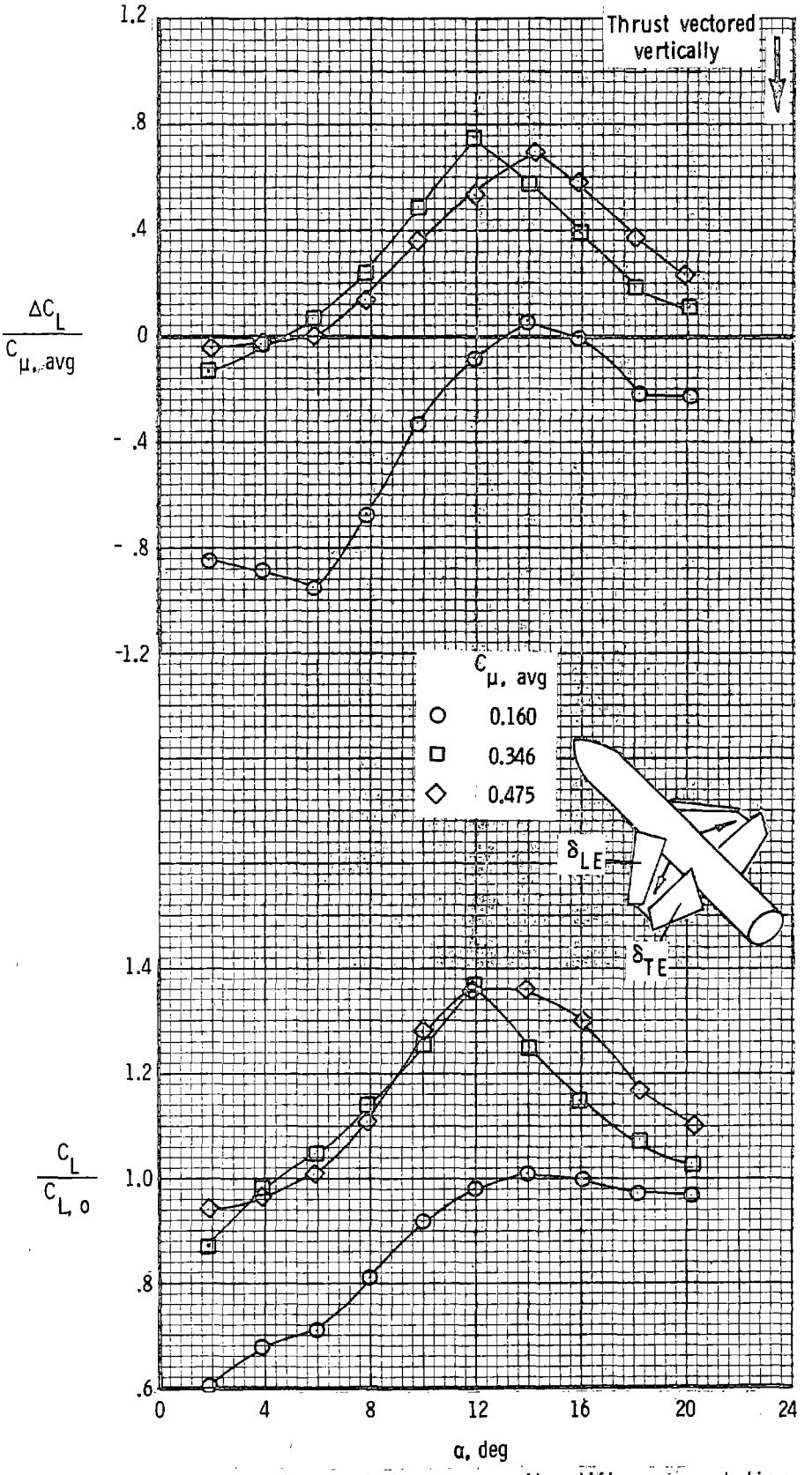

Figure 82.- Effect of α and $C_{\mu,avg}$ on the lift augmentation ratio and lift effectiveness of blowing for the "locked vortex" wing configuration for $\delta_{LE} = \delta_{TE} = 30^{o}$; $M_{\infty} = 0.15$.

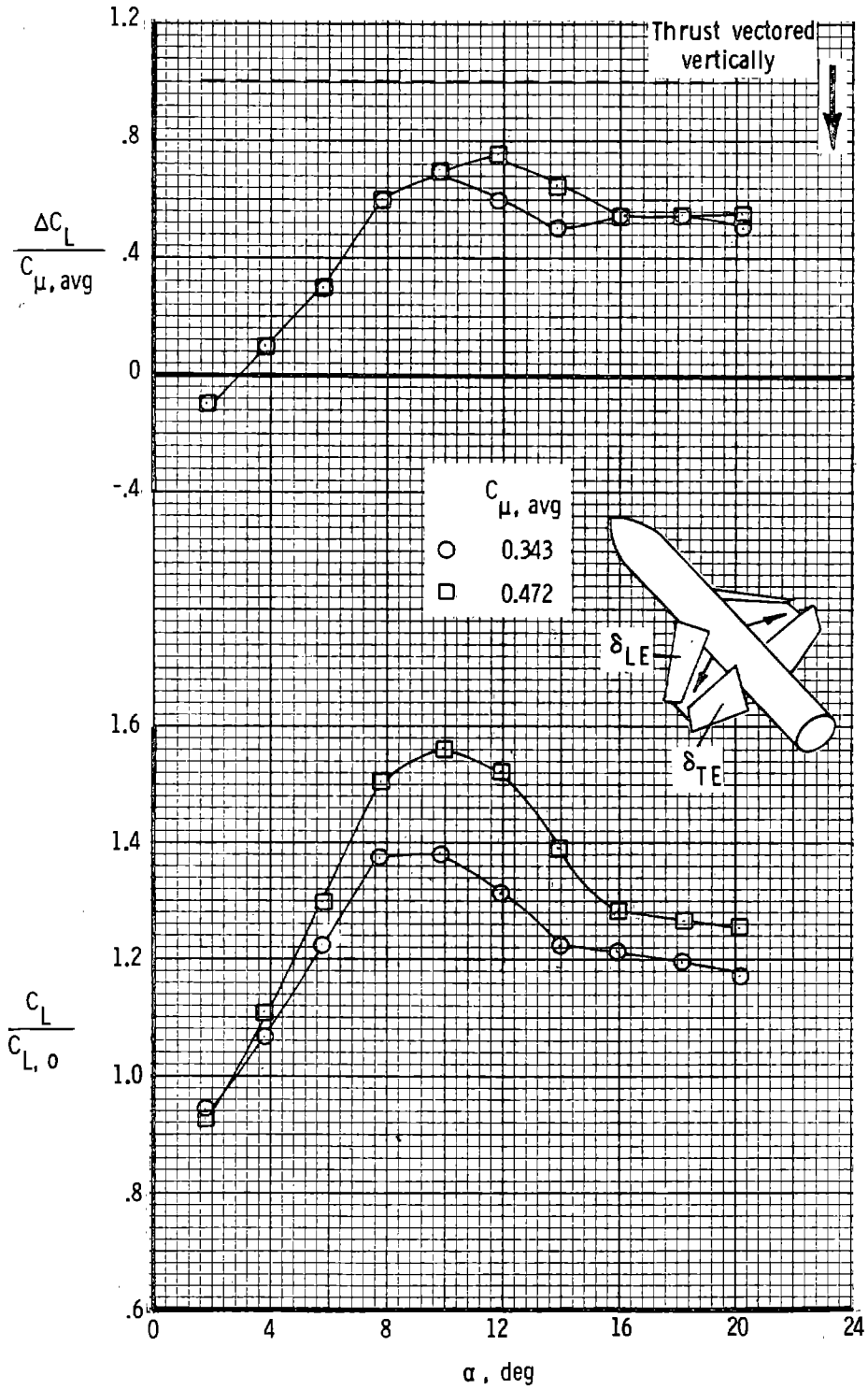

Figure 83.- Effect of α and $C_{\mu,avg}$ on the lift augmentation ratio and lift effectiveness of blowing for the "locked vortex" wing configuration for $\delta_{LE} = 45^0$; $\delta_{TE} = 30^0$; $M_\infty = 0.15$.

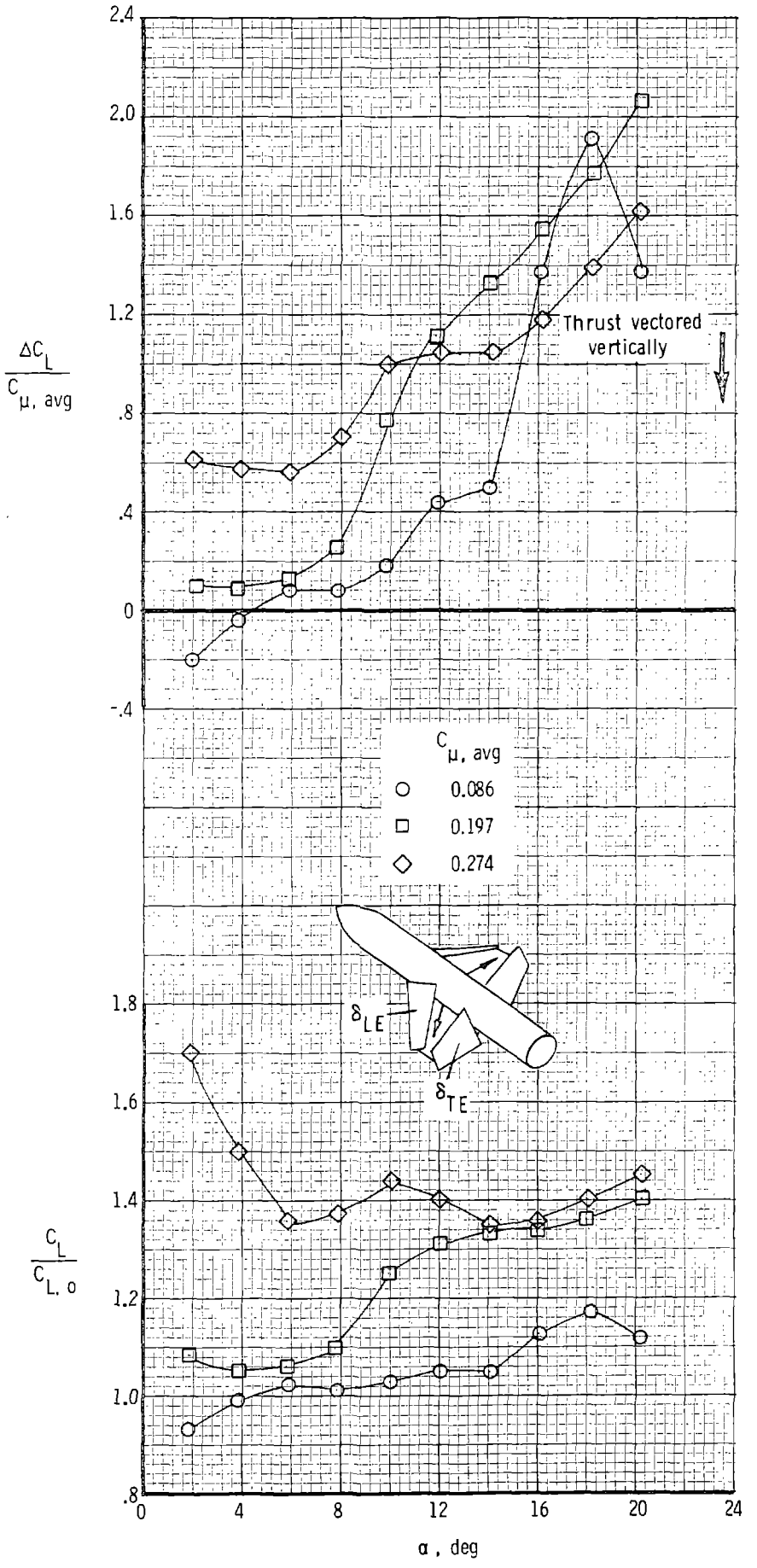

Figure 84.- Effect of α and $C_{\mu,avg}$ on the lift augmentation ratio and lift effectiveness of blowing for the "locked vortex" wing configuration for $\delta_{LE} = \delta_{TE} = 20^{o}$; $M_{\infty} = 0.20$.

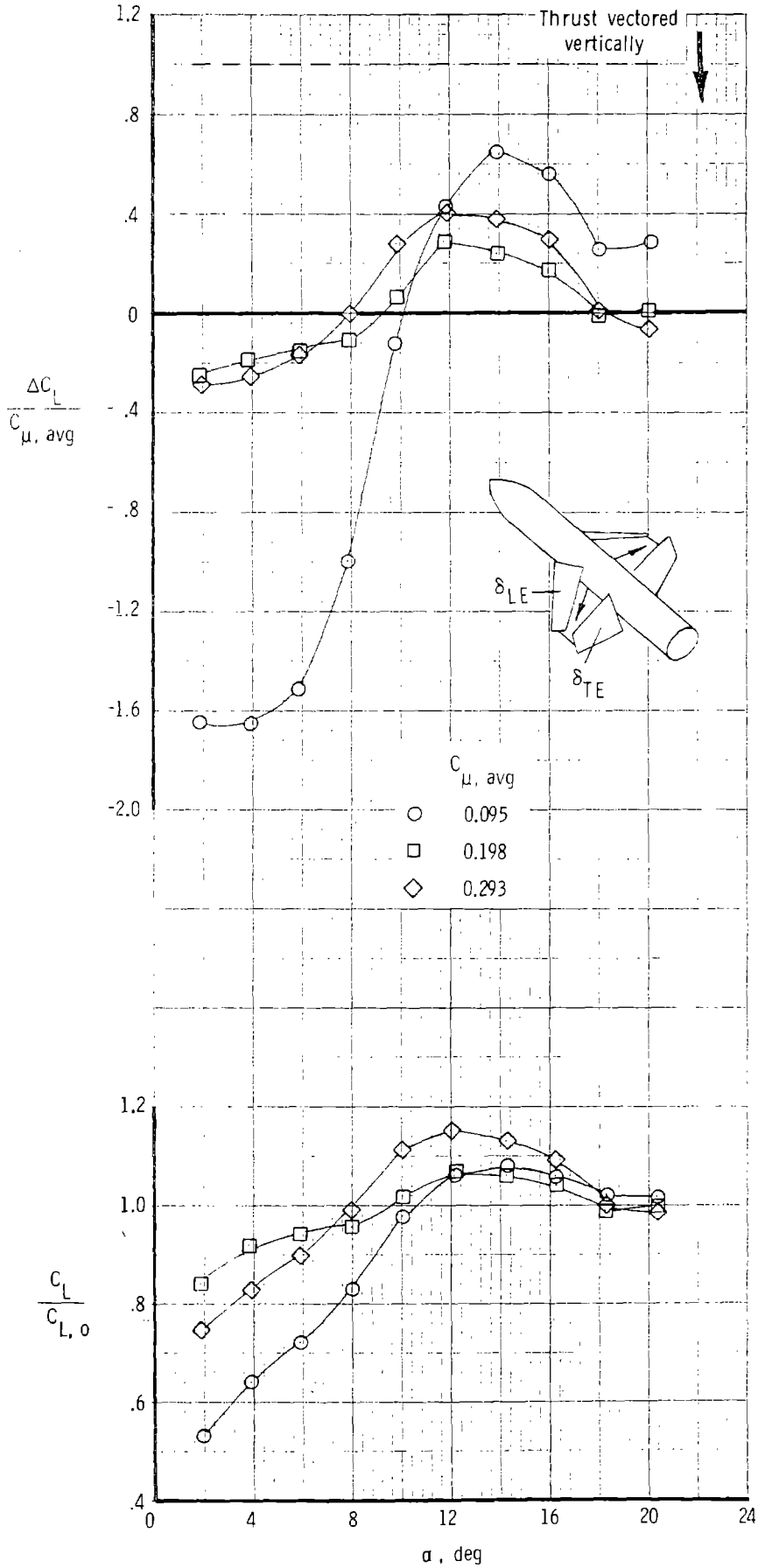

Figure 85.- Effect of α and $C_{\mu,avg}$ on the lift augmentation ratio and lift effectiveness of blowing for the "locked vortex" wing configuration for $\delta_{LE} = \delta_{TE} = 30^{o}$; $M_{\infty} = 0.20$.

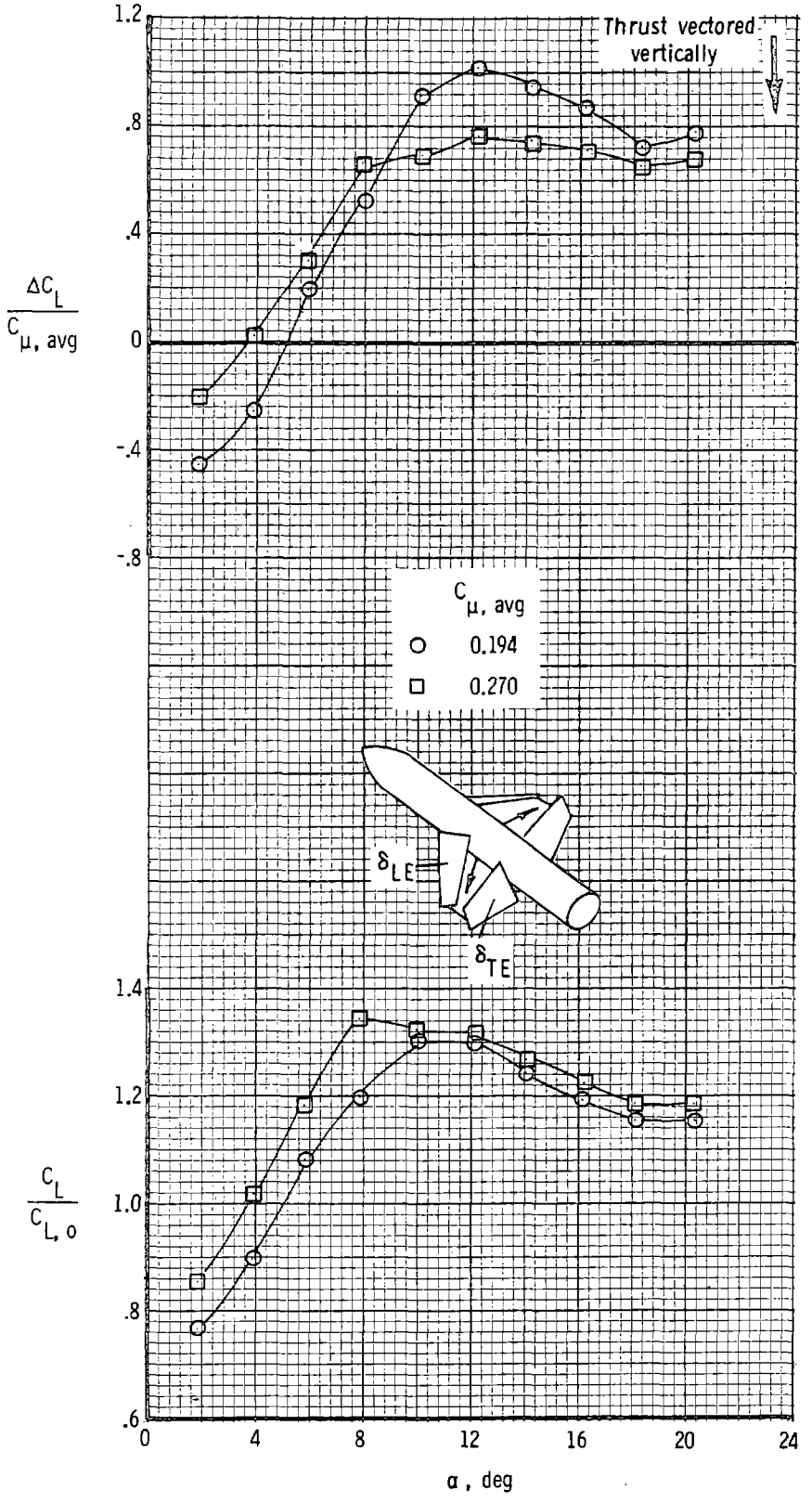

Figure 86.- Effect of α and $C_{\mu,avg}$ on the lift augmentation ratio and lift effectiveness of blowing for the "locked vortex" wing configuration for $\delta_{LE} = \delta_{TE} = 30^{o}$; $M_{\infty} = 0.30$.

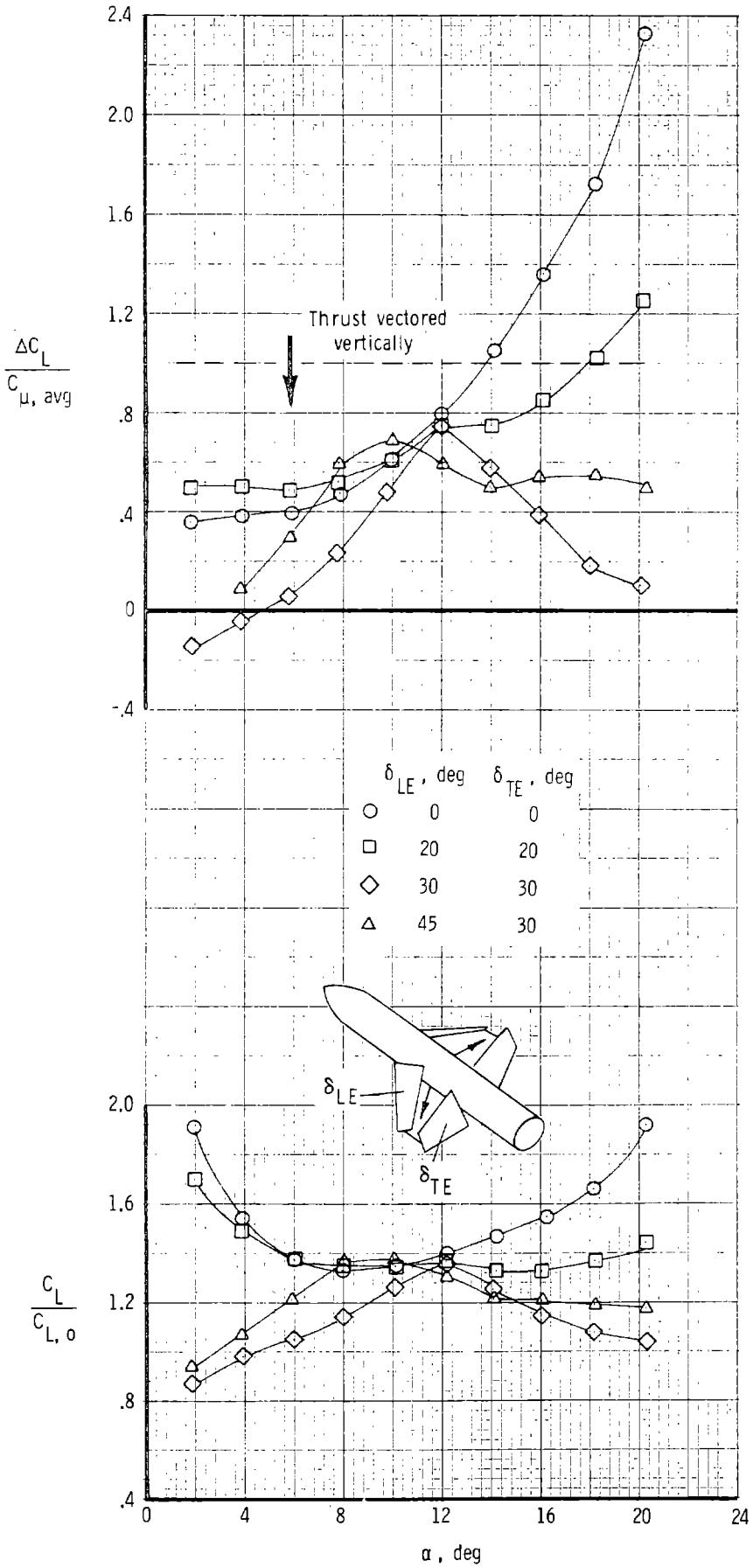

Figure 87.- Effect of α and leading- and trailing-edge flap deflection angles on the lift augmentation ratio and lift effectiveness of blowing for the "locked vortex" wing configuration; $C_{\mu,avg} = 0.340$; $M_\infty = 0.15$.

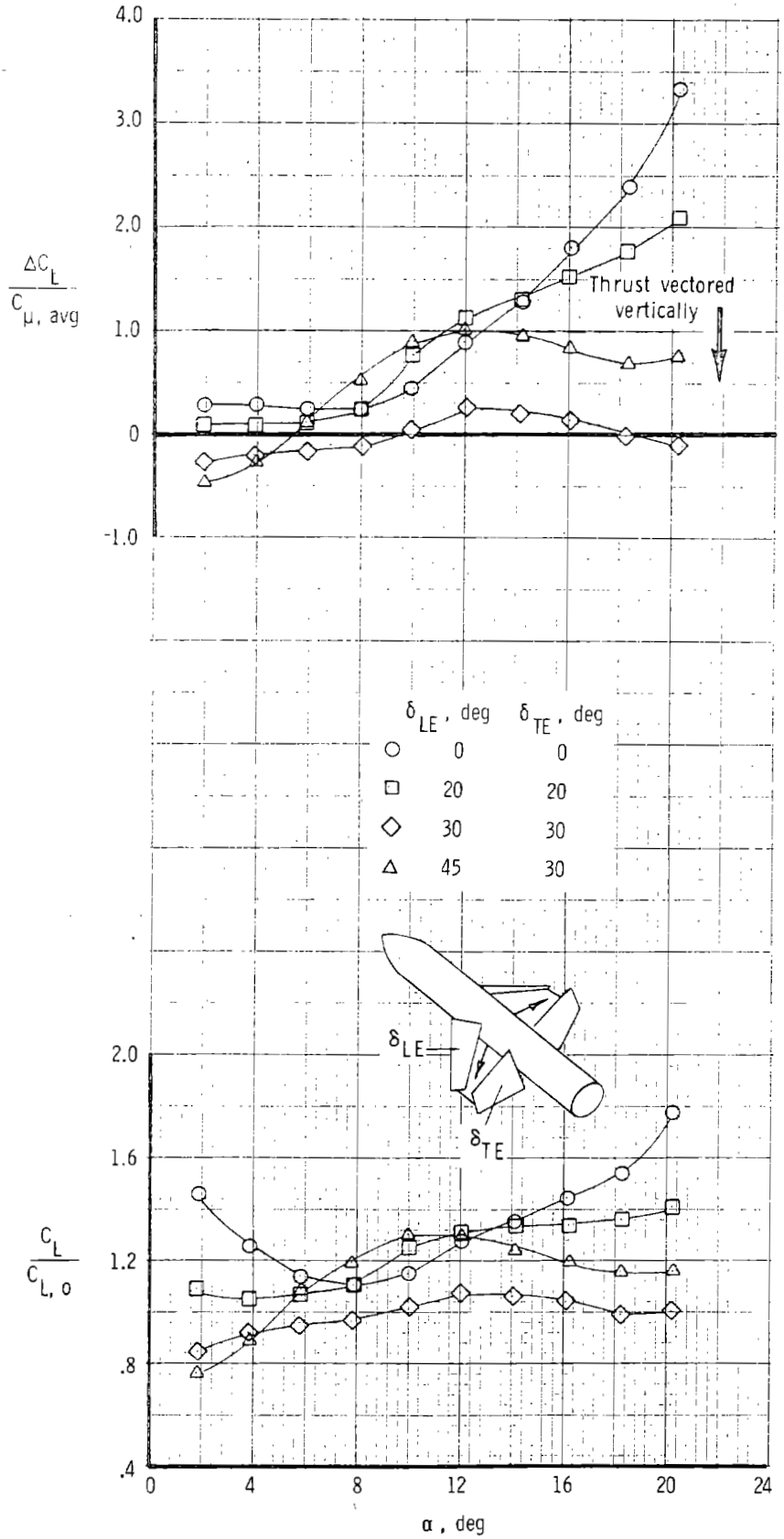

Figure 88.- Effect of α and leading- and trailing-edge flap deflection angles on the lift augmentation ratio and lift effectiveness of blowing for the "locked vortex" wing configuration; $C_{\mu,avg} = 0.195$; $M_\infty = 0.20$.

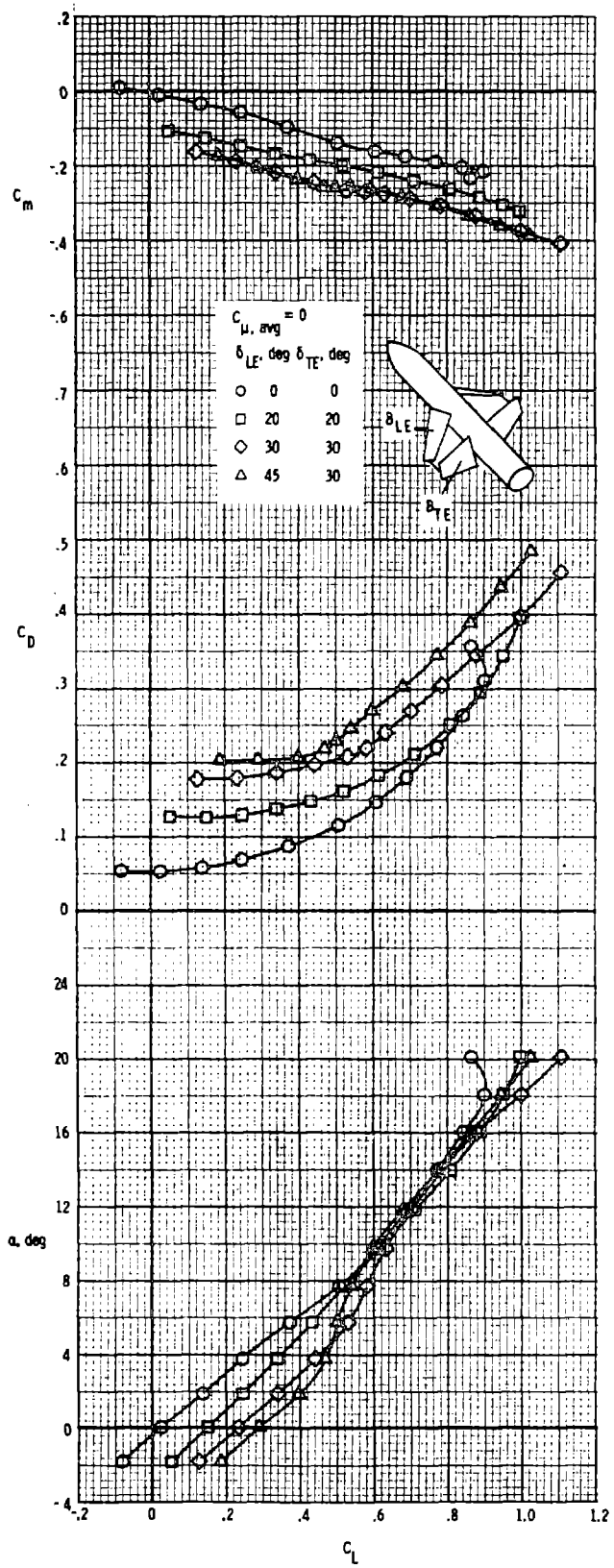

Figure 89.- Effect of leading- and trailing-edge flap deflection angles on the longitudinal aerodynamic characteristics of the "locked vortex" wing configuration with blowing off; $M_\infty = 0.15$.

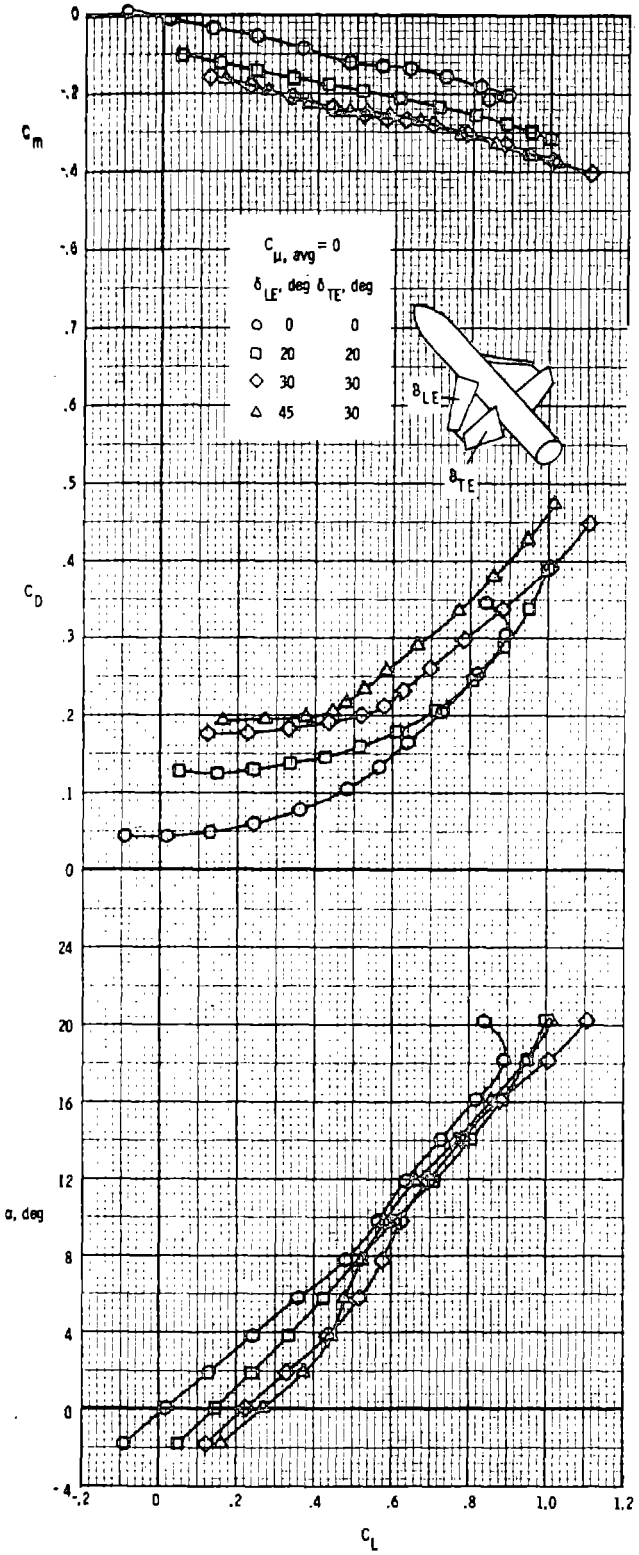

Figure 90.- Effect of leading- and trailing-edge flap deflection angles on the longitudinal aerodynamic characteristics of the "locked vortex" wing configuration with blowing off; $M_\infty = 0.20$.

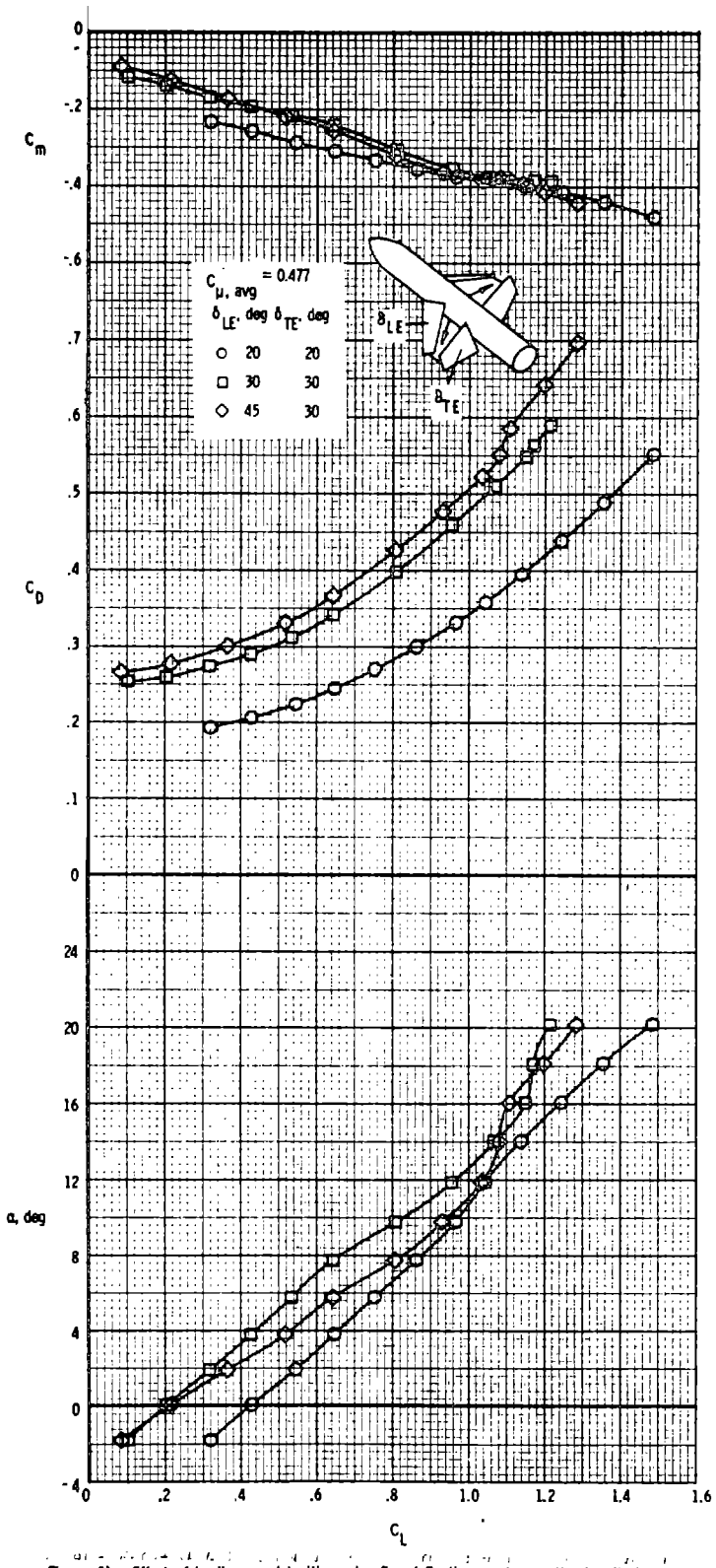

Figure 91.- Effect of leading- and trailing-edge flap deflection angles on the longitudinal aerodynamic characteristics of the "locked vortex" wing configuration with blowing on; $M_\infty = 0.15$.

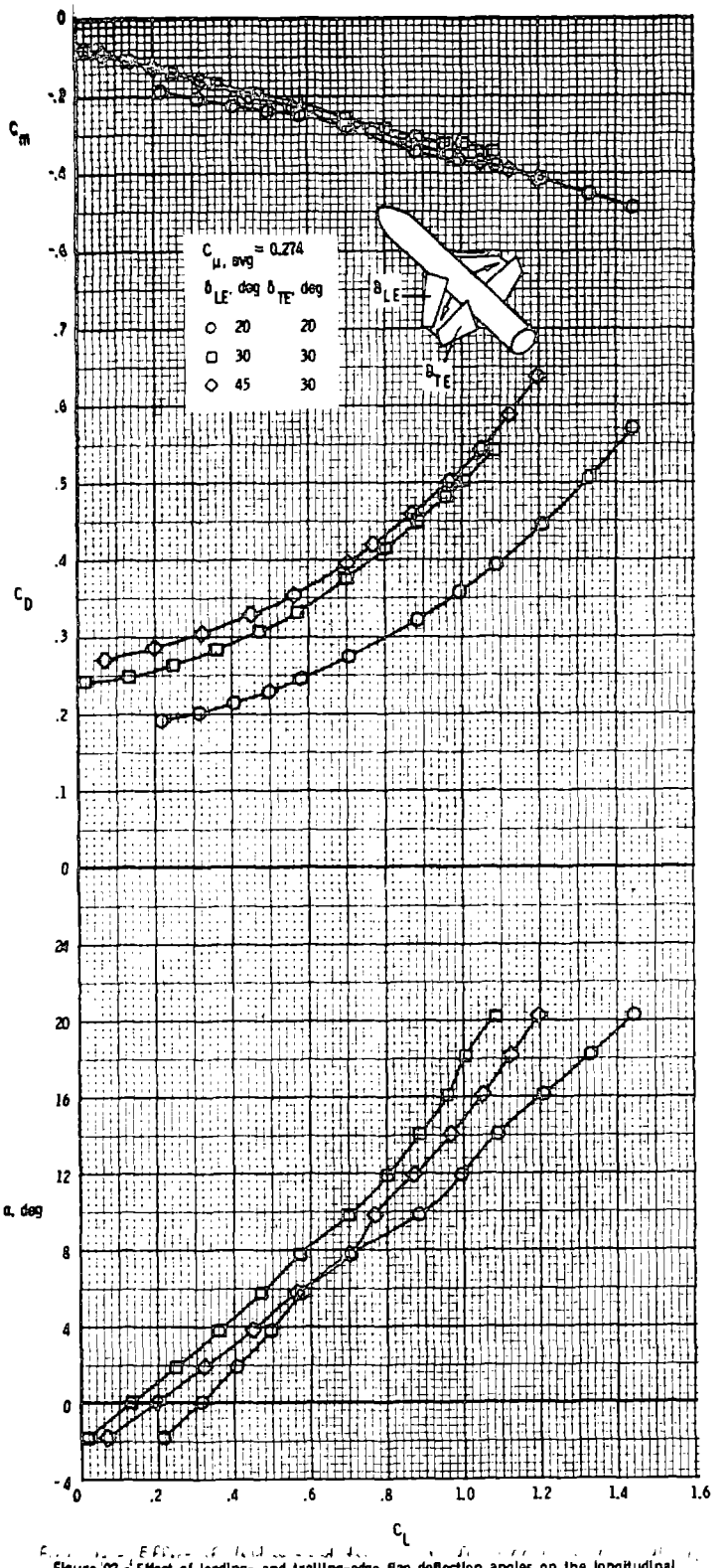

Figure 92.- Effect of leading- and trailing-edge flap deflection angles on the longitudinal aerodynamic characteristics of the "locked vortex" wing configuration with blowing on; M_∞ = 0.20.

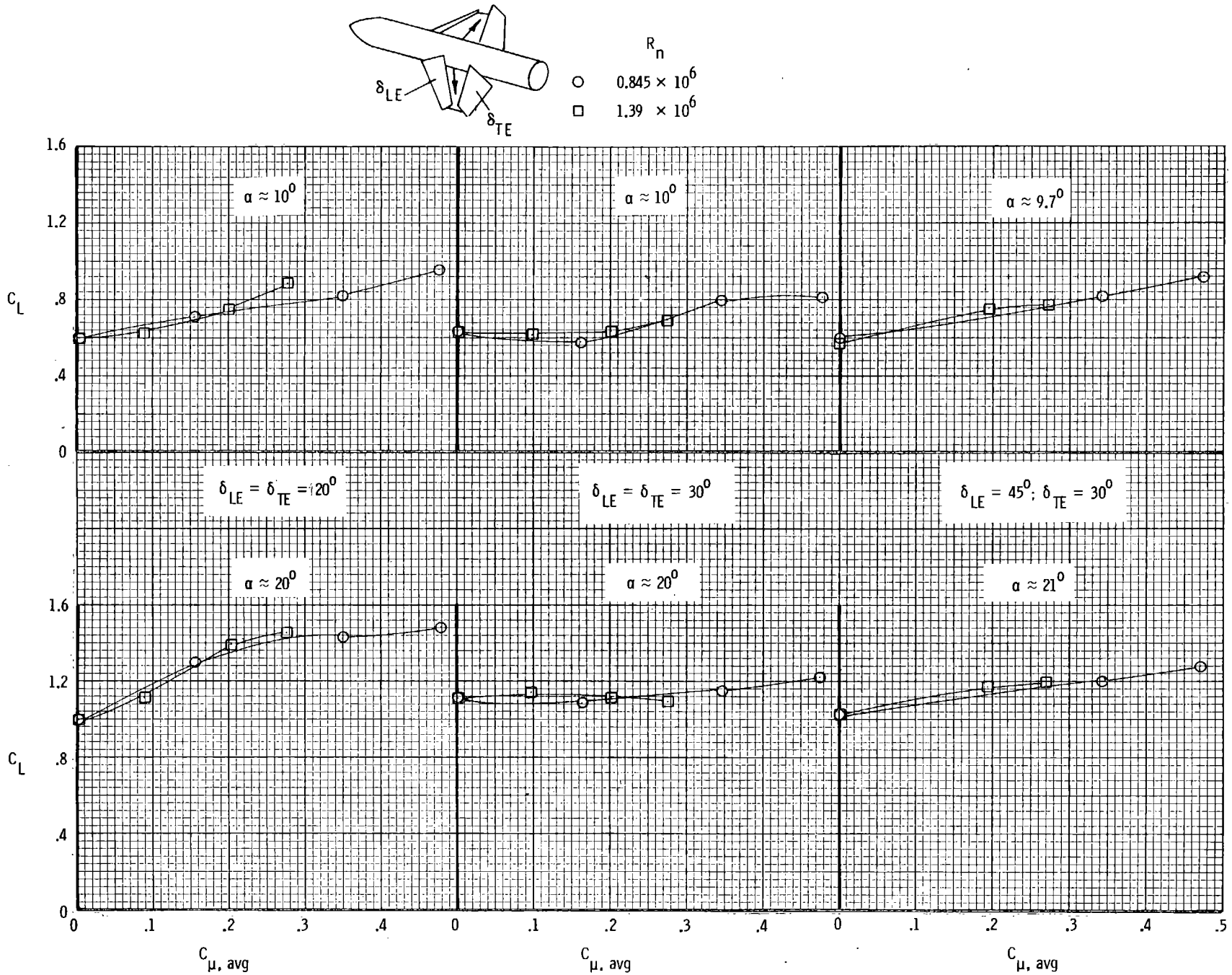

Figure 93.- Variation of lift coefficient with $C_{\mu,avg}$ for two Reynolds numbers and two angles-of-attack for the "locked vortex" wing configuration.

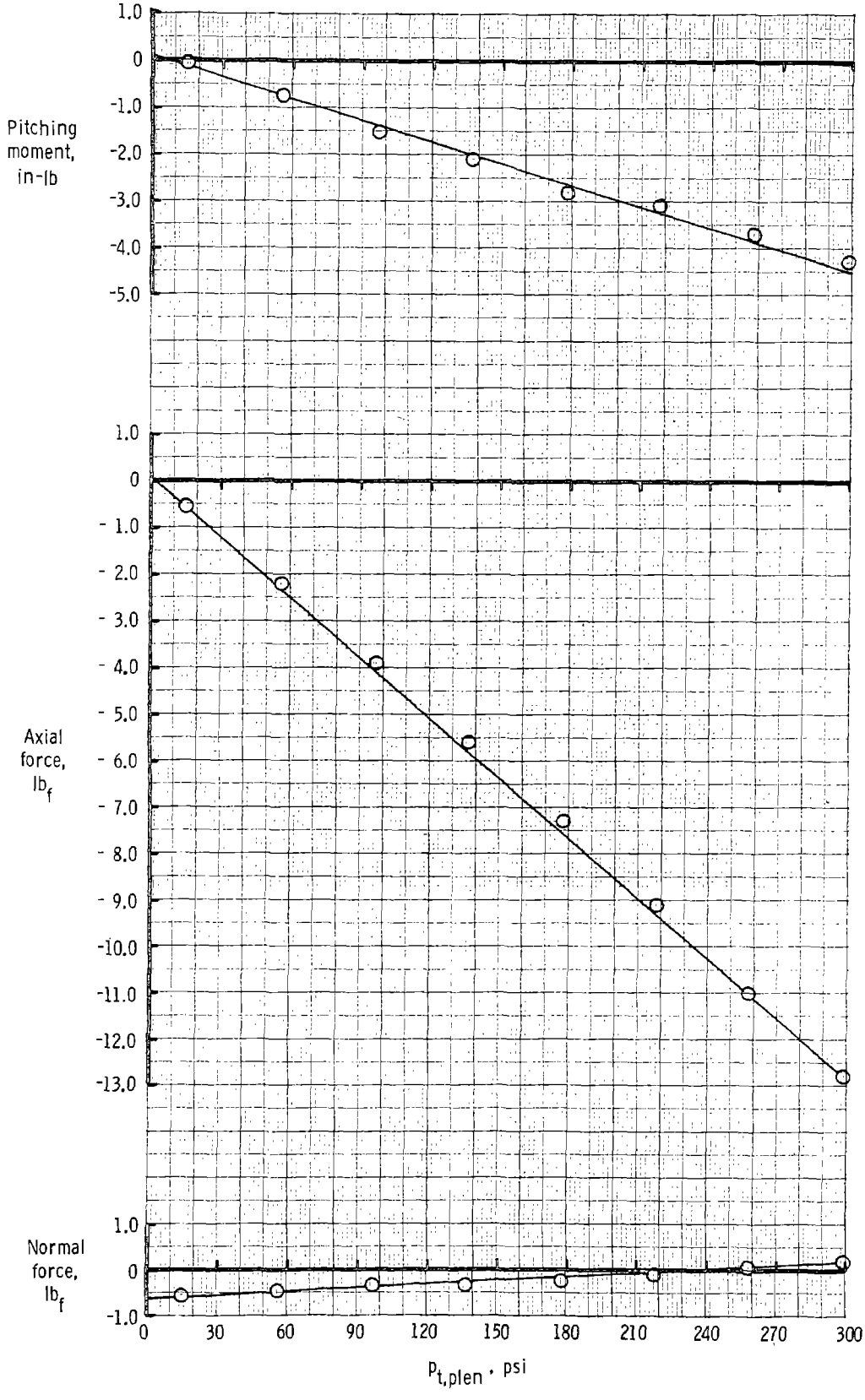

Figure 94.- Static calibration of the 44° swept trapezoidal wing nozzles.

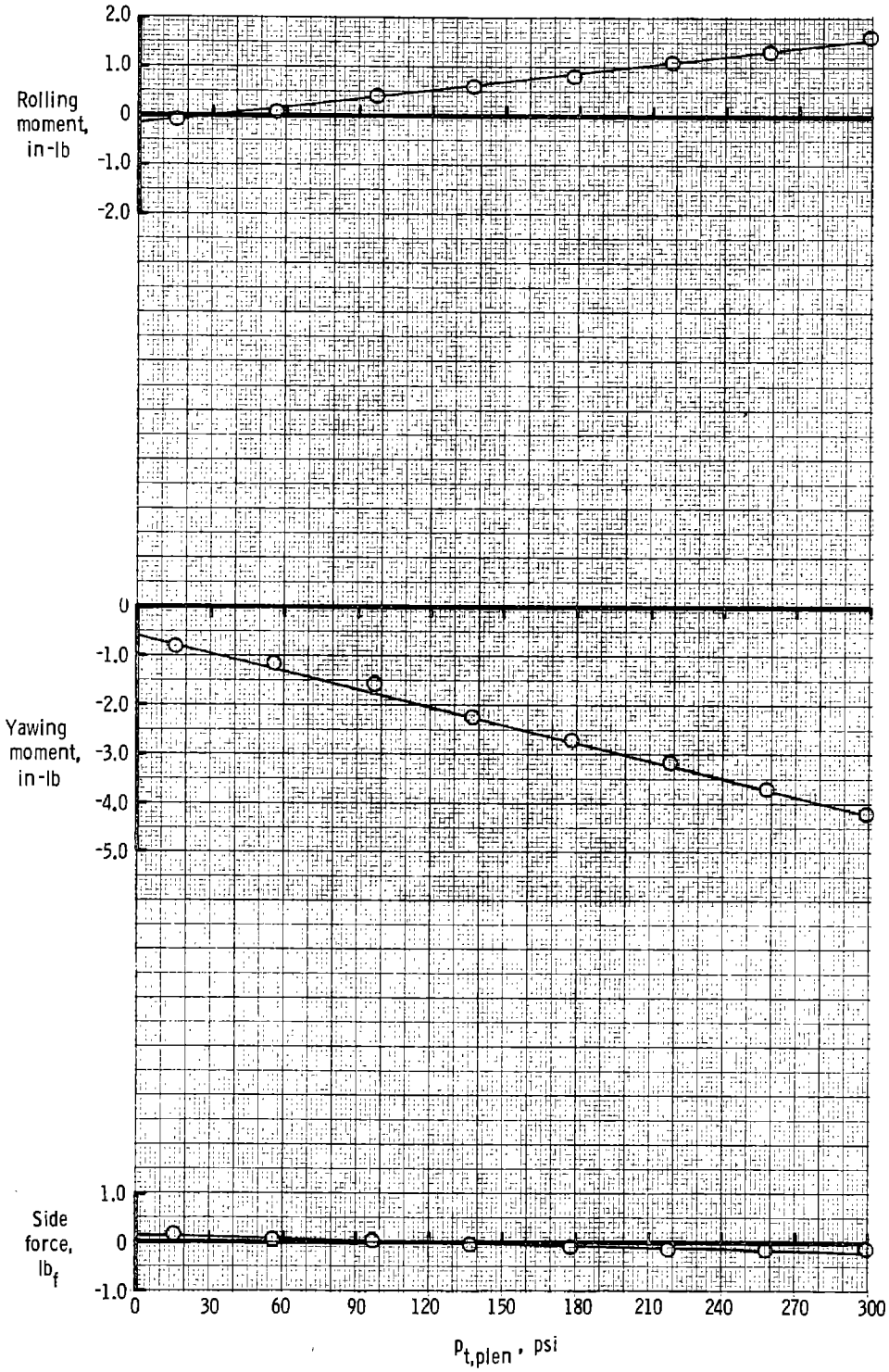

Figure 94.- Concluded.

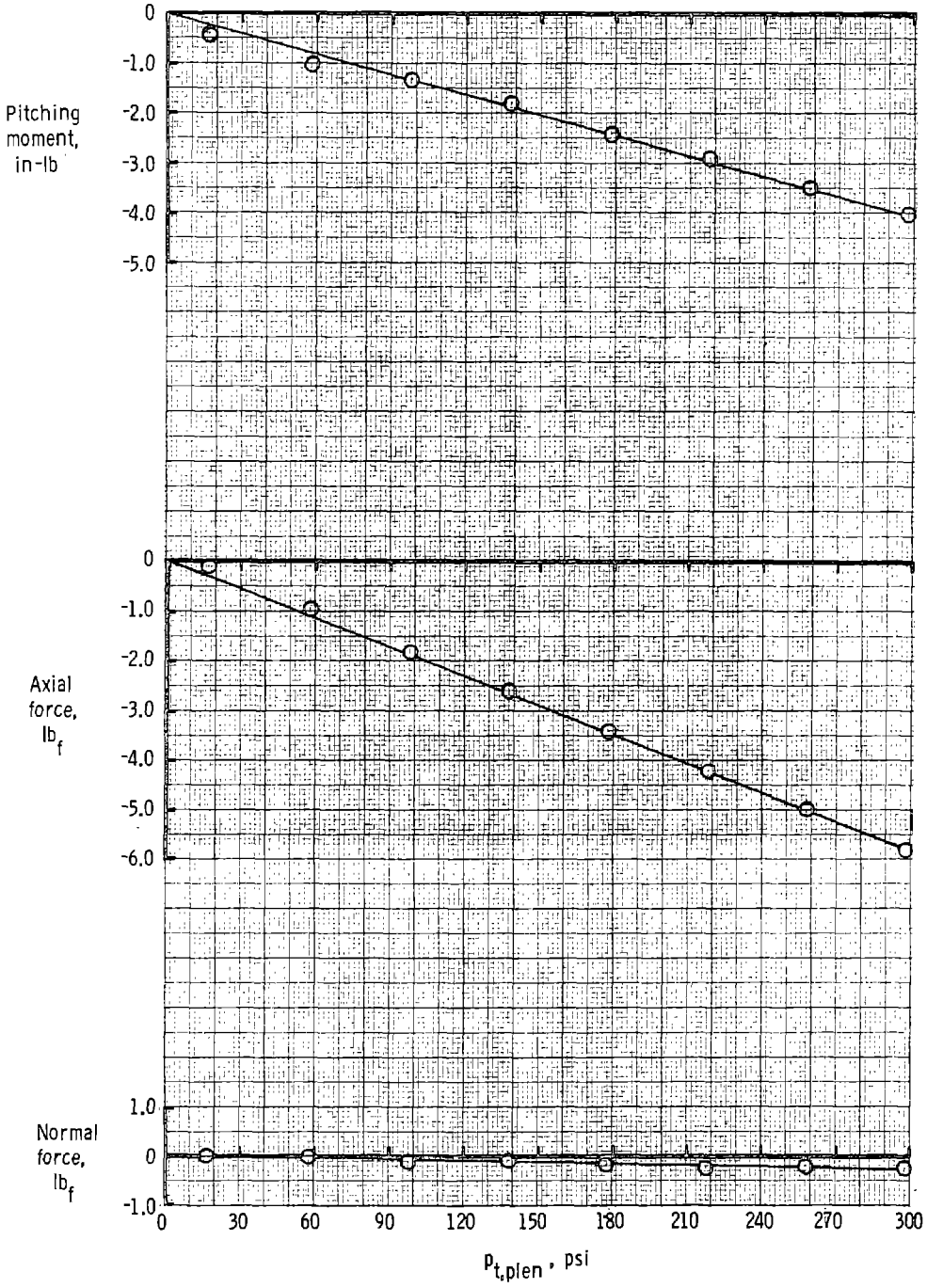

Figure 95.- Static calibration of the right 44° swept trapezoidal wing nozzle with the left wing nozzle plugged.

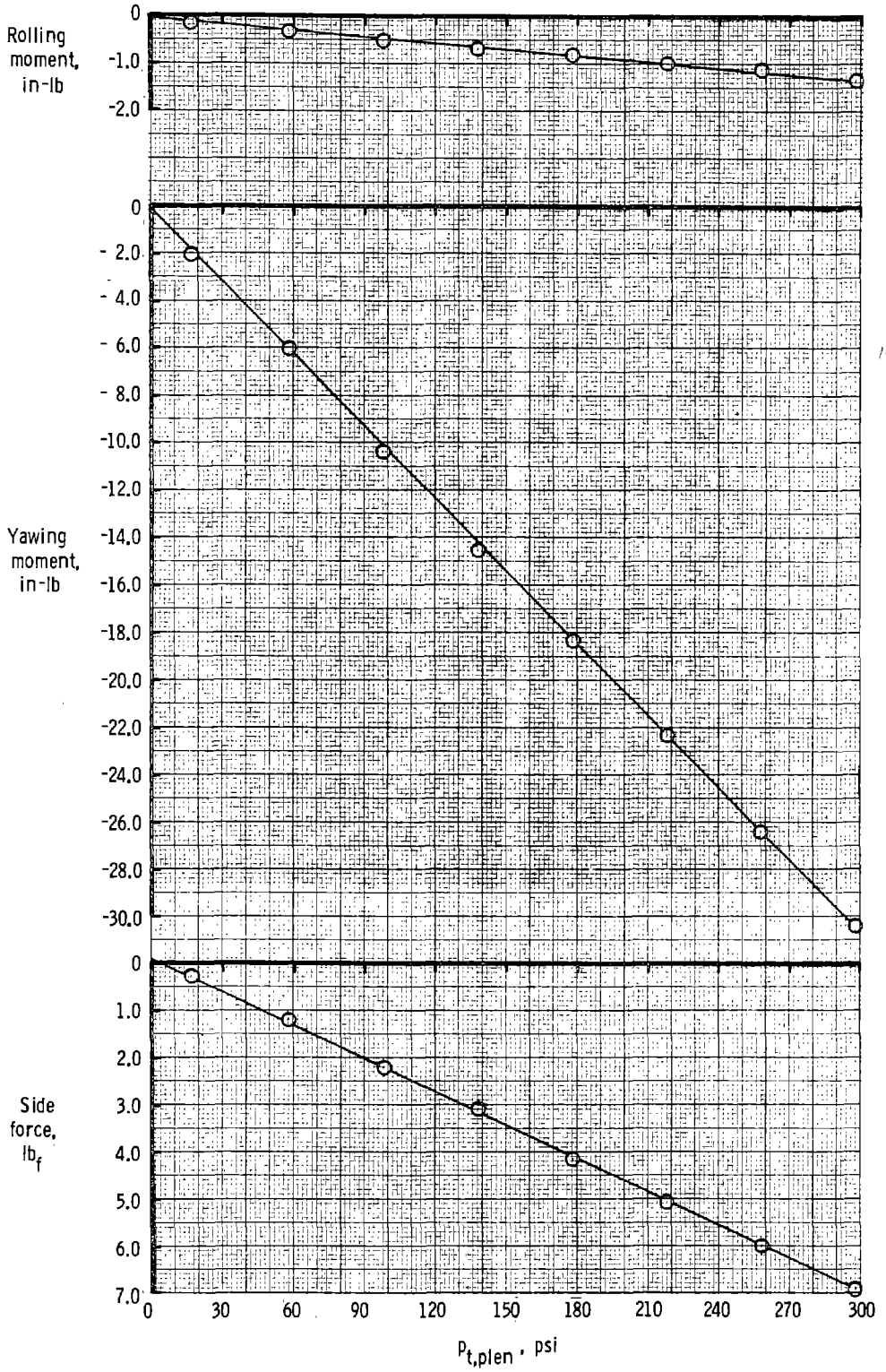

Figure 95.- Concluded.

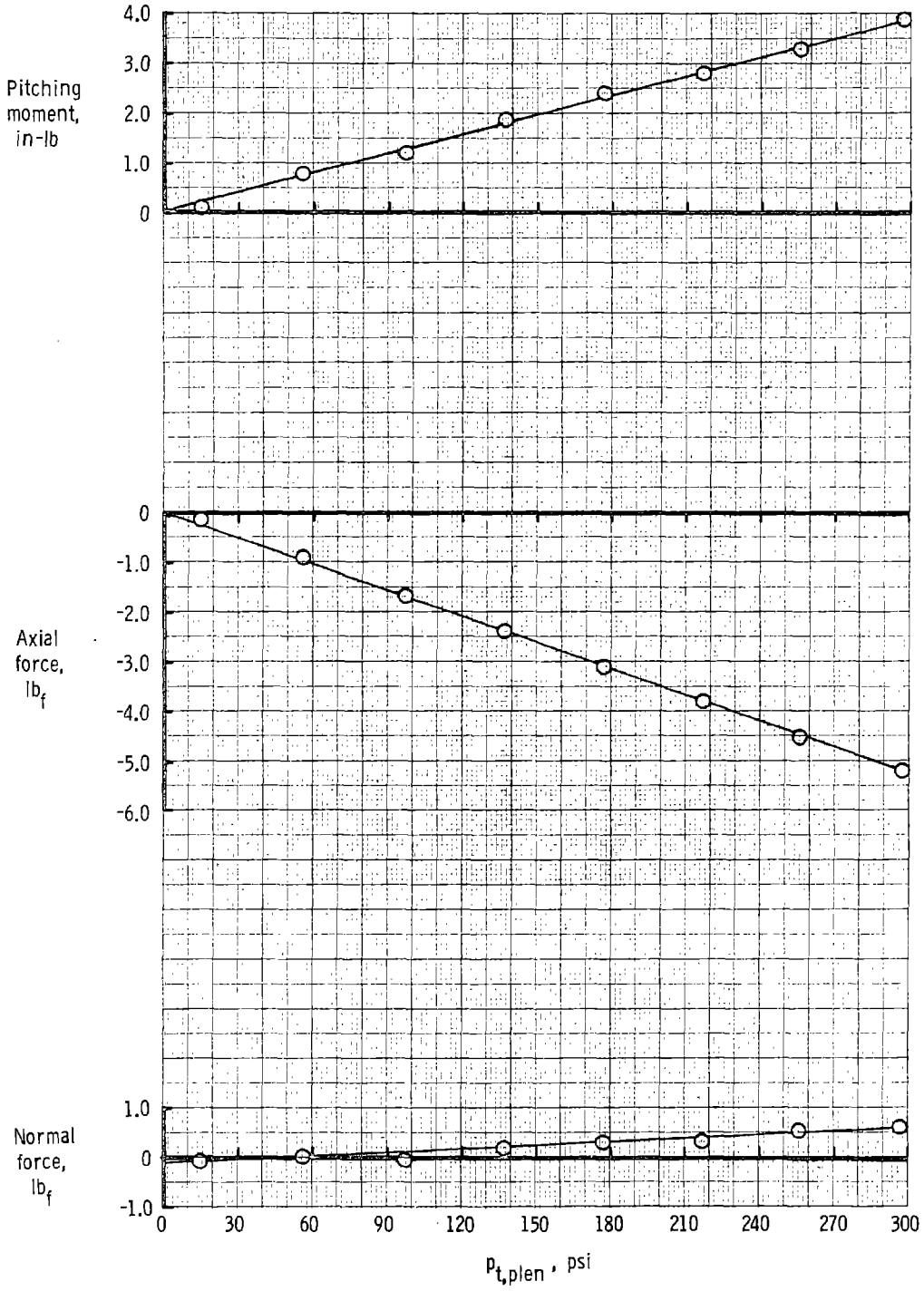

Figure 96.- Static calibration of the canard nozzles.

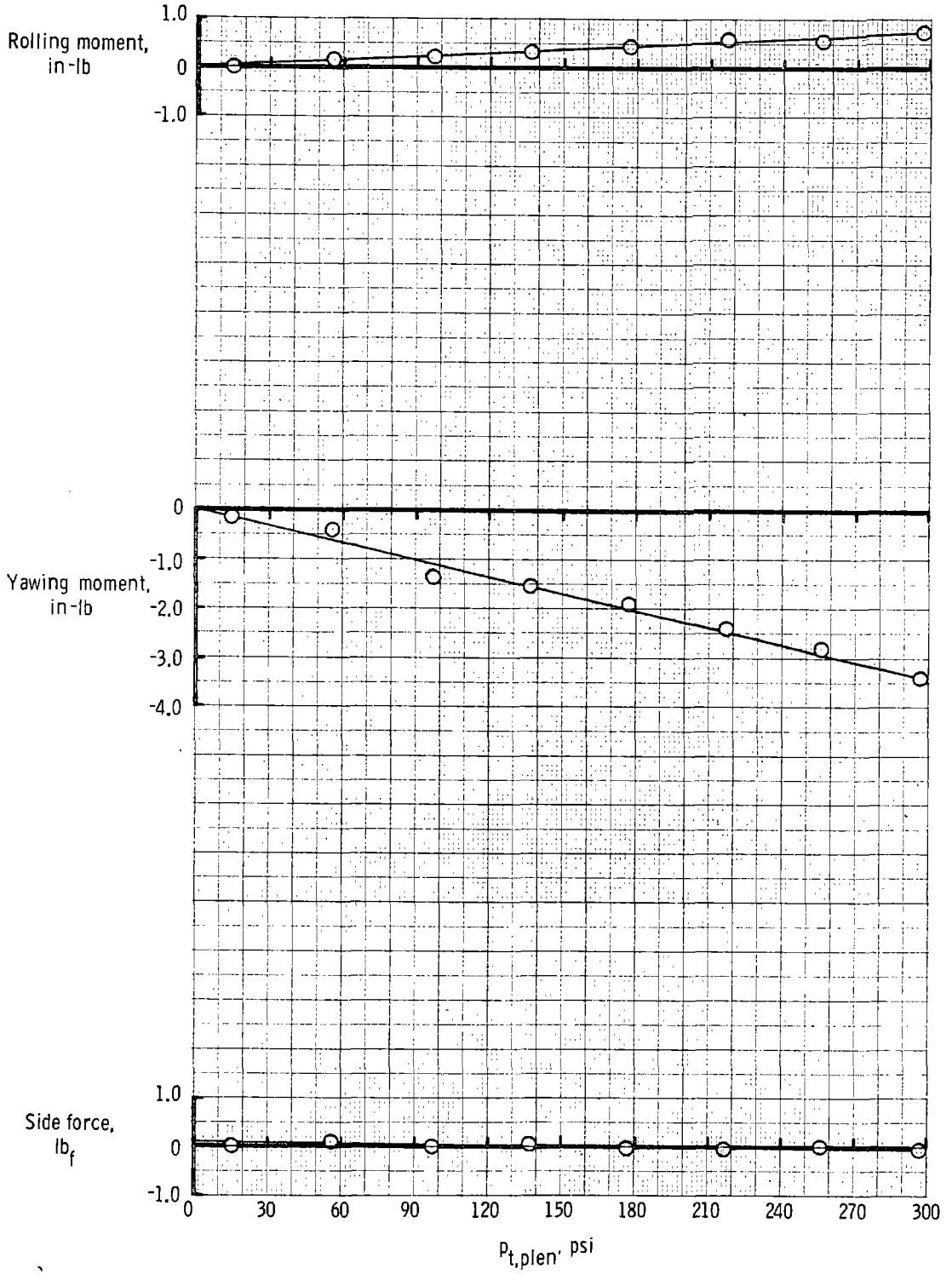

Figure 96.- Concluded.

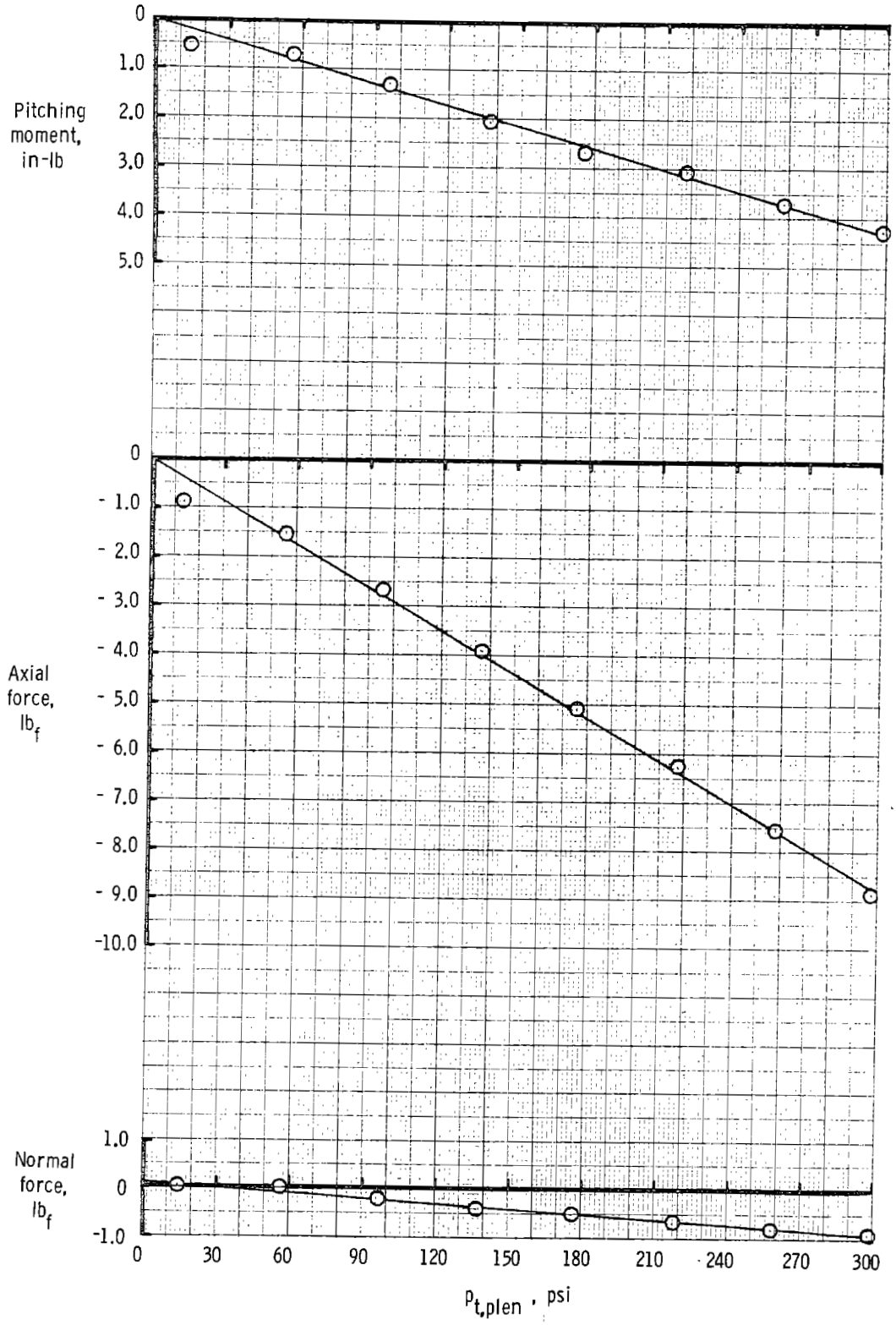

Figure 97.- Static calibration of the "locked vortex" wing nozzles.

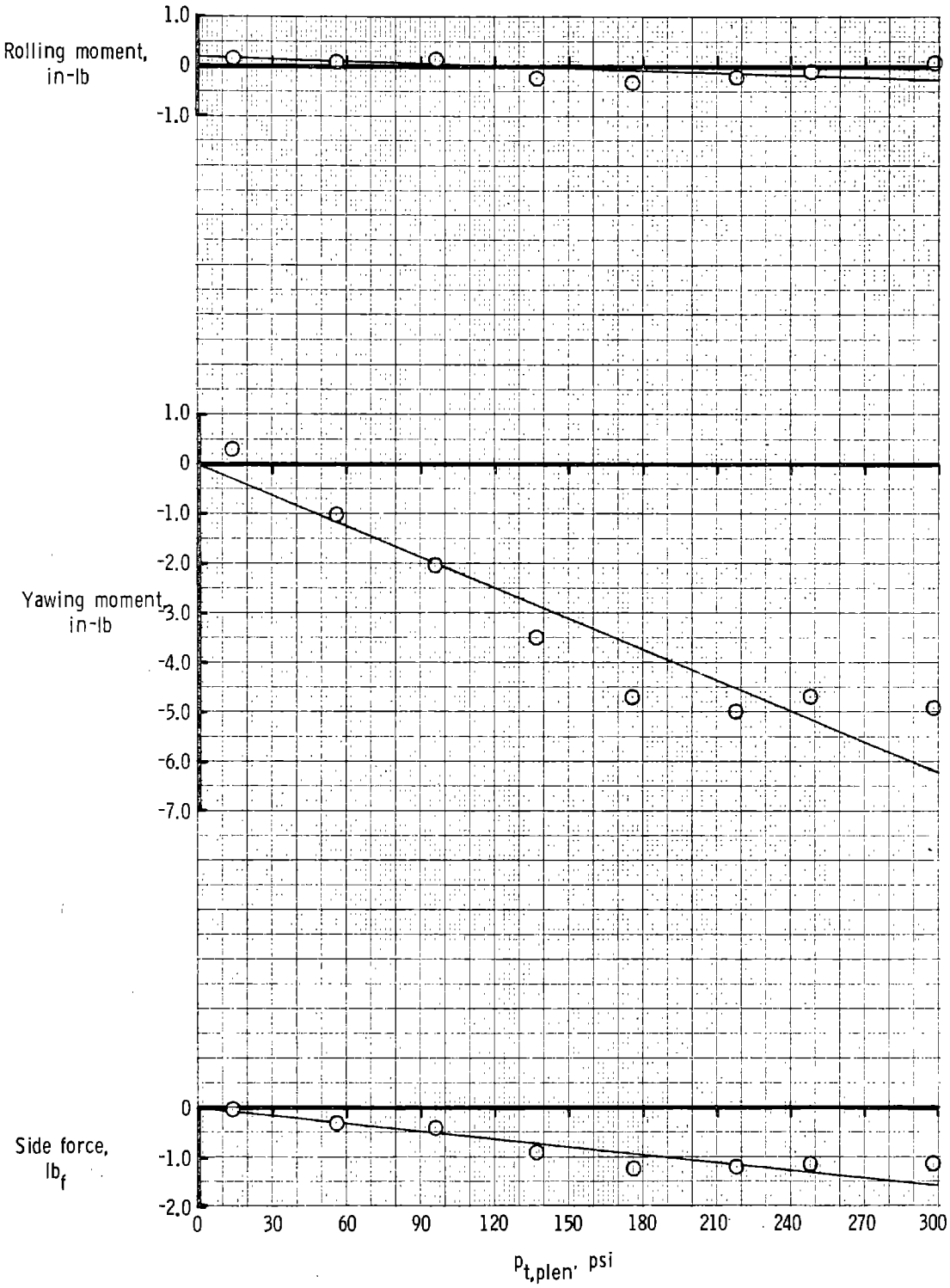

Figure 97.- Concluded.

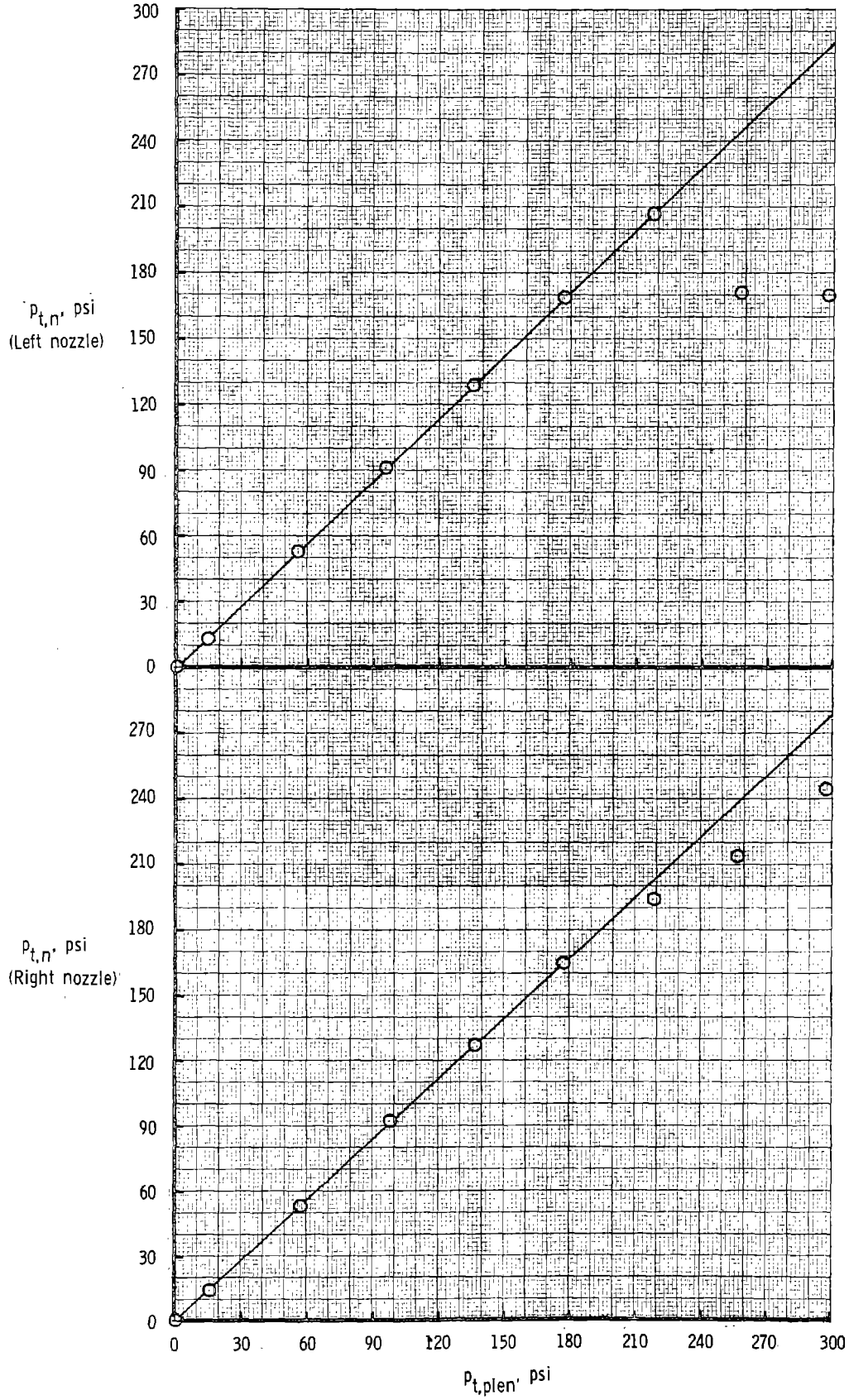

Figure 98.- Total pressure at the nozzle exit versus plenum chamber total pressure for the 44° swept trapezoidal wing nozzles.

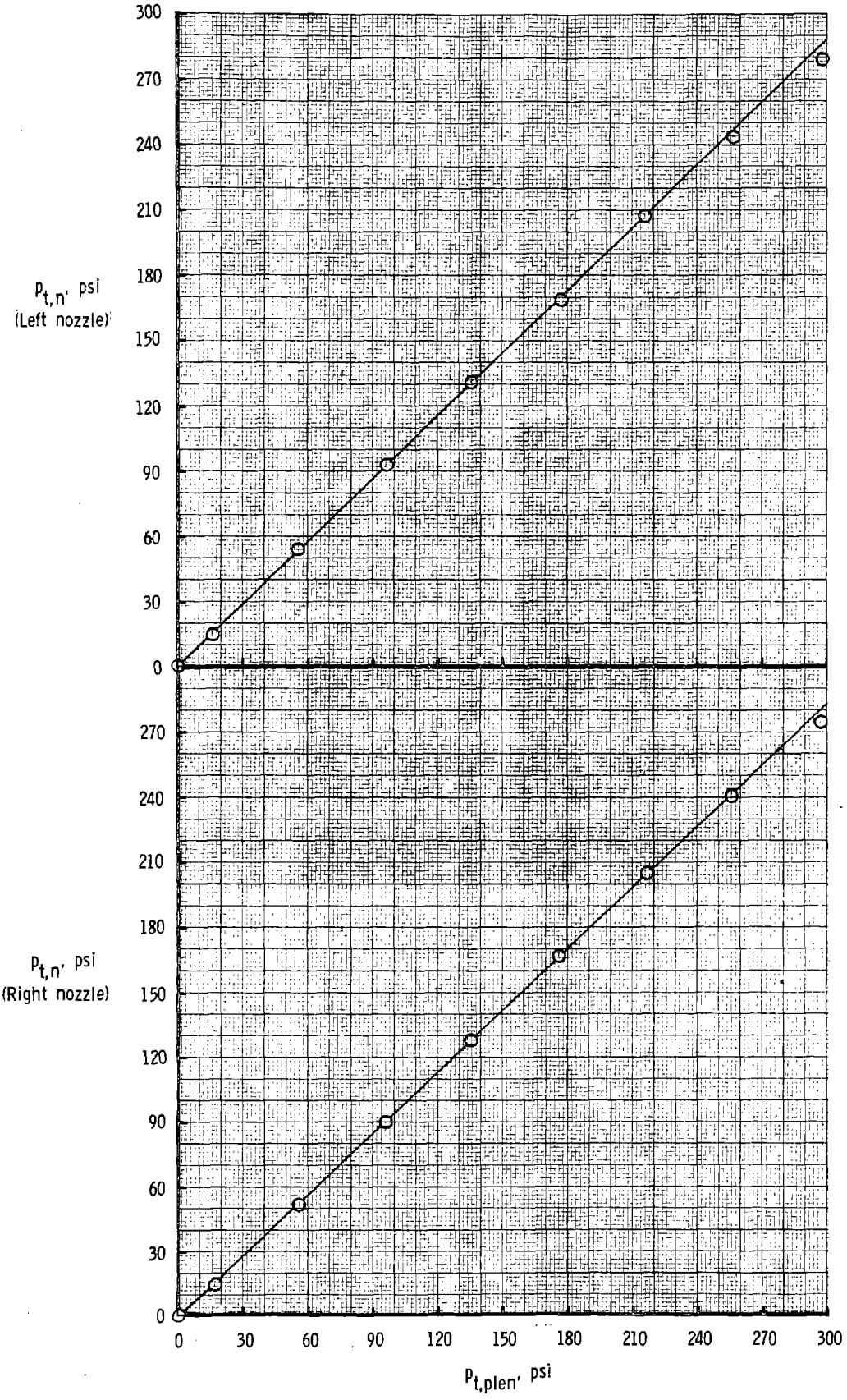

Figure 99.- Total pressure at the nozzle exit versus plenum chamber total pressure for the canard nozzles.

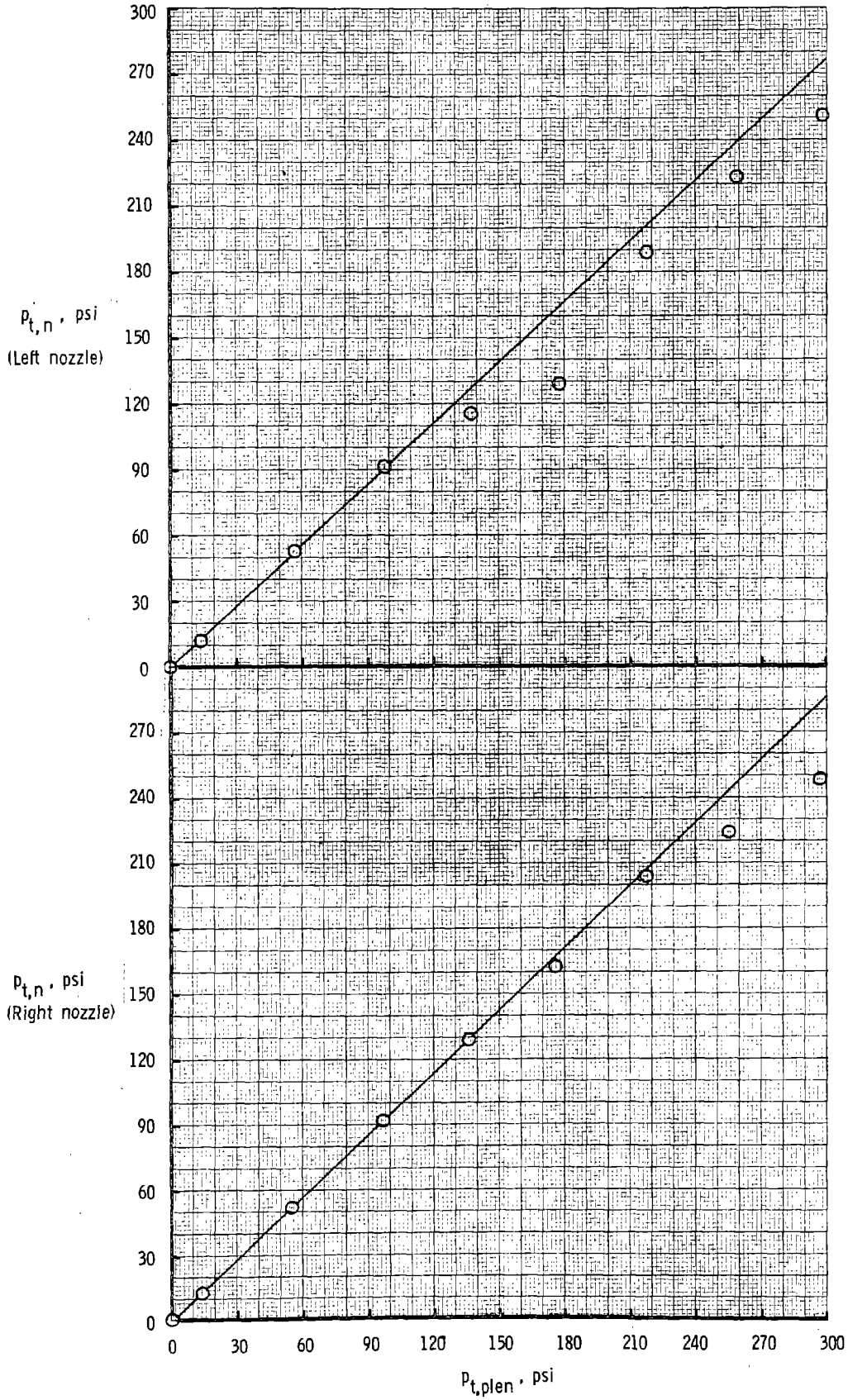

Figure 100.- Total pressure at the nozzle exit versus plenum chamber total pressure for the "locked vortex" wing nozzles.